

Modelling Photovoltaic Systems in Urban Environments

Christian Schweizer

A thesis submitted in partial fulfilment of the requirements of
De Montfort University for the degree of Doctor of Philosophy

January 2000

Institute of Energy and Sustainable Development
De Montfort University Leicester

ABSTRACT

Photovoltaic (PV) systems have found a growing interest in the last years. Several subsidising programs in Europe, the United States, and Japan, have lead to an increasing use of such systems in urban settings. For non-domestic buildings in particular, a PV array is no longer considered to be an add-on device but an integral component of the building's envelope. When used as a facade, the PV modules operate multi-functionally; they generate electricity, act as a sound barrier, as thermal insulation, as weather protection, as shading device, etc.

Facades in urban structures, however, are often shaded. Shading of a PV system decreases its yield significantly and should be avoided. If this is not possible, at least the losses should be reduced to a minimum. A computer program to model PV systems in an urban environment helps to reduce unavoidable losses and to optimise the system. In the design stage of a building it can even help to optimise the structure on solar requirements.

This thesis examines the modelling of PV systems in an urban environment. Here, the modules are often shaded or the irradiance at certain areas of the PV array is increased due to reflections of sunbeams. The thesis contributes to a better understanding of the effects of an inhomogeneously illuminated PV array. A software tool is presented that actually predicts the irradiance on PV modules considering shading and reflections, and can act as an irradiance pre-processor for further PV models. Examinations of typical urban structures conclude the work. These aid architects and systems designers in evaluating the influence of the building geometry, the surface properties, and the latitude of the site, and will help them to design 'better' PV systems and 'solar' structures.

ACKNOWLEDGEMENTS

Solar energy with its practical effectiveness in reducing greenhouse gases has been a matter of both personal and professional concern to me for a long time. Thus, I found it important to take up work in this field and to strive to find a related thesis subject. It is due to three people that I received the lucky chance of combining these two intentions and can now present this work as the result of a collaboration between De Montfort University, Institute of Energy and Sustainable Development, Fachhochschule für Technik Stuttgart (Germany), Department of Building-Physics, and ENGCOTEC GmbH, Stuttgart.

Knowing that it is impossible to thank all the people who enabled the successful conclusion of this work, I want to express my gratitude to at least those persons most directly involved, the 'front line' of support.

First of all, I am particularly grateful to Prof. Kevin J. Lomas who gave the initial ideas for the presented work. His careful support throughout and his most thorough and critical review of the thesis always kept the work 'on course'.

Further, I would like to thank Prof. Dr. Ursula Eicker for her ever friendly and helpful guidance. She was always on the site when problems seemed 'insoluble'.

At this point I would like to express my particular thanks to Mr. I. Samak. He enabled the arrangement at ENGCOTEC of my working both on practical daily business matters and on my thesis during an extended period of time. He had at all the time an open ear for my wishes or difficulties and kept my mind free from all problems. Without his help and support it is hard to imagine how this work could have succeeded.

Further, I would like to thank Dr. D. Infield for agreeing to act as external examiner and Prof. J. Blackledge as internal examiner.

John Mardaljevic is warmly thanked for reviewing the thesis at a later stage. Many thanks to him and Paul Cropper for the cooperation they afforded me whenever I spent a time in Leicester and also for their many useful tips provided by phone or email.

The Deutsche Akademische Austauschdienst (DAAD) is thanked for a scholarship which helped fund part of my work.

Finally, I want to thank my parents who always encouraged me, who always were ready with helpful advice, and who were a very reliable mainstay at all times.

Last but not least, I want to thank my wife Ute for her care and consideration and especially for her loving support throughout.

I declare that the content of this submission represents solely my own work. The contents of the work have not been submitted for any other academic or professional award. I acknowledge that the thesis as submitted complies with the conditions of the regulations. I declare that the work was carried out as part of the course of study for which I was registered and not previous or subsequent to it; and I draw attention to any relevant considerations of rights of third parties or of security which might merit a restriction on loan or access.

Christian Schweizer, January 2000

CONTENTS

Abstract.....	i
Acknowledgements	ii
Contents.....	iv
List of symbols	ix
1 INTRODUCTION.....	1
1.1 Renewable energies	2
1.2 Renewable energies in an urban environment	3
1.3 Photovoltaic systems	4
1.4 Photovoltaics in buildings	5
1.5 Modelling	5
1.6 Structure of the thesis	6
2 PHOTOVOLTAIC SYSTEMS.....	8
2.1 The photovoltaic effect.....	9
2.2 PV cells and PV modules	10
2.3 PV systems	12
2.3.1 Stand-alone systems.....	13
2.3.1.1 Serial charge controller	14
2.3.1.2 Shunt charge controller	15
2.3.2 Grid-connected systems	15
2.3.2.1 Inverter for grid-connected systems.....	16
2.3.2.2 System strategies.....	18
2.4 Inhomogeneous illuminated PV arrays.....	19
2.4.1 Parallel connection.....	20
2.4.2 Module inverters	20
2.4.3 Bypass diodes.....	21
2.4.4 Optimised wiring.....	23
2.5 Protective diodes	24
2.5.1 Block diodes.....	24
2.5.2 Bypass diodes.....	25
2.6 Designing urban PV systems.....	26
3 IRRADIANCE AND ILLUMINANCE.....	28
3.1 Solar radiation.....	28
3.1.1 Basics	30

3.1.2	Sun position	31
3.2	Irradiance on a tilted surface	34
3.2.1	Global irradiance.....	36
3.2.2	Direct irradiance	37
3.2.3	Diffuse irradiance	38
3.2.3.1	Liu / Jordan	38
3.2.3.2	Hay	39
3.2.3.3	Klucher.....	39
3.2.3.4	The Perez tilted surface model.....	39
3.2.3.5	Measurements	40
3.2.4	Ground-reflected irradiance	41
3.3	Illuminance	42
3.3.1	Sky luminance models	44
3.3.2	Overcast sky	44
3.3.2.1	Uniform sky	44
3.3.2.2	Moon & Spencer overcast sky	45
3.3.2.3	Perez overcast sky	45
3.3.3	Clear sky	46
3.3.3.1	Kittler clear sky	46
3.3.3.2	Gusev clear sky	46
3.3.4	Intermediate sky.....	47
3.3.4.1	Brunger intermediate sky.....	47
3.3.4.2	Perez 'All-weather sky model'.....	48
3.3.4.3	Matsuura intermediate sky	48
3.3.5	Blend of skies.....	49
3.3.5.1	Harrison sky blend	50
3.3.5.2	ASRC-CIE sky blend.....	50
3.4	Shading	51
3.4.1	Shading of the direct irradiance	51
3.4.2	Shading of the diffuse irradiance	52
3.5	Reflections	52
4	PV MODELLING	54
4.1	Review of PV modelling	54
4.1.1	Static electrical network analysis.....	56
4.1.2	Statistical evaluation	58
4.1.3	Time-step analysis.....	58
4.1.4	Block-oriented programs.....	60
4.2	Modelling PV systems in an urban environment	61
4.2.1	Criteria	61
4.2.2	INSEL	64
4.2.3	PVcad (ISET).....	67
4.2.4	PVEPO	69
4.2.5	PVSYST.....	70
4.3	Irradiance pre-processors	71
4.3.1	Tilted surface models.....	71
4.3.2	Models to consider shading and reflections.....	72
4.3.2.1	SHADE	72
4.3.2.2	SOMBRERO.....	72

4.3.2.3	SUNDI	73
4.3.2.4	Reflections	73
4.3.3	Criteria	73
4.3.4	Ray-tracing.....	74
4.3.5	Evaluate shading with a CAD program	76
5	TIME-VARYING SIMULATION	78
5.1	RADIANCE	79
5.1.1	Sky models.....	80
5.1.2	Input files	81
5.2	Time-varying calculations with RADIANCE	82
5.2.1	Direct calculation	83
5.2.2	The sky patch approach.....	86
5.2.2.1	Sky dome subdivision	88
5.2.2.2	Deriving the coefficients	89
5.2.2.3	Determine the irradiance	94
5.3	IPROCESS.....	96
5.3.1	Coordinates files	98
5.3.2	RTRACE options	101
5.3.3	Converter.....	102
5.4	Coupling IPROCESS to further PV models.....	103
5.4.1	Coupling to INSEL	103
5.4.2	Coupling to PVcad.....	106
5.4.2.1	Input of PV array wiring	107
5.4.3	Coupling to PVEPO.....	108
5.4.4	Conclusions.....	110
6	TIME DEMAND AND ACCURACY	111
6.1	Simulation parameters	111
6.2	RADIANCE scenes used for testing	113
6.3	Using the direct method.....	115
6.3.1	Estimating the time demand.....	115
6.3.2	Time demand depending on the parameters.....	116
6.3.3	Time demand depending on the number of trace points	118
6.3.4	Accuracy of single values	119
6.3.5	Accuracy of cumulated values	121
6.3.6	Conclusions and recommendations on parameter setting	122
6.4	Using the patch method.....	123
6.4.1	Time demand.....	123
6.4.2	Accuracy dependent on the amount of patches.....	124
6.4.3	Conclusions and recommendations on the number of patches	126
7	EVALUATION AND EXAMINATIONS	127
7.1	Sky models	128
7.1.1	Comparing different sky models.....	128
7.1.2	Intermodel comparison	129
7.1.3	Validation with measured values	131
7.2	Shading algorithms	133

7.2.1	Modelled scene and PV generators	133
7.2.2	Shading algorithms of PVcad	134
7.2.3	Yield predictions using PVcad and IPROCESS	135
7.3	Examinations of typical arrangements	136
7.3.1	Relationship between the irradiation distribution and the yield of a PV generator	137
7.3.2	Irradiation distribution at different locations	139
7.3.3	Irradiation distribution with different surface properties	142
7.3.4	Irradiation distributions at different building distances	145
7.3.5	Further validation	145
7.3.6	Conclusions	147
8	CONCLUSIONS	148
8.1	Further work	149

APPENDIX

A	PEREZ AND BRUNGER MODELS	150
A.1	The Perez tilted surface model	150
A.1.1	Circumsolar region 25°	151
A.1.2	Circumsolar region 0°	152
A.2	The anisotropic sky radiance model of Brunger	154
A.3	The Perez ‘All-weather model’	155
B	LIST OF PV MODELS	157
C	RADIANCE INPUT AND DEFAULTS	159
C.1	A simple RADIANCE scene description	159
C.2	RADIANCE <i>rtrace</i> defaults	160
D	COUPLING IPROCESS TO TRNSYS	161
D.1	Unformatted reading	162
D.2	Formatted reading	162
E	IPROCESS MANUAL	164
E.1	Preliminary remarks	164
E.2	Introduction	164
E.3	Features	165
E.3.1	Location	165
E.3.2	Irradiance.....	166
E.3.3	Scene and output	167
E.3.3.1	Scene description	167
E.3.3.2	Ray files	168

E.3.3.3	Coefficient file	169
E.3.3.4	Output file	169
E.3.4	Time period	171
E.3.5	Algorithm	171
E.3.6	Sky model	172
E.3.7	RTRACE options	172
E.3.8	Start	172
E.3.9	Convert	172
E.4	Typical working routine	173
E.4.1	Preparation of input files	173
E.4.2	Entering the settings in IPROCESS	173
E.4.3	Running the simulation	173
F	LIST OF SELECTED PUBLISHED PAPERS	175
F.1	Computation of Illuminance and Irradiance in Urban Structures	175
F.2	Dynamic Calculation of Daylighting in Urban Structures	178
F.3	Solar Irradiation on an Urban Structure	183
G	SOFTWARE DEVELOPED FOR THESIS
	List of publications and related work	190
	References	192

LIST OF SYMBOLS

Abbreviations

3D	Three Dimensional
ASCII	American Standard Code for Information Interchange
BRDF	Bidirectional Reflectance Distribution Function
CAD	Computer-Aided Design
CIE	Commission International de l'Eclairage
DXF	Data Exchange Format
I-V	Current-Voltage Characteristic
MPP	Maximum Power Point
MPPT	Maximum Power Point Tracker
PV	Photovoltaic
STC	Standard Test Conditions
TIM	Transparent Insulation Material
TMY	Typical Meteorological Year
TRY	Test Reference Year

English letter symbols

\vec{a}	vector (a_1, a_2, a_3) [-]
a	factor [-]
a/c	angular location of circumsolar region [-]
AU	Astronomic Unit $(1AU = 1.495 \cdot 10^{11} m)$ [-]
AM	Air Mass [-]
\vec{b}	vector (b_1, b_2, b_3) [-]
b	factor [-]

c	velocity of light in vacuum ($c = 2.998 \cdot 10^8 \text{ m/s}$) [m/s]
cal	calories, energy ($1 \text{ cal} = 4.19 \text{ J}$) [cal]
C	opaque cloud cover [-]
CR_t	theoretical cloud ratio [-]
d_n	day of the year (1 Jan. = 1) [-]
DF	Daylight Factor [-]
e	elemental charge ($e = 1.602 \cdot 10^{-19} \text{ As}$) [As]
E	energy ($1 \text{ Wh} = 3.6 \cdot 10^3 \text{ J}$) [J, Wh]
E_v	illuminance (on a tilted surface) [lm/m^2]
F	factor [-]
F'	Perez coefficients [-]
FF	Fill Factor [-]
h	height [m]
I	irradiance [W/m^2]
I_o	extra-terrestrial solar irradiance ($I_o = 1367 \text{ W/m}^2$) [W/m^2]
I_a	ground-reflected irradiance [W/m^2]
I_b	beam (direct) irradiance [W/m^2]
$I_{b,h}$	beam irradiance on horizontal [W/m^2]
$I_{b,t}$	beam irradiance on a tilted surface [W/m^2]
I_d	diffuse irradiance [W/m^2]
$I_{d,h}$	diffuse irradiance on horizontal [W/m^2]
$I_{d,t}$	diffuse irradiance on tilted surface [W/m^2]
I_g	global irradiance [W/m^2]
$I_{g,h}$	global irradiance on horizontal [W/m^2]
$I_{g,t}$	global irradiance on a tilted surface [W/m^2]
I	current [A]
I_{MPP}	current at Maximum Power Point [A]
I_{ph}	photo-current [A]
I_s	inverse current [A]
I_{sc}	short circuit current [A]
k	constant [-]
k	Boltzmann constant ($k = 1.38 \cdot 10^{-23} \text{ J/K}$) [J/K]

K	luminous efficacy [lm/W]
l	relative luminance distribution [-]
L	luminance or luminance distribution [$1\ cd/m^2 = 1\ lm/sr\ m^2$]
L_{bl}	luminance distribution of a blend of skies [cd/m]
L_c	luminance distribution of a clear sky [cd/m^2]
$L_{c,z}$	zenith luminance of a clear sky [cd/m^2]
L_o	luminance distribution of an overcast sky [cd/m^2]
$L_{o,z}$	zenith luminance of an overcast sky [cd/m^2]
m	relative optical air mass [-]
m	mass [kg]
MBE	Mean Bias Error [-]
n	diode factor [-]
N	nebulosity index [-]
p	pressure [bar]
P	power [W]
P_{nom}	nominal power [W]
R	resistance [Ω]
R_s	serial resistance [Ω]
R_{sh}	shunt resistance [Ω]
R	radiance or radiance distribution [$W/sr\ m^2$]
$RMSE$	Root Mean Square Error [-]
s	distance [m]
t	time [s]
t_k	temperature coefficient [-]
T	equation of time [min]
T	temperature [K]
ΔT	temperature difference [K]
V	volt [V]
V_{MPP}	volt at Maximum Power Point [V]
V_{oc}	open circuit Volt [V]

Greek letter symbols

α	azimuth [$^{\circ}$]
α_m	azimuth angle of m^{th} patch [$^{\circ}$]
α_s	solar azimuth [$^{\circ}$]
α_t	azimuth of a tilted surface [$^{\circ}$]
β	tilt angle of receiver plane [$^{\circ}$]
γ_s	angle between a surface normal and the sunbeams [$^{\circ}$]
γ_p	angle between a surface normal and an arbitrary point in the sky [$^{\circ}$]
Γ	day angle [$^{\circ}$]
δ	solar declination (north positive) [$^{\circ}$]
Δ	Perez sky brightness parameter [-]
ε	elevation or altitude [$^{\circ}$]
ε_l	Perez sky clearness parameter [-]
ε_s	solar elevation [$^{\circ}$]
η	ratio of clear sky illuminance to zenith luminance [-]
θ	zenith angle [$^{\circ}$]
θ_n	zenith angle of n^{th} patch [$^{\circ}$]
θ_s	solar zenith angle [$^{\circ}$]
θ_t	zenith angle of a tilted surface [$^{\circ}$]
κ	diffuse fraction [-]
κ_t	atmospheric clearness index [-]
λ	limiting angle [$^{\circ}$]
ξ	angle between the sunbeams and a point in the sky [$^{\circ}$]
ρ	reflection coefficient [-]
σ	sunshine probability [-]
φ	longitude (west positive) [$^{\circ}$]
φ_{st}	meridian of the local standard time (west positive) [$^{\circ}$]
ϕ	latitude (north positive) [$^{\circ}$]
ω	hour angle (0° for solar noon, 15° for each hour, morning positive) [$^{\circ}$]

Subscripts

<i>a</i>	albedo
<i>b</i>	beam, direct
<i>d</i>	diffuse
<i>g</i>	global
<i>h</i>	horizontal
<i>m</i>	index
<i>n</i>	normal, perpendicular, index
<i>p</i>	point of the sky
<i>s</i>	solar, sun
<i>t</i>	tilted (surface)
<i>v</i>	visible

1 INTRODUCTION

Seemingly inexhaustibly, the sun radiates an incredible amount of energy onto the earth. Day by day, for millions of years, a power of $1.7 \times 10^{17} \text{ W} = 170 \text{ Mio. GW}^1$ has been brought into the atmosphere and on to the ground [1]. In the early days, a large share of this energy was stored in form of fossil fuels. Nowadays, these reserves that grew over millions of years are being consumed within a few centuries.

It is not only that these fossil fuels will be exhausted in the (foreseeable) future (e.g. petroleum in about 35-45 years and hard coal in about 200 years [1, 2]) but the burning of these fuels also entails the exhaust of greenhouse gases. In the last 100 years the temperature at groundlevel has risen by about 0.6°C and the sea level by about 15 cm. Most experts are certain that this increase (or at least a part of it) is caused by the greenhouse gases. A rise of 0.6°C may not sound much, but small differences have an immense effect on the fragile balance of the earth's climate. For example, a temperature increase of 2°C is postulated as the threshold at which catastrophic reaction on the ecosystem, the climate and the feeding situation will be expected [3]. This leads to a general, world-wide agreement upon to decrease the output of climate gases such as CO_2 . One example is the Agenda 21 (The agenda for sustainable development into the 21st century) that was drawn up at the UN "Earth Summit" in Rio de Janeiro, 1992, and its successors 1997 in Kyoto, Japan. In this framework, the German government aimed to reduce the exhaust of climate gases by 25% by the year 2005 [4]. This demanding goal can be achieved only by reducing the burning of fossil fuels and promoting non- CO_2 technologies.

¹ 1-2 GW is about the power of a medium sized nuclear power station

The other main source of energy, nuclear power, generates electricity without producing greenhouse gases. However, the reserves of nuclear fuels are not endless. Following the catastrophe of Chernobyl in 1986, that caused the death of more than 4, 000 persons [5], many people consider nuclear power unsafe. Further, the problem of the nuclear waste has not been satisfactorily solved. Thus, there is a growing will in the population to build no new nuclear power stations and to close down existing ones.

The immense amount of energy that is radiated onto the earth is about 10,000 - 15,000 times larger than the actual energy demand [1, 6]. Thus, if a conversion efficiency of only 5% were assumed, as little as 0.2% - 0.13% of the earth's surface would be sufficient to cover the demand. This could be, for example, one eighth of the Sahara.

From what has been said above, it can be concluded that renewable energies will play a major role in the world's future power supply.

1.1 Renewable energies

Several different forms of 'renewables' exist. These are for example:

1. hydro-electric power
2. wave power
3. tidal power
4. wind energy
5. geothermal power
6. heat pumping
7. biomass
8. solar energy

All of the above listed forms of energy, except geothermal, and tides power, have their origin in solar radiation and can be considered as secondary solar power.

Solar energy shall be examined here to the exclusion of the others. Many different approaches exist for its use, for example:

1. solar-tower power stations (solar energy is reflected by mirrors and focused on a receiver that is mounted on a tower);
2. solar parabolic trough power stations (such a system was installed as early as 1911 [7]);
3. upwind power stations (using the chimney effect);
4. photovoltaic (direct conversion of light into electricity);
5. active solar thermal systems for domestic hot water and/or space heating;
6. passive solar systems for heating (e.g. by Transparent Insulation Material, TIM [8, 9]); and,
7. daylighting (e.g. by light guiding systems [10, 11, 12]).

Of these techniques, 1. - 3. can hardly be installed in urban environments since they demand large areas. They have mainly been installed in southern regions where the direct proportion of the solar irradiation is relatively high. Only direct sunlight (Chap. 3.2.2) can be goal-directed reflected by mirrors or focused in a trough.

The other solar techniques 4. - 7. can be installed in buildings and are enjoying a growing interest among building engineers, architects, and owners of buildings.

1.2 Renewable energies in an urban environment

Solar energy has been used in buildings for a long time. Historically, people took advantage of the sun for daylighting and passive heating. Nowadays active solar energy systems generate electricity, produce hot water, and can heat a building throughout the whole year. The development of new building components, such as TIM or photovoltaic (PV) facade elements has increased the use of solar energy [8, 9]. The latest research results show a capability of reducing the demand of electricity for artificial illumination by effective use of natural daylight and light guiding systems [10, 11, 12].

These systems and components can decrease the energy consumption significantly [13, 14] but should be viewed as an essential part of any building in order to obtain the maximum benefit. This can lead to 'zero energy' houses that need no energy for space heating [15] or even to energy self-sufficient houses that require no external energy [16].

Because of the growing awareness of ecological issues, and prospected future high energy costs, energy saving techniques are more and more applied in domestic and non-domestic buildings.

1.3 Photovoltaic systems

There is no doubt about it that the future world energy supply must be a mixture of several different sources, with a growing share of renewables. The photovoltaic systems will play a key role in this issue. They are emphasised because of several reasons:

1. The 'high-grade' **electrical** energy is generated directly. High-grade, because it can be distributed easily and can be converted into all other forms of energy at high efficiency.
2. The PV generator can be easily scaled up or down. Existing systems range over more than nine decimal decades (from mW to MW)
3. PV systems produce the energy close to where it is required. Transport expenditure and energy losses can be avoided. This can be the basis for a decentralised power supply.
4. Standard PV systems do not require any moving parts. They operate very reliably and modules are available with a guarantee of 20 years or more [17].
5. The raw material of the commonly used PV cells is silicon, one of the most widespread chemical elements.
6. The solar irradiance energy source can be accessed worldwide and is not restricted to special prerequisites.

The above mentioned reasons make PV systems very attractive for the many different applications and have led to a stable growth of annually 15-20% of the PV market in the last 15 years [18, 19]. Even large oil companies such as BP or Shell have started to produce PV modules.

However, the relatively high costs are still the major hindrance to a larger and faster dissemination of PV systems. Thus, strategies are looked for where the cost-effectiveness can be improved. One strategy is, for example, to use PV modules multi-functionally. This can be especially realised in buildings.

1.4 Photovoltaics in buildings

PV systems, especially when they are grid-connected, have a relatively simple structure and consist mainly of PV modules and inverters (Chap. 2.3.2). This makes them ideally suited for being incorporated into the building's exterior. Here, the modules can replace the 'normal' cladding and can thus act multi-functionally. One of the benefits of using PV modules in buildings is that here cost-effectiveness is not always a primary goal. For example, no one will ask for the cost-effectiveness of a marble facade.

PV modules consist mainly of glass. Thus, for example in facades, they can replace standard glass elements that are often used in modern buildings. Other than producing electrical energy, they can act, for example, as protection of the facade against climatic influences, as thermal insulation, as a shading device, or as a sound barrier. The cost of the PV generator in this application is offset by the cost of normal construction material.

However, when integrated in the facade of a building in an urban environment, the yield of the PV systems is usually reduced because of the sub-optimal tilt angle and the unavoidable shading of the modules. Thus, the planning of these systems requires more effort than standard PV systems on a tilted roof.

1.5 Modelling

Before installing a PV system on a building the owner has an interest in knowing what its benefit will be. Thus, the system is usually modelled, and its energy gains are predicted. Although many approaches exist for this, only few are suitable for application to PV systems in an urban environment. Besides the modelling of the PV system, this requires knowing the irradiance conditions on the receiver plane. Especially within an urban environment, and if mounted at facades, PV modules are often shaded, and/or the irradiance at certain areas is increased due to reflections of sunbeams. This leads to an inhomogeneous irradiance distribution at the PV array, which must be considered by the simulation.

The work presented here examines different approaches of modelling PV systems in an urban environment. A focus is placed on the irradiance conditions that are caused by shading and reflections, since these have a strong influence on the solar yield. All in all, this thesis will contribute to the better understanding of PV systems and to the distribution of solar irradiance in an urban environment. A computer tool is presented to determine the time-varying inhomogeneous irradiance on a PV array.

1.6 Structure of the thesis

A general introduction to photovoltaics is presented in Chap. 2. Besides the basic PV effects, this includes the different system technologies (Chap. 2.3) and the effects of a inhomogeneous irradiance distribution (Chap. 2.4).

The basic principles of solar irradiance are covered in Chap. 3. Different sky models to determine the irradiance on a tilted receiver plane are presented in Chap. 3.2. In this section, different sky luminance models (Chap. 3.3) and algorithms to evaluate shading (Chap. 3.4) are also presented.

A survey of different PV models, different models to simulate the solar irradiation on a tilted plane, and models to evaluate shading is presented in Chap. 4. Different criteria for computer programs are developed for devising models suitable to simulate PV systems in an urban environment.

A computer program, IPROCESS, to determine the irradiance on arbitrarily oriented receiver planes is presented in Chap. 5. This tool considers a description of the structures that surround the solar systems and determines the inhomogeneous irradiation of the receiver plane that is caused by shading and reflections of sunbeams. It can generate long-term series of irradiance data at specified points which can be used as input for further solar models. Thus, IPROCESS can be used as an irradiance pre-processor for further PV models. Coupling to some selected PV models is presented in Chap. 5.4. An approach to accelerate a simulation run using daylight coefficients is presented in Chap. 5.2.2.

IPROCESS is based on the ray-tracing program RADIANCE. This program allows adjustment of a large number of parameters that determine the accuracy and the time demand of a computation. A selection of significant parameters are examined in Chap. 6. The examinations lead to a recommendation of different parameter sets that should be used for the simulation. Further, in Chap. 6.4 the time savings with the daylight coefficient approach are examined and a number of patches that are suitable for the simulation are suggested.

Finally, the algorithms are validated and compared to others in Chap. 7. This includes a validation of the used sky model and an evaluation of the shading algorithm. Different structures that are typical for urban environments are examined on their suitability for solar systems in Chap. 7.3. Here, the effects of the geometry, of the latitude of the site, and of surface properties are examined. These examinations will aid architects and system designers to be aware of the influence of the structures on solar systems and will help them to build 'better' solar systems.

2 PHOTOVOLTAIC SYSTEMS

As mentioned in the previous chapter, it is postulated that photovoltaic (PV) systems could provide a significant share of the world's total energy demand. Since PV generators require a considerable area, an installation on the ground is only partially possible but difficult in highly populated countries such as England or Germany. In these countries, PV modules will frequently be installed on existing structures or new buildings. Thus, a large area for applications of PV systems can be found in urban environments. Here, they do not need any additional space, and they can use existing structures as support.

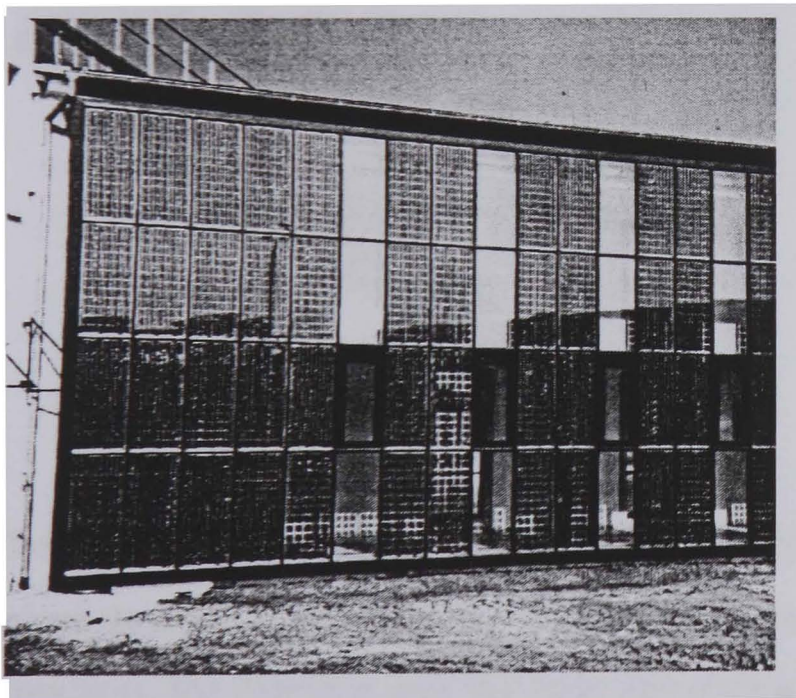


Figure 2.1
Warm facade of thermal isolating
PV elements in a post-peg construction

A PV array can be integrated into the building framework and can replace otherwise used elements. In this multifunctional use the modules act, in addition to generating electricity, for example, as a sound barrier, as a shading device, as protection for an inner facade, or as thermal insulation (Fig. 2.1). This improves the cost-effectiveness of a PV system significantly.

When used in the facades of buildings in an urban environment, PV modules are often shaded by the building itself or by surrounding structures. A serious disadvantage of PV systems is that they are very sensitive to shading, and a small shaded area can significantly reduce the system output. The reason for this and the principles of PV systems will be introduced in this chapter. This fundamental knowledge is necessary for understanding PV modelling.

2.1 The photovoltaic effect

Photovoltaic (PV) describes the direct conversion of light into electrical energy. This is achieved by semiconductors, so-called PV cells. Standard PV cells consist of layers of p-doped (e.g. by Boron) and n-doped (e.g. by Phosphorus) silicon¹. A small depletion zone occurs at the junction of the two layers (Fig. 2.2). Generally, PV cells are large-scale semiconductor diodes.

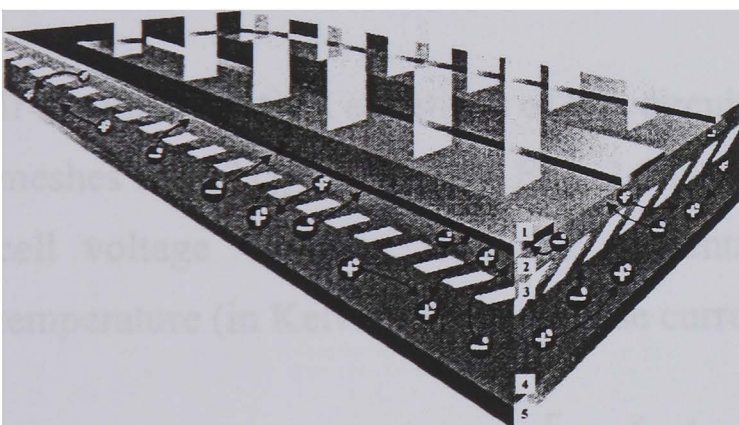


Figure 2.2
Structure principle of a PV cell comprising
1 Front side contact
2 Negative zone
3 Depletion zone
4 Positive zone
5 Reverse side contact

Sunlight in the form of photons have enough energy to crack the valence binding of an electron and to generate an electron-hole pair [20]. When a photon is absorbed near the junction, the electron and the hole are separated by the electrical field. The electron drifts into the positively charged n-zone, and the hole drifts into the negative charged p-zone. The resulting potential can be measured by a voltmeter and is about 0.5...0.6 V for silicon cells². When the two zones are contacted by a conductor, the electrons can flow through an external circuit, and their energy can be used in any electrical appliances. The structure of

¹ Although PV cells can be made of different semiconductors more than 95% of the commercial applied cells are made of silicon. All data in this chapter refer to monocrystalline silicon.

² This is the open circuit voltage (V_{OC}) of a PV cell.

a PV cell with front and reverse side contacts is shown schematically in Fig. 2.2 [17]. It should be noted that PV cells always generate a DC current.

2.2 PV cells and PV modules

A PV cell is basically a large-scale semiconductor diode. Thus, it can be described by the mathematical equation of a diode with a diode ideality factor n . The generation of the electrical (photo-) current I_{ph} can be modelled by a constant current source and the intrinsic losses by a shunt resistor R_{sh} and a serial resistor R_s . This leads to the one diode equivalent circuit diagram as shown in Fig. 2.3.

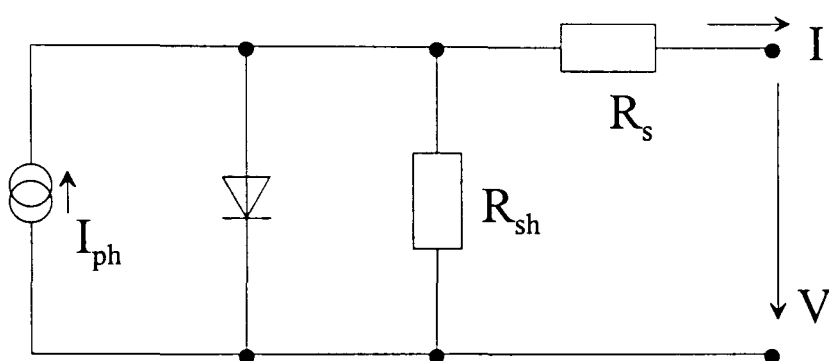


Figure 2.3

One diode equivalent circuit diagram of a PV cell and its electrotechnical symbol

If the mathematical equations of this circuit are solved according to Kirchhoff's nodes and meshes law [21], the implicit Equ. 2.1 is found for the resulting current I dependent on the cell voltage V . Here, e is the elemental charge, k the Boltzmann constant, T the temperature (in Kelvin), I_s the inverse current of the diode, and n the diode ideality factor.

$$I = I_{ph} - I_s \left[\exp\left(\frac{e \cdot (V + I \cdot R_s)}{n \cdot k \cdot T}\right) - 1 \right] - \frac{V + I \cdot R_s}{R_{sh}} \quad (2.1)$$

PV cells have a limited power and generate a small maximum voltage only. Thus, usually, single cells are combined into solar modules. The module provides mechanical protection of the fragile cells and contains several cells connected in series. The series connection increases the output voltage to a reasonable value. In many standard modules, 36 cells are connected to one string because solar modules are often used to charge a 12 V battery. The achieved voltage (i.e. 21 V_{OC}) enables charging and also overcomes system losses, cable losses, and the increased end-of-charge voltage of batteries at low temperatures.

Typical characteristic curves of a PV module with 36 cells (each 100 cm²) at Standard Test Conditions (STC) are shown in Fig. 2.4. The power output of a PV module is usually given as *Watt peak* (W_p) that is the maximum power output at STC.

STC refer to a solar irradiance of 1000 W/m², a cell temperature of 25°C, and an irradiance spectrum of Air Mass (AM) 1.5. The efficiency of a solar cell depends on the wavelength of the incident photons (i.e. the light spectrum) [20]. Thus, the declaration of an irradiance of 1000 W/m² is not sufficient, but its spectral distribution must be also given. AM 1.5 is a standardised spectral distribution [22] that is reached by the sun on average in Europe. Outside the earth's atmosphere, the solar spectrum is AM 0 and at the Equator AM 1.

In Fig. 2.4, the short circuit current I_{SC} , open circuit voltage V_{OC} and the data at the Maximum Power Point (MPP) are entered. The Fill Factor FF (Equ. 2.2) describes the quality of the solar cell [23].

$$FF = \frac{V_{MPP} \cdot I_{MPP}}{V_{OC} \cdot I_{SC}} \quad (2.2)$$

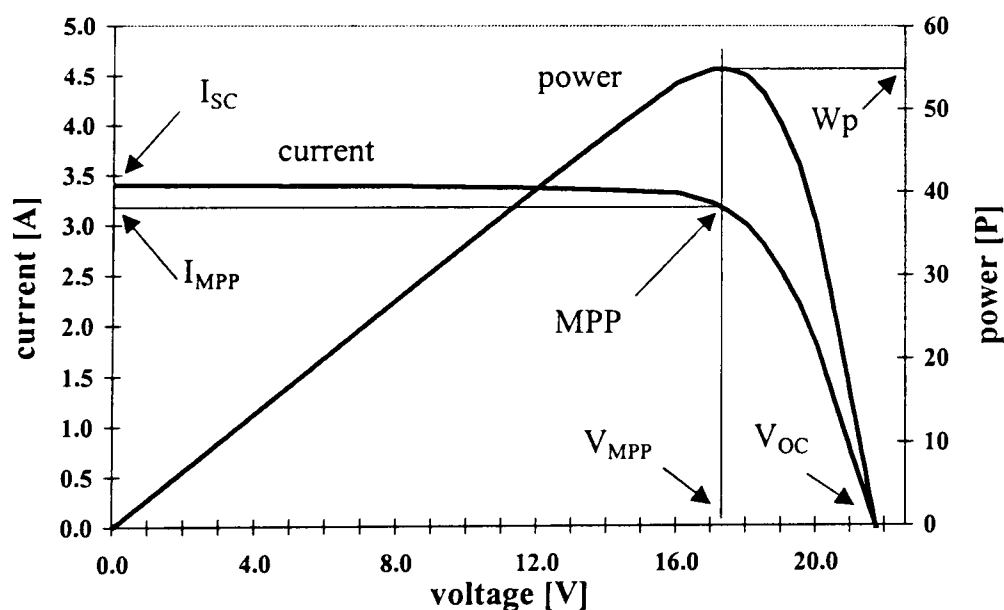


Figure 2.4
Typical I-V and power curve of a 55 W_p solar module with 36 crystalline silicon cells

The I-V curves of a solar module at a varying irradiance are printed in Fig. 2.5. Here, it can be seen that the current is directly proportional to the irradiance. When all other parameters are constant, the voltage depends logarithmically on the irradiance [22] and is nearly constant between 200...1000 W/m². Thus, the power of a solar module (in the usually considered range) is nearly proportional to the solar irradiance. The current of a PV cell is also proportional to its size (the cells used for Fig. 2.5 have an area of 100 cm²).

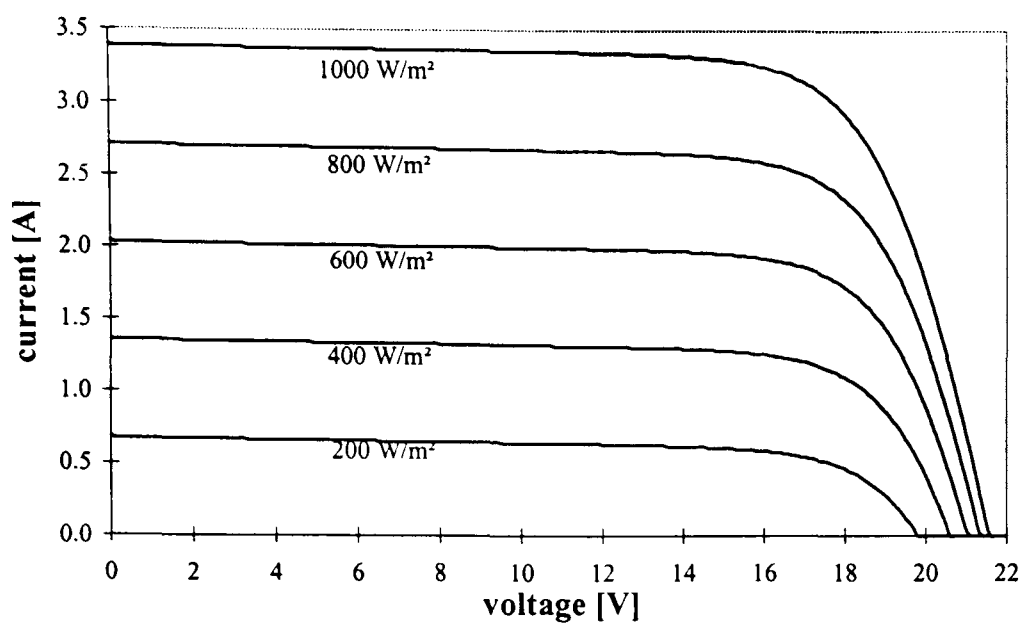


Figure 2.5
I-V curves of a solar module at a varying irradiance

Besides the irradiance, the cell temperature has a major influence on the performance of a solar module. As shown in Fig. 2.6, the current increases slightly with increasing temperature (by about 0.04 %/K). However, the voltage decreases by about 0.34 %/K [24] and consequently the power of the cell also decreases with increasing temperature.

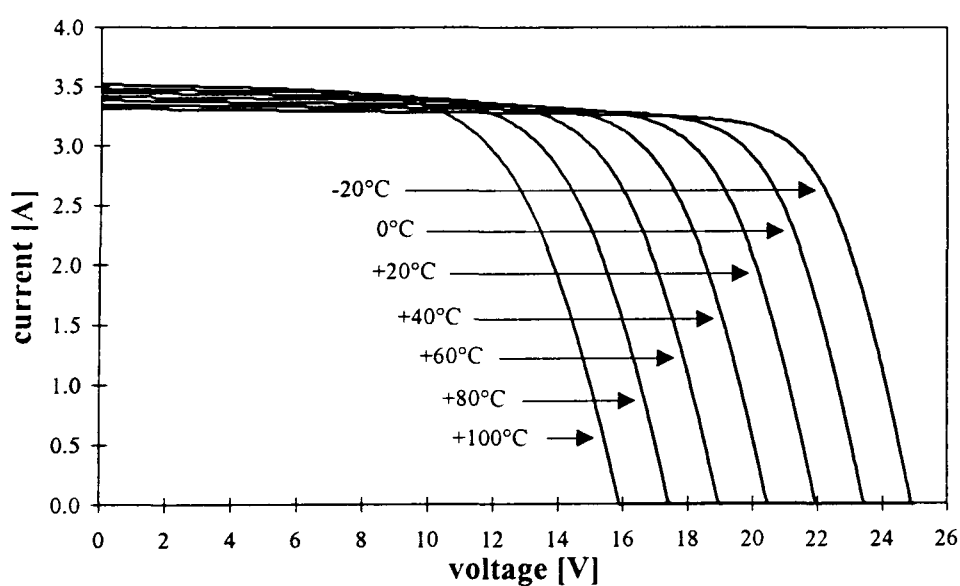


Figure 2.6
I-V curves of a solar module at varying temperatures

2.3 PV systems

Nearly all PV systems need a store for the energy because, in general, the demand and supply do not match each other exactly. An exception are solar water pumping systems, where the water is pumped only when the sun shines. However, these systems often use a reservoir as an energy store. In general, PV systems can be divided into stand-alone systems, that usually charge a battery, and grid-connected systems, where the mains are used as an infinite store. These systems will be explained in the following sections.

2.3.1 Stand-alone systems

Stand-alone PV systems usually operate a single load (e.g. the light in a solar street lamp) or a small local network. A typical system comprises a PV module, a charge controller, a battery, and the load, as shown in Fig. 2.7. However, sometimes not only PV modules but also motor generators or wind energy converters are used as the energy source. These are called *hybrid* systems. The energy store is often a lead-acid or NiCd battery, but attempts are being made to use new technologies like high-temperature batteries [25], NiMH-batteries, Lithium batteries or capacitors [20]. Another approach is to use hydrogen as a carrier for solar energy [26].

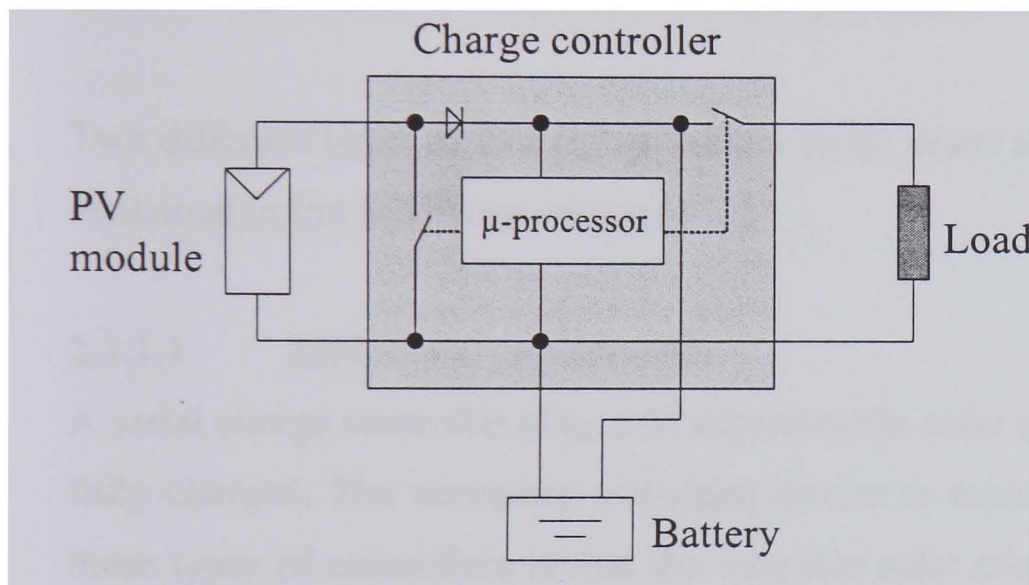


Figure 2.7
A typical stand-alone PV system comprising a PV module, a charge controller, a battery, and the load

The loads are often 12 V_{dc} appliances, developed for the car industry or for leisure activities. Sometimes inverters (to convert the DC to AC power) are applied to operate standard AC devices. These are usually connected directly to the battery and not via the charge controller. Care must be taken to ensure that deep-discharge protection is provided for the battery.

The charge controller is the core of a standard stand-alone PV system. It protects the battery from overcharge³ and deep-discharge⁴ both of which destroy it in the long-term. Charge controllers usually connect the battery directly (via some switches) to the solar

³ A battery is overcharged when more than its nominal capacity is fed into the battery.

⁴ The life time of a lead battery is inversely proportional to the amount of energy that is taken out at each usage (cycle). Thus, a lead battery should not be discharged by the full (nominal) capacity, i.e. the battery should be prevented from being deep-discharged.

modules. Thus, the operating voltage of the solar module is determined by the battery voltage.

Another option would be to use a MPP tracker [27]. Instead of a direct connection between the PV modules and the battery (or the load), this device separates its input voltage from the output voltage. It detects the maximum power point (MPP) of the solar array and operates it at the corresponding voltage (V_{MPP}). The output voltage is adjusted to the required charging voltage of the battery [20]. Thus, the PV modules can be operated in their MPP and deliver a higher output than if they were connected directly to the battery. Different control strategies for a MPP tracker can be found at [27] and [28]. However, since a MPP tracker is relatively expensive, it is seldom used in stand-alone PV systems.

Two different types of charge controllers exist: shunt and serial controllers. These will be explained in the following sections.

2.3.1.1 Serial charge controller

A serial charge controller (Fig. 2.8) separates the solar modules from the battery when it is fully charged. The necessary switching device is usually a transistor. A disadvantage of these types of controllers is that the valuable solar energy must always flow through the switching device, which causes losses.

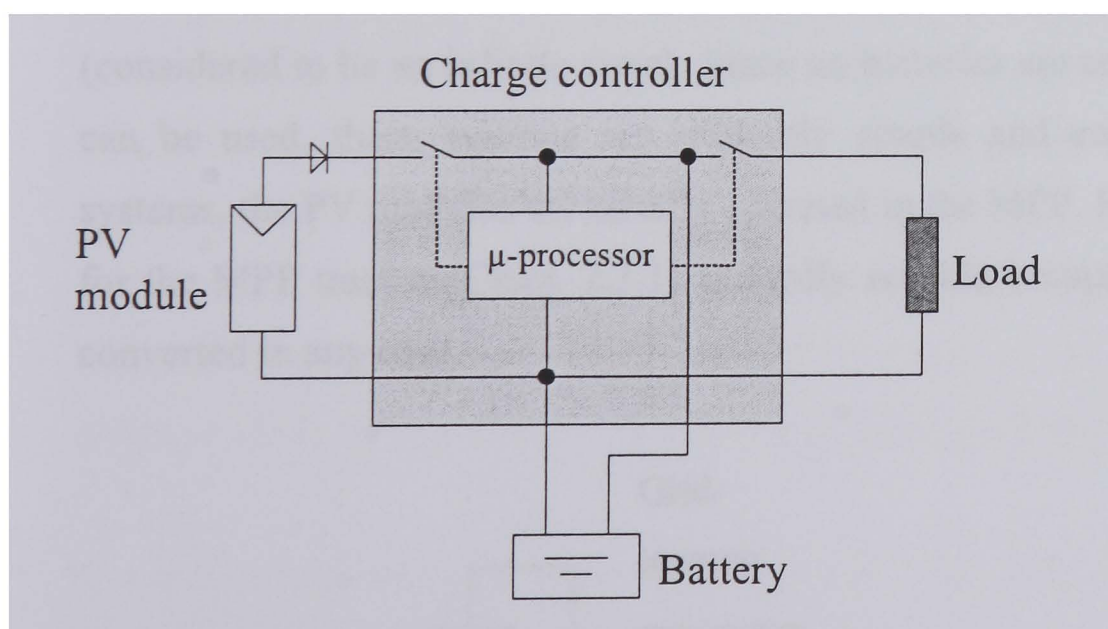


Figure 2.8
A serial charge controller
for stand-alone PV
systems

It should be noted that the controllers must have a blocking diode (Chap. 2.5.1) integrated at the output to the modules, or it must be included in the PV string (indicated in Fig. 2.8). Otherwise, the battery would discharge during the night. The second task of the charge

controller is to prevent the battery from being deep-discharged. To this purpose, it is able to separate the load from the battery by a second switch.

2.3.1.2 Shunt charge controller

Shunt charge controllers (Fig. 2.7) avoid losses due to the switching device. When the battery is fully charged, they short-circuit the solar modules to prevent a further energy flow to the battery. The switching device can causes losses only when no further energy should flow to the battery.

Short-circuiting of the PV modules is possible because the short circuit current I_{SC} of a PV module is only slightly higher than the normal operating current I_{MPP} (Fig. 2.4). However, a diode is required so that short-circuiting of the modules does not also short-circuit the battery (this would destroy the charge controller). This integrated diode is simultaneously used as a blocking diode, and no external diode is required.

2.3.2 Grid-connected systems

The other category of PV generators are grid-connected systems (Fig. 2.9). Here, the DC current that is generated by the PV modules is converted by an inverter into mains-compatible AC current. The output of the inverter is directly (or via switches) connected to the mains. Thus, the electricity can either be used in local appliances or fed into the mains (considered to be an infinite store). Since no batteries are required and standard appliances can be used, these systems are relatively simple and cost-effective. In grid-connected systems, the PV modules are usually operated in the MPP. Here, the additional expenditure for the MPP tracker (Chap. 2.3.1) is hardly notable because the module voltage must be converted in any case.

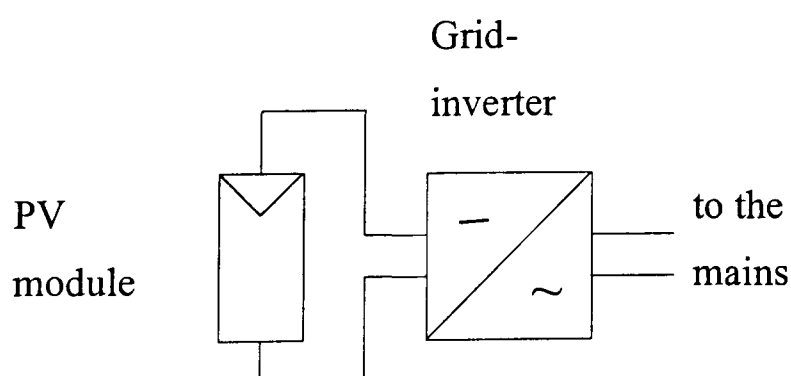


Figure 2.9
Grid-connected PV system

Although nowadays many stand-alone PV systems are installed in cities (e.g. parking ticket machine or solar street lamps), the main applications for PV modules in urban environments are grid-connected systems. They are installed on roofs or facades (Fig. 2.1) and produce enough energy to cover a share of the total energy demand of the building. Further, the multifunctional application of PV modules is more significant in grid-connected systems because these generally use a larger array. Grid-connected systems are expected to replace main power stations in future.

2.3.2.1 Inverter for grid-connected systems

An inverter for a grid-connected PV system converts the DC power of the modules into mains-compatible AC current. Most currently used inverters feed the energy in one phase of the mains only (for example this is allowed by the German law up to a power of 5 kW), however, larger inverters (with a power > 5 kW) can be applied to feed the solar energy in all three phases.

A grid-connected inverter is very different from a standard inverter for stand-alone systems which is usually connected directly to a battery. The latter generates a voltage of about 230 V_{ac} and a frequency of about 50 Hz (for European appliances) from the given DC (battery) voltage.

The grid-connected inverter must synchronise the generated sine-waves in voltage, frequency, and phase-angle exactly to those of the mains. It usually includes a MPP tracker (Chap. 2.3.1) and consequently operates the PV array at the corresponding V_{MPP} . This voltage varies with the temperature and the solar irradiance (and the shading of the module) over a certain interval but must be within the input voltage of the inverter to be accepted. It depends on the algorithm by which the inverter detects an MPP, if two different MPPs (Chap. 2.4.3) can be distinguished and if the higher one can be identified.

The basic circuit diagram of an inverter and its equivalent circuit diagram is shown in Fig. 2.10 [22]. The two switches S1 and S2 (in earlier times thyristors were used as switches which are now replaced by MOSFET's or IGBT's) are switched in such a way that an alternating voltage is applied across the transformer T1. The resulting voltage is transformed (by T1) to the desired output voltage (i.e. 230 V_{ac} if connected to the mains). Additional devices such as input and output filters or the circuit to control the switches are

neglected in the simplified diagram of Fig. 2.10. An introduction to inverters for solar systems is given in [29] and further concepts of high efficiency inverters can be found, e.g., in [30].

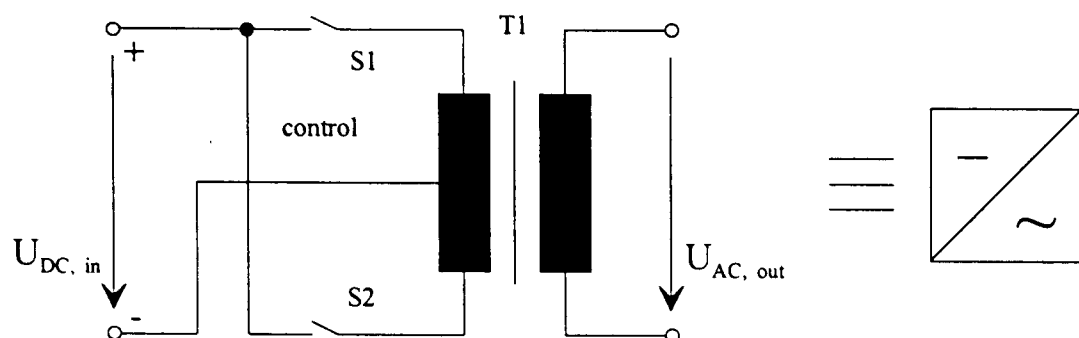


Figure 2.10
Basic circuit diagram of an inverter

Modern inverters reach an efficiency of up to 97%. Their losses can be summarised as self-consumption P_{self} , voltage losses v_{loss} , and ohmic losses r_{loss} [31]. Equation (2.3) describes the correlation between input power P_{in} and output power P_{out} .

$$P_{in} = P_{self} + (1 + v_{loss}) \cdot P_{out} + r_{loss} \cdot P_{out}^2 \quad (2.3)$$

Typically, inverters have an efficiency curve as shown in Fig. 2.11. Here, the curves of two inverters are shown that have the same efficiency at the nominal power but different intrinsic losses and a different self-consumption. This causes the higher efficiency of inverter 1 at a normalised power of 0.1.

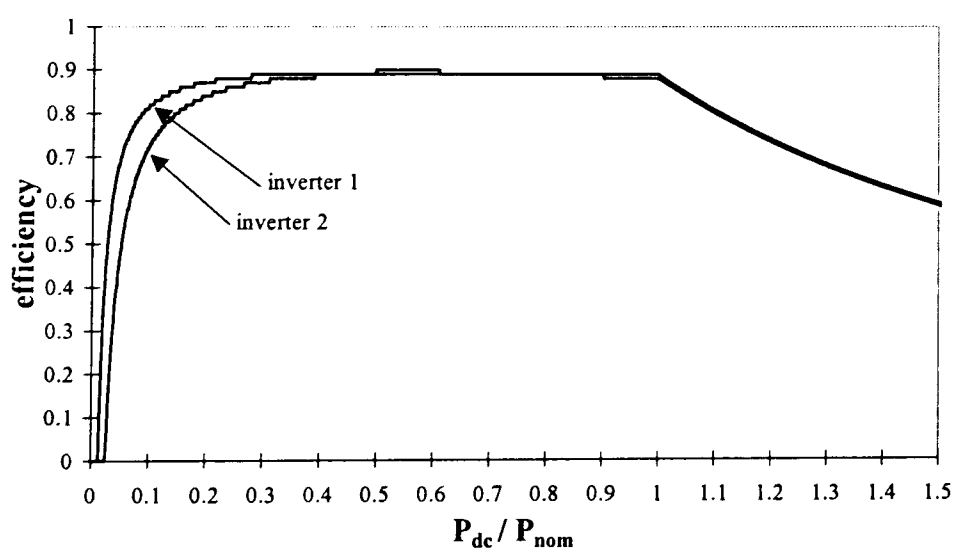


Figure 2.11
Typical efficiencies of grid-feeding inverters with different intrinsic losses but the same efficiency at the nominal power

If the possible power output of the PV array exceeds the nominal power of the inverter, it shifts the operating voltage of the PV array, so that the PV modules are not operating at a the V_{MPP} . Thus, their power output is decreased so that the inverter output power does not

exceed its maximum. This leads to the sloping part of the efficiency curves when P_{dc} is higher than P_{nom} (Fig. 2.11).

The nominal output power of a PV array that is given at the STC (Chap. 2.2), is rarely reached at northern European sites. This is because the irradiance of 1000 W/m² occurs only on some days during the year, and then the temperature is likely to be over 25°C (because it is a sunny day), and the sun light is not normal to the modules. Thus, the nominal power of a grid-inverter is usually smaller than the nominal power of the PV array (i.e. up to 30% smaller) to avoid the low inverter efficiencies at part-load.

2.3.2.2 System strategies

Different strategies for grid-connected PV systems are applied. These are:

- PV systems with a central inverter
- PV systems with string inverters
- PV systems with module inverters

The differences between them depend mainly on how many modules are connected to the inverter and its capacity (Fig. 2.12). Usually, a central inverter (Fig. 2.12a) has a capacity of more than 2.5 kW (up to 100 kW), a string inverter (Fig. 2.12b) has a capacity of 700 W ... 2.5 kW, and a module inverter (Fig. 2.12c) has a capacity of 100 ... 400 W.

The advantage of a system with a **central** inverter is that only one (large) device is required. This eases the controlling, and generally one large device is more cost-effective than several small ones. However, this concept requires a string connection box that can be neglected for the other concepts.

PV systems with **string** inverters are currently the most common systems. They are applied in PV systems with an installed power 700 Wp up to 1 MWp. Their advantage, in contrast to central inverters, is that no connection box is required and thus, installation is very simple. On the other hand, a lower number (i.e. often only one) of inverters is required as compared to module inverters.

The concept of using **modules** inverters is especially interesting for PV arrays where partial shading occurs (Chap. 2.4.2).

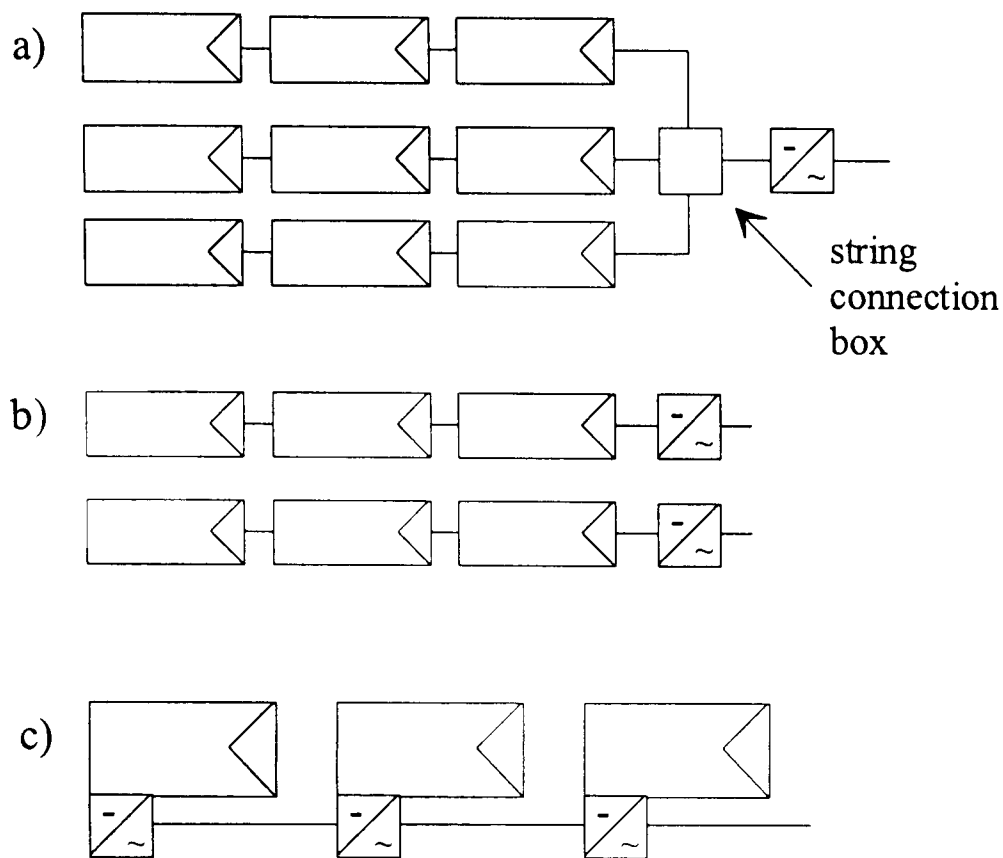


Figure 2.12
 Different strategies for grid-connected PV systems
 a) with a central inverter
 b) with string inverters
 c) with module inverters

2.4 Inhomogeneous illuminated PV arrays

When several cells⁵ are linked together, the resulting characteristic curve can be achieved by adding up the single curves. In a series connection (a so-called *string*), the voltages of the single devices must be added at a constant current; in a parallel connection the currents of the single components must be added at a constant voltage. The results of connecting one full illuminated cell⁶ in series or in parallel with a shaded⁷ one are shown in Fig. 2.13.

It can be seen that the parallel connection results in an addition of the power (at the MPP) for the full illuminated and the shaded cell. By way of contrast, the series connection of the two cells results in a power only about twice the power of the **shaded** one. This principle can be extended on the connection of many cells. Consequently, one shaded cell in a string can reduce the power of the complete string significantly.

Several strategies are applied to reduce the losses that are caused by shaded (or poorly illuminated) PV cells or modules. The most important ones are introduced in this section. It should be noticed that the principles are the same for either a single PV cell or a module, because the module usually consists of cells connected in series.

⁵ Basically, it makes no difference whether PV cells or modules are considered.

⁶ Here, only the principles are shown, the reverse breakdown of the PV cells is neglected.

⁷ *Shaded cell* is easier to understand, although *poorly illuminated cell* would better describe the reality.

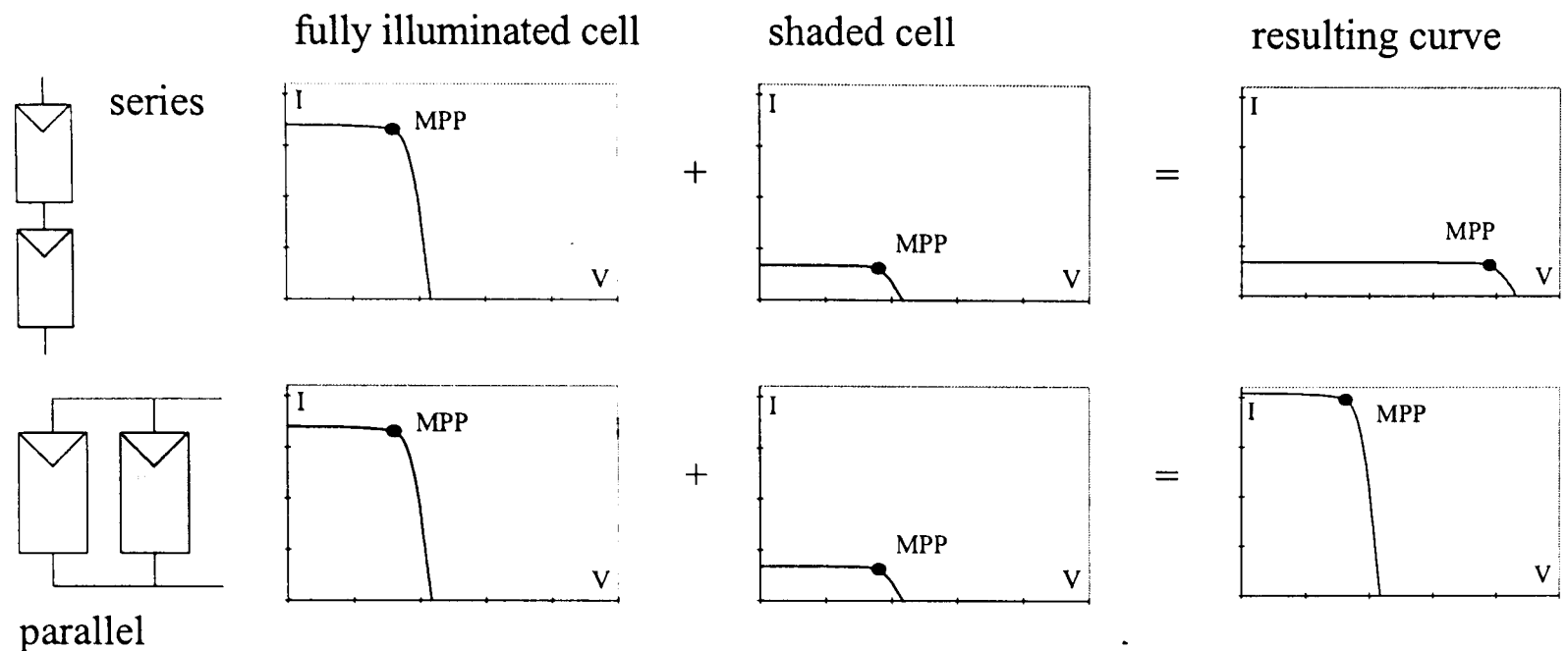


Figure 2.13 Series and parallel connection of a fully illuminated and a shaded cell

2.4.1 Parallel connection

From Fig. 2.13, it can be concluded that wiring the modules into short strings (that entail a high degree of parallel connection) reduces the risk of shading losses. However, this is only possible to a certain degree because it leads to low system voltage and high currents. This causes high losses in the electrical devices and the wires, unless very thick cables are used (which are very expensive and often impossible in practice). Further, inverters that convert the DC to AC current usually have a higher efficiency at high voltages. That is why many manufacturers offer so-called string inverters (e.g. SMA [32]) that operate at voltages as high as 550 V_{dc} and require one or two strings of up to 22 standard modules in series.

A few manufacturers (e.g. Würth [33]) offer devices for low string voltage of about 35 V_{dc} and up to seven strings wired in parallel. These inverters perform better when the solar array is inhomogeneously illuminated but require more expenditure on cabling.

2.4.2 Module inverters

Another strategy in grid-connected systems (Chap. 2.3.2) is to apply so-called module-oriented inverters (e.g. Dorfmueller [34]). Here, every solar module gets its own inverter. For example, this strategy is followed in the PV array on the German Reichstag in Berlin [35] where complex shading of the modules occurs. The advantage of these inverters is that modules are not connected to a string, and the risk of losses is reduced. Moreover,

high currents are avoided because the power is directly transformed to the mains voltage. The disadvantage of this approach is that many inverters are required which leads to high expenditure for cabling and to higher costs. Generally, the efficiency of these small inverters is lower than that of larger ones.

2.4.3 Bypass diodes

Solar modules are usually equipped with bypass diodes. These help to avoid damage to the modules by the 'hot-spot' effect (Chap. 2.5) and can also reduce the shading losses. In standard PV modules, one bypass diode is connected in parallel to 18...20 cells. The function of these diodes (here with only one diode per module) is shown in Fig 2.14.

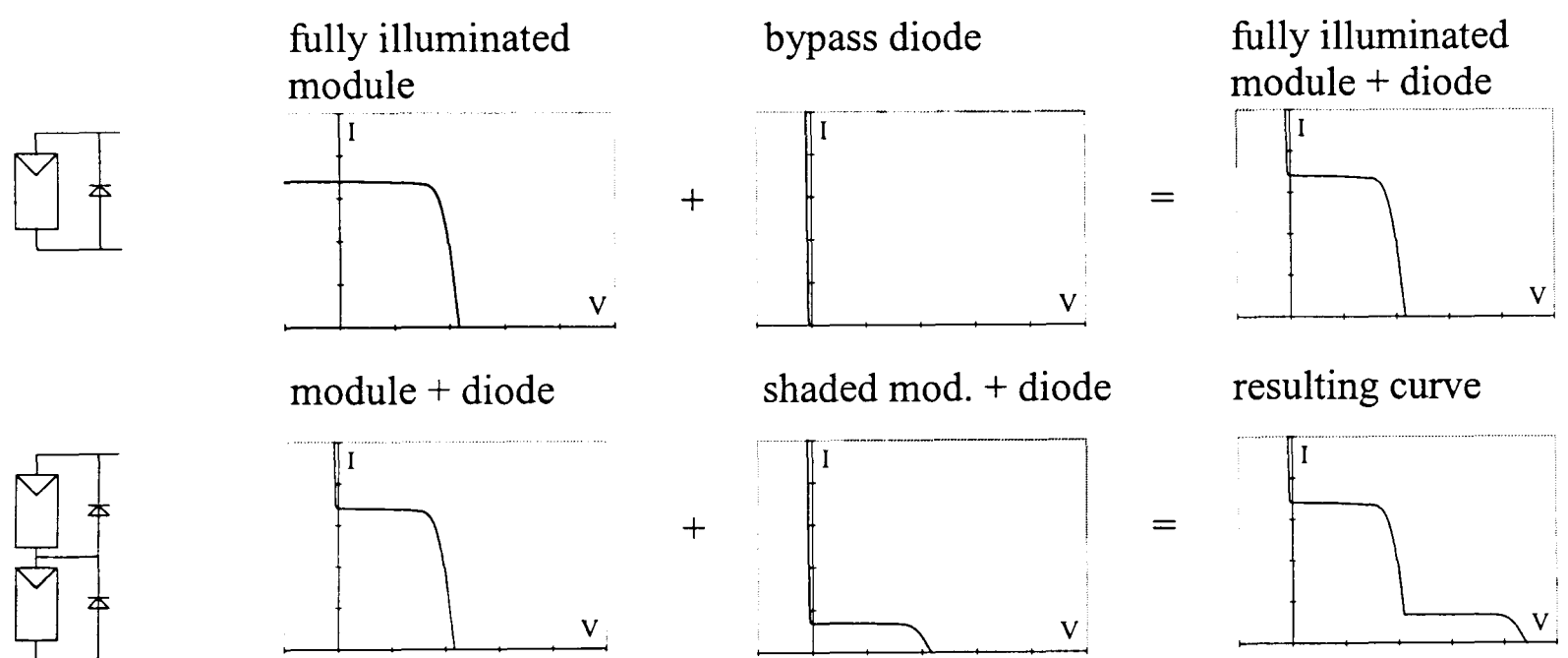


Figure 2.14 Effect of the integrated bypass diodes

When a negative voltage is applied at the module that has a bypass diode, the current flows through the diode as shown in the upper row of Fig. 2.14. If a fully illuminated and a shaded module are connected in series (lower row of Fig. 2.14), the current at high voltages is low and determined by the shaded module. At low voltages, the current may not flow through the cells but through the bypass diode and can reach the value of the fully illuminated module. This results in a (typical) step in the characteristic curve (Fig. 2.14 and 2.15) and in two MPPs at different voltages.

Depending on how many cells are bridged by a bypass diode, how many cells (or modules) are shaded, how many modules are connected to a string, and what is the remaining

illuminance on the shaded cell, the step⁸ may be more or less marked and shifted to lower or higher voltages. The I-V curve of two standard modules (of 50 Wp) connected in series, each with a bypass diode, is shown in Fig. 2.15. Here, one module is illuminated with 1000 W/m² and the other one with 500 W/m².

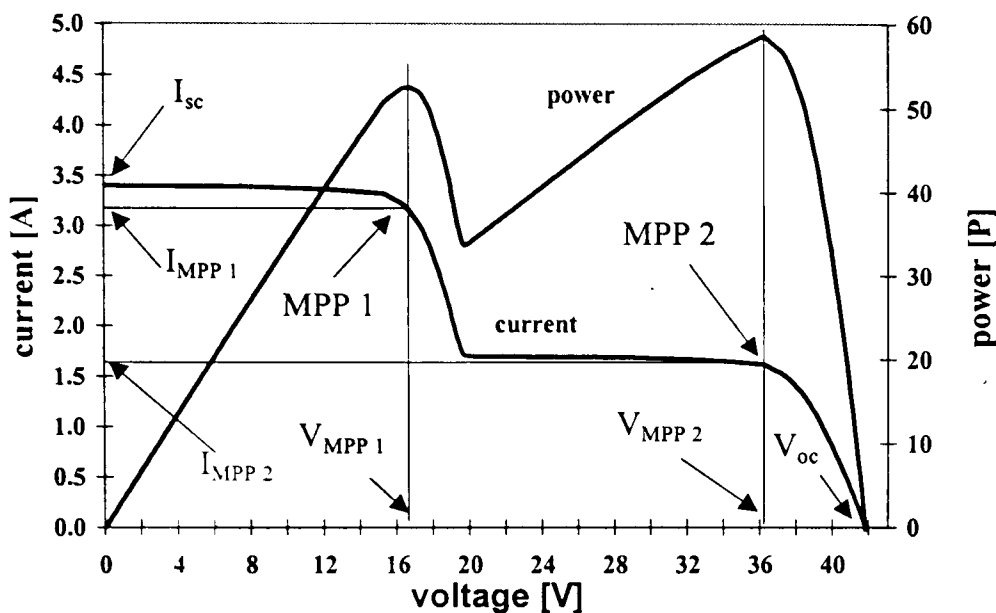


Figure 2.15
Characteristic curve of two PV modules connected in series, each with bypass diodes. One module receives an irradiance of 1000 W/m², the other one of 500 W/m².

Depending on the PV system, the bypass diodes can reduce the shading losses. In Fig. 2.15 they do not help because MPP 2 is higher than MPP 1, but MPP 2 would be also reached without diodes. Bypass diodes can only increase the yield if the MPP at the lower voltage is higher than the MPP at the higher voltage. Another stipulation is that the system must be able to operate at the low voltage. This is usually not the case when the PV array charges a battery, because then the system operates at a fixed voltage (Chap. 2.3.1). In grid-connected systems (Chap. 2.3.2) it depends on the permissible input voltage of the inverter. If the MPP at the lower voltage is still within the allowed range it can be adjusted, but the algorithm to detect the MPP must be able to distinguish two MPPs.

The step in the curve caused by the bypass diodes is shifted towards higher voltages as the number of cells that are bridged by the diode decreases (assuming only some of these cells are shaded). Thus, attempts have been made to integrate the diode into the PV cell structure to obtain one bypass diode per cell [36, 37]. Other approaches try to avoid the additional expenditure for the diodes and to use modules without them [38, 39]. However, because of the risk of the 'hot-spot' effect (Chap. 2.5), it is recommended that modules with bypass diodes are used in grid-connected and stand-alone PV systems.

⁸ Or several steps when several modules are illuminated differently.

2.4.4 Optimised wiring

Another strategy to reduce the shading losses is to optimise the string wiring. If some modules in a PV array that consists of two strings are shaded, then it is best if these modules are connected to one string with the fully illuminated modules in the other string. This yields a higher power than a mixture of differently illuminated modules in both strings.

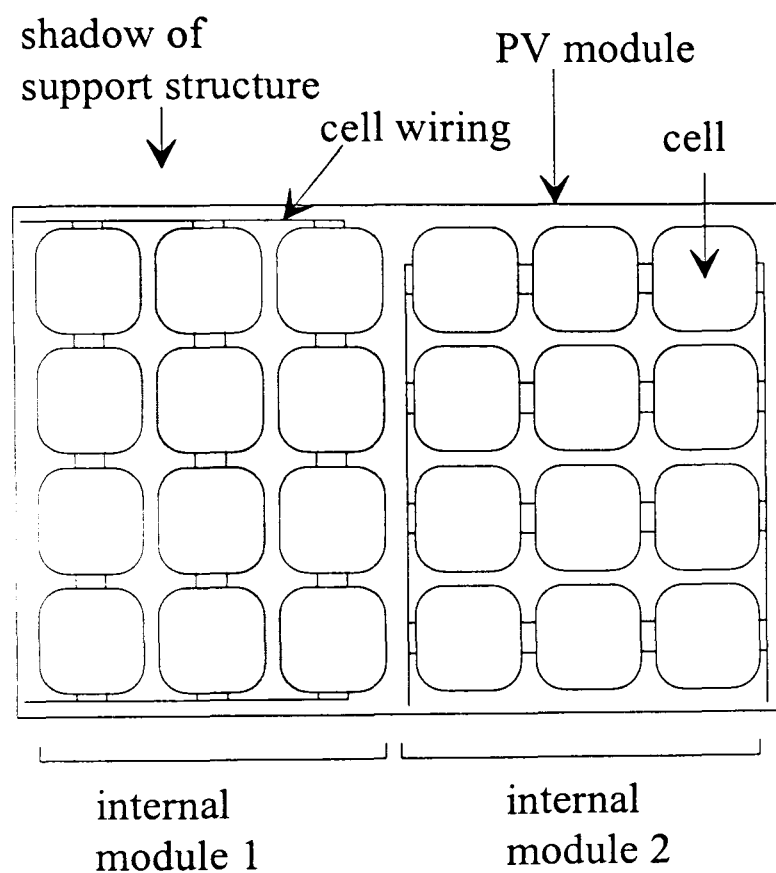


Figure 2.16

The so-called 'Module in Module' technology. The wiring of the cells in the module was fitted to the shadow of the support structure.

A PV system designer would try to arrange the wiring in such a way that, if shading is unavoidable, all the modules in one string are simultaneously shaded. However, this is not always possible because of the variable silhouette of a shading obstacle on the PV array. A computer program (e.g. PVEPO, Chap 4.2.4) can help to optimise the wiring of the array. It calculates the power for different wiring options and suggests which modules should be connected to each string.

In a specific situations even the wiring of the cells inside the module can be optimised. For example, for the PV generator on the new building for the German President in Berlin custom-made modules were used [40] where the wiring of the cells was fitted to the silhouette of the support structure (Fig. 2.16).

2.5 Protective diodes

PV modules connected in series with unshaded modules can become a load on the array, rather than, as intended, a source of current (Fig. 2.17, 2.19). The unshaded array can cause a reverse voltage or a reverse current which heats the module, the so-called hot-spot effect. The heated cell can be damaged, or even destroyed, by the high temperature. To avoid this blocking diodes which prevent a reverse current and bypass diodes that prevent a (high) reverse voltage are used in PV arrays. These diodes play a protective role as well as, as noted above, helping to avoid power losses due to shading.

2.5.1 Blocking diodes

Blocking diodes prevent a reverse current in the PV modules. They are connected in series with a string as shown in Fig. 2.17.

Consider a design in which several modules are connected in two parallel strings without blocking diodes, where one string is less illuminated than the other (Fig. 2.18). Now, if the electrical circuit is not closed because, for example, no load is connected, the open circuit voltage (here U_I) will be applied to the strings. The total current that is generated in the fully illuminated modules (I_I) must also flow through the shaded modules, but in the reverse direction ($-I_I$). This may lead to the shaded modules becoming a hot-spot. Whether or not these modules are destroyed depends on the number of modules per string, the number of parallel strings, and the actual (low) irradiance on the shaded module.

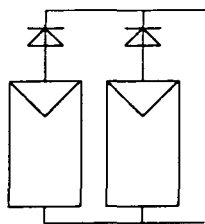


Figure 2.17
Solar array with one blocking diode per string

A reverse current through a module may also appear in battery charging systems at night when the irradiation is zero but the battery is connected to the module. Then the battery voltage applies across the module and the battery discharges through the module. Blocking diodes prevent the reverse current through the modules. Unfortunately, blocking diodes entail a voltage drop in the string and cause power losses thus. Diodes with a low voltage drop are to be used (e.g., Schottky-Diodes [41]) to reduce the power losses.

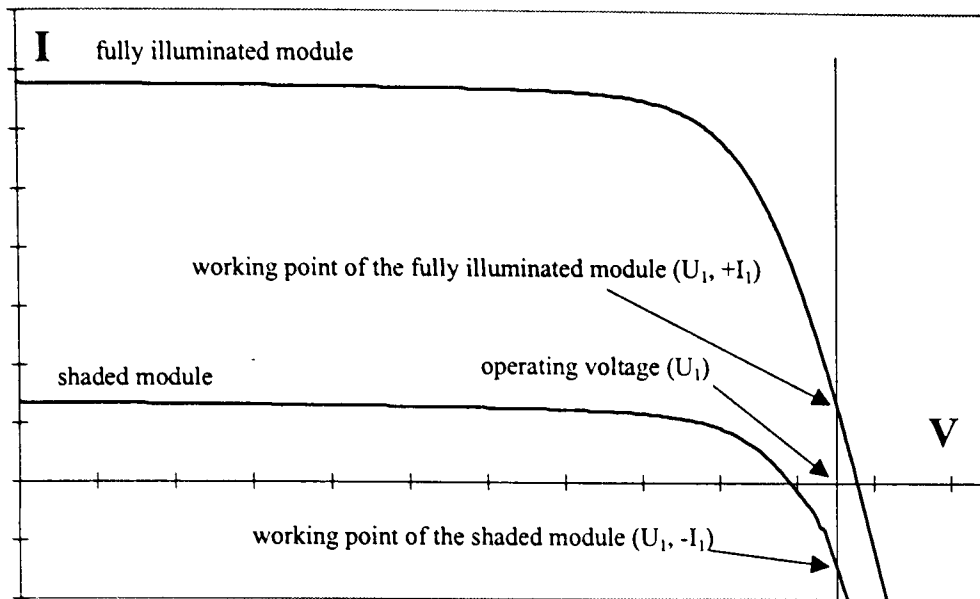


Figure 2.18

A fully illuminated and a shaded string without blocking diodes connected in parallel (same voltage U_1 across both strings). If this array is operated without having a load connected, a reverse current $-I_1$ flows through the shaded module.

In currently applied PV systems, blocking diodes can be neglected in stand-alone systems (Chap. 2.3.1) (because it is integrated the charge controller) and in grid-connected systems with a module or a string inverter (Chap. 2.3.2.2) (because only one ‘string’ is connected in parallel). In grid-connected systems with a central inverter, blocking diodes are generally applied, but attempts have been made to avoid [39] them even in those systems.

2.5.2 Bypass diodes

The function of bypass diodes in reducing shading losses has already been described in Section 2.4.3. They can also help to protect modules from the hot-spot effect caused when two modules in the same string are illuminated differently. When such a string is short-circuited the positive voltage of the fully illuminated module (U_1) is applied inverse across the shaded module ($-U_1$) as shown in Fig. 2.19⁹. A string is short-circuited for example by a shunt charge controller (Chap. 2.3.1.2) to prevent a battery from overcharging. However, this happens not only when a string is short-circuited but also at normal operating voltages such as 12 V in a battery charging system or at the V_{MPP} [42].

When this negative voltage ($-U_1$) is applied across a PV module (without a bypass diode), it operates as a load and is heated by the current (hot-spot). The temperature may destroy the module, but, as noted above, this depends on the number of modules per string, the number of shaded cells, and the irradiance on the shaded module.

⁹ Again, the reverse characteristic of a PV cell is neglected.

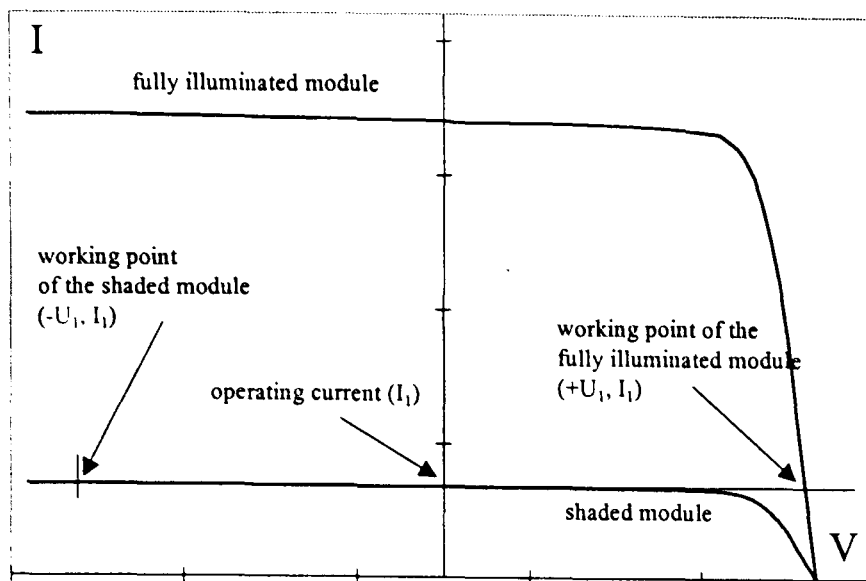


Figure 2.19

A fully illuminated and a shaded module without a blocking diode in one string (same current I_1 through both devices). If this string is short-circuited, a reverse voltage $-U_1$ is applied at the shaded module.

If a PV module has a bypass diode, any reverse current flows through the diode and not through the module. Thus, the module is prevented from becoming a hot-spot, but the diode must be able to carry the total current. Bypass diodes produce hardly any losses during the normal (unshaded) operation of a PV array. Only the diode reverse current is lost, but this is generally very small, e.g., 10 pA for silicon diodes [41]. Thus, standard modules incorporate a bypass diode.

2.6 Designing urban PV systems

As previously said, PV systems in an urban environment are mainly grid-connected systems installed on the roof of a detached house - a detached house because with multiple dwellings, problems with the ownership often occur. Usually, string inverters are applied because then the system consists mainly of PV modules and an inverter. These systems require hardly any designing. The PV array is chosen according to the desires of the client (i.e., the money he will spend or the area of the roof) and then a (string) inverter with a capacity of about 30% lower than the installed PV power (Chap. 2.3.2.1) is used. Since these systems are usually installed on the roof, hardly any shading occurs, or it can be avoided by finding the right location for the PV modules.

The situation is different for PV roof generators on non-domestic buildings. The arrays of these systems are often very extended and partial shading can not always be avoided (e.g., Fig. 2.20 [43] or Fig. 5.19 [44]). Then, these systems require a detailed shading analysis to optimise the array wiring and to generate to maximum power yield. According to the shading and to a cost-benefit analysis, an adequate system configuration of Chap. 2.3.2.2 will be chosen.

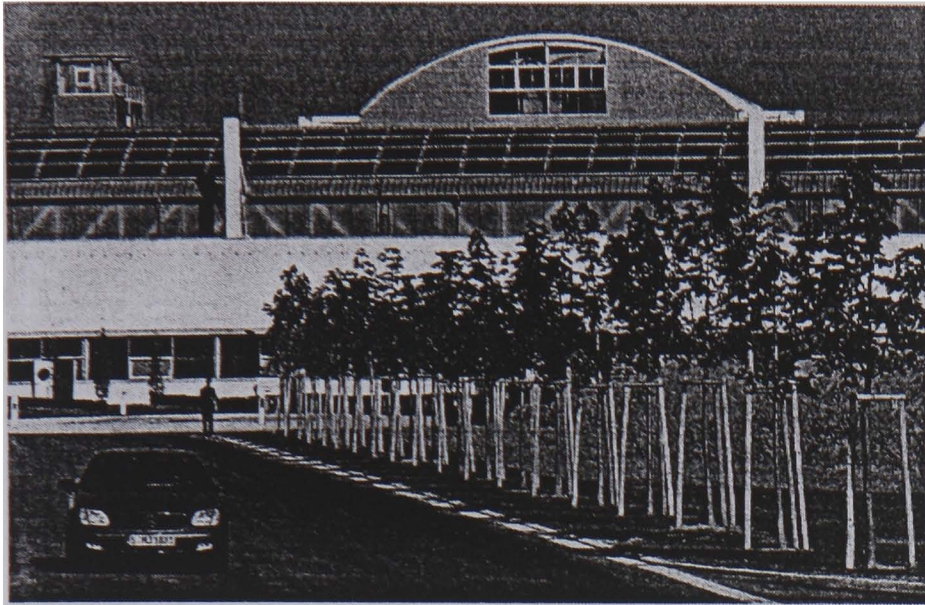


Figure 2.20

Solar generator with an installed power of 435 kWp on the roof of the Daimler-Chrysler factory in Stuttgart, Germany. Partial shading occurs at some hours caused by the roof support (white poles).

The same is valid for a PV generator where the modules are integrated on a facade (Fig. 2.1). In these systems, often shading by neighbouring buildings or by the structure itself cannot be avoided. However, solar facade generators are generally multi-functional. The modules act additionally as facade cladding (e.g. curtain wall facade), as thermal insulation (warm facade) or as shading devices for offices. Then, a cost-benefit analysis of the PV approach alone is not sufficient since the other function(s) must be also taken into consideration.

3 IRRADIANCE AND ILLUMINANCE

All solar energy systems use the irradiation coming from the sun. The input to a system, i.e., the solar irradiation on the receiver plane, is important when the system's yield should be predicted. This requires an accurate modelling of the sun and the sky. However, the irradiation on a receiver plane varies with the fluctuating sky conditions and with the sun position.

The following Section 3.1 will present the fundamental equations for calculating the position of the sun. It is used to model the direct irradiation (that comes directly from the sun) on an arbitrarily oriented solar receiver plane. Different approaches to determine the diffuse irradiation (that comes from the whole sky dome) and the Albedo, the ground reflected irradiance, are introduced in Chap. 3.2. Algorithms to calculate a sky luminance distribution will be introduced in Chap. 3.3. They describe different skies, ranging from overcast to clear sky conditions. The irradiance on a receiver plane can be derived from the irradiance models or the sky luminance models. The latter has the advantage that any objects that are situated between the sky and the receiver can be considered.

Besides the solar irradiance, shading determines the illumination of a sunlit surface. Often shading is desirable, e.g. to prevent buildings from overheating or to control daylighting, but should be minimised to obtain the maximum yield of a solar energy system. Fundamental approaches for considering shading are introduced in Chap. 3.4.

3.1 Solar radiation

Solar radiation is generated by nuclear fusion in which four protons are melted to a stable helium nucleus. During this process, mass is transformed into energy according to the famous law of Einstein.

$$E = m \cdot c^2 \quad (3.1)$$

At present, the sun loses weight at a rate of about 4×10^6 t per second to maintain its luminous power of about 1.2×10^{18} J. However, only a small part of this energy reaches the earth. Different measurements to determine the extraterrestrial irradiance have been carried out with slightly differing results ($\pm 3\%$ of the variation comes from the varying distance between the sun and the earth, Chap. 3.1.1). The current standard according to the World Radiation Centre (WRC) [45] is given by Equ. (3.2).

$$I_0 = 1367 \text{ W/m}^2 \quad (\text{WRC}) \quad (3.2)$$

However, sometimes the earlier value of $I_0 = 1353 \text{ W/m}^2$ according to measurements of the NASA [46] is used.

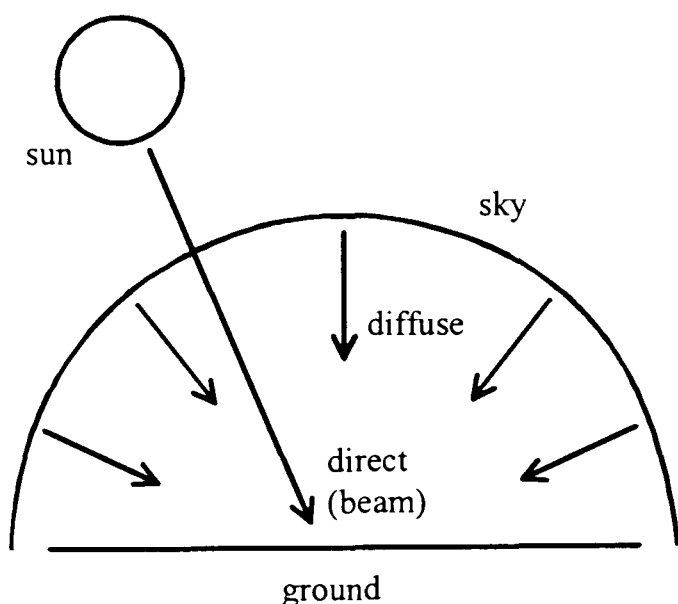


Figure 3.1
Global irradiance on earth

More than 97% of the sun's energy is emitted in the form of short-wave irradiation with a wavelength between 0.28 and $3.0 \mu\text{m}$ [46]. When the sun's rays hit the atmosphere, part is reflected back to space. The rest either passes through directly or is scattered by particles, the so-called Rayleigh, diffuse or Mie scattering [47]. Thus, the total (or *global*) irradiation on the earth is composed of the *direct* (or *beam*) and the *diffuse* irradiation (Figure 3.1). The beam irradiation comes from the direction of the sun but there is no direction related to the diffuse part. It is distributed over the complete hemisphere.

While passing through the atmosphere, the spectral distribution of the sunlight changes significantly. The stratospheric ozone absorbs nearly all irradiation with a wavelength below $0.29 \mu\text{m}$ [48]. Further effects like scattering and H_2O -vapour absorption attenuate

the intensity at longer wavelengths. To compare different solar receivers (e.g. PV modules), some spectral distributions are standardised¹ using the so-called Air Mass [49].

3.1.1 Basics

Our sun is a normal yellow dwarf star that lies near the centre of our galaxy. With a diameter of about 1.4×10^6 km, the sun subtends an angle at the earth of 0.53° . Since its size is more than 100 times that of the earth, all sunbeams arrive nearly parallel. This assumption will be used throughout this thesis.

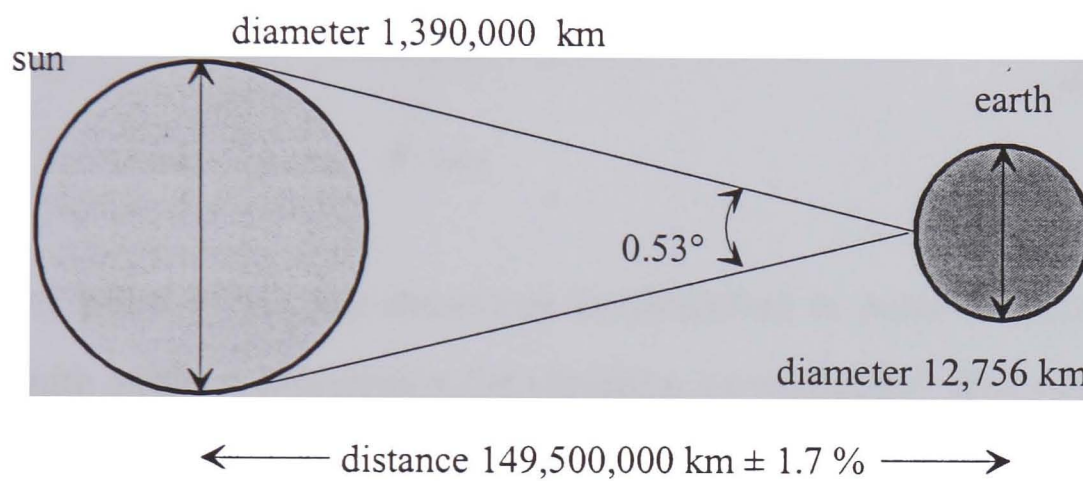


Figure 3.2
*Basic relationship
between the sun and
the earth*

The earth revolves around the sun in 365.26 days on a nearly circular orbit [50]. The distance between them varies during the year but only by about $\pm 1.7\%$ [46]. The standard average distance is called 1 Astronomic Unit (AU).

$$1 \text{ AU} = 1.495 \cdot 10^8 \text{ km} \quad (3.3)$$

Besides its orbit around the sun, the earth revolves around itself with an axis inclined by 23.45° . This inclination has a strong influence on the weather on the earth; it creates the seasons and it causes differences in the length of days in summer and winter.

Nearly all calculations connected with solar systems are based on the position of the sun. Usually, it is given in polar coordinates by the solar azimuth α_s and the solar zenith angle θ_s . In agreement with most definitions given in the literature, 0° will be used for south, angles towards east are counted positive and angles towards west counted negative. Only

¹ To compare solar modules, a standardised spectral distribution Air Mass (AM) of 1.5 is used.

for locations on the globe, the western longitude is positive and the eastern negative. However, sometimes a different terminology is used.

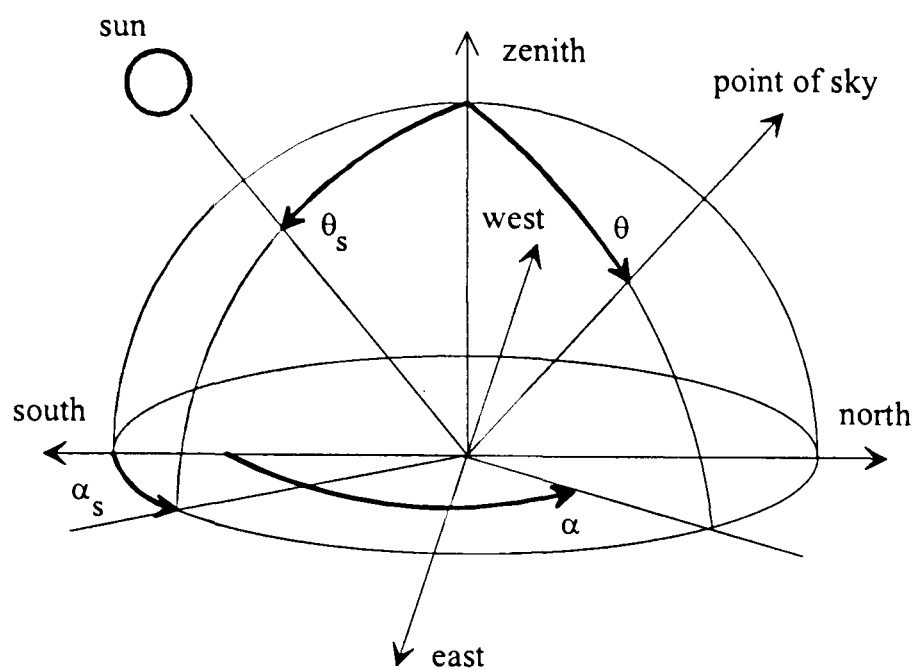


Figure 3.3
*Definition of angles
defining the sun position*

Any point of the sky dome can be described in polar coordinates by the azimuth α and zenith angle θ . Sometimes the elevation ε (or altitude) above the horizon is used instead of the zenith angle. They can be converted into each other by

$$\varepsilon = 90^\circ - \theta . \quad (3.4)$$

3.1.2 Sun position

The sun position is crucial to irradiance calculations. When, for example, the direct normal irradiance is to be converted to direct horizontal irradiance for low solar elevations, small errors in the zenith angle can cause large differences. In the following, the most accurate equations found in the literature are quoted.

The solar azimuth α_s and zenith angle θ_s (Figure 3.3) depends on the local latitude ϕ , the local longitude φ and the time. They can be calculated by a series of equations from the time and the day of the year d_n [47]. The day angle Γ (1st Jan. = 1, 31st Dec. =365 and February always with 28 days) is given by Equ. (3.5).

$$\Gamma = \frac{360}{365}(d_n - 1) \quad (3.5)$$

The solar declination δ (Figure 3.4) describes the tilt of the earth's axis to the orbital plane. It is similar to the elevation angle measured to the sun when seen from the equator at solar noon. Different equations are presented for δ , the one given by Spencer [51] has a maximum error of 0.034° .

$$\delta = \frac{180}{\pi} (0.006918 - 0.399912 \cos(\Gamma) + 0.070257 \sin(\Gamma) - 0.006758 \cos(2\Gamma) + 0.000907 \sin(2\Gamma) - 0.002697 \cos(3\Gamma) + 0.00148 \sin(3\Gamma)) \quad (3.6)$$

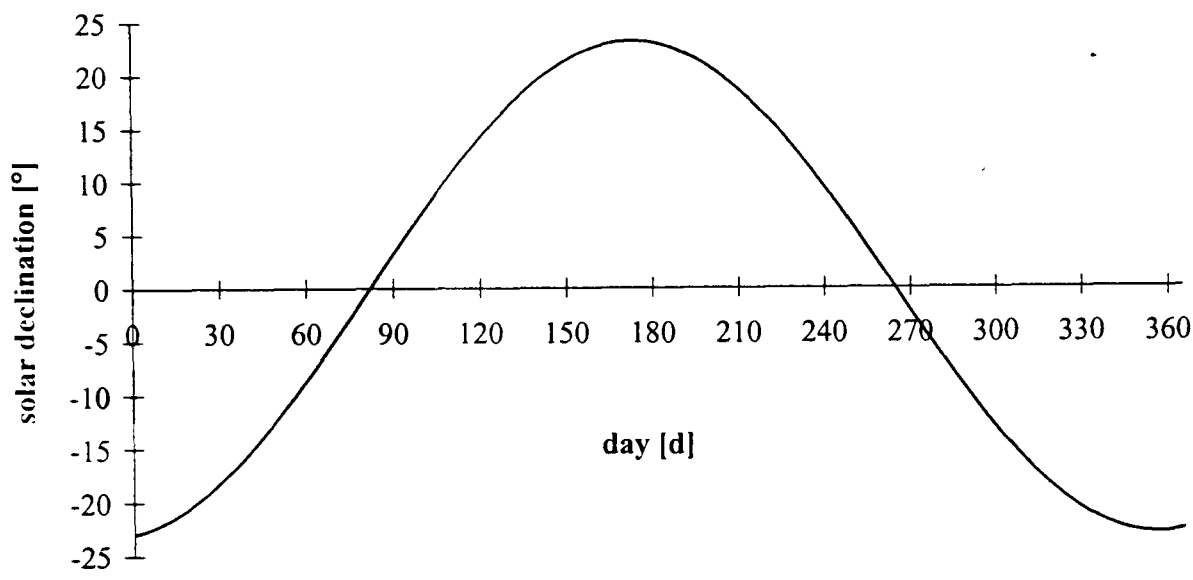


Figure 3.4
Solar
declination

The hour angle ω is measured between the sun meridian at 12:00 and the observer meridian (15° for every hour, 0° for solar noon, morning positive, e.g. 11:00 \equiv 60 min \equiv 15°).

$$\omega = 0.25 (720 - \text{solar time in minutes}) \quad (3.7)$$

The solar zenith angle θ_s (or the solar elevation ε_s) and solar azimuth α_s can be calculated from the above given equations with Equ. (3.8) and (3.9).

$$\cos(\theta_s) = \sin(\varepsilon_s) = \sin(\delta) \sin(\phi) + \cos(\delta) \cos(\phi) \cos(\omega) \quad (3.8)$$

$$\cos(\alpha_s) = \frac{\cos(\theta_s) \sin(\phi) - \sin(\delta)}{\sin(\theta_s) \cos(\phi)} \quad (3.9)$$

for

$$0^\circ \leq \alpha_s \leq 90^\circ$$

$$\cos(\alpha_s) \geq 0$$

$$90^\circ \leq \alpha_s \leq 180^\circ$$

$$\cos(\alpha_s) \leq 0$$

In all these equations time refers to solar time this means it is 12:00 at the highest solar elevation. To convert solar time to local standard time, the equation of time T (in minutes) and the deviation of the local latitude φ to the meridian of the local standard time φ_{St} must be considered [52]. The longitude correction is positive when the local latitude is east of the standard time meridian φ_{St} . The daylight saving time may be added.

$$\text{solar time} = \text{local standard time} + 4 \cdot (\varphi_{St} - \varphi) + T + \text{daylight saving time} \quad (3.10)$$

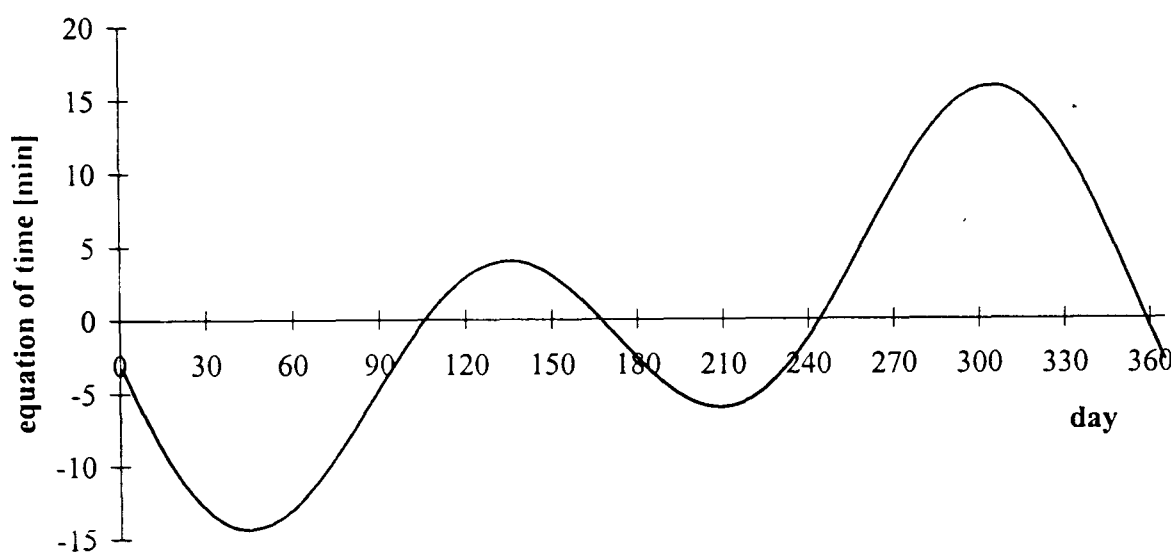


Figure 3.5
Equation of
time

Again different expressions for the equation of time are given. Spencer [51] presented Equ. (3.11) with a maximum error of 0.14 min.

$$T = (0.000075 + 0.001868 \cdot \cos(\Gamma) - 0.032077 \cdot \sin(\Gamma) - 0.014615 \cdot \cos(2\Gamma) - 0.04089 \cdot \sin(2\Gamma)) \cdot 229.18 \quad (3.11)$$

Sun path diagrams (Figure 3.6) can be used to quickly estimate the sun path on any day of the year. They show the polar coordinates of the sun as seen from a specific point. Usually, the sun paths of several days are given, and the paths of further days can be estimated by interpolation. Sun path diagrams also give an impression of the sunset and sunrise times on any day of the year. It should be remembered that they are valid for one location only and usually refer to solar time (highest sun elevation at 12:00).

Sun path diagrams can also be used to determine the hours when the sun, seen from a specific point, is hidden behind surrounding objects [53]. To do this, the angles (in polar coordinates) defining the outline of the shading object must be entered in the diagram. The

time when the point cannot be reached by sunbeams is indicated by the intersection of the sun path with the object (Figure 3.6).

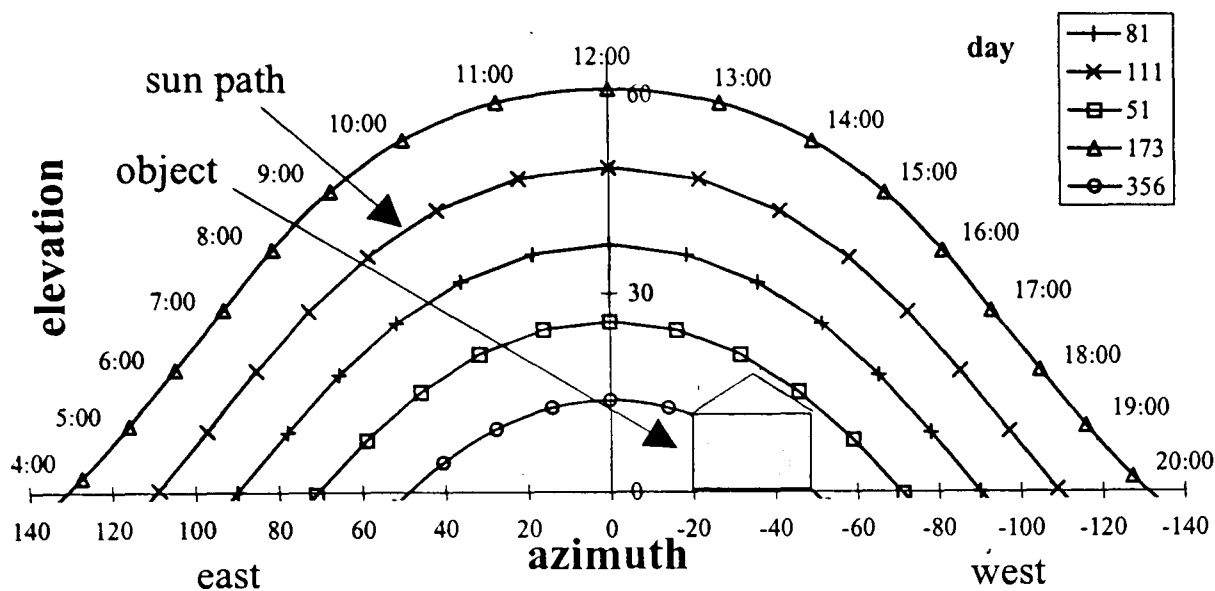


Figure 3.6
Sun path
diagram for
Leicester, UK,
(52.7°N,
1.1°E) given
for solar time

3.2 Irradiance on a tilted surface

To calculate the energy gain from a solar system, the irradiance on the receiver must be known. At the earth's surface the irradiance on a tilted surface comprises three components (Figure 3.7)

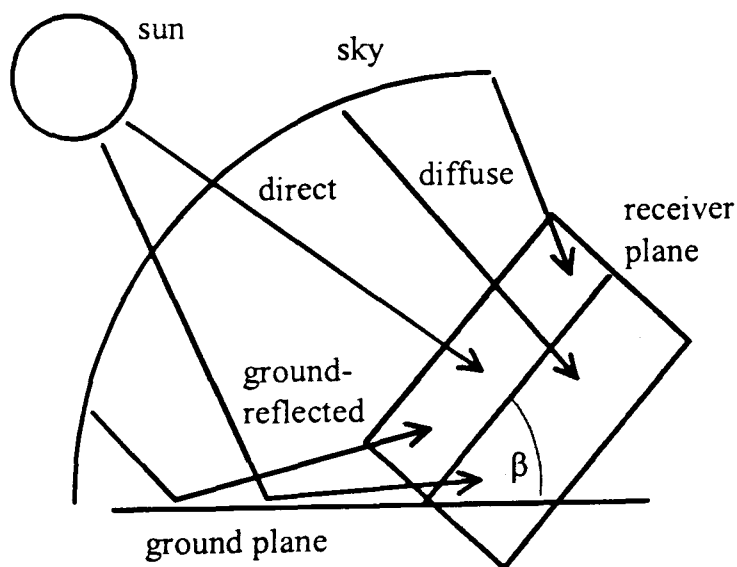


Figure 3.7
Global irradiance on a tilted
receiver plane, composed of
direct, diffuse and ground-
reflected

- the diffuse irradiance from the sky I_d
- the ground-reflected irradiance I_a (subscript a stands for albedo, the reflection coefficient)
- the direct irradiance from the sun (often also called beam irradiance²) I_b

² The expression *beam irradiance* is usually used for the direct irradiation at normal incidence. Here, the subscript b is used for direct irradiance throughout because d is utilised for diffuse irradiance.

If the irradiance is to be calculated, the incidence angle of the sunbeams on the plane must be known. Several different definitions for the angles can be found in the literature, but here the following terms (Figure 3.3 and 3.8) will be used throughout.

All azimuth angles α start from south and are positive in the easterly direction. Zenith angles range between $0^\circ \leq \theta \leq 90^\circ$ because only surfaces facing upwards are considered. The tilt angle of a surface to the horizon is given by β . The angle between a surface normal and the sunbeams, γ_s , can be calculated by, [54],

$$\cos(\gamma_s) = \cos(\beta) \cdot \cos(\theta_s) + \sin(\beta) \cdot \sin(\theta_s) \cdot \cos(\alpha_s - \alpha_t) \quad (3.12)$$

Equation (3.12) also returns the angle between the surface normal and an arbitrary point in the sky, γ_p , if solar azimuth and zenith angles (α_s and θ_s) are replaced by the angles to the point α_p and θ_p .

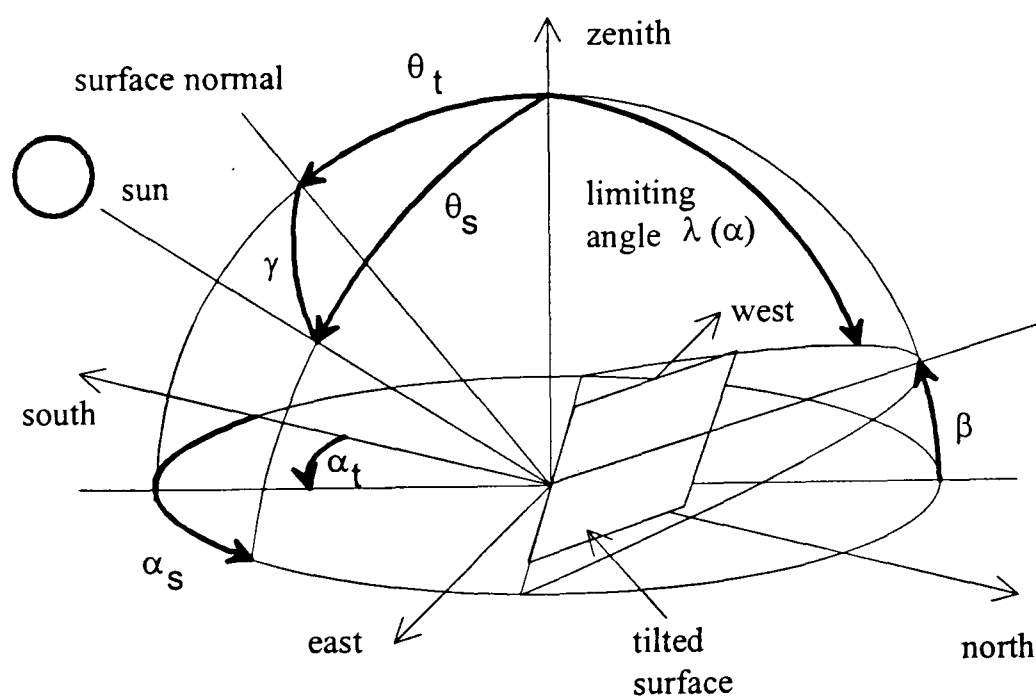


Figure 3.8
Definitions to calculate the incidence angle of sunbeams on a solar receiver

A limiting angle $\lambda(\alpha)$ is defined as the angle from the zenith to an imaginary curve produced by the intersection of an infinite tilted surface with the sky. This line varies with the azimuth and can be computed following [55] by Equ. (3.13).

$$\sin(\lambda(\alpha)) = \sqrt{1 + \tan^2(\theta_t) \cdot \cos^2(\alpha - \alpha_t)} \quad (3.13)$$

for

$$\alpha > \alpha_t + 90^\circ \text{ and } \alpha < \alpha_t - 90^\circ$$

otherwise

$$\lambda(\alpha) = 90^\circ$$

3.2.1 Global irradiance

The global or total irradiance I_g can be either calculated or measured. On a horizontal surface, $I_{g,h}$ can be calculated from the direct horizontal irradiance $I_{b,h}$ and the diffuse horizontal irradiance $I_{d,h}$

$$I_{g,h} = I_{b,h} + I_{d,h} \quad (3.14)$$

To calculate the global irradiance on a tilted surface $I_{g,t}$, the ground-reflected share I_a must be added.

$$I_{g,t} = I_{b,t} + I_{d,t} + I_a \quad (3.15)$$

The global irradiance is measured by a pyranometer (Fig. 3.9). This instrument compares the temperature difference between a black and a white surface. It is important to compensate for changes in the ambient temperature and to protect the surface from wind. Thus, the sensor is usually hidden behind a glass dome. Flat glass covers are not ideal because of the different reflection coefficients at different incidence angles.

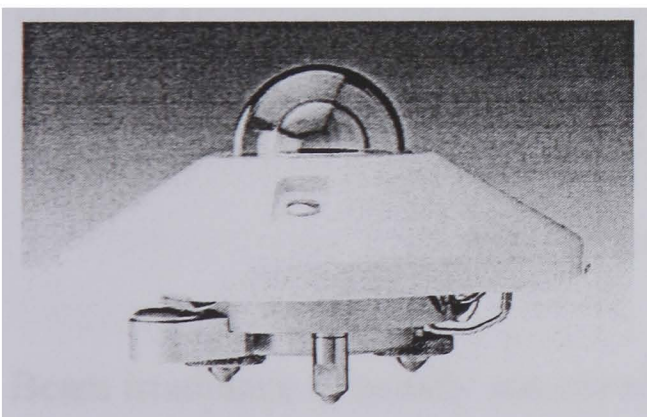


Figure 3.9
Pyranometer (Kipp & Zonen CM 11) to measure the global irradiance

The accuracy of measured values depends on influences such as temperature, non-linearity, bearing mismatch, time response, time mismatch, etc. The following data are typical for an ISO 9060 class 1 pyranometer [56]:

temperature sensitivity	$\pm 2\%$
non-linearity	$< 1.5\%$
bearing mismatch	$< 20 \text{ W/m}^2$ at 1000 W/m^2
tilt error	$< 1.5\%$
time response	$1/e^5 \text{ sec} = 0.006738 \text{ sec.}$

If the high instantaneous accuracy of a pyranometer comparing the black and white surfaces is not required, the global irradiation can be measured with a calibrated solar cell. This instrument is much cheaper, less than £ 150 compared to £ 840 for a class 1 pyranometer (1999). In a comparison from Auer [57], 90% of the measured values of a cell lay within an error of $\pm 4.4\%$ if a period of one month was considered. However, for a measuring period of only one hour, 90% of the values lay in an error interval of $\pm 15\%$. The conclusion is that the calibrated solar cell is suited for long-term measurements of more than one month but not for short periods such as one hour.

3.2.2 Direct irradiance

Climate data files often supply direct horizontal irradiance $I_{b,h}$ or direct normal irradiance $I_{b,n}$ (often referred to as DNI). One can be calculated from the other by using the angle of incidence, e.g. from [47].

$$I_{b,h} = I_{b,n} \cdot \cos(\theta_s) \quad (3.16)$$

Equation (3.17) from [49] can be used to calculate the beam irradiance on a tilted surface $I_{b,t}$ from horizontal values ($I_{b,h}$) or normal values ($I_{b,n}$).

$$I_{b,t} = I_{b,n} \cdot \cos(\gamma_s) = I_{b,h} \frac{\cos(\gamma_s)}{\cos(\theta_s)} \quad (3.17)$$

Beam irradiance is usually measured with a tracked pyrhelimeter (Fig. 3.10) that follows the path of the sun. This instrument is equipped with a tube to measure the solar radiation which has an effective opening angle of 5° ³. Thus, the diffuse radiation from the sky is excluded. The direct horizontal irradiance $I_{b,h}$ can also be obtained by subtracting diffuse horizontal irradiance $I_{d,h}$ from global horizontal irradiance $I_{g,h}$ (Equ. 3.18).

$$I_{b,h} = I_{g,h} - I_{d,h} \quad (3.18)$$

³ This 'wide' angle is chosen to account for mechanical tracking problems.

This is often done because the automated tracking of a pyrheliometer is very expensive (in the range of £ 8000), compared to a shadowband that allows measuring of the diffuse component (about £ 80) for a pyranometer (Section 3.2.3.5).

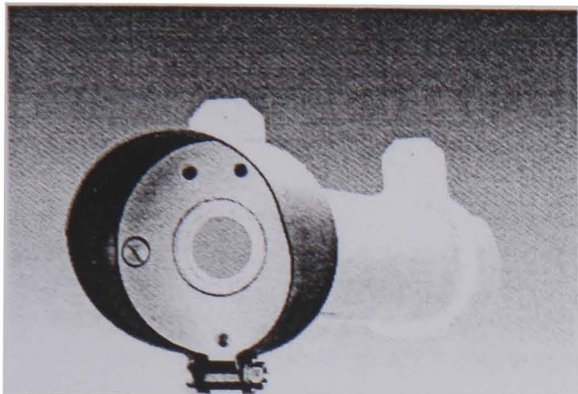


Figure 3.10
Pyrheliometer (Kipp & Zonen CUVB2/CUVA2) to measure the direct normal irradiance

3.2.3 Diffuse irradiance

The diffuse irradiance on a tilted surface $I_{d,t}$ is either measured or calculated from diffuse horizontal irradiance $I_{d,h}$ and a more or less complex scaling factor. For this factor, several tilted surface models have been developed [58, 59, 60, 61, 62]. The related equations describe the part of the sky that is visible to the surface and the brightness of that part. The different models use either an isotropic or an anisotropic radiance distribution.

If the sky radiance distribution $R(\alpha, \theta)$ is a known function from azimuth and zenith angle, the irradiance on a tilted surface can be calculated with Equ. 3.19. The bound of the inner integral is the limiting angle λ (Fig. 3.8).

$$I_{d,t} = \int_0^{2\pi} \int_0^{\lambda} R(\alpha, \theta) \cdot \sin(\theta) \cdot \cos(\gamma) d\theta d\alpha \quad (3.19)$$

3.2.3.1 Liu / Jordan

The simplest sky (radiance distribution) model assumes uniformly (isotropically) distributed sky radiance. This model is often referred to as the Liu / Jordan model, [58], or uniform sky model. Due to its simplicity (it can be used even with pocket calculators) it is widely disseminated and used in many computer simulation programs.

$$I_{d,t} = I_{d,h} \cdot \frac{1 + \cos(\beta)}{2} \quad (3.20)$$

3.2.3.2 Hay

Real skies never have a uniform radiance distribution. Thus, when compared with measurements, the Liu / Jordan model often performs poorly. Real skies have an anisotropic radiance distribution. Usually, they have a bright zone around the sun (circumsolar brightening) and near the horizon (horizon brightening). The model of Hay [59] superimposes a circumsolar zone on the isotropic sky.

$$I_{d,t} = I_{d,h} \cdot \left[\frac{1 + \cos(\beta)}{2} \left(1 - \frac{I_{b,n}}{I_0} \right) + \frac{I_{b,n}}{I_0} \cdot \frac{\cos(\theta_t)}{\cos(\theta_s)} \right] \quad (3.21)$$

3.2.3.3 Klucher

Further models, for example by Klucher [60], superimpose a circumsolar zone and a horizon brightening zone on the uniform sky.

$$I_{d,t} = I_{d,h} \cdot \frac{1 + \cos(\beta)}{2} \cdot \left[1 + (1 - \kappa^2) \sin^3\left(\frac{\beta}{2}\right) \right] \cdot \left[1 + (1 - \kappa^2) \cos^2(\gamma_s) \cdot \sin^3(\theta_s) \right] \quad (3.22)$$

The diffuse fraction κ in Equ. (3.22) is defined as

$$\kappa = \frac{I_{d,h}}{I_{g,h}} \quad (3.23)$$

3.2.3.4 The Perez tilted surface model

Perez et al. introduced [61, 62], a model for irradiance on a tilted surface that has become almost a standard and is used in many simulation programs. The model consists of a geometric description of the sky dome with the superposition of an isotropic sky, a circumsolar component and a horizon zone. These three parts are weighted by empirical coefficients F_1' and F_2' . The complex model presented in [61] had a variance in the opening angle of the circumsolar zone. It was simplified in [62], in which two models were presented, the second one reduces the circumsolar zone to a point and is easier to use. This model has been shown to perform very well by many validation studies, [63, 64].

$$I_{d,t} = I_{d,h} \left[(1 - F_1') \frac{1 + \cos(\beta)}{2} + F_1' \frac{\cos(\theta_t)}{\cos(\theta_s)} + F_2' \cdot \sin(\beta) \right] \quad (3.24)$$

The coefficients F_1' and F_2' depend on the Perez parameters: sky brightness Δ and sky clearness εl (originally only ε but here this symbol is already used in another context). These are given by Equ. (3.25) and (3.26) with θ_s measured in radians.

$$\varepsilon l = \frac{\frac{I_{d,h} + I_{b,n}}{I_{d,h}} + 1.041 \cdot \theta_s^3}{1 + 1.041 \cdot \theta_s^3} \quad (3.25)$$

$$\Delta = \frac{I_{d,h} \cdot m}{I_0} \quad (3.26)$$

Robledo and Soler [65] pointed out that the model's accuracy could be increased when the coefficients were fitted to the site in question or even to the orientation of the receiver plane. The Perez coefficients and some further readings are given in the Section A.1.

3.2.3.5 Measurements

The diffuse horizontal irradiance $I_{d,h}$ is usually measured with a pyranometer, for recording the global irradiance, fitted with a shading device (Fig. 3.11). This is often a shadowring that excludes the direct beams of the sun throughout a day.



Figure 3.11
Pyranometer with a shadowring to measure the diffuse irradiation

The shadowring must be adjusted about every week to ensure that it obliterates the sun at all times. Since the shadowring obstructs the sun and a part of the sky, the measured irradiance must be multiplied by a factor, the so-called shadowring correction [66, 67], to obtain the correct value.

An alternative to using the shadowband would be to shade out the sun by a small circular plate. It must be held at a distance from the sensor by a mounting rod and follow the sun path. If the plate is small enough no correction factor is required. However, this causes adjustment problems and an expensive tracking system is necessary. Diffuse irradiation data may also be obtained by measuring the global horizontal irradiance and subtracting the beam irradiance.

3.2.4 Ground-reflected irradiance

When no measurements are available the ground-reflected irradiance I_a can be calculated by a model. The often used model from Ineichen [68] assumes a constant reflection coefficient (albedo) ρ that depends only on the site.

$$I_a = \rho_{(site)} \cdot I_{g,h} \quad (3.27)$$

Other models, for example Nkemdirim [69, 70], include a dependency on the sun position (Equ. 3.27) where a is a positive factor, ε_s the sun elevation in degree and ρ_0 the albedo at an solar elevation of 90° .

$$\rho = \rho_0 \cdot \exp(a \cdot (90^\circ - \varepsilon_s)) \quad (3.28)$$

Nearly all computer models apply Equ. (3.29) to calculate the ground-reflected irradiance onto a tilted surface. It is computed from the global horizontal irradiance, the reflection coefficient and the tilt angle of the surface [47, 63].

$$I_{a,t} = I_{g,h} \cdot \rho \cdot \frac{1 - \cos(\beta)}{2} \quad (3.29)$$

This equation assumes an infinite ground plane in front of the receiver, no obstacles and a uniform reflection from the plane. Under real conditions this will never be true. However, as investigations from Ineichen et al. [71] show, this model performs very well if the albedo of the site under consideration is known. Often this is not the case and ρ is set to

0.2. A list giving the albedo of different surfaces can be found in Tab. 3.1 according to Quaschnig [3].

surface	albedo	surface	albedo
grass (July, August)	0.25	asphalt	0.15
grass	0.18 ... 0.23	forest	0.05 ... 0.18
dry grass	0.28 ... 0.32	heathen and sand	0.10 ... 0.25
farmland	0.26	water ($\varepsilon_s > 45^\circ$)	0.05
soil	0.17	water ($\varepsilon_s > 30^\circ$)	0.08
gravel	0.18	water ($\varepsilon_s > 20^\circ$)	0.12
concrete, weather-beaten	0.20	water ($\varepsilon_s > 10^\circ$)	0.22
concrete, clean	0.30	fresh snow	0.80 ... 0.90
cement	0.55	old snow	0.45 ... 0.70

Table 3.1 Albedo of different acreage surfaces

If the ground-reflected irradiance should be measured, a normal pyranometer for global irradiance is used that is mounted upside-down (Fig. 3.12). Since the data depend on the reflectivity of the local ground they are valid for a limited area only.

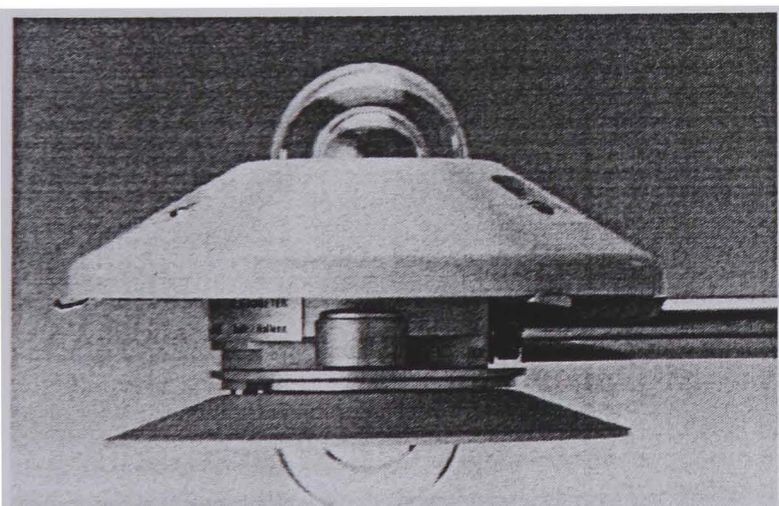


Figure 3.12
Two pyranometers (Kipp & Zonen CM 7B / CM14), one mounted upside-down to measure the ground-reflected irradiance

3.3 Illuminance

In practice it is not easy to distinguish illuminance from irradiance. The latter describes the energy flux in terms of total energy, whereas illuminance refers to the response of the human eye. Each person's eyes responds differently, but, in general, the visible part of the

electro-magnetic spectrum ranges from about 380 to 780 nm, between the ultraviolet (100 ... 400 nm) and the infrared (780 ... 1000 nm) [73].

The importance of light on our lives cannot be overestimated, and much effort is put into designing of the illuminance of rooms and work places. The Daylight Factor (DF) is often used to evaluate the daylighting capabilities of buildings. It compares the outside diffuse illuminance with the indoor illuminance [74]. The basis of calculating the DF is the sky luminance distribution $L(\alpha, \gamma)$ which can be either measured or modelled. Direct sunlight causes unwanted reflections that are usually avoided by blinds or similar devices. Thus, only the diffuse illuminance is taken into consideration for daylighting⁴ purposes (e.g., [74]).

Detailed sky luminance measurements with scanners have been made at more and more sites. A standard was established that specifies 145 measurement points [75], which are more or less equally distributed over the sky dome. The azimuth and altitude of the measurement points are given in Tab. 3.2 [76].

zenith angle of sky element	number of measuring points	azimuth angle between measuring points	solid angle of sky patch [sr]
0°	1	0°	0.0344
12°	6	60°	0.0455
24°	12	30°	0.0445
36°	18	20°	0.0429
48°	24	15°	0.0407
60°	24	15°	0.0474
72°	30	12°	0.0416
84°	30	12°	0.0435

Table 3.2 Coordinates and distribution of sky illuminance measuring points

Illuminance can be converted to irradiance with the luminous efficacy factor K . The German DIN [74] uses a constant factor for overcast skies (Equ. 3.30).

$$K = 115 \frac{lm}{W} \quad (3.30)$$

⁴ Daylighting is the expression for illumination of rooms by natural light.

However, K depends on the spectral luminance distribution and varies for different sites, sun positions and diffuse lighting conditions. Different equations for K are given in [77, 78, 79, 80].

3.3.1 Sky luminance models

At many places horizontal illuminance data integrated over the sky dome are measured. From this data a sky luminance distribution can be modelled. It is remarkable that the sky radiance R and the sky luminance L distribution are very similar [55], but not the skylight or colour distribution. According to the findings of Michalsky [81] some radiance models perform even better for luminance than purely luminance models. Robledo and Soler [65] validated the Perez-point-source model (Chap. 3.2.3.4) with illuminance values measured in Madrid on horizontal and vertical south, east, west and north facing surfaces. The model performed very well, especially with a set of local coefficients.

Different models have been developed to simulate the sky luminance distribution under different sky conditions [74, 77, 82, 83, 84]. Depending on the amount of cloud, they describe a clear, an intermediate, or an overcast sky.

Similar to Equ. (3.19) the illuminance on a tilted surface E_v can be calculated from the sky luminance distribution $L(\alpha, \theta)$.

$$E_v = \int_0^{2\pi} \int_0^\lambda L(\alpha, \theta) \cdot \sin(\theta) \cdot \cos(\gamma) d\theta d\alpha \quad (3.31)$$

3.3.2 Overcast sky

Overcast skies are simpler to model than other sky conditions. They have a relatively homogeneous light distribution (depending of the amount of clouds) and are only slightly brighter at the zenith (overcast zenith brightness: $L_{0,z}$).

3.3.2.1 Uniform sky

The simplest model assumes a constant luminance for the whole sky dome.

$$\frac{L_o(\alpha, \theta)}{L_{o,z}} = 1 \quad (3.32)$$

This formula corresponds via Equ. (3.31) with the tilted surface model for a uniform sky given by Equ. (3.20). However, as discussed for the tilted surface models, in reality even an overcast sky is anisotropic. So, this equation is only a relatively poor description of a real overcast sky.

3.3.2.2 Moon & Spencer overcast sky

A more realistic model that reflects the brighter area at the zenith was developed by Moon & Spencer (Equ. 3.33).

$$\frac{L_o(\alpha, \theta)}{L_{o,z}} = \frac{1 + b \cdot \cos(\theta)}{1 + b} \quad (3.33)$$

This model was accepted by the CIE and the German DIN [74] with a value of $b = 2$ as the ‘CIE standard overcast sky’ (Equ. 3.34).

$$\frac{L_o(\alpha, \theta)}{L_{o,z}} = \frac{1 + 2 \cdot \cos(\theta)}{3} \quad (3.34)$$

This model can be scaled to measured data or, if not available, the zenith luminance $L_{o,z}$ according to Equ. (3.35) can be used. Here, the zenith luminance is only dependent on the solar zenith angle θ_s . This is consistent with the observation that the luminance of heavily overcast skies does not vary with the azimuth angle.

$$L_{o,z} = \frac{9}{7\pi} (300 + 21000 \cdot \cos(\theta_s)) \frac{cd}{m^2} \quad (3.35)$$

Using a data set collected in England, Enarum and Littlefair [85] found that this model performed better than many others, even more recent ones.

3.3.2.3 Perez overcast sky

Perez presented an exponential model for an overcast sky with two modelling coefficients. In a publication from Kittler and Valko [86] they propose to use the values $a = 3.5$ and $b = -0.56$ as standard values.

$$\frac{L_o(\alpha, \theta)}{L_{o,z}} = \frac{1 + a \exp\left(\frac{b}{\cos(\theta)}\right)}{1 + a \cdot \exp(b)} \quad (3.36)$$

3.3.3 Clear sky

Modelling clear sky luminance is more complex than modelling overcast conditions because the brightness varies over the sky dome and depends strongly on the sun's position. Two versions of one model have been established. It should be remembered that only the sky itself is modelled and not the sun. However, the sun is always visible under clear sky conditions.

3.3.3.1 Kittler clear sky

Kittler proposed Equ. (3.37) that became the '*CIE standard clear sky*' [87]. All angles are given in radians.

$$\frac{L_c(\alpha, \theta)}{L_{c,z}} = \frac{\left(1 - \exp\frac{-0.32}{\cos(\theta)}\right) \left(0.91 + 10 \cdot \exp(-3 \cdot \xi) + 0.45 \cdot \cos^2(\xi)\right)}{\left(1 - \exp(-0.32)\right) \cdot \left(0.91 + 10 \cdot \exp(-3 \cdot \theta_s) + 0.45 \cdot \cos^2(\theta_s)\right)} \quad (3.37)$$

$$L_{c,z} = 300 + 3000 \cdot \cot(\theta_s) \frac{cd}{m^2} \quad (3.38)$$

3.3.3.2 Gusev clear sky

For a more polluted sky, a slightly different equation was proposed by Gusev. The German DIN [74] decided to use this model for German conditions. As above, the clear sky zenith luminance $L_{c,z}$ depends only on the sun's position.

$$\frac{L_c(\alpha, \theta)}{L_{c,z}} = \frac{\left(1 - \exp\frac{-0.32}{\cos(\theta)}\right) \left(0.856 + 16 \cdot \exp(-3 \cdot \xi) + 0.3 \cdot \cos^2(\xi)\right)}{\left(1 - \exp(-0.32)\right) \cdot \left(0.856 + 16 \cdot \exp(-3 \cdot \theta_s) + 0.3 \cdot \cos^2(\theta_s)\right)} \quad (3.39)$$

$$L_{c,z} = 900 + 6500 \cdot \cot(\theta_s) \frac{cd}{m^2} \quad (3.40)$$

3.3.4 Intermediate sky

The overcast and clear sky models described above are well suited to evaluating daylight under static conditions. The models can be used to design blinds and artificial lighting inside non-domestic buildings. However, if energy savings due to daylighting are to be calculated, a time-varying simulation is necessary. It must consider the fluctuating sky conditions that never remain purely clear or overcast. To carry out a time-varying simulation, real skies must be modelled either by an intermediate sky model or by a blend of overcast and clear skies.

3.3.4.1 Brunger intermediate sky

Brunger [88] found that real sky radiance distributions depend strongly on the position of the sun, the diffuse fraction, and the clearness index. He presented the following equations [82], which describe the sky luminance (or sky radiance) by an analytical equation dependent on four empirically found coefficients a_i

$$\frac{R(\theta, \alpha)}{I_{d,h}} = \frac{a_0 + a_1 \cdot \cos(\theta) + a_2 \cdot \exp(-a_3 \cdot \xi)}{\pi \left(a_0 + \frac{2}{3} a_1 \right) 2 a_2 F(\theta_s, a_3)} \quad (3.41)$$

$$F(\theta_s, a_3) = \frac{1 + \exp\left(\frac{-\pi \cdot a_3}{3}\right)}{a_3^2 + 4} \left[\pi - \left(1 - \frac{2(1 - \exp(-\pi \cdot a_3))}{\pi a_3 \left(1 + \exp\left(\frac{-\pi \cdot a_3}{2}\right)\right)} \right) \cdot (2\theta_s \sin(\theta_s) - 0.02 \pi \sin(2\theta_s)) \right] \quad (3.42)$$

The coefficients a_i are given in a matrix (Section A.2) and depend on the diffuse fraction κ and the atmospheric clearness index κ_t

$$\kappa = \frac{I_{d,h}}{I_{g,h}} \quad (3.43)$$

$$\kappa_t = \frac{I_{g,h}}{I_{o,h}} \quad (3.44)$$

In a comparison of seven models with records from four sites [89], this model and the Perez ‘All-weather sky model’ performed best.

3.3.4.2 Perez ‘All-weather sky model’

Another intermediate sky model that has attracted much attention is the Perez ‘All-weather sky model’ [84]. It is given as a relative sky luminance $l(\theta, \xi)$ (Equ. 3.45)

$$l(\theta, \xi) = \left(1 + a \cdot \exp\left(\frac{b}{\cos(\theta)}\right) \right) \left(1 + c \exp(d \xi) + e \cdot \cos^2(\xi) \right) \quad (3.45)$$

that can be either scaled to diffuse horizontal irradiance or to the zenith luminance as shown below.

$$\frac{L_{i(\theta, \xi)}}{L_{i,z}} = \frac{l(\theta, \xi)}{l(0, \theta_s)} \quad (3.46)$$

The five coefficients $a - e$ depend on the sky brightness parameter Δ (Equ. 3.26) and the sky clearness parameter εI (Equ. 3.25), which were already introduced for the tilted surface model. They can be calculated by a set of empirically found values (Section A.3). These parameters are the same as used for the tilted surface models. It should be mentioned that for a particular choice of parameter ($a = 1$, $b = -0.32$, $c = 10.989$, $d = -3$, $e = 0.4945$) this model is similar to the CIE standard clear sky (Equ. 3.37). Later, Perez upgraded his model [90] to take real skylight variations due to random cloud patterns into consideration.

3.3.4.3 Matsuura intermediate sky

The intermediate sky model of Matsuura [91] was proposed by the CIE working committee.

$$\frac{L_{i(\theta, \xi)}}{L_{i,z}} = \frac{A(\varepsilon_s, \varepsilon) \cdot \exp\left(\xi \cdot B(\varepsilon_s, \varepsilon)\right)}{A(\varepsilon_s, \pi/2) \cdot \exp\left(\theta_s \cdot B(\varepsilon_s, \pi/2)\right)} \quad (3.47)$$

with

$$A_{(X,Y)} = \frac{1.35(\sin(3.59Y + 0.009) + 2.31) \cdot \sin(2.6X + 0.316) + Y + 4.799}{2.326} \quad (3.48)$$

and

$$B_{(X,Y)} = -0.563((Y + 1.059)(X - 0.008) + 0.812) \quad (3.49)$$

In contrast to the other intermediate sky models (Chap. 3.3.4.1 and 3.3.4.2), this model does not require any empirical parameter. Thus, it is much easier to handle and might be less site-sensitive.

3.3.5 Blend of skies

It is also possible to simulate real skies by using a blend of different sky conditions, i.e., clear L_c and overcast L_o skies. Several models that use a linear blend dependent on the sunshine probability σ , nebulosity index N , or the opaque cloud cover C [77, 92] can be found in the literature. The basic equation for a linear blend based on sunshine probability is given by Equ. (3.50).

$$L_{bl} = \sigma \cdot L_c + (1 - \sigma) \cdot L_o \quad (3.50)$$

Sometimes, the same equation is used with the opaque cloud cover C or the nebulosity index N instead of σ .

The nebulosity index N is dependent on the theoretical cloud ratio CR_t and the ratio η of clear sky luminance to zenith luminance (ε_s in degree).

$$N = \frac{1 - \frac{Ev_{h,d}}{Ev_{h,g}}}{1 - CR_t} \quad (3.51)$$

$$CR_t = \frac{\eta \cdot L_{c,z}}{\eta \cdot L_{c,z} + \frac{125000 \cdot \sin(\varepsilon_s)}{1 + 0.45 \cdot \operatorname{cosec}(\varepsilon_s)}} \quad (3.52)$$

$$\begin{aligned} \eta = & 6.9731 + 0.042496 \cdot \varepsilon_s - 8.5375 \cdot 10^{-4} \cdot \varepsilon_s^2 - 8.6088 \cdot 10^{-5} \cdot \varepsilon_s^3 \\ & + 1.9848 \cdot 10^{-6} \cdot \varepsilon_s^4 - 1.6222 \cdot 10^{-8} \cdot \varepsilon_s^5 + 4.7823 \cdot 10^{-11} \cdot \varepsilon_s^6 \end{aligned} \quad (3.53)$$

3.3.5.1 Harrison sky blend

The blend of a special clear L_C and overcast sky L_O was presented by Harrison [92]. This model uses in Equ. (3.50) the opaque cloud cover C instead of σ .

$$L_O = 0.4 + 0.21 \cdot \theta_s + 0.27 \cos(\theta) + 1.45 e^{-2.4 \xi} \quad (3.54)$$

$$L_C = \left(1.28 + 1.47 \cdot e^{-11.1 \cdot \xi} + 4.28 \cos^2(\xi) \cdot \cos(\theta_s) \right) \left(1 - \exp \frac{-0.42}{\cos(\theta)} \right) \left(1 - \exp \frac{-0.67}{\cos(\theta_s)} \right) \quad (3.55)$$

In a comparisons of Ineichen [89] and Perez [93] no measured data for C could be found, so they used the diffuse fraction κ (Equ. 3.23). However, with this approximation, the model showed poor results.

3.3.5.2 ASRC-CIE sky blend

Perez et al. [93] introduced a model consisting of a linear blend of four skies - Moon & Spencer overcast sky (Equ. 3.33), Kittler clear sky (Equ. 3.37), Gusev clear sky (Equ. 3.39) and Matsuura intermediate sky (Equ. 3.47). These models were blended according to the sky clearness parameter εl (Equ. 3.25) and the sky brightness parameter Δ (Equ. 3.26).

$$\varepsilon l \leq 1.2 \quad L_{bl} = (1 - a) L_{O(Moon)} + a L_{i(Matsuura)} \quad (3.56)$$

$$\text{with} \quad a = \min \left\{ 1, \max \left\{ 0, \frac{\varepsilon l - 1}{0.2}, \frac{\Delta - 0.05}{0.4} \right\} \right\} \quad (3.57)$$

$$1.2 < \varepsilon l < 3 \quad L_{bl} = (1 - b) L_{i(Matsuura)} + b L_{c(Gusev)} \quad (3.58)$$

$$\text{with} \quad b = \frac{\varepsilon l - 1.2}{1.8} \quad (3.59)$$

$$\varepsilon l > 3 \quad L_{bl} = (1 - c) L_{c(Gusev)} + c L_{c(Kittler)} \quad (3.60)$$

$$\text{with} \quad c = \min \left\{ 1, \frac{\varepsilon l - 3}{3} \right\} \quad (3.61)$$

In the comparisons of Littlefair [77], this model and a blend of the CIE overcast and the Gusev clear sky performed best, even better than the Perez ‘All-weather sky model’ which was developed later.

3.4 Shading

Shading has a major influence on the illuminance of a plane that is exposed to sunlight. At windows, particularly of non-domestic buildings, shading is necessary to avoid overheating or reflections at PC monitors. Shading of solar systems however reduces the yield and should be avoided.

When the reduced illuminance of a solar receiver is to be calculated, the shading of the direct and the diffuse irradiance must be distinguished.

3.4.1 Shading of the direct irradiance

The shading of the direct irradiance is usually computed by a geometrical method [72, 94, 95] that uses algorithms to project the shading object on the considered plane, i.e. usually the solar receiver (Fig. 3.13). It is normal to distinguish between far and near shading [94].

Far shading is caused by the horizon (mountains) or by other obstacles far away. It is defined as condition when the sun is not visible from the (complete) plane of a solar receiver. Then the plane is only illuminated by the diffuse irradiation. The occurrence of far shading depends on the sun position.

Near shading is usually caused by the building itself (e.g. overhangs) or by surrounding structures, and affects only a part of the solar receiver. The *near shading factor* as given in Equ. 3.62 is determined by the sun position and changes throughout a day.

$$\text{near shading factor} = \frac{\text{illuminated area of receiver}}{\text{total area of receiver}} \quad (3.62)$$

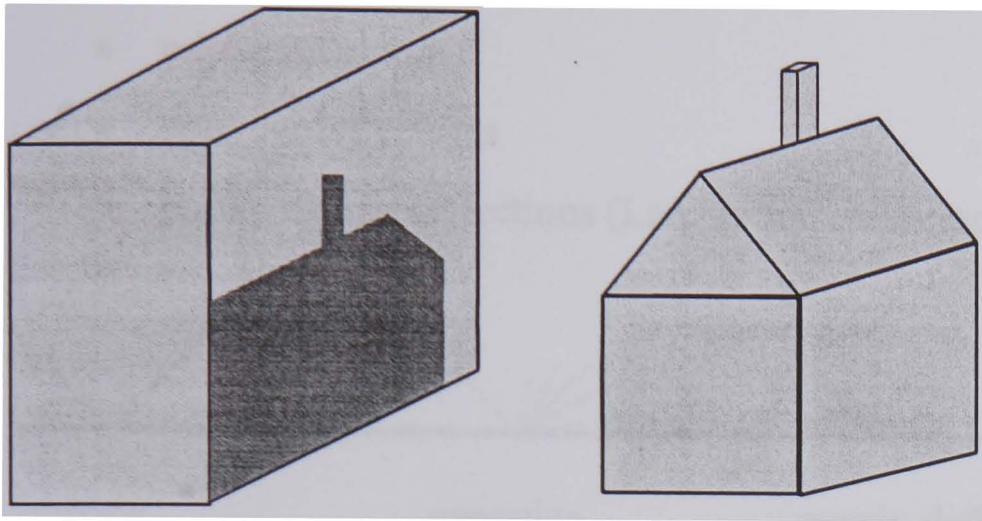


Figure 3.13
Geometrical projection of a shading object

3.4.2 Shading of the diffuse irradiance

When a plane is shaded by an obstacle, not only the direct light is affected but also the diffuse irradiance. This comes from the complete sky dome, but the obstacle may block a part of it. The *view factor* (Equ. 3.63) determines the fraction of the unobstructed sky that is 'seen' by a solar receiver.

$$\text{view factor} = \frac{\text{solid angle of visible sky}}{\text{solid angle of visible sky} + \text{solid angle of obstructed sky}} \quad (3.63)$$

At solar systems with fixed receivers, this factor remains constant throughout the year and does not depend on the sun position. The diffuse irradiation is permanently reduced by this factor. However, a problem of this method is that, strictly speaking, the view factor is valid for one point of the receiver only. At extended receivers, two points situated apart from each other will have different view factors. Another limitation is that this approach assumes a uniform sky distribution that does not represent the real sky, as many validations have showed [55, 89].

3.5 Reflections

Reflections of sunlight from nearby buildings or other surfaces can increase the irradiance on the plane of a solar receiver. The reflection of diffuse solar radiation from the sky vault, may also have an effect, but is probably less important as the irradiation intensity is usually less. The amount of light reflected depends on the materials of which a surface is made and

the way these interacts with light. Three different reflection characteristics can be distinguished:

- mirror reflections
- specular reflections
- purely diffuse reflections (Lambertian reflection)

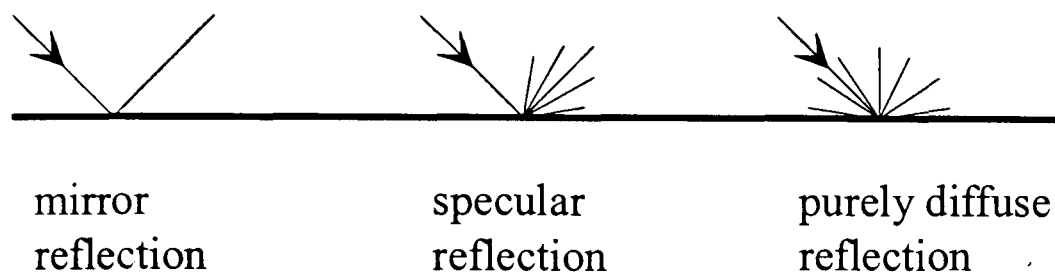


Figure 3.14
Different reflection characteristics

With a mirror reflection, all light rays are reflected with the same angle as the incidence angle. With a purely diffuse reflection light is scattered equally in all directions. The specular reflection is a combination of both.

The reflection coefficient of a surface is given by:

$$\rho = \frac{\text{total incident radiation intensity}}{\text{total reflected radiation intensity}} \quad (3.64)$$

Buildings are largely constructed of opaque materials which are diffuse reflectors. Thus most models of urban irradiance assume such a reflection characteristic. However, the windows are specular reflectors and in extreme cases, buildings can have large areas of (metal) coated glazing and are thus mirror like reflectors.

Usually, surfaces have a reflection coefficient that is independent of the angle of the incident radiation (an extensive list of reflection coefficients of surfaces can be found in the RADIANCE software, Chap. 5.1). However, for dielectric materials like glass or water, the reflectance depends on the angle of the incident radiation.

4 PV MODELLING

The modelling of PV systems has many different aspects, and thus several different modelling methods exist. In research institutes other objectives shall be reached than, for example, in planning offices. The former often use PV models to look at details and to obtain precise data to improve components or the complete system. In planning offices, PV models are usually used to predict the total system yield and for a cost-benefit analysis.

According to the different objectives, different approaches are used to model PV systems. The most relevant ones are introduced in this Chapter. Afterwards, a survey of known PV models follows. Criteria are developed for determining features which have to be implemented in a PV model to be suitable to simulate systems in an urban environment. The surveyed programs are classified according to these criteria.

The irradiation on the PV modules is crucial to the system's performance. Especially if a part of a PV array is shaded by surrounding obstacles. Thus, different models to predict the irradiance on a tilted surface will be introduced as well as some computer programs which address shading. The ray-tracing approach allows modelling of a scene and the computation of the irradiance at arbitrarily chosen trace points considering shading and reflections of the structures within the scene.

An alternative approach to determining the shading losses using a CAD program is introduced at the end of the section.

4.1 Review of PV modelling

System designers often use a computer-based simulation program to predict the yield of a PV generator. A large variety of such programs exist [96, 97] for different purposes. A list of PV models including contact addresses can be found in the Appendix B. According to their applications, the programs have a higher degree of complexity and allow detailed simulation, or they work on a general basis with limited input parameters and limited accuracy.

Tool	static	statistic	time step	block
ASHLING			✓	
INSEL				✓
ITE-BOSS				(1)
PHOTO			✓	
POWACOST		✓		
PV			✓	
PVcad (ISET)			✓	
PV CAD (PV IR)			✓	
PV CALC		✓		
PV DIM			✓	
PVEPO			✓	
PV F-CHART		✓		
PV FORM			✓	
PV ISRAEL			✓	
PV NetSim	(2)			(2)
PV NODE	(1)			
PV SOL			✓	
PVS for Windows			✓	
PVSYST			✓	
PV-TAS			(1)	
SAM	(3)			
SOMES			✓	
TRNSYS				✓
WATSUN PV			✓	

(1) for internal use only, program not freely available

(2) program under development, not ready yet

(3) only single components of PV systems can be simulated

Table 4.1 Classification of known PV simulation programs

By extending the classification in [97] the computer tools can be divided into four categories: programs for a static network analysis, a statistical evaluation, a time-step

analysis and block-oriented programs. Table 4.1 presents an overview of known PV models classified according to the different approaches. These will be introduced in the following sections.

4.1.1 Static electrical network analysis

Programs that carry out a static simulation are derived from electrical network models and compute the actual working conditions of a PV system rather than making long-term yield predictions. The input of such programs is the specific wiring and the electrical components of the PV generator. In older programs this is done with a text editor (e.g., PV node [42]). More recent programs allow graphically supported input (e.g., PV NetSim [98] that uses the network analyser PSpice [99] and SCHEMATICS [100]).

Usually the user can choose between predefined components such as PV cells, protective diodes, resistors, etc. The characteristic equations of these devices (e.g. the current of a PV module according to Equ. 2.1) are defined in the program. Several parameters, for example the irradiance and the temperature of PV modules, can be varied to study their effects and different working conditions.

In the example of Fig. 4.1 a (blocking) diode between node 1 and node 2, a PV cell between node 2 and node 3, a bypass diode between node 2 and node 3, and so on, must be entered. Then an electrical network analysis is carried out. During the analysis a system of equations is built. It is assured that the sum of all currents flowing into one electrical node is zero and that the sum of all voltages in one closed mesh is also zero (Kirchhoff's laws [21]). Here, the direction of the current and the voltage must be considered. It is conventional to assume that the current towards a node and the voltage anticlockwise in a mesh is positive. An example for Fig. 4.1 would be:

$$\text{node 2: } I_1 + (-I_2) + (-I_3) = 0 \quad (4.1)$$

$$\text{node 3: } I_2 + I_3 + I_4 + I_5 = 0 \quad (4.2)$$

$$\text{mesh 1-2-3-0: } V_{12} + V_{23} + V_{30} + (-V_{10}) = 0 \quad (4.3)$$

By choosing $V_{10} = 0$, the short circuit current $I_{1,sc}$ is calculated, and by choosing $I_1 = 0$, the open circuit voltage $V_{10,oc}$ is computed. To obtain the I-V curve in the range where it is normally used, the voltage V_{10} must be gradually increased from 0 ... V_{oc} .

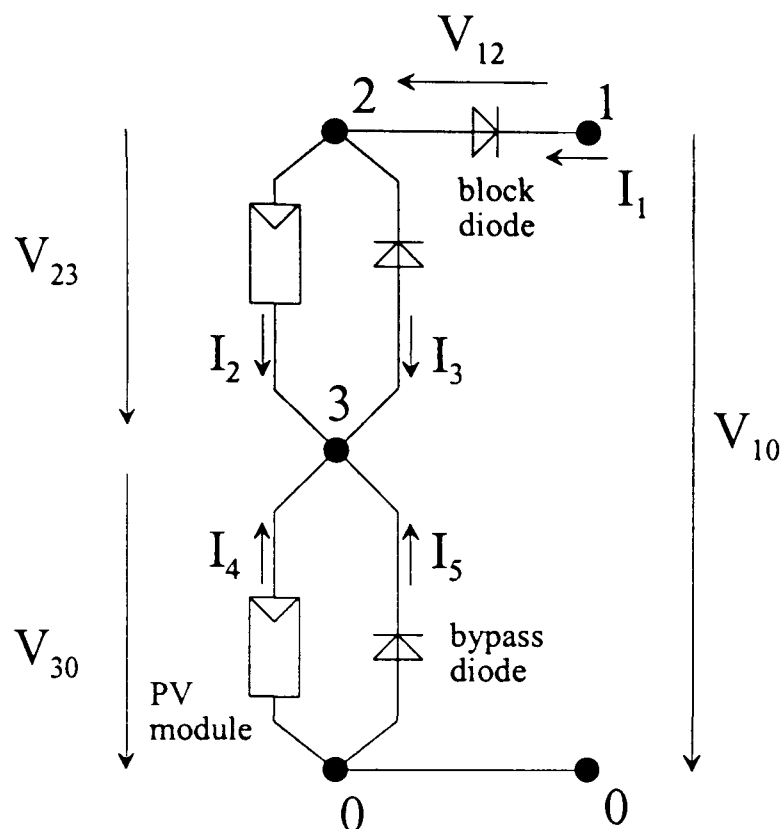


Figure 4.2
Typical PV network

If the circuit is modelled with electrical components, this can be done by inserting a virtual voltage source between the nodes 1-0 or by inserting a resistor at the same place whose value changes from 0 to ∞ . The maximum power point (MPP), the point where a PV array yields the maximum power, can be derived from the I-V curve.

In principal the programs of this category are able to fulfil the task of simulating PV systems with an inhomogeneous solar irradiance distribution. Their limitations are that they are designed to carry out a static electrical network analysis rather than to calculate the long-term yield of a complete PV system. To meet this aim, the programs should have a simple option to rerun them for each time step (this is implemented in PV NetSim). Further, a way must be found to include an inverter in the simulation. This is not yet done in PV node. A problem might be that inverters are usually described by their characteristic power equation (Equ. 2.3). To use them for a static network analysis, MPP tracking must be included and the power curve must be expressed in terms of current and voltage.

4.1.2 Statistical evaluation

Programs that work on a statistical basis do not use a series of irradiation data for their calculations. The aim of these programs is either to suggest quickly the design of a solar system from a few input parameters or to determine quickly the annual yield of a grid-feeding PV generator. Often only average irradiation data are used or even only the month with the lowest irradiation.

These programs calculate the yield of grid-connected systems by reference to systems that have been monitored over a period of time. Their yields are documented (e.g. [101]) and the programs assume that similar systems will perform in the same way. However, site-dependent influences such as shading cannot be taken into account.

If PV stand-alone systems are to be simulated, the output of the programs is often a system design that will supply enough energy to a consumer. Another typical output (mainly for grid-connected systems) is the monthly or annual yield or the fraction of the total energy demand that is covered by the solar yield. Programs of this category are limited to standard system configuration but, due to restricted input parameters, are easy to use.

4.1.3 Time-step analysis

Models of this category work with a constant time step, often one hour, to simulate a more or less complex PV system. Usually, global horizontal (and/or direct normal) irradiance data are used as input. These data are provided, for example, by files in the TMY (Typical Meteorological Year) or TRY (Test Reference Year) [102] format and exist for many stations in Europe and America.

The systems are classified into: stand-alone systems, hybrid systems (e.g. solar and diesel generator), grid-connected systems, PV pumping systems, etc.

In contrast to Section 4.1.1, programs in this category calculate the energy flow rather than accurate working conditions. By changing the parameters the user can follow-up the resulting system behaviour. As an example, the following equations show how the yield of

a solar module is calculated without temperature effect (Equ. 4.4) and with temperature effect (Equ. 4.5).

$$P_{out} = P_{nom} \frac{I_{glob}}{1000 \frac{W}{m^2}} \quad (4.4)$$

$$P_{out} = P_{nom} \frac{I_{glob}}{1000 \frac{W}{m^2}} (1 + t_k \cdot \Delta T) \quad (4.5)$$

P_{out} power of the solar module [W]

P_{nom} nominal power of a solar module at standard test conditions (STC) [W_p]

($I = 1000 \text{ W/m}^2$, $T_{cell} = 25^\circ\text{C}$, spectral solar irradiance distribution: AM 1.5)

I_{glob} solar irradiance in the plane of the array [W/m^2]

t_k temperature coefficient [1/K]

ΔT temperature difference between actual cell temperature and the nominal cell temperature of 25°C [K]

If several modules are connected together, the resulting power is simply multiplied by the number of modules. For a simple stand-alone system comprising only loads, a battery, and a module, the energy flow is calculated according Equ. 4.6.

$$P_{PV} = P_{Load} + P_{Battery} + P_{losses} \quad (4.6)$$

Programs of this category are well suited for a detailed simulation of standard solar systems. Depending on the parameters and the input data, they can predict the yield of a given system with high accuracy. The output is often relatively extensive and ranges from current flow or voltage variations to the monetary pay-back period, as short-time or annual values. Recent programs even consider losses due to shading of the PV modules, different orientations of single PV sub-arrays, and some are able to generate hourly irradiation data for the specific site from monthly mean values [94, 103].

The limitation of these programs is their lack of flexibility. They are restricted to predefined system categories that are determined within the software and cannot simulate any arbitrary system configuration. If, for example, the program allows the user to consider

only two different orientations of the PV modules, it is impossible to model a curved PV array with several different orientations. A typical program of this category is PVcad [103] or PVSYST [94].

4.1.4 Block-oriented programs

Block-oriented programs are a mix between a computer programming language and a simulation program. A solar system is described by special language elements, so-called blocks. The user can build up a solar system by linking several blocks together. Always any one input must be linked to only one output but one output may be linked to several inputs.

In contrast to computer programming languages such as C or PASCAL, the keywords of block-oriented programs do not refer to commands but to predefined blocks. The blocks describe different system components or additional functions. For example, a *solar module* block calculates the PV power output using the solar irradiation on the module as input. A *solar irradiation processor* block would calculate the irradiance on a tilted surface from horizontal values.

Within such programs, a solar system can be modelled using the blocks without formulating the specific mathematical algorithm. There are hardly any restrictions to the number of blocks of which a modelled system may consist. Usually, the only limitation is the computer memory. The same block can be reused several times in one circuit. This offers the opportunity to simulate virtually any solar system, and only the kind of predefined blocks limit the complexity of the system. However, most block-oriented programs offer a large number of blocks, e.g., INSEL [104] more than 100. Further, INSEL, and most block-oriented programs offer the opportunity to write user-defined blocks to model new components.

Block-oriented programs are very flexible with regard to the system configuration and output data they permit. They are able to compute the I-V curve of a specific PV array wiring as well as the annual yield of a complete system. With block-oriented programs, usually all standard systems can be modelled using a time-step approach (Chap. 4.1.3).

Further, it is possible to set up a configuration to execute a statistical simulation (Chap. 4.1.2). An electrical network analysis (Chap. 4.1.1) can also be executed (with some small limitations) but the input is not given in the form of an electrical circuit diagram but as a block diagram. Thus, block-oriented programs can usually solve all tasks described in the preceding chapters.

4.2 Modelling PV systems in an urban environment

In this section the different PV models will be considered for their use in simulating PV systems in an urban environment. Firstly, selection criteria are developed, and then the models are compared with these criteria.

4.2.1 Criteria

The common characteristic of PV systems in an urban environment is that they are grid-connected (specially in European countries), and other structures are built around the solar generator. Until recently, most grid-connected PV systems are installed on a either flat or tilted roof of a building. There, the PV arrays are rarely shaded, if at all. However, nowadays solar facade generators (Fig. 2.1) are attractive to many architects. The problems of facades are that they are often partly shaded, especially in an urban environment. Further to shading, reflections of sunbeams may light up a certain area of a facade. If then a PV array is mounted on the facade, it is inhomogeneously illuminated (at least at some hours of a day). As described in Chap. 2.4, this leads to losses that should be minimised. A model for PV systems in an urban environment should be able to consider the inhomogeneous illumination by calculating with a separate irradiance for each module. The different irradiance values can be either generated by an implemented shading generator or read from an external file. Then the data must be created with a separate irradiance pre-processor.

Accurate yield predictions help a system designer to minimise losses caused by an inhomogeneous illumination of a PV array. Further, they may help an architect to find an optimised solar design right from the first draft of a building.

	price (1)	program available	grid-connected systems	yield predictions	solar module library	inverter library	WINDOWS supported	inhomogeneous irradiance	shading generator	import of CAD models
ASHLING		✓	✓	✓	✓	✓	✓	-	-	-
INSEL	DM 500.-	✓	✓	✓	✓	✓	✓	✓	-	-
ITE-BOSS		-	✓	✓	(4)	(4)	-	(4)	(4)	-
PHOTO		✓	✓	✓	-	-	-	-	-	-
POWACOST		✓	✓	✓	-	-	-	-	-	-
PV		-	✓	✓	-	-	-	-	-	-
PVcad (ISET)	50,- (2)	✓	✓	✓	✓	✓	✓	✓	✓	✓
PV CAD (PV IR)		✓	✓	✓	✓	-	-	-	-	-
PV CALC		✓	✓	✓	✓	-	✓	-	-	-
PV DIM		-	✓	✓	-	-	-	-	-	-
PVEPO	(2)	✓	✓	✓	✓	✓	-	✓	-	-
PV F-CHART		✓	✓	✓	✓	✓	✓	-	-	-
PV FORM		✓	✓	✓	-	-	-	-	-	-
PV ISRAEL		✓	✓	✓	-	-	-	-	-	-
PV NetSim		(3)	✓	✓	✓	✓	✓	✓	-	-
PV NODE		-	-	-	✓	-	-	✓	✓	-
PV SOL	DM 550.-	✓	-	✓	✓	✓	✓	-	-	-
PVS for Windows	DM 890.-	✓	✓	✓	✓	✓	✓	-	-	-
PVSYST	CHF 400.-	✓	✓	✓	✓	✓	✓	-	✓	-
PV-TAS		-	✓	✓	(4)	(4)	✓	-	-	-
SAM	DM 99,-	✓	-	-	✓	✓	✓	(✓)	-	-
SOMES	DFL 250.-	✓	✓	✓	-	-	✓	-	-	-
TRNSYS	US\$ 2000.-	✓	✓	✓	-	-	-	✓	-	-
WATSUN PV		✓	✓	✓	✓	✓	✓	-	-	-

(1) Prices from 1998

(2) freely available in the Internet

(3) under development

(4) not known

Table 4.2 Features of PV simulation programs

To be suitable for modelling PV systems in an urban environment the following criteria are important.

1. Simulation of grid-connected PV systems.

2. Prediction of the yield for a certain time period.
3. The option to import pre-calculated irradiance data (one value per module) or a built-in shading generator (this requires the use of short-time irradiance data).

Other features that make a program easy to use are:

4. A library to select standard PV modules.
5. A library to select standard inverters.
6. Operation on a PC using WINDOWS.
7. If the program uses a built-in shading generator it should offer the possibility to import external created CAD models of houses or city districts.

It is also important that:

8. The program is available and not written for internal use only.
9. The price of the program does not exceed the budget.

The reviewed programs are listed in Tab. 4.2 with respect to these items. Criteria that prevent the program from simulating systems in an urban environment are a '-' in one of the categories: '*program available*', '*grid-connected*' or '*yield predictions*'. Further, the program must be either able to import a pre-calculated inhomogeneous irradiance distribution ('*inhomogeneous irradiance*') or must have '*shading generator*'. A '-' in both categories leads also to an exclusion of the program. It must be mentioned that the programs given in Tab. 4.2 are not able to process CAD models (except PVcad) and that the TRNSYS [52] types for PV systems are very limited.

From the criteria, the discussion of the fundamental approaches and the above-given items it can be said that:

- Programs working on statistical basis (POWACOST, PV CACL, PV F-CHART) are not able to fulfil the task of simulating PV systems in an urban environment because they cannot take site-dependent influences into account.
- TRNSYS can be used in principle but it is not recommended because of the missing special PV blocks. INSEL works very similarly (also block-oriented) and is preferable because of its larger capabilities in modelling PV systems and its useful graphic interface.

- Programs of the category ‘static network analysis’ could be used in principle but they are either under development (PV NetSim), or are for internal use only (PV NODE).

The other models that are in principle able to simulate PV systems in an urban environment are INSEL, PVcad, PVEPO, and PVSYST. With the restriction that INSEL requires pre-calculated irradiance values since it does not own a shading processor. These programs will be discussed in the following sections.

4.2.2 INSEL

INSEL is computer program for an interactive simulation of renewable electrical energy supply systems [104]. It is a block-oriented program, specially written to simulate PV and further electrical energy systems. Because of its block structure, nearly any system configuration can be modelled. However, INSEL is complex and requires a certain level of training to be used effectively, and the system of interest must be known well.

block	category	description
GH2GT	solar irradiation	calculates the irradiation on a tilted surface from horizontal values
PVI	photovoltaic	returns the current of a PV module
BTU	storages	calculates the output voltage of a battery
HOY	clocks and time conversions	calculates the hour of the year
AND	logical relations	checks whether two inputs are both equal to one
CONST	mathematics	returns a constant value
ABS	mathematics	returns the absolute value of the input signal
DO	program flow	a counter with start, stop and step
PLOT	output	to plot graphical results on the screen
READ	file handling	reads up to hundred values from a file

Table 4.3 A selection and categorisation of different blocks of INSEL

INSEL is built up from different blocks. A small selection of more than one hundred available blocks is given in Tab. 4.3. Further blocks for wind turbines, pumps, diesel generators, etc. exist, but here only the capabilities to model PV systems are of interest.

The blocks contain a mathematical description or function of the modelled component. In contrast to the network analysis of Chap. 4.1.1 where only $I(V)$ equations are allowed, the blocks may have any physical value as input, for example the DC power. The user has to take care that the required value is available. The blocks usually require special input data and return output values according to their implemented function and to the specified parameters. There is only a small difference between *inputs* and *parameters*. Usually, *inputs* vary during a simulation (for example the irradiance on a PV module) whereas parameters are fixed values (for example the size of the PV module).

The modelled system is described in a plain ASCII file. This can be created with a text editor, but this is somewhat awkward. To make the program more user-friendly, the last INSEL release 5.02 includes a graphical interface (HP-VEE). It allows menu-driven selection of different blocks and graphically aided linking of the inputs and outputs. An example to model and plot the I-V curve of a PV module at an irradiance of 1000 W/m^2 is given in Fig. 4.2. Whereas outputs can generally be left unconnected, it depends on the specific block whether all or only some inputs require data from preceding blocks.

INSEL offers a good opportunity to simulate simple and complex PV systems. It is possible to model virtually any system configuration. The implemented blocks offer the opportunity to read hourly irradiance values from an external file or to generate the hourly data from monthly mean values. The converter GH2GT allows to calculate the irradiance on a tilted surface from horizontal values using one often different models, e.g., Liu-Jordan (Equ. 3.20), Hay (Equ. 3.21), Klucher (Equ. 3.22), Perez (Equ. 3.24), etc.

Unfortunately, there is no block available that considers shading. This reduces the capabilities of INSEL to predict the yields of PV systems in an urban environment. A block that would allow modelling of structures and calculating the reduced irradiance at certain points where the PV modules should be placed would be necessary. Since such a block is not implemented yet, the irradiance on the PV modules in an urban environment

(considering shading) must be calculated with an external program and read with the INSEL data reader. Then it is possible to simulate an inhomogeneously illuminated PV system and assign a separate irradiance to each module. However, to calculate the long-term yield of such a system is difficult if it comprises more than one string per inverter. For one string, the implemented blocks enable a direct computation of the yield. If several strings are to be connected to one inverter only the I-V curves (a list of numerical values for each hour that should be simulated) can be calculated with INSEL, but the related maximum power points (MPP) must be determined by an external program. These can be re-entered to INSEL to determine the system yield.

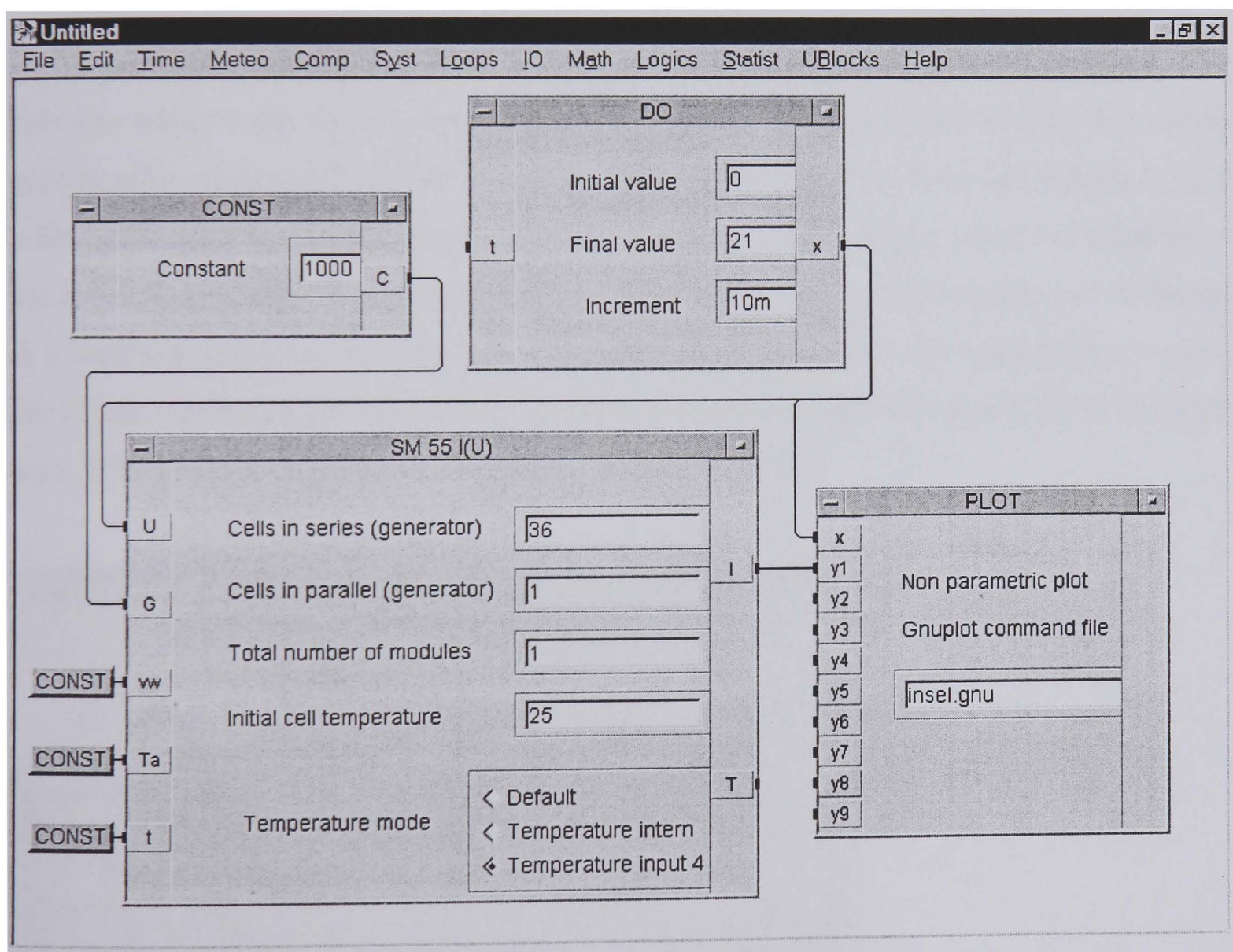


Figure 4.2 INSEL input to model and plot the I-V curve of a PV module at an irradiance of 1000 W/m^2

Thus, INSEL is well suited to modelling PV systems in an urban environment if the system consists of one string only and if an irradiance pre-processor is used. However, it requires accurate knowledge of the modelled system and the input of extensive PV systems will be

somewhat awkward. At installations with more than one string per inverter it is somewhat complicated to use INSEL to determine the long-term yield of a PV system.

4.2.3 PVcad (ISET)

PVcad [105] (two programs with this name are listed in Tab. 4.1 but here, the one written by the ISET Institute is referred to) is a recently developed model to simulate and design PV facades. It works on a time-step basis but offers nearly the same modelling flexibility as block-oriented programs. Its main advantage is that shading of the PV generator from surrounding structures can be considered.

First the program requires information about the location of the planned PV generator. The user can select a site from a very extensive database. Then, if available, the user has to specify a file with hourly irradiance data (global horizontal and diffuse horizontal). If such a file is not available it can be generated from monthly mean values, which are supplied in the attached database. The generated file is saved (with *.sct extension) and can be reused in a later simulation or for other purposes. Further, PVcad offers the opportunity to use a file of pre-calculated irradiance data, where one value is stored for each module and each hour. If this option is used, the site specification is neglected.

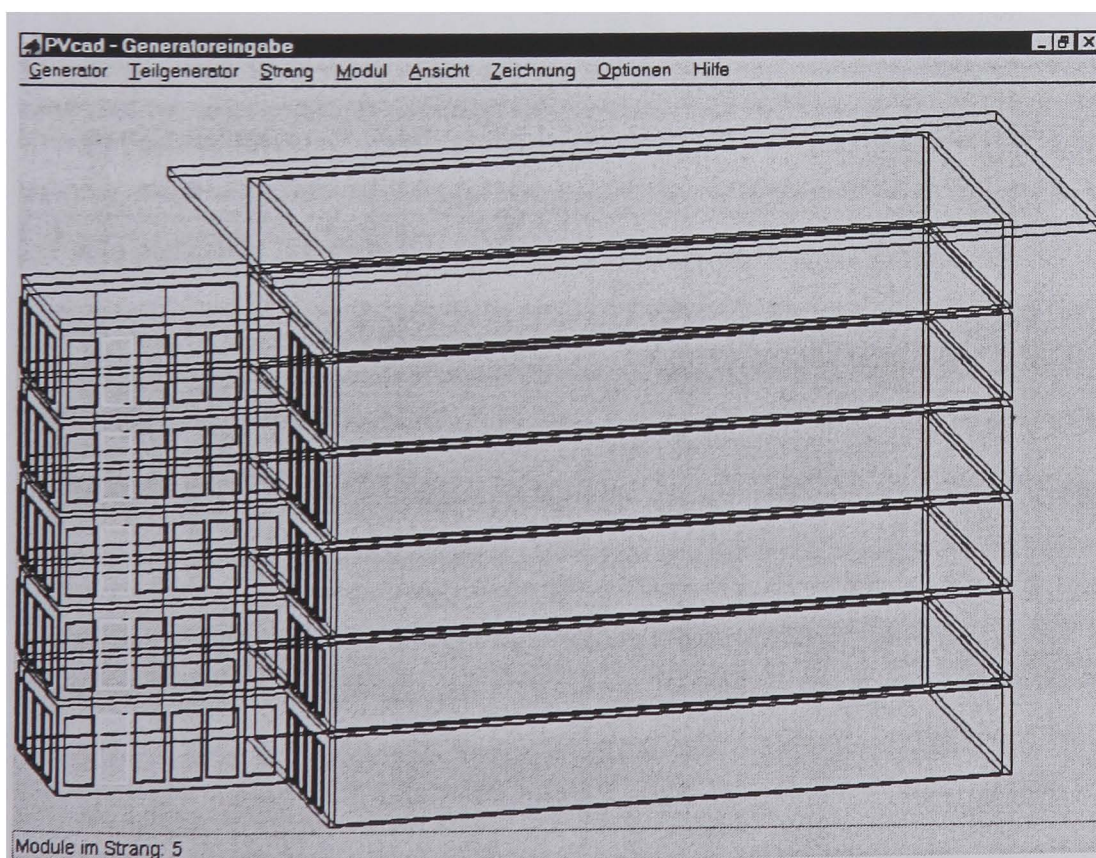


Figure 4.3
Graphical interface of
PVcad to enter the PV
generator

In the second step, the site is specified. It includes the building, the PV generator, and the surrounding structures. They have to be modelled with a 3D-CAD program (usually AutoCAD) and saved in the DXF format. Walls and solid building elements must be assigned to a different layer than the PV array to be distinguished from each other. Each PV module must be entered as a separate rectangle to enable correct wiring. PVcad converts the DXF file to a *.egb file, where all geometrical information about the building, surrounding structures and the PV array are stored.

The third step is to specify the PV generator. In a graphical interface (Fig. 4.3), the building and the PV modules are displayed in different colours. The user can link several modules to one string by clicking on the related square. Then the module type can be selected from an extensive database. One or several strings are linked to an inverter that can be also selected from a large database. Finally, the information about the PV generator must be stored in a *.gen file.

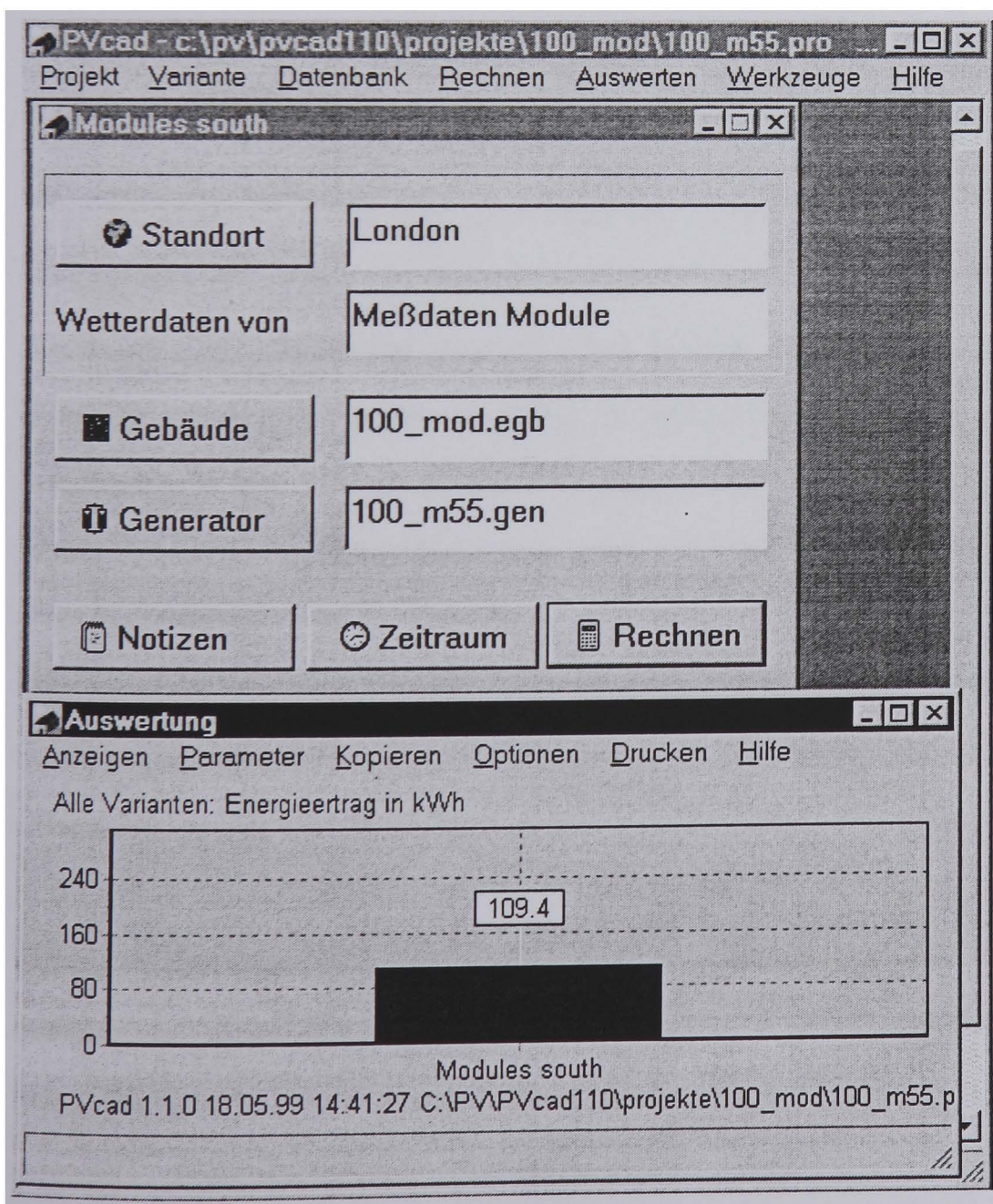


Figure 4.4
PVcad, a tool to simulate PV generators

If the above-described entries are made, the user can specify a time interval and start the simulation. After completion, the results can be displayed either as text output or as a diagram. A limitation of PVcad is that only one value, the final yield of PV generator, is displayed. Fig. 4.4 shows typical entries and the result of a simulation with PVcad.

PVcad is a very good tool for simulating PV generators in an urban environment. In particular the opportunity to generate irradiance data from a database should be mentioned as well as the option to select PV modules and inverters from an extensive database. Thus, the problem of obtaining this data can be neglected and simplifies the work significantly.

The opportunity to model the structures and the PV generator with a CAD program and to take shading into account is a unique feature, not achieved by other programs. However, working with a 3D-CAD program requires some experience and might be a hindrance for a new user. The opportunity to import pre-calculated irradiance values makes it ideal to couple PVcad to other irradiance pre-processors.

4.2.4 PVEPO

The program PVEPO [106], written by Monika Grötzner, can determine the optimised wiring of a PV array. As shown in Chap. 2.4, the yield of an inhomogeneously illuminated PV array depends on the internal array wiring. Because of the varying sun position and the fluctuating sky radiance, shading or reflections will lead to a decreased or increased irradiance at any corner of the PV plane. Thus, the inhomogeneous illumination of a PV array will change throughout the year. An optimised wiring would connect modules with the same irradiation to one string. Because of the fluctuating illumination this optimised wiring may vary from one time step to the next. A computer model to determine an optimised overall PV array wiring must calculate the yield for different wirings at different illumination distributions throughout a year. PVEPO does this.

The program has been developed to study different wiring options rather than to precisely predict the yield of a PV generator. As input, PVEPO requires separate irradiance data for each module and information about the generator design (i.e., how many modules in series and how many strings are connected to the inverter). The output is an ASCII file that states

the PV generator yield at a specific wiring. Different wiring options with the corresponding yields are returned, arranged in a way that option with the highest output comes last.

In the past, the program was Internet-based and had a graphical interface for data exchange, but it was recently removed from the server. Now, access to the program is only possible via the author (email: mg@litt.rwth-aachen.de). Further documentation can be achieved under <http://telemann.litt.rwth-aachen.de/pvepo-doku>.

A minor limitation of the program is the special format of the input irradiance file (Appendix E). This format is seldom used, and a file might become very large, for example, 20 MB if 100 modules are to be simulated for one year. Depending on the Internet access, the transfer of the file via the net might take a very long time or may be even impossible. Because generally the quality of the Internet access increases steadily and compressing of the file is also possible, this limitation will become less significant in the future. However, a stand-alone version would be appreciated because this simplifies the access significantly. Till now the program runs under UNIX, and it is not clear how access to the program will be enabled in the future.

4.2.5 PVSYST

PVSYST [94] is a time-step based program to model stand-alone and grid-connected PV systems. Its PV modules and inverter database makes it relatively easy to use. An advantage of PVSYST is that it delivers a large variety of output values. Many different data such as DC power, AC power, global irradiance on the PV array, inverter efficiency, and much more are delivered.

The built-in shading generator is an important feature. PVSYST was one of the first programs to offer such a tool. It allows to model grid-connected PV system considering shading from surrounding structures. Since this is an integrated feature, the user may not be accustomed to a, usually relatively complicated, 3D-CAD program. However, a limitation of the program is that only simple structures can be entered easily. A complex scene such as a city district can hardly be modelled. The manual [94] says: “A global scene can theoretically be constituted of an unlimited number of PV fields or shading obstacles.

However, it is advisable to restrict oneself to simple representations of the systems, as the calculation time of the shadows quickly becomes prohibitive”.

Another limitation is that all PV modules must have the same orientation. Internally PVSYST does not compute with different irradiance values for the different modules. The non-linear effects of shading of PV array are thus not considered. These aspects and the missing option to import CAD models restrict the use of PVSYST for simulating PV systems in an urban structure.

4.3 Irradiance pre-processors

Most of the programs listed in Chap. 4.2 comprise an converter that calculates the irradiance on a tilted surface from horizontal data. However, most of the converters (except the one of PVcad and PVSYST) do not consider shading of the PV array. Then, or if a non-implemented sky model should be used, an external irradiance pre-processor must be applied and its results imported to the PV model.

Different programs that can be used as irradiance pre-processor will be introduced in this section.

4.3.1 Tilted surface models

Usually, several tilted surface models (Chap. 3.2.3) are implemented in the PV models of Chap. 4.2. If these are part of the output (e.g. PVSYST [94]), the program can be used as an irradiance pre-processor. Especially the block-oriented programs like INSEL [104] or TRNSYS [52] can be used in this way because they allow the connection of the block that converts the horizontal irradiance to irradiance on the tilted surface to the output block.

A program that purely computes the irradiance on a tilted surface is IRRAD [107]. It requires the direct normal incidence and the global horizontal irradiance as input and applies either the Liu-Jordan (Equ. 3.20), the Hay (Equ. 3.21), the Klucher (Equ. 3.22), or the Perez (Equ. 3.24) model.

The programs INSEL, TRNSYS, and IRRAD can be used as irradiance pre-processors to other models or to examine the irradiance purely. However, all three models do not consider a potential shading of the tilted surface.

4.3.2 Models to consider shading and reflections

Shading generators determine either the irradiance on an arbitrarily oriented plane directly, or they compute shading factors. If the latter are resulted, the irradiance on the tilted surface must be post-computed with the shading factors separately.

4.3.2.1 SHADE

A model that determines the geometrical projection of a shadow on a plane is SHADE [110]. This program allows the modelling of (complex) objects consisting of rectangular planes. Then a receiver surface can be defined, and a grid is placed over it. SHADE calculates for a given time period if anyone of the grid points is shaded by the object. The information shaded/not shaded is entered in a matrix and can be used in further solar modelling. However, this will be somewhat awkward because first the irradiance on the tilted receiver plane must be calculated and then the reduced irradiance must be reduced determined with the shading matrix. Diffuse shading (Chap. 3.4.2) or a view factor (Equ. 3.63) is not determined by this model, only I/O information. The user has to decide carefully how to deal with this data.

SHADE offers additionally a screen output to visualise the silhouette. This is helpful to experienced solar system designers for quickly finding a good location for a solar system. The algorithms of SHADE were also implemented in PVcad but in an extended form.

4.3.2.2 SOMBRERO

Another model for determining shading is SOMBRERO [108]. This model also uses a geometrical projection of an object on the considered plane to determine a geometrical shading coefficient (GSC). The GSC is the proportion of shaded area and is one result of the program. Further outputs of SOMBRERO are view factors, one for the sky according to Equ. 3.63 and one for the ground. Thus, the diffuse shading as mentioned in Chap. 3.4.2 can be considered with this tool.

A limitation to the model is that it calculates the results for one plane only. Each separate plane that could be for example PV modules, requires a separate simulation. Since a program run requires considerable time, the simulation of a standard grid-connected PV system (usually more than ten modules) is prohibitive.

Further limitations are that it is very complicated to couple SOMBRERO to other solar models, and only the uniform sky radiance distribution can be modelled.

4.3.2.3 SUNDI

The model SUNDI [109], developed by Quaschnig, calculates the irradiance on a tilted surface considering direct shading (Chap. 3.4.1) and diffuse shading (Chap. 3.4.2). Similar to SHADE and SOMBRERO, the model also uses a geometrical projection. Its advantage is that the irradiance on a solar receiver plane is directly returned and is not only shading coefficients. This simplifies its use as irradiance pre-processor significantly.

A limitation of the program is that shading objects must be defined by their azimuth and elevation angles. Even for a simple scene this is a very long-winded procedure. Another limitation of SUNDI is that it calculates the results for one point only.

4.3.2.4 Reflections

All the reviewed PV models calculate the irradiance on a receiver plane according using the tilted surface model (Chap. 3.2). These models do not allow account for reflections.

Advanced lighting simulation programs such as RADIANCE (Chap. 5.1) are able to model single or multiple reflections between surfaces thus they are, in principle, suited for use as pre-processors to PV models.

4.3.3 Criteria

All the above-mentioned programs have limitations that restrict their use as a irradiance pre-processor for PV systems in urban environment. Such an pre-processor should have the following features:

- It should allow easy modelling of an architectural space. Preferably it should comprise an option to import a drawing that was created with a standard CAD program. These programs are optimised to model complex spaces.
- It should allow easy coupling to further PV (or solar) models. Preferably it should produce a file with the irradiance values directly (and not just shading factors), since many programs (e.g. INSEL, TRNSYS, PVcad, PVEPO) can read such a file.
- The irradiance should be computed at arbitrary points. Neither the location nor the orientation (view direction) should be restricted.
- Shading of surrounding structures and possibly even reflection of sunbeams should be considered.
- The irradiance should be computed at several points at the same time. In this way an inhomogeneously illuminated PV generator can be modelled easily.
- Modelling of the sky should not be restricted to the uniform sky, but more realistic skies should be available.

4.3.4 Ray-tracing

In principle, ray-tracing [111] can fulfil all criteria developed in Chap. 4.3.3. It is thus possible to develop an irradiance pre-processor for PV systems in a urban environment that satisfies all demands based on ray-tracing.

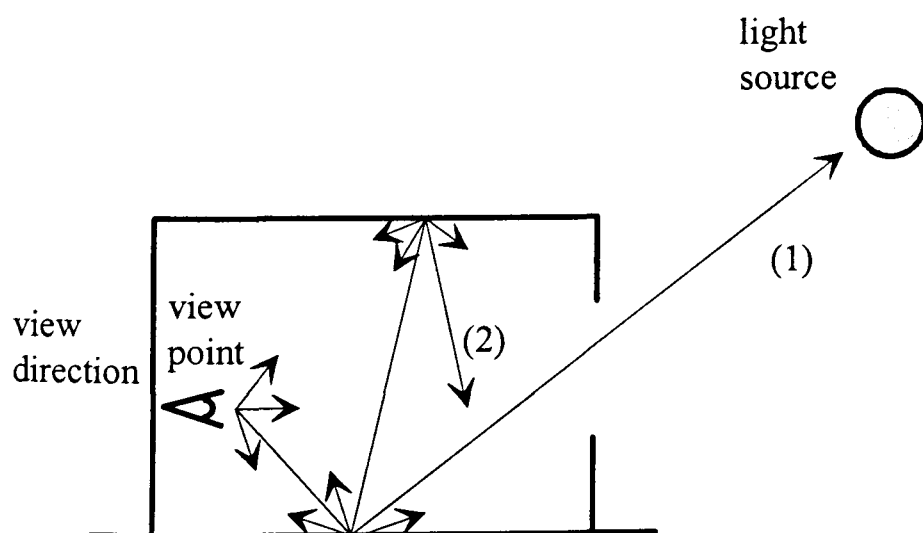


Figure 4.5
Rays are traced until they hit a light source (1) or until the limit of reflections is reached (2)

For ray-tracing, a scene must be modelled in a format that is fitted to the corresponding program. Then a specific point of interest, the view point (vp) (Fig. 4.5), and a view direction (vd) are defined. Rays are sent out from the vp in the vd and traced until they hit a

surface. From there a bundle of further rays is sent out. This procedure is repeated until a ray either hits a light source (1) or the specified limit of reflections is reached (2) so that its contribution to the final result will drop below a certain threshold (at each reflection the ray is attenuated). One of the problems of ray-tracing is to decide how long it is worth continuing tracing because this will influence the computation time significantly.

Originally, ray-tracing was used to generate photo-realistic images of architectural spaces. In this application, the view point represents the position of the virtual camera. Since images are a superposition of the luminance values of different colours, the illuminance or the irradiance at the view point can also be determined with the ray-tracing approach. An important advantage is that the irradiance at several arbitrarily chosen view points can be determined simultaneously.

Further, the reflections of the rays can be treated according to the bidirectional reflectance distribution Function (BRDF) of the surface (Fig. 4.6). This allows to consider different reflection characteristics like diffuse, specular or mirror reflections. Different spectral (colour) characteristics can be considered if several channels, e.g. for red, green, and blue are used.

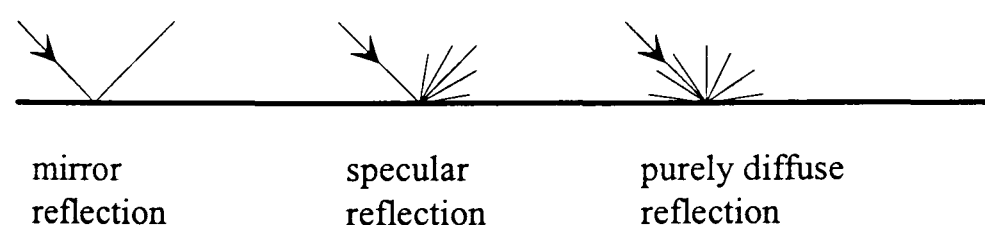


Figure 4.6
Different reflection characteristics of surfaces

The above described features of ray-tracing allow the modelling of virtually any space and the determination of the irradiance at any point of interest (trace point). It depends on the specific ray-tracing program if it comprises an option to import CAD models. For example, the ray-tracing program RADIANCE [112, 113] includes a converter for the standard DXF files. This program also allows to model a sky according to a uniform luminance distribution (Equ. 3.32), a diffuse (3.34), an intermediate (Equ. 3.47), a clear sky (Equ. 3.37), or according to the Perez 'All-weather sky' luminance distribution (Equ. 3.45), including or excluding a sun.

However, RADIANCE allows only a static simulation, i.e. for one sky condition and one sun position only. To use it as irradiance pre-processor it must be run for each time step (i.e. each hour) with the corresponding sky radiance distribution and sun's position.

4.4 Evaluate shading with a CAD program

CAD (computer aided design) programs like AutoCAD [114] are the up-to-date tools to design architectural spaces. They allow 3D-modelling of a scene and visualisation of the structure from different viewpoints. Moreover, modification of a design can be done very quickly and thus, different options can be examined easily.

In AutoCAD, full 3D-drawing and rendering allows visualisation and a virtual walk in a planned building. Also the impact of sunlight and daylighting of interior spaces can be visualised. For this, a light source that representing the sun can be modelled and placed at the desired position. An ambient light level controls the constant illumination of all surfaces to make them visible. However, modelling a standardised sky luminance distribution is not implemented yet. This would be necessary to predict the illuminance or the irradiance at the outside of a building.

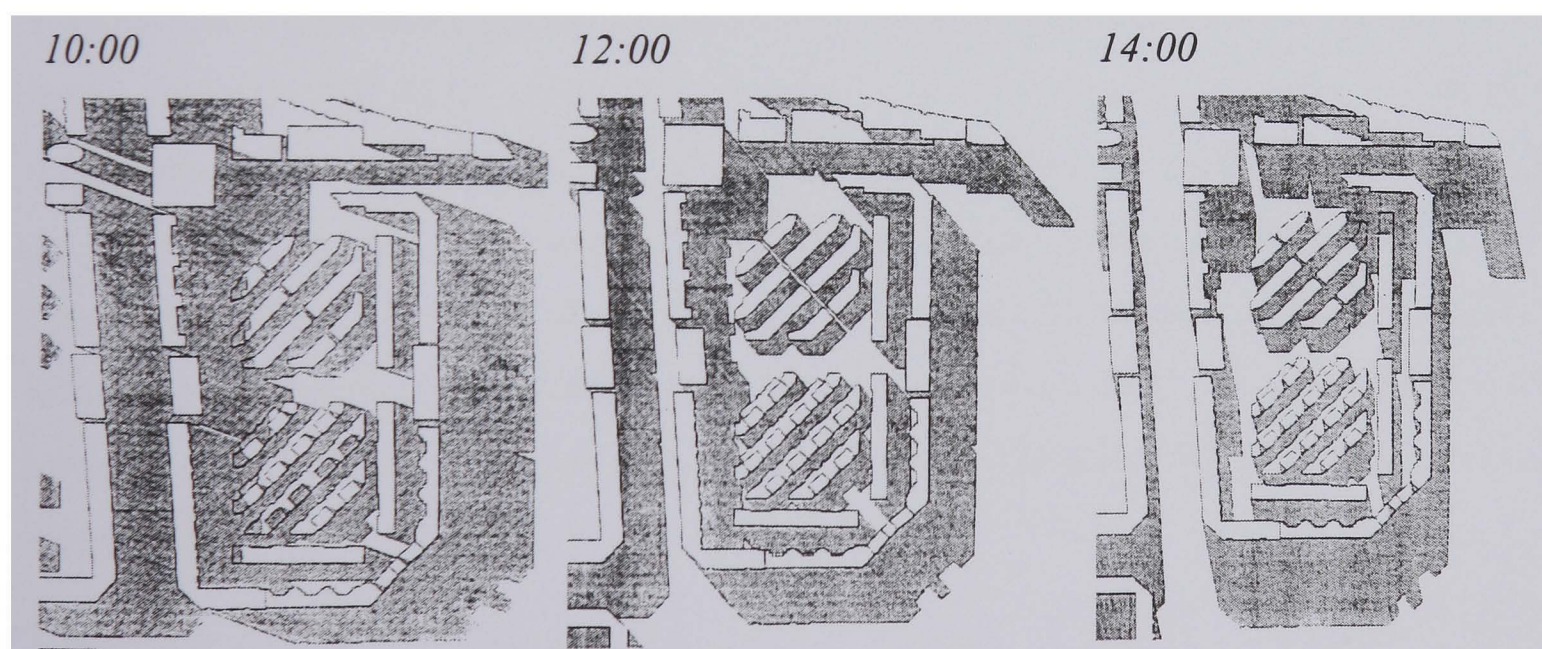


Figure 4.7 Silhouette of an arrangement of buildings showing the solar shading at different times of the day

Figure 4.7 shows the silhouette of an arrangement of buildings at different sun positions [115]. In this way it can be evaluated when buildings are shaded by surrounding structures. In the same way, the shaded area of a solar receiver can be determined. This allows the

estimation of the yield reduction of a solar system when the output is proportional to the shaded area. The yield of a PV system is however not linear with the shaded area of the PV array (Chap. 2.4). Thus, predictions of how much the yield of a PV system is reduced by shading should not be based on the shaded area of the modules. Only very rough estimations are possible.

5 TIME-VARYING IRRADIANCE PREDICTIONS

Modelling PV systems in an urban environment is a complex task. In the previous chapter, criteria were developed which PV models must fulfil in order to achieve this task. Several existing models were reviewed but all, except PVcad, are either incomplete for modelling PV systems in an urban environment, or they display major restrictions that limit their practical operation. An irradiance pre-processor that accounts for shading and reflections in the simulation is required.

Various existing computer programs were examined for their use as irradiance pre-processors for PV models, but again major restrictions were found. This makes the development of a new computer code necessary. As shown in Chapter 4.3.4, the ray-tracing model RADIANCE [112, 113] can be used for this purpose. It allows the direct computation of irradiance values at arbitrarily chosen points, accounting for shading and the inter-reflected light. However, a way must be found to enable an efficient time-varying simulation with RADIANCE to generate a time series of irradiance data, considering different sky conditions and different sun positions. This was realised within a new program called IPROCESS [116, 117]. RADIANCE and IPROCESS will be introduced in this section.

IPROCESS predicts global irradiance values at the trace points. These can be examined as they are or can be fed to a further PV model. The models INSEL (Chap. 4.2.2), PVcad (Chap. 4.2.3), and PVEPO (Chap. 4.2.4) are ideal for this; INSEL to look at details such as I-V curves, PVEPO to optimise PV array wiring, and PVcad for long-term yield predictions.

5.1 RADIANCE

RADIANCE [112, 113] is a physically based ray-tracing program to visualise lighting designs. It is suited to predicting, with precision, illumination values at specific points of interest as well as the production of photo-realistic images of architectural spaces. Basically, RADIANCE is not just one program but a system containing many different programs. RADIANCE was originally written for UNIX and is freely available via the Internet at the server of the Lawrence Berkeley Laboratories (<http://hobbes.lbl.gov>). There is also a PC version of RADIANCE within the ADELIN package [118]. However, ADELIN must be bought from the Fraunhofer Institute for Buildings Physics, Stuttgart, Germany. In this context, the PC version is referred to if not otherwise mentioned.

To simulate any space, a RADIANCE format scene description must first be created. The scene file(s) comprise the three-dimensional geometry of all the objects (buildings, furniture, trees, windows, walls, lamps, etc.) and their surface properties. Then the light falling on the specified point of the scene can be calculated, or a photo-realistic image can be produced. RADIANCE uses three channels, red, green, and blue, that are superimposed to generate a coloured picture. This can be sent to the screen or to a printer [119, 120].

RADIANCE commands can be used to simplify the scene creation and to model more complex objects with aid of a generator. They can create for example a rectangular box (*genbox*), a curved surface (*gensurf*) or even the description of a sky including the sun with a position according to a given day and hour (*gensky*). A generator can be either executed within the RADIANCE scene file or it is possible to run it externally and to append the created code with the >> command to the scene file.

The central programs of the RADIANCE package are *rview*, *rpict*, and *rtrace*. *Rview* and *rpict* are used to generate the image, seen from the *view point* in the *view direction*. Here, *rview* produces an image where the right parameters (e.g., view point, direction, angle, ambient brightness) can be set interactively whereas *rpict* produces a high resolution image that may take some minutes or hours to render depending on the parameters and the scene complexity.

Rtrace is used to compute either the radiance of specified rays or the irradiance values at specified trace points. The irradiance calculation is used for IPROCESS.

In order to obtain an accurate result, many different calculations parameters have to be set correctly. For photo-realistic images, the numerical accuracy is less important because a change in the brightness of 5-20% from one pixel of a picture to the next is hardly visible. However, for computation of irradiance values a much more accurate setting of the parameters is required but this leads to longer computation times. The parameter settings can have a large influence on the rendering time and the accuracy of the results [113]. With poor settings RADIANCE will return inaccurate or even arbitrarily results.

5.1.1 Sky models

RADIANCE includes the two programs *gensky* [119] and *gendaylit* [121] that generates various sky radiance distributions based on theoretical models.

Gensky allows modelling of a uniform sky (Equ. 3.32), CIE standard overcast sky (Equ. 3.34), Matsuura intermediate sky (Equ. 3.47), and the CIE standard clear sky (Equ. 3.37). Whereas the clear and the intermediate sky can be modelled with or without a sun, the uniform and the overcast skies are always modelled without sun. Further commands at the call of *gensky* allow adjusting the radiance of the sky according to the horizontal diffuse irradiance (*-B* command) and the radiance of the sun according to the horizontal direct irradiance (*-R* command). To create, for example, a clear sky with sun, a sun position of $\epsilon_s = 70^\circ$ and $\alpha_s = 20^\circ$, a horizontal diffuse irradiance of 300 W/m², and a horizontal direct irradiance of 500 W/m², the following line must be entered.

```
gensky -ang 70 20 +s -B 300 -R 500
```

Gendaylit generates a sky according to the Perez ‘All-weather sky’ (Equ. 3.45) model. It can be also created with or without a sun. Different options are available to enter the radiance of the sun and the sky. In this context however, entering the direct normal and the diffuse horizontal irradiance is most convenient. To generate, for example, a Perez sky

with a sun position of $\varepsilon_s = 70^\circ$ and $\alpha_s = 20^\circ$, a direct normal irradiance of 600 W/m^2 , and a diffuse horizontal irradiance of 300 W/m^2 the following line must be entered.

```
gendaylit -ang 70 20 -W 600 300
```

In RADIANCE the azimuth angle is measured from south whereas the convention is from north (clockwise in both cases). It should be noted that the *gensky* model is available in the UNIX and the PC version of RADIANCE (ADELINE) whereas the *gendaylit* model is available for UNIX only.

All the above-mentioned models were made available within IPROCESS with the extension that all *gensky* models can be created with or without sun.

5.1.2 Input files

A RADIANCE scene description (scene file) consists of so-called *primitives*. They have always the same form, as indicated below.

<i>modifier type identifier</i>	modifier type name
<i>n S1 S2 ... Sn</i>	string arguments
<i>0</i>	integer arguments
<i>m R1 R2 ... Rm</i>	real arguments

Several predefined primitives exist to model spatial objects like spheres, cylinders, cones, polygons, etc. The surface of an object can be either self-luminous (light, glow, illum, etc.) or have a predefined interaction with light (mirror, plastic, metal, etc.), or both. Further materials like *dielectric* allow modelling of the correct physical behaviour of glass. Additionally, a texture or a pattern may be assigned any to. A red self-luminous sphere in the centre of the coordinates with a diameter of one is modelled as follows. A complete RADIANCE scene description is given in the Appendix C.1.

```
# this is comment, the following primitive defines a red colour
void light red
0 0
3 500 10 10
```

```

# this is comment, the following primitive defines sphere with red surface
red sphere ball
0      0
4 0 0 0 1

```

Except for the primitives, only three further formats are allowed in a RADIANCE scene file.

<i># comment</i>	to write a comment
<i>modifier alias identifier reference</i>	to use an alias
<i>! command</i>	to execute a command

If a very complex scene is to be rendered, the geometry of the objects can be drawn with a 3D CAD program and then stored in the standard DXF format. The ADELIN package (but not UNIX RADIANCE) possesses the *dxconf* program to convert a standard DXF file into a RADIANCE scene description. However, not the complete range of CAD commands can be used since only special surfaces are allowed (see the *dxconf* manual [119] for which CAD objects can be converted). The material properties (colours and textures) must be added manually to the input file.

It should be noted that in RADIANCE coordinates system the X-vector shows to east, the Y-vector towards north, and the Z-vector towards the zenith.

Another input file to RADIANCE is a so-called ray-origin file if the irradiance at several trace points is to be calculated with *rtrace*. This file must contain the coordinates of the trace points and the view direction. If the irradiance on a plane is to be calculated the view direction is equal to the surface normal. To calculate the irradiance on a south-facing wall at a location of 3 / 3 / 3 the ray file must contain the following line.

```
3      3      3      0      -1      0
```

A ray file with trace points as above given will be used for IPROCESS.

5.2 Time-varying calculations with RADIANCE

RADIANCE [122] is well suited to calculate the irradiance at given points of interest (trace points). This can be done for different trace points and thus, the inhomogeneous irradiance

distribution over a PV array can be calculated. However, the irradiance is calculated with one sky model and one sky position only. For long-term yield predictions of PV systems the inhomogeneous irradiance distribution must be calculated for a certain time period, i.e. for each hour of a complete year. This can be done by repeated calculations with RADIANCE, modelling the different sky conditions with *gensky* or *gendaylit*.

5.2.1 Direct calculation

A computer program *dcalc* (direct calculation) was written to control the repeated calls of RADIANCE. It is programmed in the computer language C because this creates a fast program, it can be also compiled for UNIX, and it is possible to run it from a batch file.

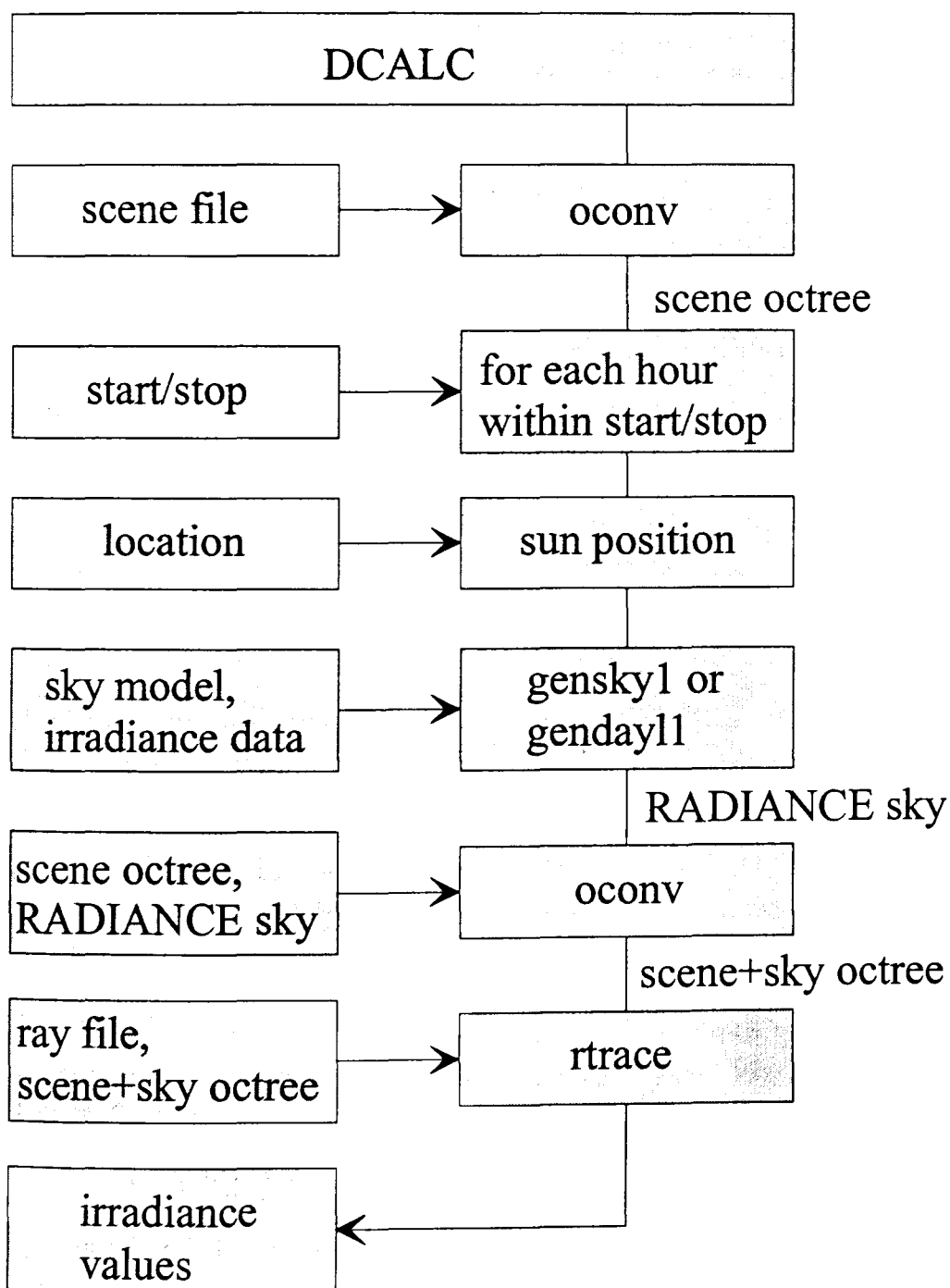


Figure 5.1
Block structure of *dcalc*
(*oconv* and *rtrace* are original RADIANCE programs, *gensky1* and *gendayl1* are modified RADIANCE programs)

For each hour of a specified time period *dcalc* calculates the sun position according to the entered location and the time of the year. It uses the algorithms as given in Chap. 3.1.2 (Equ. 3.5-3.11) for this. However, as mentioned above, the azimuth angle is measured clockwise from south. Dependent on an input parameter, the sun position is determined at local time or at solar time, i.e. considering the equation of time (Equ. 3.10, 3.11). Then *dcalc* reads irradiance data from an external file and then applies *gensky* or *gendaylit* to model a RADIANCE sky according to the command as given in Chap. 5.1.1. Actually, not the original programs were used but *gensky* was extended (to *gensky1.exe*) to enable the modelling of the uniform sky and the overcast sky including a description of sun. Further, the (UNIX) C code of *gendaylit* was transferred (to *gendayl1.exe*) to enable a compilation for PC's.

The generated sky and one (or up to three) scene file(s) (Chap. 5.1.2) are merged and the RADIANCE program *oconv* is applied to generate a RADIANCE octree which is stored in a temporary file. Actually, a frozen octree (see RADIANCE *oconv* manual RADIANCE [119]) of the scene is generated only once and the octree of the sky is added for each hour to save computation time. The temporary file and a ray file (Chap. 5.1.2) are used to calculate the irradiance values with *rtrace*. A block structure of *dcalc* is given in Fig. 5.1.

option	argument	choices	default
-a	<i>latitude</i>	-90° ... +90° (+ north / - south)	37.82° N
-o	<i>longitude</i>	-180° ... +180° (+ west / - east)	122.04° W
-m	<i>meridian</i>	-180° ... +180° (+ west / - east)	120.0° W
-s	<i>sky model</i>	0: uniform without sun 1: uniform with sun 2: overcast without sun 3: overcast with sun 4: intermediate without sun 5: intermediate with sun 6: clear sky with sun 7: Perez with sun	7
-b	<i>start_month</i> <i>start_day</i>	1 ... 12 1 ... 31	1 1
-e	<i>stop_month</i> <i>stop_day</i>	1 ... 12 1 ... 31	1 1
-f	<i>control file</i>	file name	control.con

Table 5.1 Parameters to be entered in the command line to start dcalc

Parameters that are necessary for the program are given in Tab. 5.1. They can be entered in the command line to run the program. If a parameter is not specified a default is assumed. For example, *dcalc* can be started with the following line.

```
dcalc -a 42.5 -o -9.12 -m -15 -s 7 -b 5 27 -e 5 30 -f control.con.
```

IRRADIANCE FILE c:\weather\try\berlin.try	path and name of the file that contains the irradiance data
TIME MODE 0	0: local time 1: solar time
FILE START MONTH 1	month in which the records of the irradiance file start
FILE START DAY 1	day in which the records of the irradiance file start
FILE TYPE try	TMY (the formats are described in the manual, Appendix E) TRY SCT
CONVERSION FACTOR 1	conversion to W/m ²
COORDINATES FILE c:\iprocess\sample.inp	path and name of the file that contains the location and the view direction of the sample points
ACTPATH c:\iprocess\	path to the program
SCENE PATH c:\iprocess\L-house\	path to the file(s) that contains the scene description
SCENE FILE1 material.rad	name of the 1 st file that contains the scene description
SCENE FILE2 walls.rad	name of the 2 nd scene file if the scene description is stored in more than one file
SCENE FILE3 [empty line]	name of the 3 rd scene file if the scene description is stored in three files
OUT FILE c:\iprocess\L-house\3may.out	path and name of the output file, if it exists it will be overwritten
OUT FILE FORMAT 0	0: standard (with header) 1: no header 2: global irradiance + temperature 3: output for PVEPO (the formats are described in the manual Appendix E) 4: output for PVcad
RTRACE PARAMETER -I -aa 0.4 -ab 2 -ad 64 -ar 16	<i>rtrace</i> parameters as described in [119] (-I is necessary if irradiance should be calculated)
COEFFICIENTS FILE step.cof	path and name of the coefficients file (these lines are not used for <i>dcalc</i>)

Table 5.2 Example of a control file that is used by dcalc

Further parameters must be specified in a control file that is referred to after the *-f* parameter. A sample of how this might look is given in Tab. 5.2, but only the text in the left-hand column must appear in the control file, comments are not allowed. The text under COEFFICIENTS FILE is not used here and will have no effect. The resolution of the ambient calculation can be adjusted with the RTRACE PARAMETER. They are explained in the RADIANCE manual [119]. Here, the *-I* parameter is necessary to calculate the irradiance. Otherwise *rtrace* would result the radiance at the trace point. If this is required, *dcalc* can also calculate a time series of radiance values.

It is assumed that the irradiance input data are given in terms of Wh/m². Sometimes, the climate data files contain irradiance data in kJ/m², cal/cm² or other formats. For example, if the data are given in cal/cm² the CONVERSION FACTOR 11.628 (Tab. 5.2) must be entered. For data given in kJ/m² the required factor is 0.2778. The results will always be in Wh/m² units.

The different FILE TYPE formats enable the reading of irradiance data that were recorded or generated in different formats. These are described in the IPROCESS manual (Appendix E.) as well as different output formats that simplifies coupling to further PV models.

5.2.2 The sky patch approach

A disadvantage of *dcalc* and its algorithms is that the irradiance computation with the above described direct approach can take a very long time. For example, a complex scene like a city district, a long time period of one year (at hourly values), and 100 scattered trace points can take up to 13 hours to be calculated (the time refers to PC with PENTIUM 130 MHz and 48 MB RAM).

An attempt to accelerate the computations is the patch approach that is based on the daylight coefficients approach from Tregenza and Waters [123]. Here, the contribution C to the irradiance I_k at the trace point k made by every infinitely small zone of the sky is computed separately. The total irradiance I_k is then calculated by multiplying C with the sky radiance R and integrating over all components according to Equ. 5.1.

$$I_k = \int_0^{2\pi} \int_0^{\pi/2} C_k(\varepsilon, \alpha) \cdot R(\varepsilon, \alpha) \cdot \cos(\varepsilon) d\varepsilon d\alpha \quad (5.1)$$

To be used for numerical computation, a real extent must be assigned to each small zone of the sky. The thus created zones are called sky patches. Their extent is described by the solid angle S . Equation 5.1. can now be written in the form of Equ. 5.2 [123]

$$I_k = \sum_i C_{i,k} \cdot R_i \cdot S_i \quad (5.2)$$

where i refers to the considered patch. All patches together must cover the complete sky dome.

For the computations, the sky dome is discretised and subdivided into small emitter patches (Fig. 5.2). Then, the irradiance at the trace points is computed by fading out all patches except one and assigning a standardised radiance to this patch. For this approach the sky is usually modelled as a sphere or as a spherical polyhedron. It must be secured that sphere radius is large enough that all points of the scene are with sufficient precision in the centre of the sphere. The calculated irradiance values serve as (daylight) coefficients [123, 124, 125] (or also called form factors [75]) for the following computation of time-series irradiance data. The total irradiance at the considered trace point I_k is computed by multiplying the coefficients $C_{i,k}$ (i : number of considered patches, k : number of considered trace point) with the real radiance $R_i(\alpha, \varepsilon)$ of the sky at the position of the patch and its solid angle S_i and cumulating the results over all patches as given in Equ. 5.2.

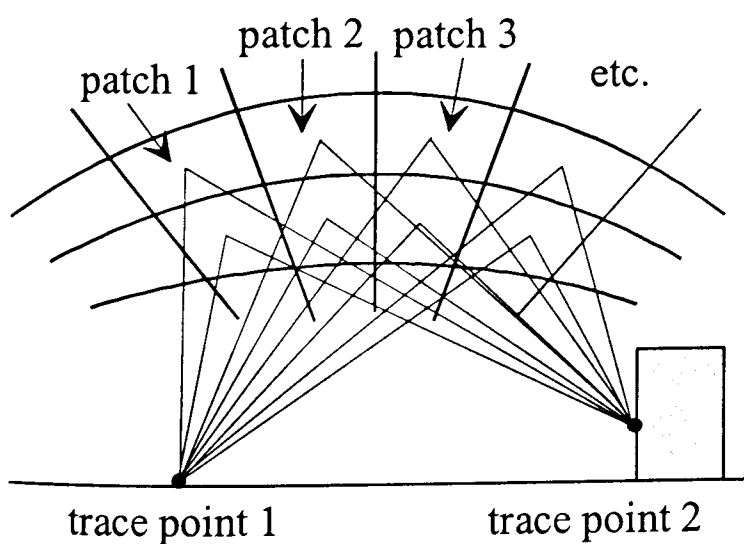


Figure 5.2
A set of coefficients is calculated, one for each trace point to each patch, to apply the sky patch approach

The time-consuming process of this calculation is the determination of the $i \times k$ coefficients. However, this must be done only once and then the coefficients can be stored in an external file. The time series calculation of irradiance data can recall the coefficients and only the sky radiance distribution must be updated for each time step. Since this requires only the relatively fast computations according to Equ. 5.2 the total computation time is reduced significantly, however, dependent on the number of patches. It should be noted, that the computation of one patch takes about the same time as the computation of one sky (at the direct approach). Since a year has about 4,400 daylight hours, the patch approach is potentially more efficient when the number of patches is less than this number.

5.2.2.1 Sky dome subdivision

Several methods to discretise the sky dome can be found in the literature. Cesarano [126] used an equi-angular division where the sky vault was divided into m bands along the latitude ($0 < \varepsilon < 90^\circ$). Each band was then divided into $n (= 4 \times m)$ 'quadrangles' (in spherical polar-coordinates the resulting patches are only approximately quadrangles). By this way the spatial angles between the centres of the patches remain the same. However, since the sky band becomes shorter at an increasing altitude, also the patches will be smaller at higher altitudes.

zenith angle of sky band	number of patches	azimuth angle between centres of patches
0°	1	0°
12°	6	60°
24°	12	30°
36°	18	20°
48°	24	15°
60°	24	15°
72°	30	12°
84°	30	12°

Table 5.3
Measuring points
of sky scanner

Another option is to place the centres of the patches according to the pattern shown in Tab. 5.3. In this way, 145 patches will be created. This subdivision is described by Tregenza [127] and became a standard for sky scanner measurements. However, a disadvantage of this fixed distribution is that it does not allow variation of the number of patches. Mardaljevic [125] used this discretisation for indoor daylight coefficients to validate RADIANCE using scanner measurements.

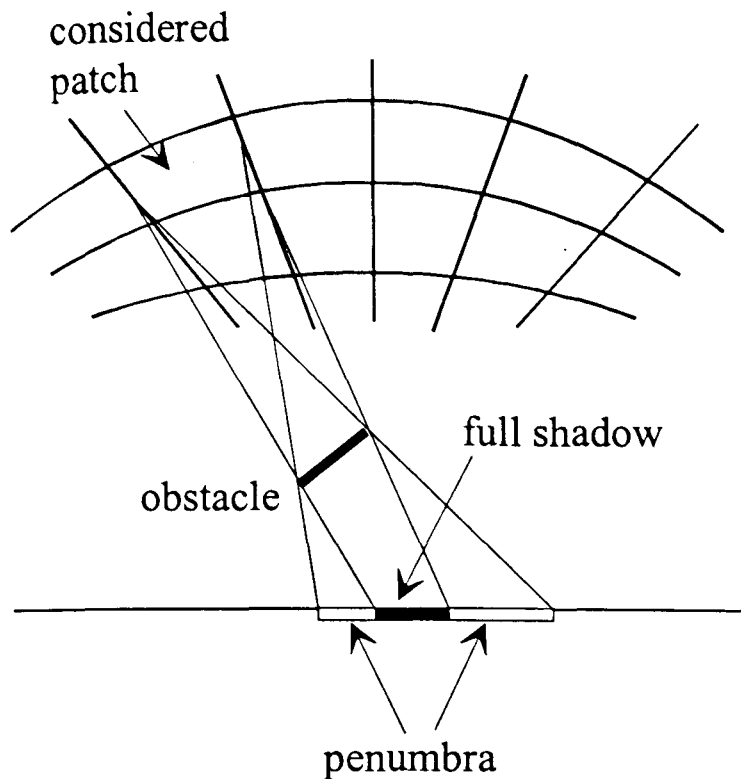


Figure 5.3
Considering penumbras from one patch

Cropper [124] suggested to model a sky from triangles. The advantage is that: “They can be arranged to completely cover the sky dome, and because they can be recursively subdivided to achieve any degree of discretization”. To vary the size of patches and consequently their number is important to find an optimum between accuracy and computation time. The shape of the patches is however only important if its whole area contributes to the computation of the form factors. This will lead to an accurate consideration of penumbras (Fig. 5.3) that are caused by one single patch. Another option is use only the centre of a patch as a (point) light source. This will neglect penumbras and the shape of the patches does not matter.

5.2.2.2 Deriving the coefficients

It is possible to derive the coefficients as described in Chap. 5.2.2 with RADIANCE (Chap. 5.1). If the shape of the patches should be considered they must be modelled as RADIANCE *glow* type. This will cause a stochastically sampling of the complete patch area and penumbras are considered. However, stochastically sampling is relatively time-consuming and is thus opposed to the aim to reduce the time demand. Further, in contrast to daylight coefficients for indoor calculations, penumbras will have only a very small influence on a time series of irradiance data computed for the outer wall of a building. Depending on the number of patches, the possible error could become insignificant.

Because of the above mentioned it is advantageous to sample the patches deterministically. This can be done with RADIANCE by assigning the *light* type to a patch. Now, only one ray will be sent to the centre of a patch. Actually, the term ‘patch’ is not correct for this approach but will however be used to simplify the understanding. In the following, the term *patch* always refers to the centre of the patch.

The best way to model such a patch within RADIANCE is to use the *source* type and assign the *light* property to it. A *source* is rather a solid angle than a surface that is far away. Thus, no problems regarding the distance between the patch and the scene will appear and distance to the ‘patch sky’ may not be adjusted according to the scene size.

The *light* property allows to assign a normalised radiance to the patch. The resulting coefficient is exactly equal to the normalised radiance if the surface normal (where the trace point is placed) points directly towards the centre of the patch, if no obstacles are in the way and if the light is not reflected. Due to reflections (e.g. the albedo) the coefficient may be higher than the normalised radiance. This approach to compute the (patch) coefficients was realised in a computer program *pcoef*. Because of the same reasons as given for *dcalc*, it was also written in the programming language C.

New approach for sky dome subdivision

The sky dome subdivision (and thus the distribution of the patches) was realised as a mixture of the methods give in Chap. 5.2.2.1. On the one hand, the number of patches should be variable and, on the other hand, the distance between them should approximately equal because this should produce an statistically uniform error [124].

The distance (and number of patches) depends on a *step* that is chosen by the user. The sky-dome is divided into n equi-angular bands (Fig. 5.4) similar as suggested by Cesarano (Chap. 5.2.2.1). The angle between the bands is equal to the *step*. To obtain an equal longitudinal placing and to avoid patches with a zenith angle of 90° ($\theta = 90^\circ$), the bands are shifted by half a *step* at all values except 4, 12, 20, and 40. The zenith angle θ_n of the patches of the band n is determined by Equ. 5.3 and 5.4.

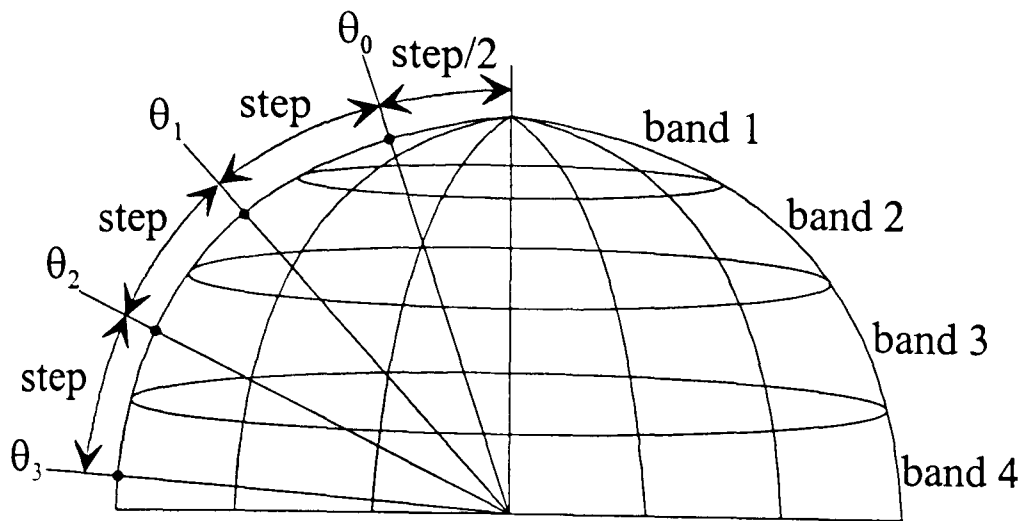


Figure 5.4
Division of the sky for
the patch approach

$$\text{step} \neq 4, 12, 20, 36 \quad 0 < \theta_n \leq 90^\circ \quad \theta_n = \text{step} \cdot \left(\frac{1}{2} + n \right) \quad n = 0, 1, 2, 3 \dots \quad (5.3)$$

$$\text{step} = 4, 12, 20, 36 \quad 0 < \theta_n \leq 90^\circ \quad \theta_n = \text{step} \cdot n \quad n = 1, 2, 3 \dots \quad (5.4)$$

To obtain an equal azimuthal spacing (size) of the patches, their azimuth angles α_m depends on the zenith angle θ_n of the considered band. In a first attempt the azimuth angles were computed according to Equ. 5.5.

$$0 \leq \alpha_m < 360^\circ \quad \alpha_m = \frac{\text{step}}{\sin \theta_n} \cdot m \quad m = 0, 1, 2, 3 \dots \quad (5.5)$$

By this algorithm one patch of each band has an azimuth of zero, that, in itself, is permitted. However, it was found that this leads to an overpredicting of the irradiance at south facades at small number of patches because the points are not evenly distributed over the hemisphere. Thus, the azimuth of the first patch was shifted to obtain a better distribution of the patches around $\alpha = 0^\circ$. Equ. 5.6 was found to produce a suitable distribution. Additionally, a further patch is generated at $\theta = 0^\circ$.

$$0 \leq \alpha_m < 360^\circ \quad \alpha_m = \frac{\text{step}}{\sin \theta_n} \cdot \left(\frac{1}{2} + m \right) \quad m = 0, 1, 2, 3 \dots \quad (5.6)$$

The number of patches that will be generated with these algorithms are given in Tab. 5.4 and an empirically found equation to approximate this relation in Equ. 5.7. The values of Tab. 5.4 and Equ. 5.7 are entered in the diagram of Fig. 5.5. The number of patches mainly determines how long a computation with this approach will take.

$$\text{number of patches} \approx \frac{20628}{\text{step}^2} \quad (5.7)$$

step	2	3	4	5	6	7	8	9
number of patches	5157	2293	1293	828	574	428	311	255
step	11	13	15	17	19	21	24	27
number of patches	164	126	93	66	63	43	41	25
step	30	33	35	38	40	45	50	55
number of patches	24	23	22	12	12	11	11	10

Table 5.4 Number of steps dependent on the chosen step value

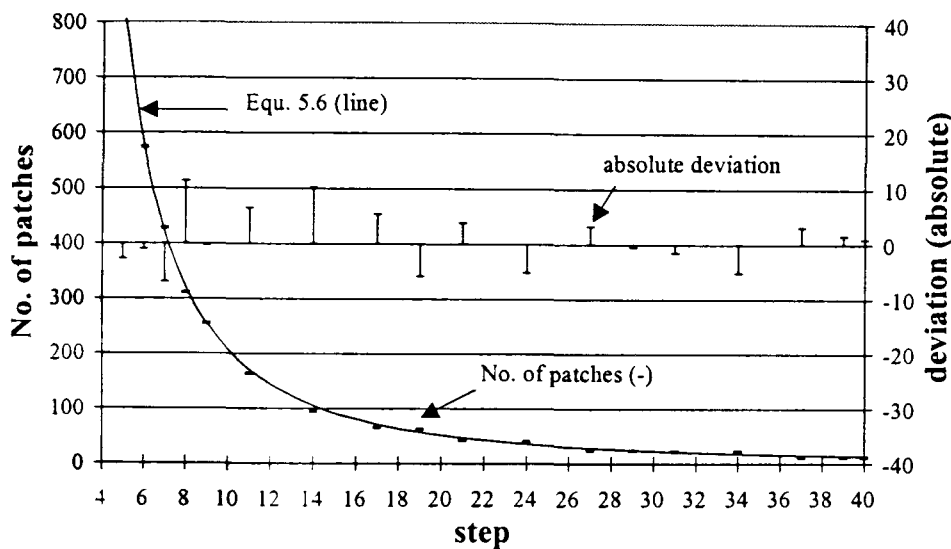


Figure 5.5 Correlation between the chosen step and the number of patches

step	24				
n	-	0	1	2	3
zen_n	0	12	36	60	84

m	azi_m				
0	0	57.7	20.4	13.9	12.1
1		173.2	61.2	41.6	36.2
2		288.6	102.1	69.3	60.3
3			142.9	97.0	84.5
4			183.7	124.7	108.6
5			224.6	152.4	132.7
6			265.4	180.1	156.9
7			306.2	207.8	181.0
8			347.1	235.6	205.1
9				263.3	229.3
10				291.0	253.4
11				318.7	277.5
12				346.4	301.7
13					325.8
14					349.9

Table 5.5 Zenith and azimuth angles of the patches that will be generated with a step of 24 (e.g. the patch m=2 at band n=1 has a zenith angle of 36° and an azimuth of 102.1°)

As an example, the zenith angles (zen_n) and azimuth angles (azi_m) of the 41 patches that will be generated with a *step* of 24 are given in Tab. 5.5. It can be seen that the azimuth angle of the patches varies around $\alpha = 0^\circ$.

Computer code

To calculate the coefficients *pcoef* requires, similar as *dcalc*, a RADIANCE scene. The program uses the same control file as given in Tab. 5.2 but reads however only the required information. The coefficients will be stored together with the zenith θ and azimuth α angle of the patch in a file that is specified under COEFFICIENTS FILE. A block diagram of the program run is given in Fig. 5.6.

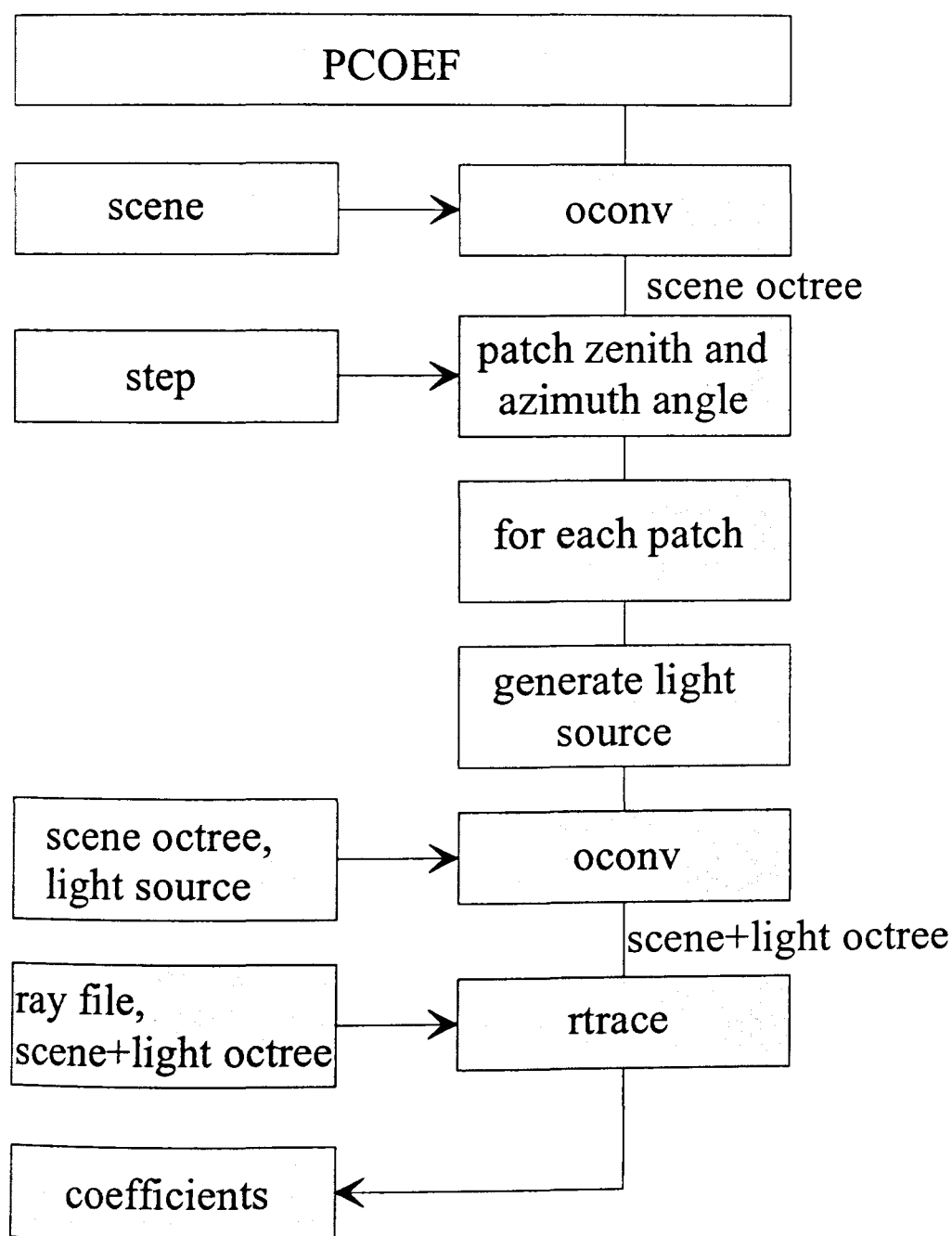


Figure 5.6
Block structure of *pcoef*
(*oconv* and *rtrace* are
RADIANCE programs)

In the command line *pcoef* accepts only two parameters: the step and the name of the control file. For example, the program can be started with:

```
pcoef -s 13 -f control.con
```

5.2.2.3 Determine the irradiance

To determine the irradiance at a trace point the normalised coefficients must be multiplied with real world sky radiance and the results must be cumulated according to Equ. 5.2. This algorithm was realised in a further C program, *pcalc* (patch calculation).

Here, the patches are not only used for the (diffuse) irradiance from the sky but also for the (direct) irradiance from the sun. It is tested in which patch the sun appears. Then the direct normal irradiance $I_{d,n}$ is multiplied with the coefficient of the related patch and for the considered trace point. This is the share of the direct irradiance at the trace point.

With very large patches this can lead to some inaccuracies. For example, when the (real) sun appears in a corner of the patch and is visible from the trace point but the patch centre (that references the complete patch as said in Chap. 5.2.2.2) is not visible, the direct part is neglected (Fig. 5.7). However, the probability that this error occurs depends on the patch size and can be reduced by reducing the patch size. Further, in a time series calculation the error will be levelled out because sometimes the patch centre will be visible but not the sun.

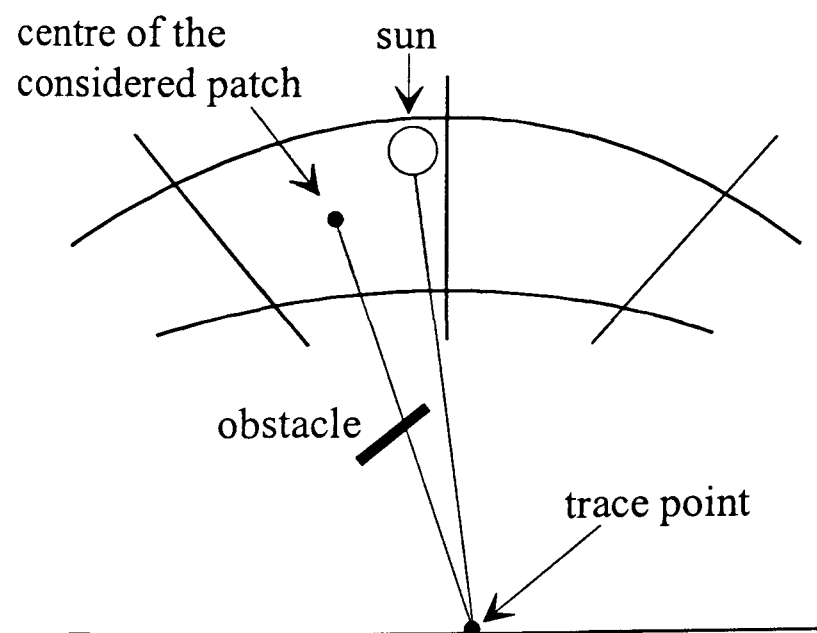


Figure 5.7
If the sun is visible from a trace point but not the patch centre, the direct share is neglected

To assign a real world radiance to the sky, the same sky models as for *dcalc* (Chap. 5.1.1) are also implemented in *pcalc*. They are programmed according to the same equations (Equ. 3.32-3.47). Furthermore, the Brunker sky model is implemented according to Equ. 3.41.

In principle, *pcalc* demands the same input as given in Tab. 5.1 only the Brunger sky model can be additionally chosen as sky model 8. The same control file as shown in Fig. 5.2 is used but only the required entries are read. The other data can be arbitrary. For example, the following command line will start the program:

```
pcalc -a 42.5 -o -9.12 -m -15 -s 7 -b 5 27 -e 5 30 -f control.con.
```

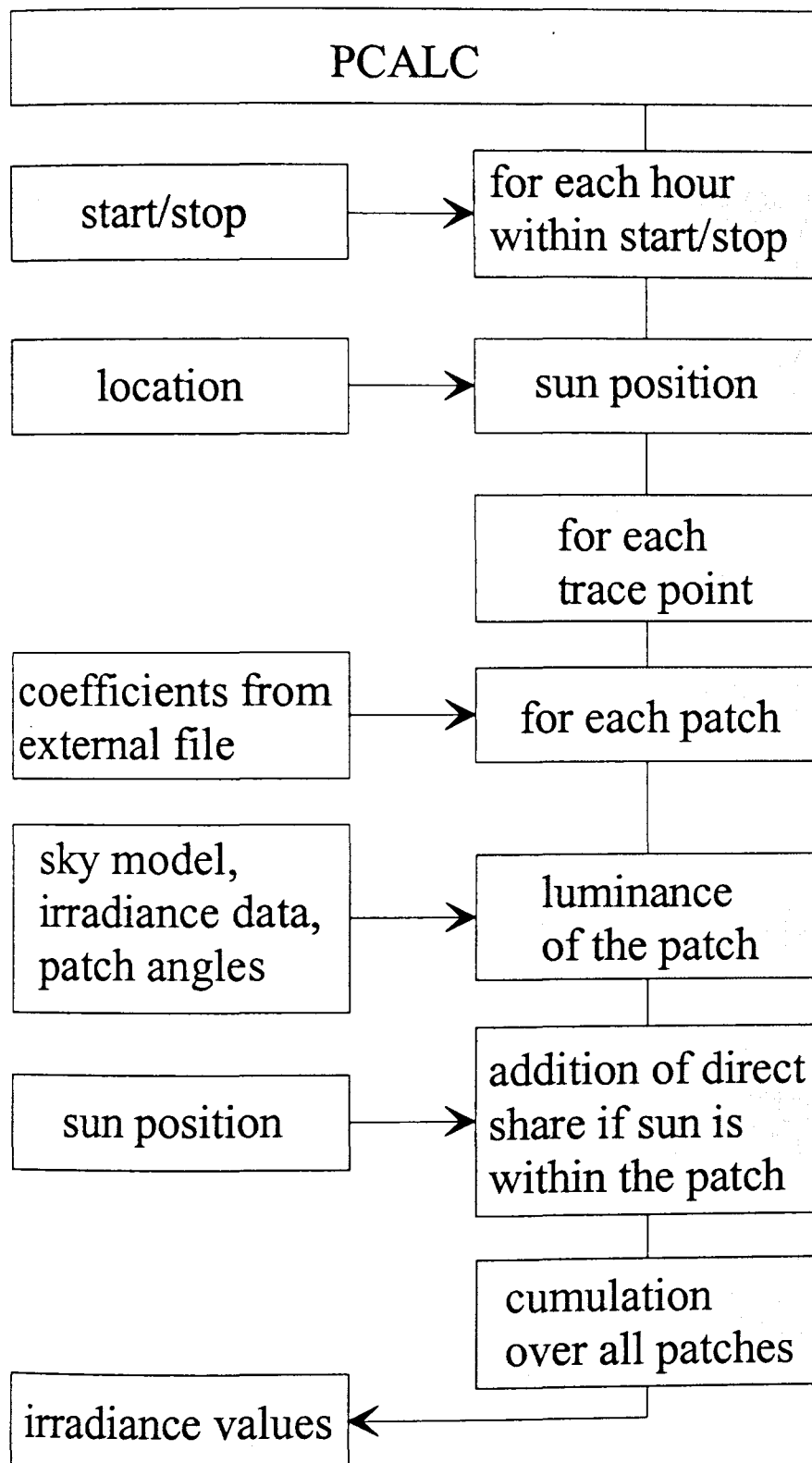


Figure 5.8
Block structure of *pcalc*,
this program does not
require RADIANCE

It should be noted that, in contrast to *pcoef*, this program does not require RADIANCE. Furthermore, it can also use coefficients generated with any program as long as the zenith and azimuth angles are stored within the file and the format is met. Then, a scaling of the coefficients as described in Chap. 5.2.2.2 might be necessary. The block structure of the program is given in Fig. 5.8.

5.3 IPROCESS

The algorithms and computer codes that were described in Chap. 5.2 enable a time-varying calculation with RADIANCE. However, the input of parameters via a command line and control files are not very user friendly. Modern software offers menu-driven, self-explaining input. A ‘visual’ computer language like Visual Basic [128] is usually used.

Therefore, the program IPROCESS (a block structure is given in Fig. 5.10) was written (in Visual Basic) that controls the different inputs and C programs that are required for a time-varying calculation. It is mainly a comfortable input mask (Fig. 5.9) to the codes *dcalc*, *pcalc*, and *pcoeff*, but has also some built-in features to simplify its use. These are mainly:

- a database with the location of different sites that be extended by the user
- an aid to place the trace points in a visualised scene and to generate a *coordinates file*
- a converter to convert files of a different output format into each other.

Figure 5.9
Main menu
of
IPROCESS

Further, access to the ADELIN program *dxconv* (Chap. 5.1.2) is enabled to convert a DXF file (usually generated with AutoCAD) into a RADIANCE scene description. A block diagram of the structure of IPROCESS is given in Fig. 5.10. More details of the program can be found in the manual (Appendix E).

5.3.1 Coordinates files

The coordinates file contains the 3D-coordinates of the points of interest (trace or sample points), where the irradiance is to be calculated. For the subsequent calculation of the annual yield of a PV generator (e.g. with PVcad) or wiring optimisation (with PVEPO) the trace points are to be placed in the centre of each module. For a detailed shading study, e.g. shading of a module by a rod (Fig. 5.11), the trace points can be also placed in the centre of each single cell. The results of such an irradiance calculation will usually be fed into INSEL, for a static analysis or to compute the yield of one selected day.

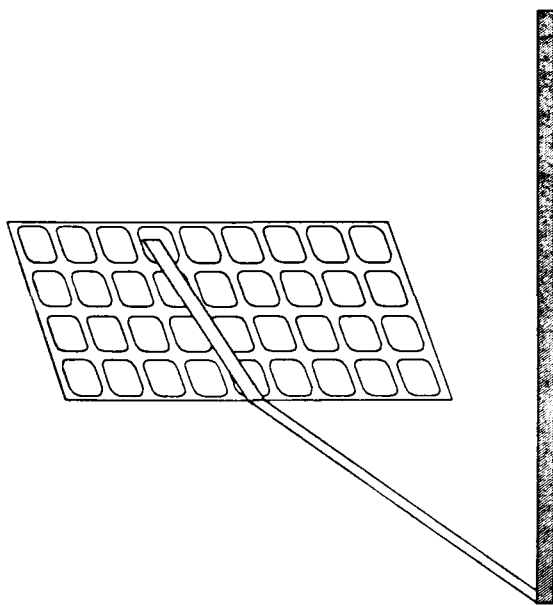


Figure 5.11
Shading of a PV module by a rod.

The coordinates file must contain the location of the trace points and the view direction. The latter is a vector in the direction of the half-dome from where the irradiance is to be calculated. This is generally the surface (or PV module) normal. Thus, six data are required for each sample point, three for the coordinates and three for the direction. The *Create coordinates file* sub-menu (Fig. 5.12) of IPROCESS assists the visualised input of the data.

The four buttons *With VIEW - Including trace points - With OBJVIEW - Including trace points* will visualise the scene with or without existing trace points, respectively, that are given in the coordinates file. Existing trace points are displayed as arrows in different colours (Fig. 5.13). The buttons use different options and, depending on the scene size and

its complexity, either can work better. The difference between the two options is that for the visualisation *with VIEW* a sun and a sky according to

```
gensky 6 6 15 +s -R 100 -B 200
```

is generated and *rview* (see *rview* manual in [119]) is called with the parameters

```
-pe 0.1 -vp 0 -10 10 -vd 0 1 -0.5 -vv 70 -vh 70
```

(-pe: exposure, -vp: view point, -vd: view direction, -vv vertical view size, -vh horizontal view size). The visualisation *with OBJVIEW* uses the RADIANCE command *objview* (see *objview* manual in [119]) whereby some light sources and a sensible viewpoint are generated internally.

	X	Y	Z
Sample point	142	120	30
Second point	167	120	32
Third point	156	120	39

	X	Y	Z
Sample point	142	120	30
Direction	0.00000	-1.00000	0.00000

Figure 5.12
The 'Create coordinates file' sub-menu of IPROCESS

It is suggested that users visualise the scene mainly *with VIEW* and enter a sensible view point manually. The other option is useful if the user is very uncertain about the scene and when he does not know where it is located. In some rare circumstances a problem may occur when using *objview* for very large scenes. Sometimes, when the dimension of the scene exceeds about 1000 units, the rendering will not start. It helps just to scale down the scene, for example to divide each value by 10.

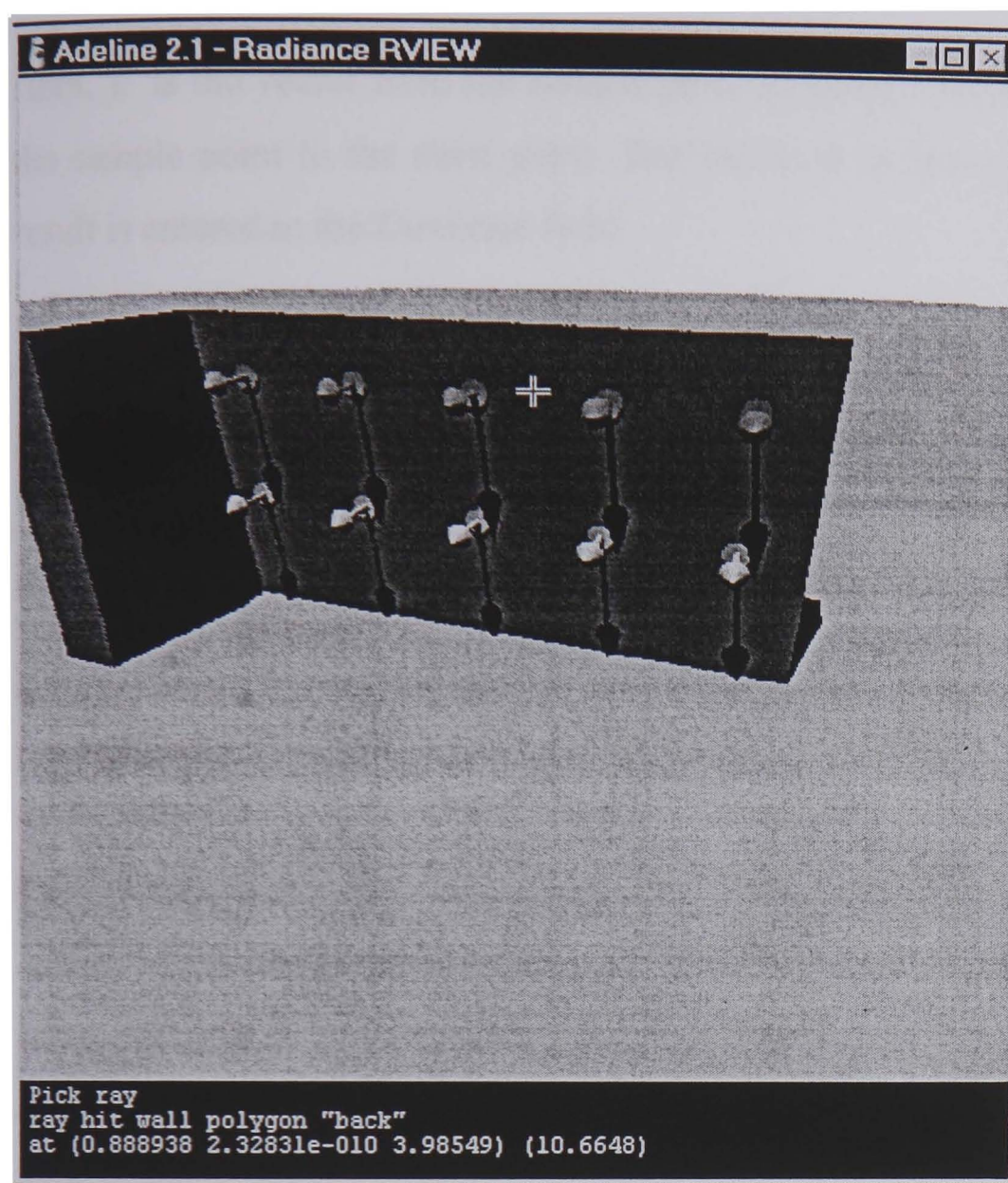


Figure 5.13
A visualised scene where existing trace points are displayed as arrows. The *t*-command displays the coordinates of the mouse in the command line. They can be entered in the create coordinates file form (Fig. 5.12) to be added to the coordinates file and to determine the surface normal.

Once the scene is visualised, the *t*-command can be used to selected any point with the mouse and display its 3D-coordinates (Fig. 5.13). They can be entered into *Enter coordinates - Sample point* box (Fig. 5.12). The same data will immediately appear under *Data written to coordinates file - Sample point*.

If the surface (or PV module) normal is known the vector can be entered under *Direction*. Otherwise, two further points on the plain can be located and entered anticlockwise under *Second* and *Third point*. Then the normal vector \vec{n} is calculated according to the cross product (Equ. 5.8) [129]. This results a vector that is perpendicular to the plane defined by the two vectors.

$$\vec{a} \times \vec{b} = \begin{pmatrix} a_2b_3 - a_3b_2 \\ a_3b_1 - a_1b_3 \\ a_1b_2 - a_2b_1 \end{pmatrix} = \vec{n} \quad (5.8)$$

Here, \vec{a} is the vector from the sample point to the *second* point and \vec{b} is the vector from the sample point to the *third* point. The vector \vec{n} is then normalised (Equ. 5.9) and the result is entered in the *Direction* field.

$$\frac{\vec{n}}{|\vec{n}|} = \frac{\vec{n}}{\sqrt{n_1^2 + n_2^2 + n_3^2}} \quad (5.9)$$

If the data are correct they can be added to the coefficients file by pushing the *Add data to coordinates file* button. The user should take care that the sample point is not falsely hidden closely behind the surface. This may happen due to rounding errors. It is always recommended to place the point slightly in front of the plain.

The RADIANCE *rview* commands (see *rview* manual in [119]) allow one to ‘move’ around in the visualised scene to look at different details and to find the surface where a sample point is to be placed. The most important ones in this context are *aim*, *move*, *rotate* and *view*.

5.3.2 RTRACE options

IPROCESS uses the RADIANCE program *rtrace* to calculate the irradiance values. Several options and parameters can be set in the program to optimise the calculation speed and the accuracy. Within IPROCESS, three parameter sets were predefined to enable a *fast*, *accurate*, or *detailed* calculation of irradiance values in an urban environment. These refer to the following *rtrace* parameters:

- fast: aa 0.4, ab 1, ad 32, ar 16
- accurate: aa 0.4, ab 2, ad 64, ar 16
- detailed: aa 0.3, ab 3, ad 128, ar 64

All other parameters were set to the default (Appendix C.2). The dependency of calculation speed and accuracy on the different parameters and how the above given parameter sets were derived is examined in Chap. 6. For special purposes it is also possible to enter user defined parameters. Then, care should be taken that the parameter *-I* is entered if the irradiance is to be calculated.

5.3.3 Converter

The menu item *Converter* allows conversion of output files from the formats *standard*, *no header*, *PVcad* or *PVEPO* to the formats *PVcad*, *PVEPO* or to a file with *Summarised data* (Fig. 5.14). This is helpful if a file is generated for example in the ‘*standard*’ format but should be used as input to *PVcad*.

If an output file is converted to *Summarised data* a file will be created where all the irradiance values for one trace point are totalled for the given time interval. By this, the (e.g. annual) irradiance on a facade can be visualised. For the example given in Fig. 5.15 100 trace points were equally distributed over a facade in a 10 x 10 matrix. The irradiance at the trace points for January was calculated and the results converted as described above.

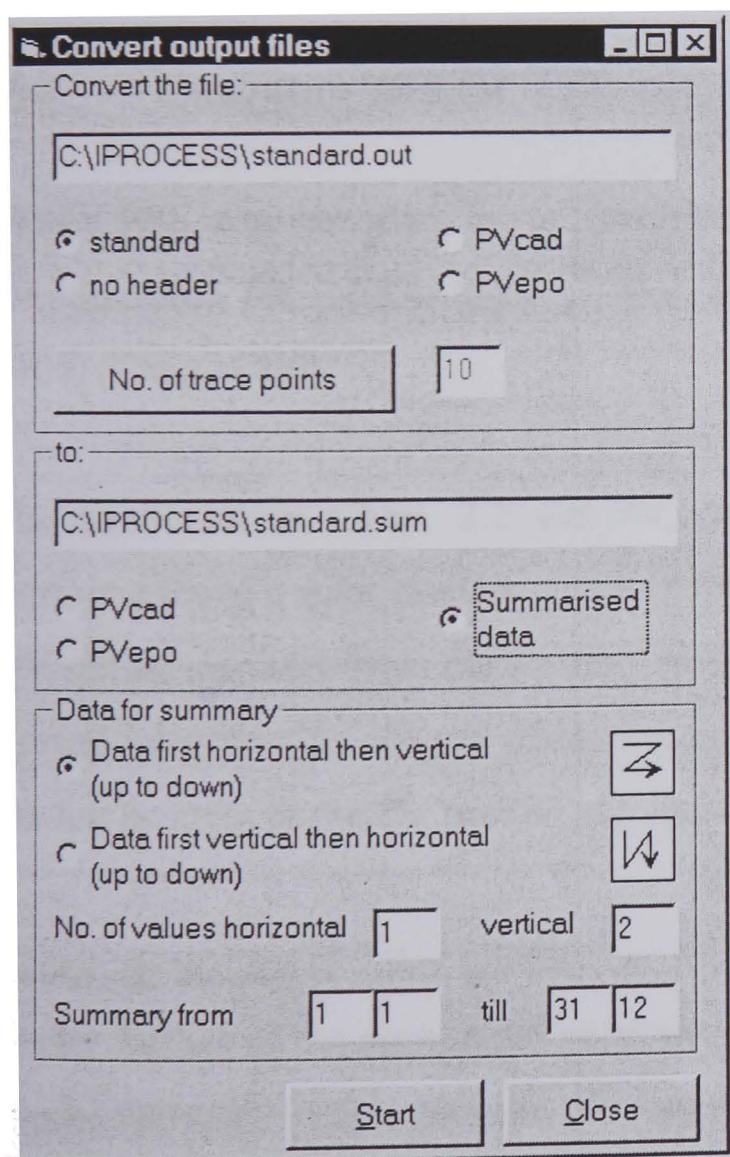


Figure 5.14
The ‘Create coordinates file’ form of IPROCESS

The resulting file can be displayed with standard software such as EXCEL (EXCEL was used for Fig. 5.15). Images like this give a first and rough impression of ‘dark’ corners of a facade and an overview where PV modules can be placed advantageously.

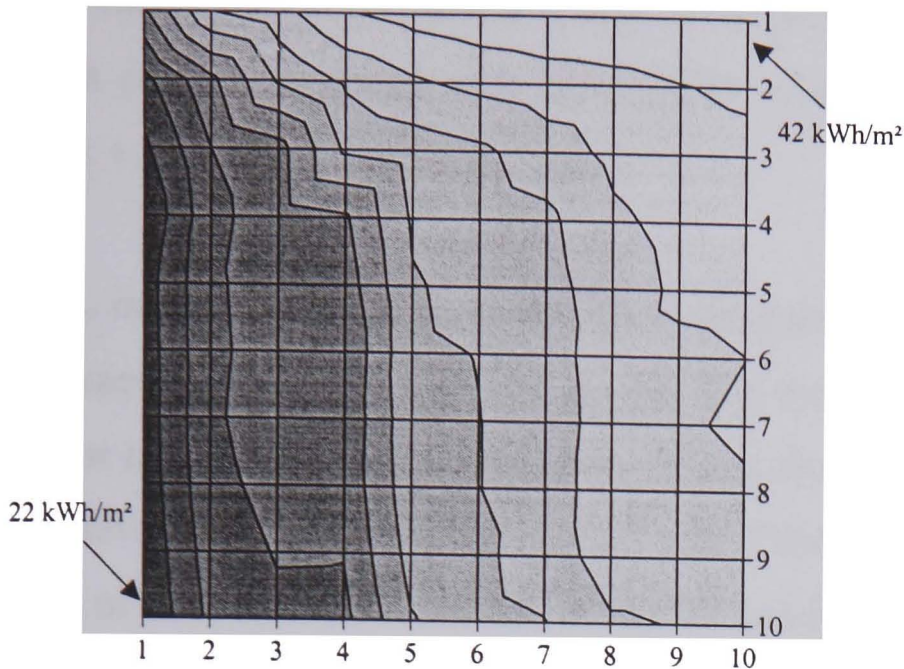


Figure 5.15
*Determination of
 'dark' corners of a
 facade using the
 Summarise data
 option*

In the *convert output file* sub-menu it must be specified how many trace points were used, in how many rows and columns, and how their order is in the coordinates file.

5.4 Coupling IPROCESS to further PV models

IPROCESS can be used as an irradiance pre-processor to PV models. This will be demonstrated for INSEL [104] (Chap. 4.2.2), PVcad [103] (Chap. 4.2.3), and PVEPO [106] (Chap. 4.2.4).

As mentioned in Chap. 2.2 the PV cell temperature has a major influence on the performance of a solar module. Each of the above mentioned PV models can determine the PV cell temperature from the ambient temperature (and incident radiation). Thus, this value is read from the (irradiance) input file and printed without modifications in the output file for use as input to the PV model (see Appendix E.3.3.4 for the different output formats).

Coupling to further solar models can be done in a similar way, depending on the data reader facility of the considered program. As an example, coupling to the thermal building model TRNSYS [52] is given in the Appendix D.

5.4.1 Coupling to INSEL

INSEL [104] (Chap. 4.2.2) can be used to model a PV system and to predict its yield. To consider an inhomogeneous irradiance distribution on the PV array, pre-calculated

irradiance values should be used, it is best to use a separate series of data for each module. These data can be generated with IPROCESS using the options 'no header' or 'global irradiance + temp'.

An INSEL input file according to the block diagram of Fig. 5.16 will determine the yield of a PV generator over a certain time period. The modelled generator consists of one string with two or more solar modules (or more precise *module blocks* because each block might comprise several PV modules) and one inverter. INSEL does not care if the inverter is grid-connected or stand-alone. It calculates only the power output regardless whether the power is used or not.

The *DO* block (Fig. 5.16 and 5.17) determines the number of records to be read and thus, the length of the time period. To calculate for example the January (744 hours), the *DO* loop must count from 0 to 743.

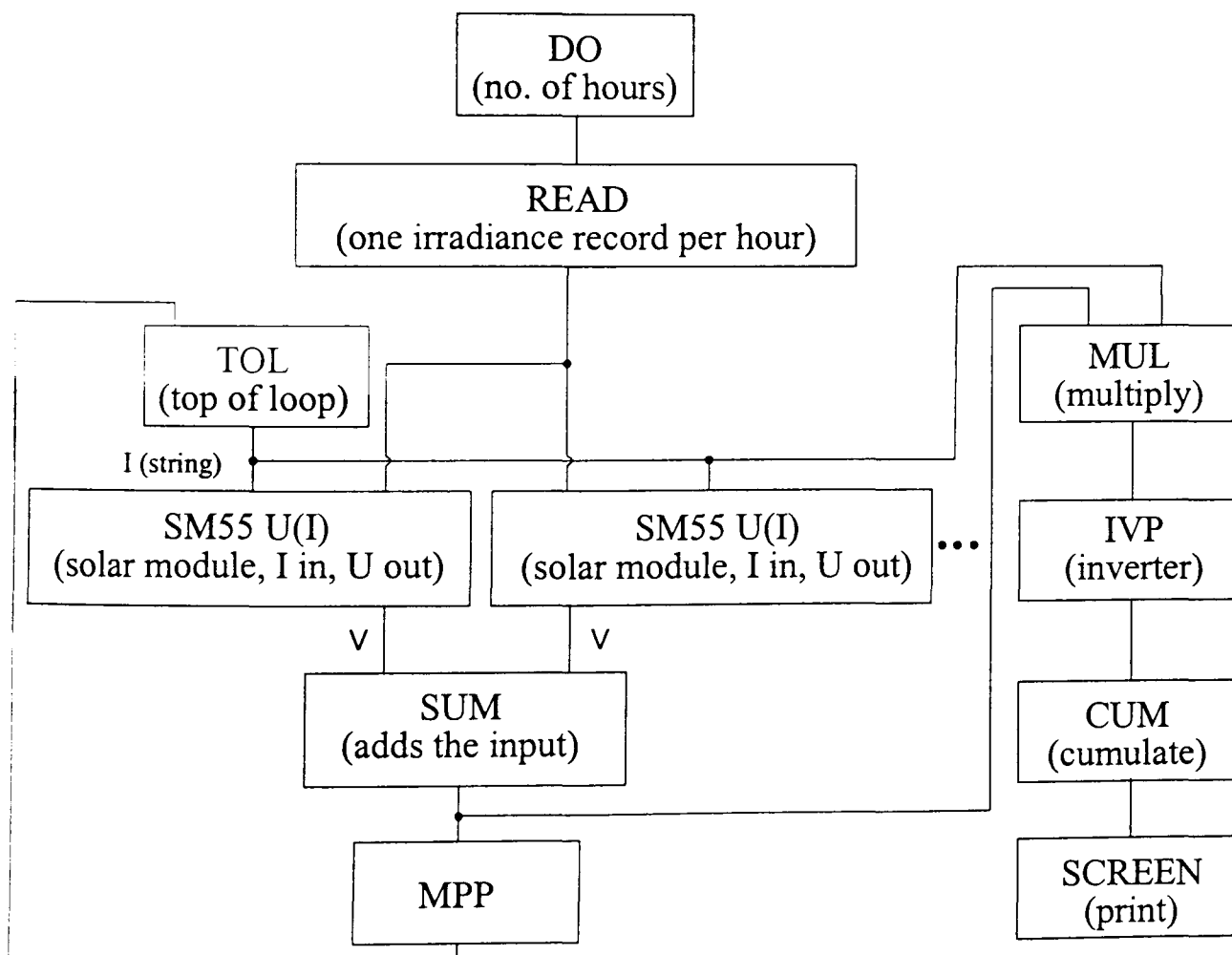


Figure 5.16
INSEL
block diagram to calculate the yield of a PV system

The irradiance file and the (FORTRAN) format of the records must be specified in the *READ* block (Fig. 5.16 and 5.17). This format assumes that all records have the same length. Several letters are used to describe the data format but X and F are sufficient to read the data.

X to skip the specified number of digits, e.g. 21X means to skip 21 digits

F to read a float number, e.g. F6.1 means to read a total of 6 digits, consisting of 4 numbers, one comma and one digit after the comma

The number of records that must be skipped at the beginning of the file must be also entered in the *READ* block. For example, to calculate the irradiance in February, 744 lines must be skipped.

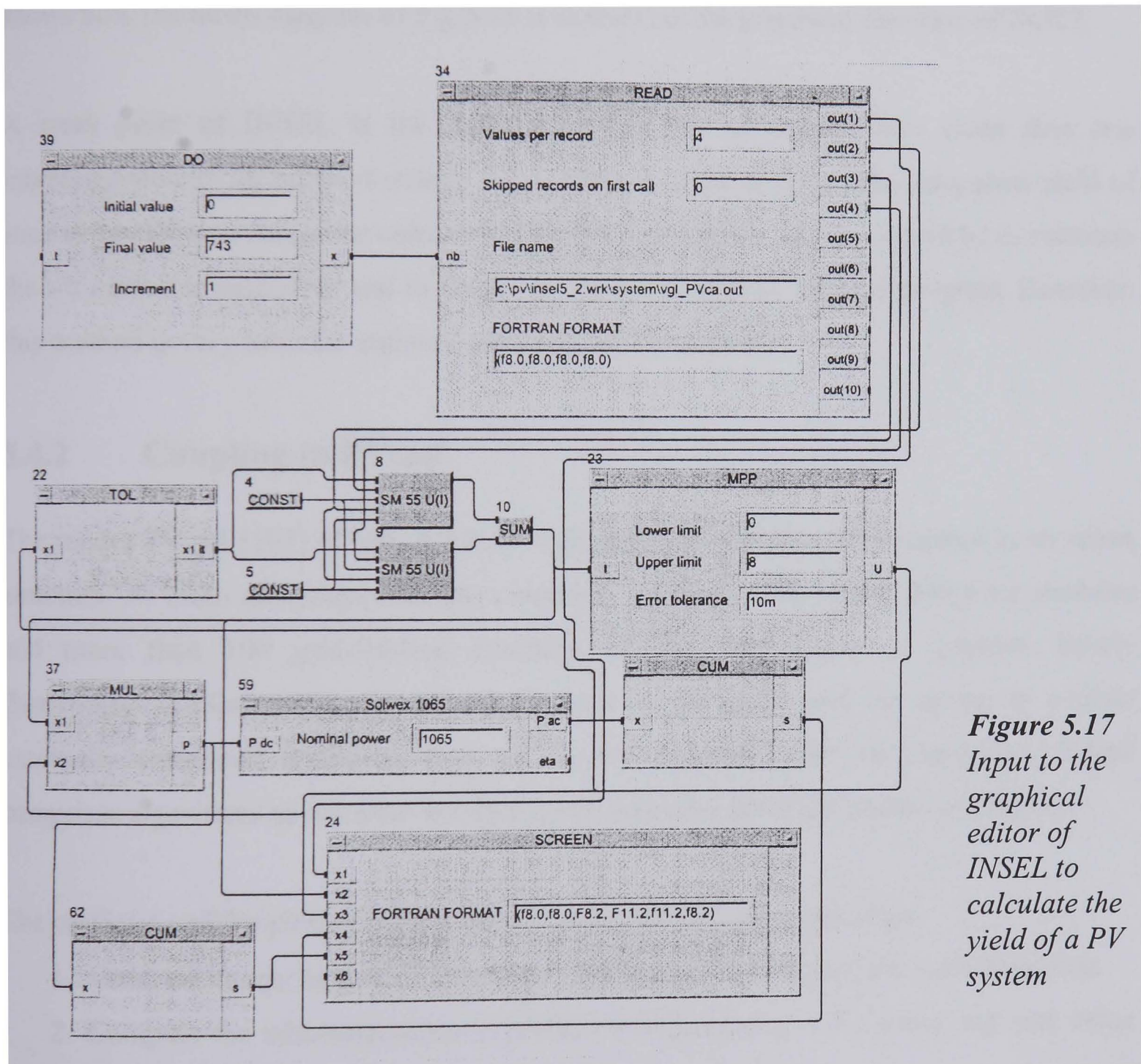


Figure 5.17
Input to the graphical editor of INSEL to calculate the yield of a PV system

The voltage-from-current block of the solar modules (*SM55 U(I)*) calculates the voltage of the PV module (type: SM 55) using the current, the irradiance, the temperature and some further data as input. The voltage of two or more modules is summed in the *SUM* block which leads to the series connection of the modules to one string. The total voltage is then fed to the *MPP* block (Maximum Power Point). It varies its output (i.e. the current input of

the modules) until the MPP is found. The *TOL* block (top of loop) is required for the internal sorting of the algorithms. Finally, the PV current and voltage at the Maximum Power Point (MPP) are multiplied by the *MUL* block and used as input to the *IVP* block that calculates the inverter losses.

The results are cumulated (*CUM* block) over the total time period and printed on the screen (*SCREEN* block). Again the FORTRAN format is used to display the results. Figure 5.17 shows how the block diagram of Fig 5.16 is realised in the graphical interface of INSEL.

A weak point of INSEL is the modelling of a PV generator where more than one inhomogeneously illuminated strings are connected to an inverter. The long-term yield of such an installation cannot be calculated directly with INSEL. A way would be to calculate the I-V curves at each hour and to determine the MPP with an external program. However, this method is very intricate and will normally not be realised.

5.4.2 Coupling to PVcad

The model PVcad [103] (Chap. 4.2.3) is well suited to simulate PV systems in an urban structure. Its main advantages are the extensive databases with nearly 300 solar modules and more than 100 grid-feeding inverters. Further, the ability to generate hourly (horizontal) irradiance data for almost any site on the globe and the option to process externally computed irradiance data on the PV modules must be mentioned. PVcad comprises algorithms to consider the shading of modules, these are studied in Chap. 6.

The prediction of the yield of a PV system can be divided into three steps.

1. Generate hourly horizontal irradiance and temperature data of the considered site.
2. Compute the inhomogeneous irradiance distribution on a PV array, e.g. one value per module.
3. Determine the (annual or monthly) yield of the PV system

PVcad can solve all these tasks. Alternatively, task 2 can be solved by IPROCESS and its results can be fed back to PVcad. Thus, IPROCESS can be coupled to PVcad to determine the long-term yield of a PV system or to evaluate its urban modelling capabilities.

PVcad comprises an extensive climate database with monthly mean values of temperature and irradiance. It is possible to generate hourly values from the database by a built-in procedure and store them in a separate file. PVcad's own SCT format is used for this file. IPROCESS has an option to read this format if the related entries are done.

A limitation of PVcad is that only the total yield is calculated. More detailed examinations where, for example, the I-V curve or the voltage of a generator needs to be evaluated, are not possible.

5.4.2.1 Input of PV array wiring

To enter the PV array wiring a comfortable graphical interface is implemented in PVcad. The modules that belong to one string can be selected with the mouse and then several strings can be connected to one inverter. Fig. 4.3 shows a screen image of this interface.

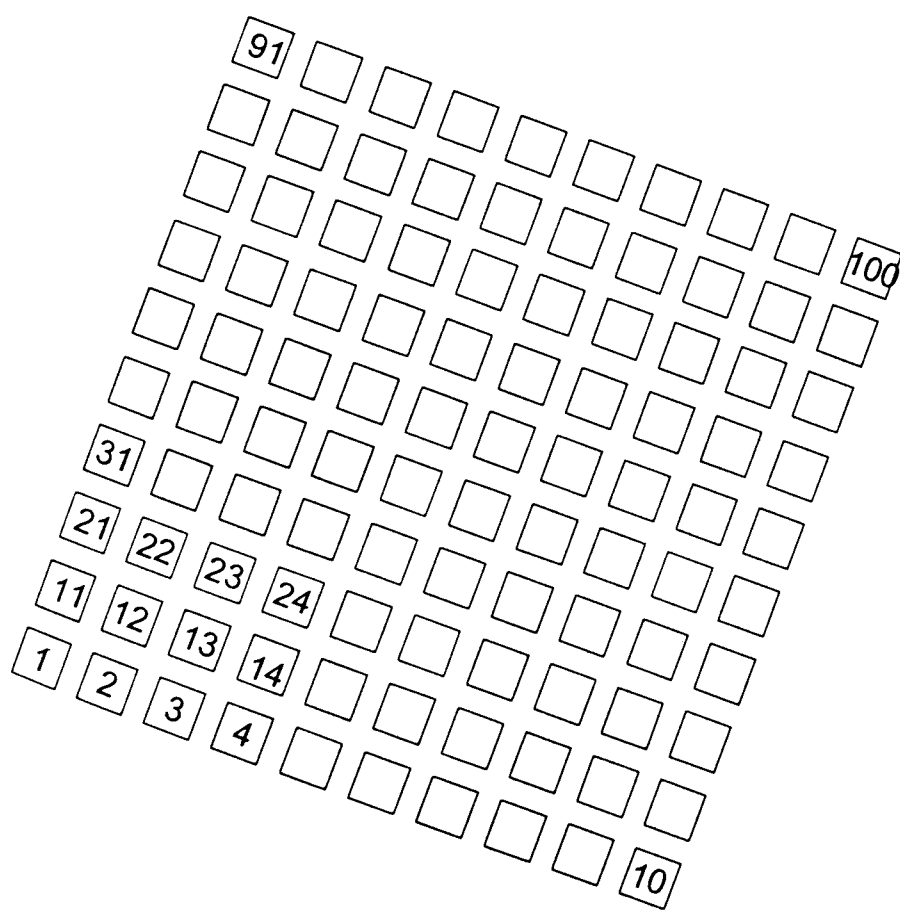


Figure 5.18
Entering the properties and the wiring of a solar generator in PVcad using the 100_mod.egb file that is supplied with IPROCESS.

However, this interface requires that the building and the objects are entered as a DXF file, usually generated with a 3D CAD program. If a PV system designer is not accustomed to such a program this might be a significant hindrance. To simplify the use of PVcad in connection with IPROCESS, the file, 100_mod.egb, is included to IPROCESS. This file

contains the (DXF) description of a PV array of 10 x 10 modules (Fig. 5.18) that was converted to the PVcad format (*.egb).

This file can be loaded in PVcad instead of a building description and can be used to wire the PV array. Each square represents one solar module. For example, to create an array with 15 PV modules in three strings, the squares 1-5, 6-10, and 11-15 are to be selected. Square one references to the first irradiance value in the output file of IPROCESS, square two to second, and so on.

5.4.3 Coupling to PVEPO

PVEPO [106] (Chap. 4.2.4) is a program to determine the optimised wiring of a PV array. As input, it requires hourly irradiance data for the considered time interval, one series of data for each module. To produce these data with IPROCESS, the option *output for PVEPO*, must be chosen. A simulation with PVEPO for a real design project is discussed in the following example.

A solar generator comprising of two arrays with 50 solar modules each was to be installed on the roof of an historical building (Fig. 5.19). Due to the statuettes in the foreground and the towers on the left and the right, the PV array would be inhomogeneously illuminated. The wiring of the arrays needed to be optimised. For this, the roof and the relevant building parts were modelled with RADIANCE, and the irradiance on each module calculated with IPROCESS.

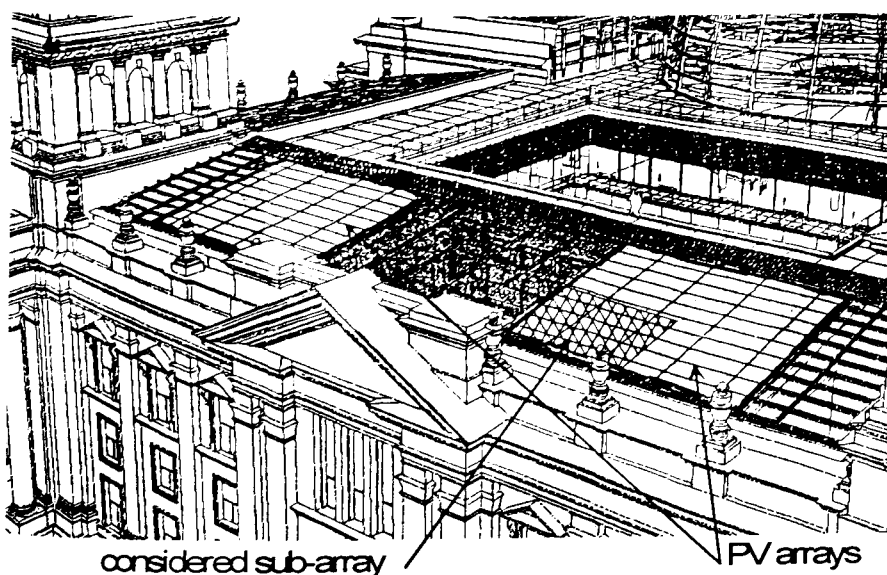


Figure 5.19
Historical building with two PV arrays, each 50 modules. The wiring shall be optimised with PVEPO.

First, only the sub-array as indicated in Fig. 5.19 and 5.20 was examined. The sub-array consists of 15 modules, to be wired in three strings. The irradiance data for January were used as input to PVEPO to optimise the arrangement.

Intuitively, a system designer would wire the five modules of one column into one string (Fig. 5.21a). Starting from this configuration, PVEPO improved the wiring gradually (Fig. 5.21b-c). The final version achieved a 5.4% higher yield than the intuitive version. However, a disadvantage is the high expenditure for the cabling. It is in the responsibility of the system designer to weigh the higher performance against the more complicated wiring.

10	20	30	40	50
9	19	29	39	49
8	18	28	38	48
7	17	27	37	47
6	16	26	36	46
5	15	25	35	45
4	14	24	34	44
3	13	23	33	43
2	12	22	32	42
1	11	21	31	41

Figure 5.20

The right-hand PV array of the historical building with the part where the wiring is to be optimised

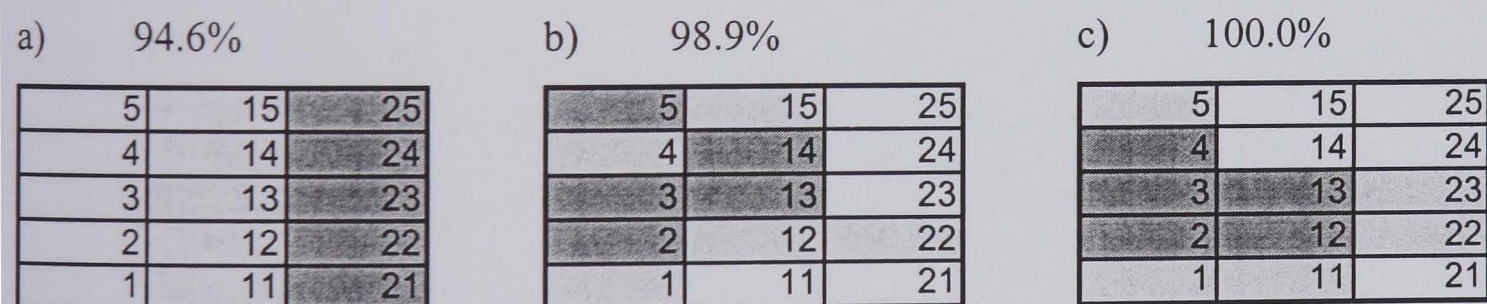


Figure 5.21 *PVEPO improved the wiring gradually of the sub-array starting from the left configuration. Modules indicated by the same colour form one string. The given percentages states the relative yield in January.*

In a second simulation, both PV arrays (of Fig. 5.19) and the yield for a complete year were considered. Then, energy gains due to different wirings were below 0.5%. The reason for this was that most of the energy is yielded in summer when the sun altitude is very high. Then, hardly any shading occurs on this sample and the array obtained an almost homogeneous irradiance. Thus, no gains due to optimised wiring could be achieved. Also,

the irradiance levels are much higher, so the significance of the January results is less than that suggested by the 5.4% difference.

5.4.4 Conclusions

Coupling of IPROCESS to further PV models was introduced in this chapter. Usually, the different models are applied for different tasks. INSEL, to look at details such as the current flow in a shaded PV array or to study the effect of shading on the PV module (hot-spot).

PVEPO can predict the long-term yield of a PV generator under consideration of different wiring options. However, since the inverter database is limited, it will mainly be used for comparative studies using one inverter type only.

The array wiring, determined either with PVEPO or defined by other methods, will be fed into PVcad for long-term yield predictions. PVcad is preferred for such tasks because of its comprehensive database of PV modules and inverters.

6 TIME DEMAND AND ACCURACY

Two approaches to predict the time-varying irradiance in an urban environment were introduced in the previous chapter and were realised in the computer code, IPROCESS (Chap. 5.3). Both approaches, the direct calculation and the sky patch approach, will be examined in the following section with special regard to the time demand and the (relative) accuracy. Both are influenced by varying the simulation parameters (RTRACE options see Chap. 5.3.2). The aim is to find an optimum parameter set for maximum speed at reasonable accuracy.

6.1 Simulation parameters

The two RADIANCE [113] programs *oconv* (to build the RADIANCE *octree*) and *rtrace* (to actually calculate the results) are used for the time-varying irradiance calculations and require most of the computation time. Normally, it would be necessary to build a new octree for each new sky radiance distribution, but *oconv* allows splitting up of the building of the octree into several stages. Thus, the octree of the scene can be built once and then reused for the single time steps (this is illustrated in Fig. 5.1 and 5.6). The octree of the different skies is added at the time steps. This reduces the time demand of the computation of complex scenes significantly, for example to one third for the annual calculation of scene (E) in Chap. 6.2. Further accelerations with *oconv* are hardly possible, and most of the total computation time is required by *rtrace*. Thus, the following discussion is limited to the *rtrace* parameters. They can be modified in the 'RTRACE options' box in the IPROCESS main menu (Fig. 5.9) or in the corresponding line of the control file (Tab. 5.2).

The parameters having the most significant influence on the time demand and the accuracy in calculating the irradiance in an urban environment are: ambient accuracy (aa), ambient

bounces (*ab*), ambient divisions (*ad*), and ambient resolution (*ar*). These are explained, following. The contents of the RADIANCE manual [120] is given in Tab. 6.1.

Name	Parameter	Description
aa	ambient accuracy	This value will approximately equal the error from indirect illuminance interpolation. A value of zero implies no interpolation.
ab	ambient bounces	This is the maximum number of diffuse bounces computed by the indirect calculation. A value of zero implies no interpolation.
ad	ambient divisions	The error in the Monte Carlo calculation of indirect illuminance will be inversely proportional to the square root of this number. A value of zero implies no interpolation.
ar	ambient resolution	This number will determine the maximum density of ambient values used in interpolation. Error will start to increase on surfaces spaced closer than scene size divided by the ambient resolution.

Table 6.1 Most significant rtrace parameters on time demand and accuracy, calculating the time-varying irradiance in an urban environment

The parameter *ambient bounces* (*ab*) defines the maximum number of diffuse bounces that are computed by the indirect calculation. For example, a value of $ab = 0$ means that only the irradiation that come directly from the sun is considered. A value of $ab = 1$ includes the diffuse irradiation from the sky, the direct irradiation from the sun, and all direct irradiation that is reflected at one surface only.

The parameter *ambient divisions* (*ad*) defines how many rays are sent out from the trace point in the hemisphere that is defined by the view direction (Chap. 5.3.1). More rays will lead to a higher accuracy.

The *ambient resolution* (*ar*) limits the maximum distance between cached values that are used for the interpolation of the ambient calculation. The higher the value, the larger is the distance and thus, the error increases.

The *ambient accuracy* (*aa*) limits the error of the indirect irradiance interpolation. Smaller values result in closer spacing of indirect calculations, at a commensurate cost [113].

Several optimisation algorithms are applied within RADIANCE. Thus, there is no general correlation between the parameter value and the resulting computation time. This depends on the rendered scene itself, its size, the distance between the objects and the number and position of the trace points. The RADIANCE manual [119] states the general correlation as given in Tab. 6.2.

Name	Effect on calculation time	Min.	Default	Max.
aa	direct, doubling this value approximately quadruples rendering time	0.5	0.2	0*
ab	direct, doubling this value can double rendering time	0	0	8
ad	direct, doubling this value may double rendering time	0	512	4096
ar	direct, effect depends on scene, can quadruple time for double value	8	128	0*

* *disables optimisation*

Table 6.2 *Effects of the parameters on computation time, and minimum, maximum, and default values*

6.2 RADIANCE scenes used for testing

The influence of the four above described parameters *aa*, *ab*, *ad* and *ar* on the time demand and the accuracy was examined at different scene descriptions. Typical arrangements of houses in an urban environment as described under (A - E) were used.

(A) A scene with an L-shaped house as shown in Fig. 6.1. However, the complete building was not modelled but only the two front surfaces, relevant for the irradiance at the sample points (RADIANCE scene size 120, two surfaces, seven trace points).

(B) The same arrangement as (A) but with one additional wall that has no influence on the irradiance at the sample points. (RADIANCE scene size 120, three surfaces, seven trace points).

- (C) Two opposed houses as shown in Fig. 6.2. Similar as for (A), only the two relevant (inner) surfaces were modelled (RADIANCE scene size 120, two surfaces, seven trace points).
- (D) The same arrangement as for (C) but with one additional wall, again without influence on the irradiance at the trace points (RADIANCE scene size 120, three surfaces, seven trace points).

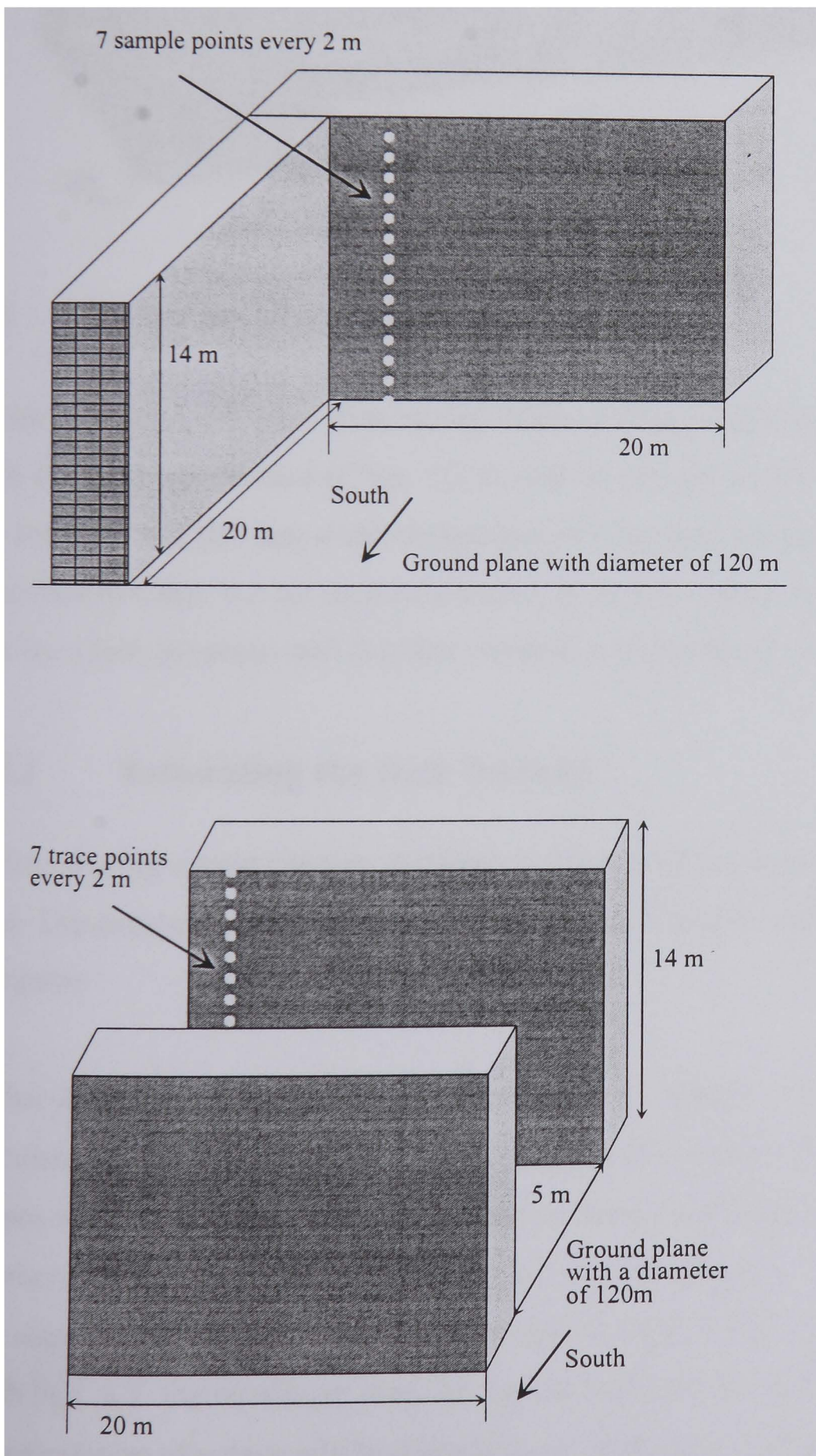


Figure 6.1
L-shaped house to test time demand and accuracy

Figure 6.2
Opposing houses to test time demand and accuracy

(E) The complete scene description of the campus of the De Montfort University in Leicester as shown in Fig. 6.3 (RADIANCE scene size 507, very complex scene with more than hundred surfaces, two trace points).

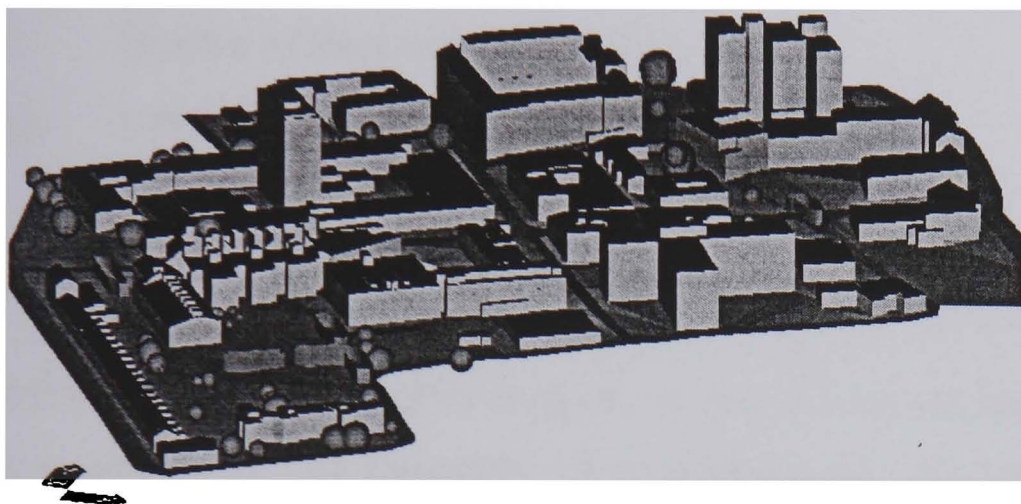


Figure 6.3
Campus of the
De Montfort
University (DMU)
to test time demand
and accuracy

6.3 Using the *direct* method

In the following sections, first, a fast method to generally predict the total computation time of the *direct* method (Chap. 5.2.1) will be presented. Then, it will be examined how the accuracy and the time demand depends on the *rtrace* parameters. For this, the scenes as described in Chap. 6.2 are used as samples. A recommendation of three different parameter sets for a *fast*, *accurate*, and *detailed* simulation is presented in the end.

6.3.1 Estimating the time demand

Before starting a long-running calculation it is of interest to know how long it will take in total. Depending on this, the computation can be executed during the night or on a spare computer.

A fast and easy method exists to estimate the maximum time demand of a time-series calculation since it is nearly linear-dependent on the number of considered days (at least at scenes with a ‘normal’ complexity). The maximum time demand for the calculation of any number of days can be estimated from the time demand for one sample day. This sample day should have 12 hours daylight, thus, usually the 80th day, i.e. 21 March, will be chosen. With Equ. 6.1. the maximum time for the calculations of n days can be estimated. Usually, the calculation of n days will be slightly faster than given in Equ. 6.1 since the scene *octree*

is built only once for a simulation, regardless if one day or one year is to be calculated (Chap. 5.2.1).

$$t_{n \text{ days}} \approx t_{80} \cdot n \quad (6.1)$$

n number of days to be calculated

t_{80} time demand for the calculation of the 80th day

6.3.2 Time demand depending on the parameters

The influence of the parameters as given in Tab. 6.1 on the time demand was studied for the arrangements (A - E). Generally, all parameters were set to their defaults as given in the App. C.2 and only the considered parameter was varied. However, the *ambient bounces* were set to *ab 2* because the default value *ab 0* neglects the diffuse irradiance from the sky. The computation times as given in Figures 6.4-6.7 refer to the calculation of one day with 12 hours daylight (24 March) and using a PC with a Pentium 133 MHz processor and 48 MB RAM.

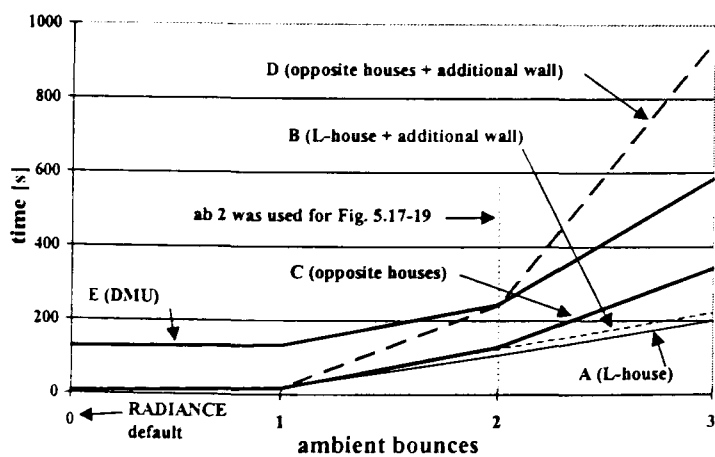


Figure 6.4 Time demand for one day varying *ab*

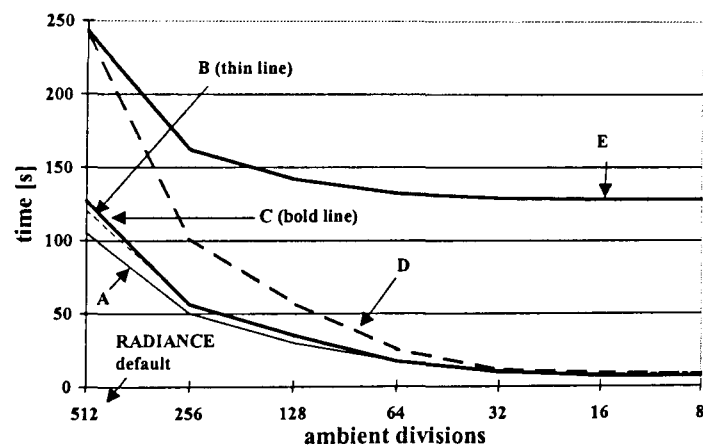


Figure 6.5 Same as Fig. 6.4 but varying *ad*

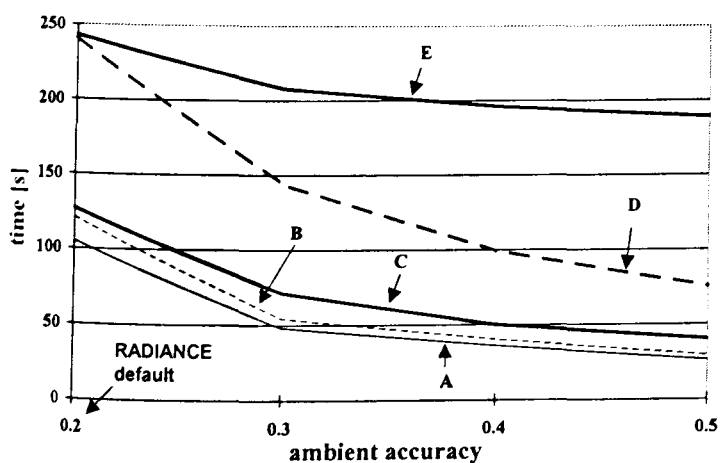


Figure 6.6 Same as Fig. 6.4 but varying *aa*

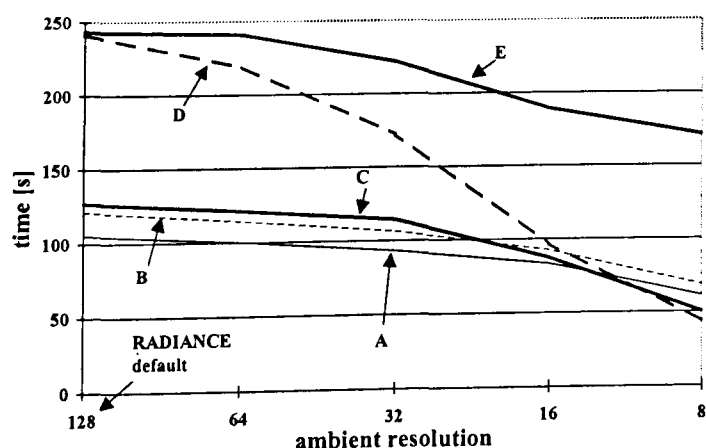


Figure 6.7 Same as Fig. 6.4 but varying *ar*

Because of the implemented RADIANCE optimisation algorithms, the correlations as given in Tab. 6.2 are not always valid here. The diagrams show that the parameters have a significant influence on the time demand and, further, that just one additional surface can more than double the calculation time. Thus, the parameter values should be chosen carefully, and the scene should contain relevant surfaces only in order to accelerate the computation. However, to erase the unused surfaces would demand a considerable effort by the user.

From the results as shown in Figures 6.4-6.7, it was empirically concluded to continue the examinations using the parameters: *aa* 0.4, *ab* 2, *ad* 64, and *ar* 16. At these parameters, there seems to be no further acceleration possible because the curves reach an asymptotic level. However, *ab* was left at a value of 2 to include the albedo (Chap. 3.2.4).

The above described calculations were repeated for the arrangements (A), (C), and (E) with the new parameter set. The time demand using these values was compared to the time required with the default setting (and *ab* 2) and is given in Tab. 6.3. It must be noted that the minimum computation time with an empty scene and a very low parameter setting is about 7 seconds for one day. Thus, the time demand using the parameter values *aa* 0.4, *ab* 2, *ad* 64, and *ar* 16 can hardly be further reduced.

Parameter	L-house	opposing houses	DMU
ab 2, rest default	106 sec	124 sec	243 sec
aa 0.4, ab 2, ad 64, ar 16, rest default	9 sec	9 sec	131 sec

Table 6.3 Time for the calculation of one day using different parameters values

The time dependencies simulating scene (C), using the new parameter set (*aa* 0.4, *ab* 2, *ad* 64 and *ar* 16) as basis and varying only the considered parameter are shown in Figures 6.8-6.11. Here not just one day but the all values for the complete month April were calculated.

The shapes of these curves resemble very much the ones given in Figures 6.4-6.7. This shows that the principal correlation between the time demand and the value of one

parameter is more or less independent from the setting of the other parameters, at least in this application.

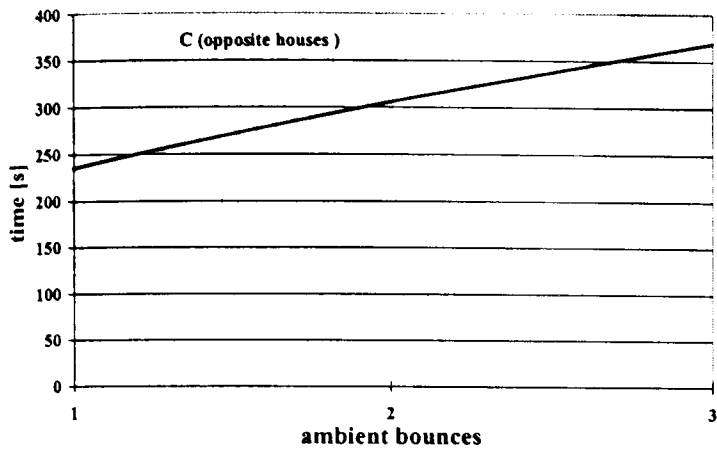


Figure 6.8 Time demand for one month using the 'new' parameter set, varying ab

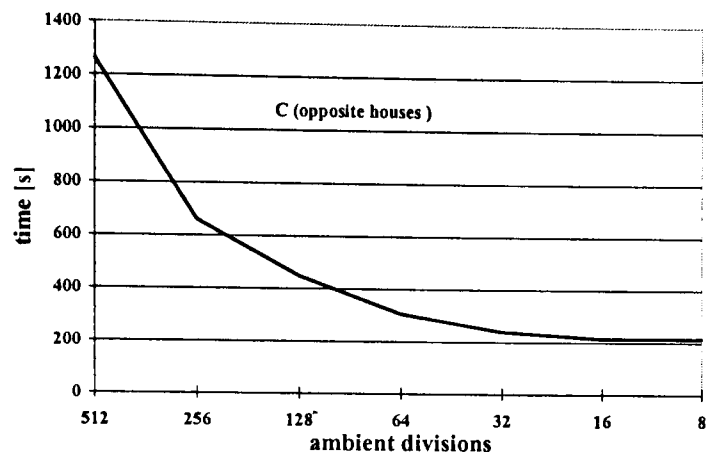


Figure 6.9 Same as Fig. 6.8 but varying ad

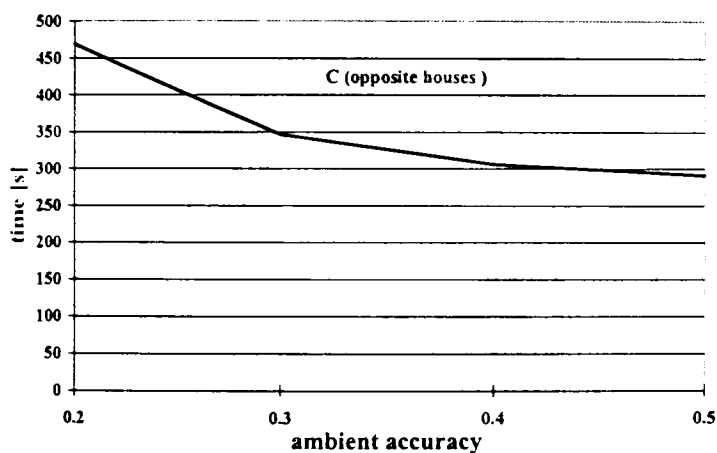


Figure 6.10 Same as Fig. 6.8 but varying aa

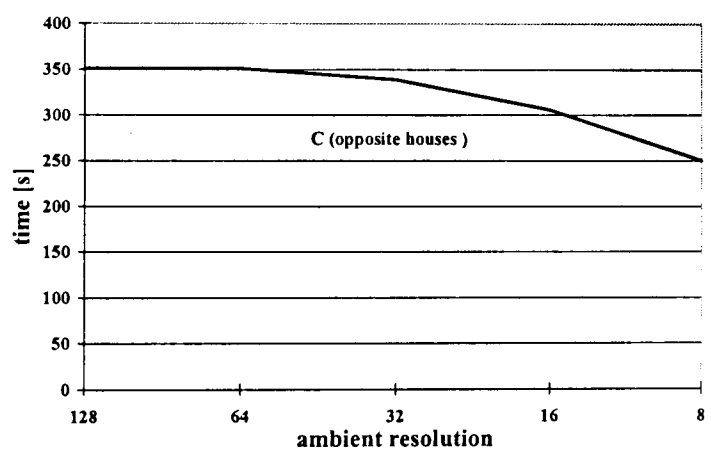


Figure 6.11 Same as Fig. 6.8 but varying ar

It should be noted that storage resistant programs like the screen saver can increase the time demand significantly. These programs should be switch off before using IPROCESS.

6.3.3 Time demand depending on the number of trace points

There is no linearity between the number of trace points and the time demand. This depends on the scene, the placement of the trace points and the parameter values, especially the value of aa . The results as shown in Tab. 6.4 were achieved by using the parameters: aa 0.4, ab 2, ad 64, ar 16 and calculating one day¹.

¹ Because of uncontrolled circumstances the time may vary by some seconds.

It can be seen that the time demand increases only very slightly with an increasing number of trace points. Thus, it is suggested to calculate the time series of irradiance values at all trace points at a single IPROCESS run to enable the RADIANCE optimisation algorithms.

Number of sample points	opposing houses	DMU
2	8 sec	131 sec
5	9 sec	133 sec
7	10 sec	131 sec
20	11 sec	135 sec

Table 6.4 Time demand, dependent on the number of trace points at aa 0.4, ab 2, ad 64, ar 16

6.3.4 Accuracy of single values

In this section, the accuracy of the single values (i.e. at one time step only) will be examined. For the 'L-house' and the 'opposite houses' the seven sample points (as shown in Figures 6.1 and 6.2) were used and two arbitrarily chosen sample points within the 'DMU scene'. Different hours during one day (24 March) were considered to account for different sun positions. However, values smaller than 40W/m^2 were removed from the records because they have a small influence (on the yield of a PV system) only.

It is expected that the deviation of the single values will generally be larger than the deviation of cumulated values since possible errors (at the single time steps) are both positive and negative. Thus, they may compensate each other to a certain degree. When modelling a PV system in an urban environment, usually the system yield during a certain time period is of interest. The yield is calculated cumulating the results at the single time steps over the considered time period. However, the accuracy of the single values will be examined here to provide a basis for the following examinations of the cumulated values.

The accuracy of the calculation of single values was studied for the arrangements (A), (C), and (E). The irradiance at the trace points was calculated and the single results were compared with each other. The irradiance that was returned using the default values for the parameters (and *ab* 2) was generally used as reference (deviation = 0). Only the reference irradiance to examine the dependency on *ab* was achieved with *ab* 3.

Figures 6.12-6.15 show the relative (to the reference value as described above) deviation of the irradiance at the trace points using the above mentioned parameters. It was found that:

- the results converge (to the results achieved with the default setting), so that the difference becomes very small (except *ab* that will be discussed in Chap. 6.3.5) when the parameters approximate the defaults. It is noted that the default settings lead to very accurate results because RADIANCE is able to calculate accurately at defaults (see discussion in Chap. 7.3.5).
- high deviations occurred only when a low irradiation was predicted. However, these values will be of minor significance at a time-series calculation (Chap. 6.3.5).
- a deviation of up to 100% occurs at *ab* 0. This happens when the input irradiance is purely diffuse. The setting of *ab* 0 neglects the diffuse irradiation and will then predict an irradiance of zero, so a deviation of 100%.

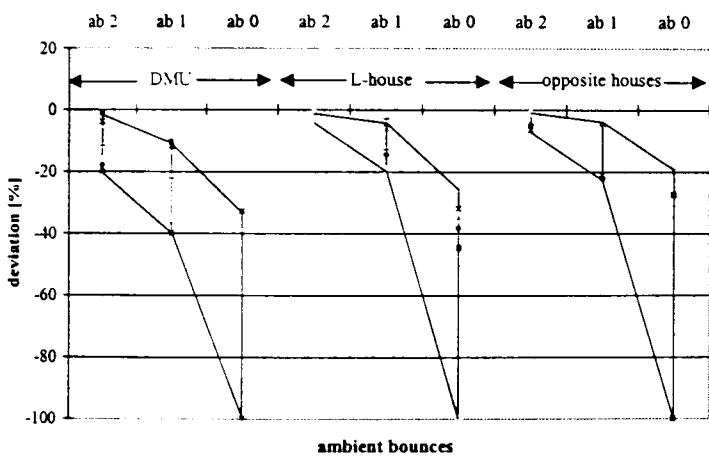


Figure 6.12 Accuracy of the 7 single values (Fig. 6.1 and 6.2) varying *ab*

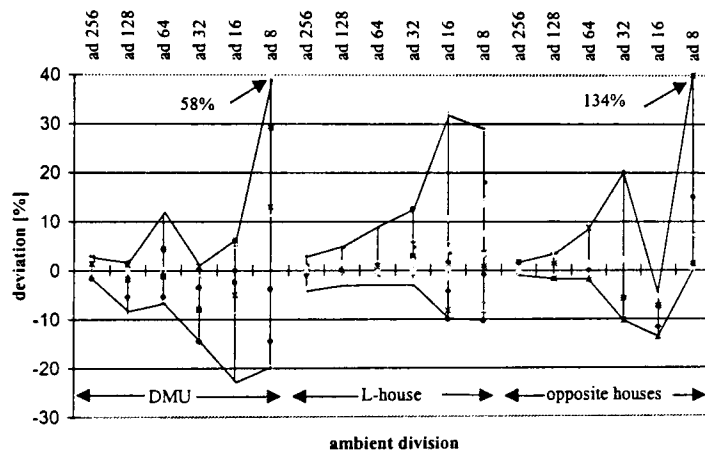


Figure 6.13 Same as Fig. 6.12 but varying *ad*

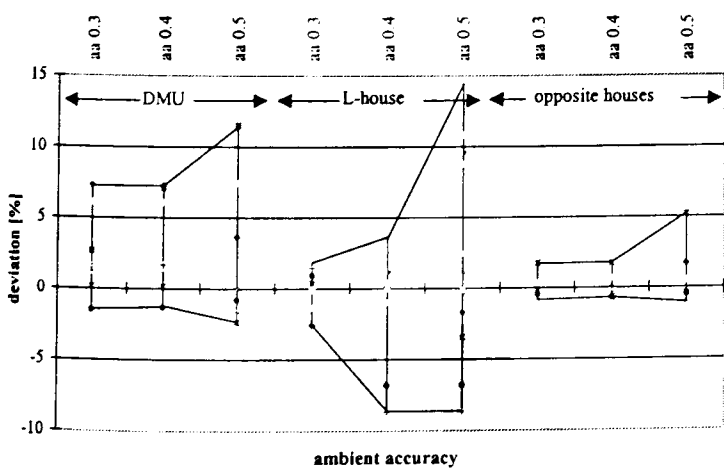


Figure 6.14 Same as Fig. 6.12 but varying *aa*

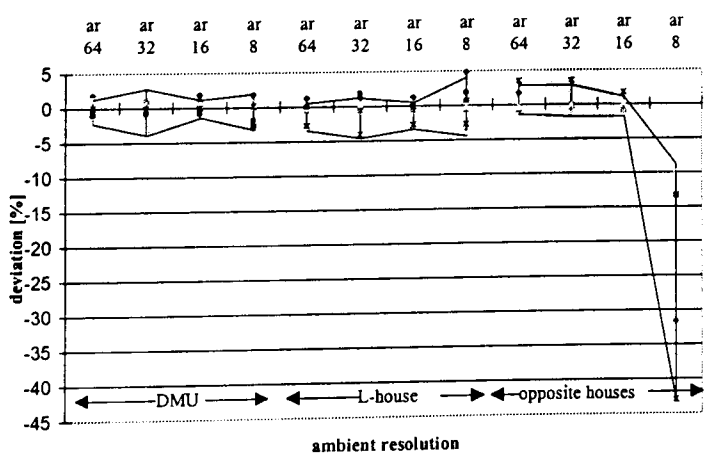


Figure 6.15 Same as Fig. 6.12 but varying *ar*

6.3.5 Accuracy of cumulated values

The yield of a solar energy system is usually calculated as monthly or annual cumulated values. As mentioned in Chap. 6.3.4, this will decrease the deviations as given for the single values. This was confirmed repeating the above described computations for scene (C) but cumulating the irradiance values over one month (April).

Figures 6.16-6.19 show the deviations of the cumulated values at the seven single trace points, varying the considered parameter. Again the default settings were used to compute the reference values, with the exception that the ambient bounces were set to *ab 2* (to *ab 3*, respectively, for Fig. 6.16). Consequently, the deviations at the settings *aa 0.2*, *ab 3*, *ad 512* and *ar 128* are zero.

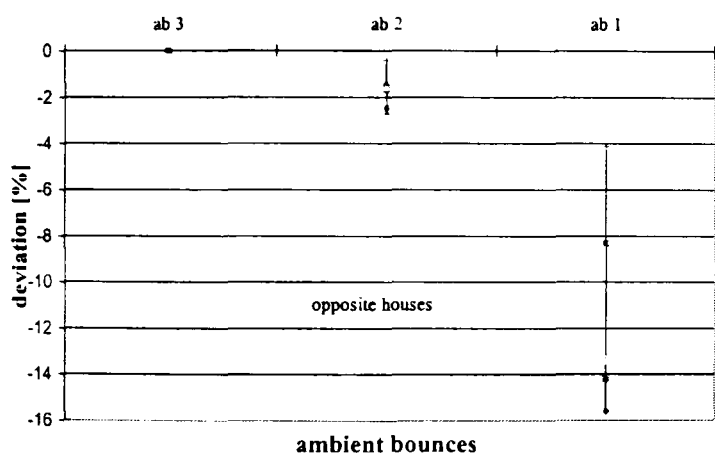


Figure 6.16 Accuracy of monthly cumulated values varying *ab*, the spread refers to the seven sample points as given in Fig. 6.2

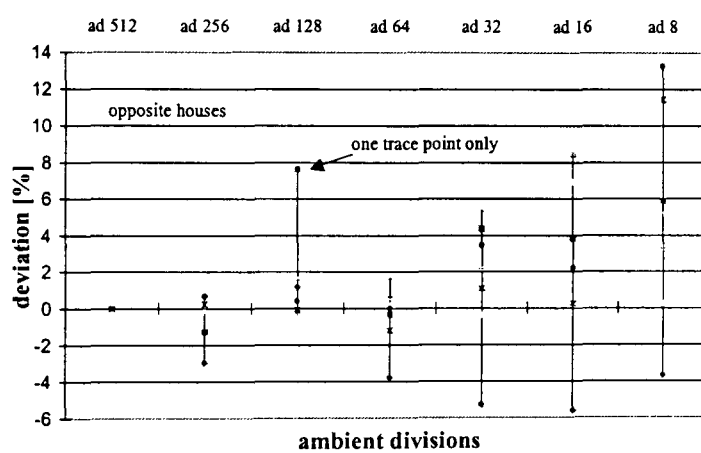


Figure 6.17 Same as Fig. 6.16 but varying *ad*

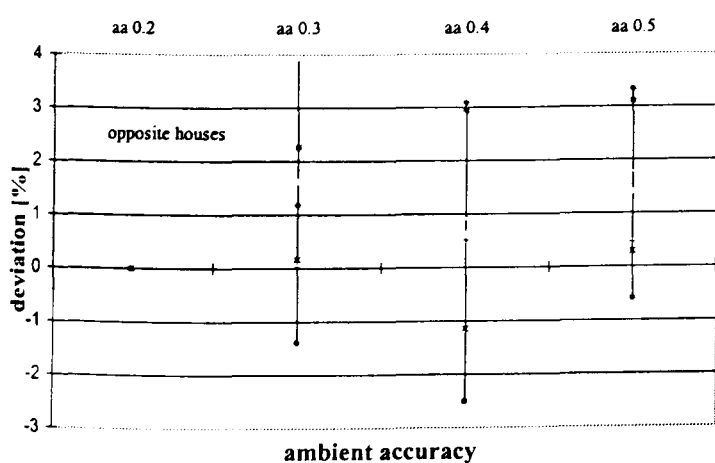


Figure 6.18 Same as Fig. 6.16 but varying *aa*

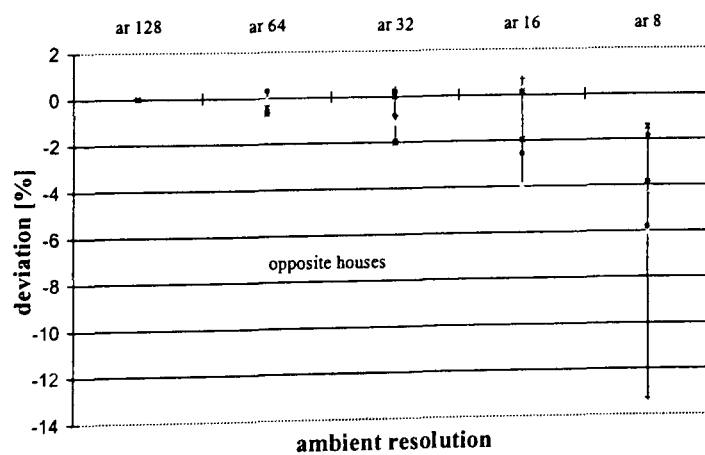


Figure 6.19 Same as Fig. 6.16 but varying *ar*

The figures show that now the accuracy converges even faster than before (Chap. 6.3.4) and also for the parameter *ab*. An exception is the ambient accuracy where decreasing *aa* does not decrease the deviation. However, since the deviation is very low this is not further regarded. It must be noted that the deviation of 8% in Fig. 6.17 at ad 128 is caused by one trace point only. The deviations at the other points remain below 2%.

6.3.6 Conclusions and recommendations on parameter setting

From the above described examinations, three empirically determined parameter sets (Tab. 6.5) are suggested to execute a *fast*, *accurate* or *detailed* simulation. These parameter sets will be used if the corresponding option is applied in IPROCESS. They will enable focusing either on speed (*fast*) or on accuracy (*accurate*). The third parameter set should only be used in simple scenes where very detailed examinations are necessary or for short time periods. The given accuracy shall be understood as relevant to cumulated values of one month or more. However, the actually achieved accuracy depends strongly on the scene and the placement of the trace points. In special circumstances it can vary significantly.

Setting	parameter	accuracy for a time-series computation
fast	aa 0.4, ab 1, ad 32, ar 16	< 20%
accurate	aa 0.4, ab 2, ad 64, ar 16	< 10%
detailed	aa 0.3, ab 3, ad 128, ar 64	< 5%

Table 6.5 Recommendation on parameter settings

When the irradiance at several trace points is to be calculated, it is always recommended to do this at one IPROCESS run to enable the RADIANCE optimisation algorithms. Splitting the calculation for the different trace points will increase the total time significantly and is only recommended if several spare computers can be used.

The time demand for the annual calculation of the above given scenes and the *accurate* parameter set is given in Tab. 6.6. It can be seen that the calculation of complex scenes (DMU) takes a very long time with the direct method. The sky patch approach (Chap.

5.2.2) will accelerate the computations significantly. It should be recalled that the calculations refer to the hardware as mentioned in Chap. (6.3.2). An up-to-date PC (e.g. PENTIUM III, 500 MHz) will be about three times faster.

Opposing houses	L-house	DMU
3684 sec = 61 min	3600 sec = 60 min	46440 sec = 12h 54 min

Table 6.6 Time demand for an annual calculation using the 'accurate' setting

6.4 Using the *patch* method

In the previous chapter, the effects of the *rtrace* parameters on the time demand and the accuracy were examined using the direct method (Chap. 5.2.1). In the following, the sky patch approach (Chap. 5.2.2) will be examined. However, it is not the *rtrace* parameters but the dependencies on the amount of sky patches which are evaluated. *Rtrace* parameters are generally set to *accurate* (Tab. 6.5) if not otherwise mentioned.

6.4.1 Time demand

Executing a time-series calculation of irradiance values with the sky patch approach consists of two processes, generating the coefficients and calculating the irradiance (Chap. 5.2.2). The time demand of both must be regarded separately from each other but later added together, to obtain the total computation time.

1. The coefficients must be generated regardless of the considered time period. Thus, the time demand for this process arises if calculating only one day or a complete year.
2. Calculating the irradiance values is done with the C program *pcalc* (Chap. 5.2.2.3). It works completely without RADIANCE and is independent from the scene. Thus, the time demand depends linearly on the number of patches, the number of days, and the number of trace points.

Since the time demand of both processes depends linearly on the number of patches, Fig. 5.5 shows additionally the dependence between the computation time and the chosen *step* (Chap. 5.2.2.2). The time demand to produce a one-year time series of irradiance data for

the scenes (C) and (E) but with 20 trace points (Chap. 6.2) at different steps is displayed in Fig. 6.20. The curves for generating the coefficients, the final irradiance values, and the total time demand are printed separately.

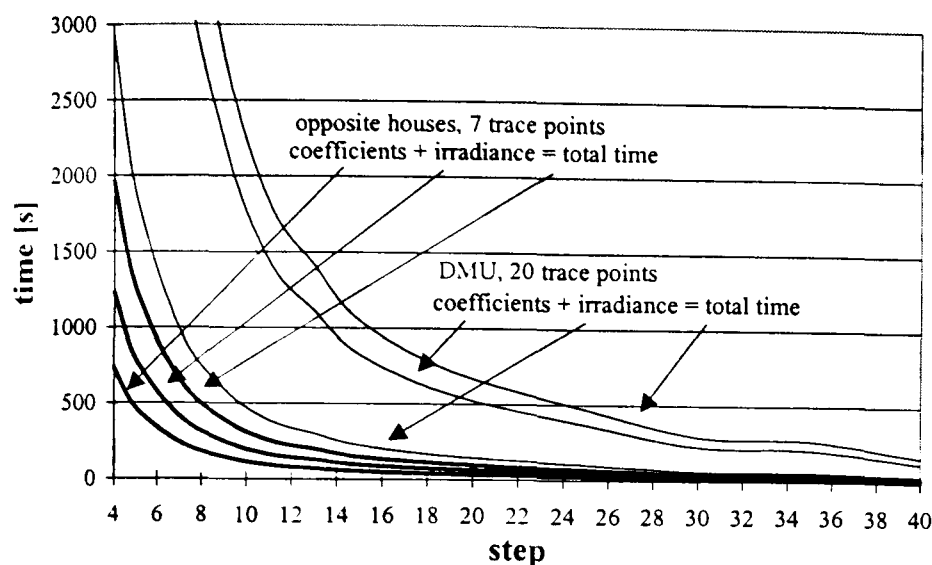


Figure 6.20
Time demand to generate a one-year time series of irradiance data using the patch approach with different steps

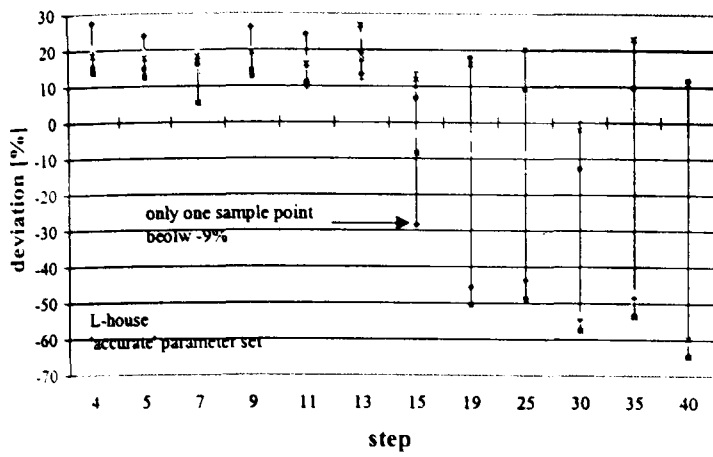
The total time demand using the patch approach with, for example, a step of 13 and the time demand using the direct approach (Tab. 6.6) are listed in Tab. 6.7. It can be seen that the computation time can be reduced by factor 18 ... 32 using a step of 13. However, the achieved accuracy must be examined.

	Opposing houses	L-house	DMU
direct	3684 sec = 61 min 24 sec	3600 sec = 60 min	46440 sec = 12 h 54 min
patch	200 sec = 3 min 20 sec	197 sec = 3 min 17 sec	1410 sec = 23 min 30 sec

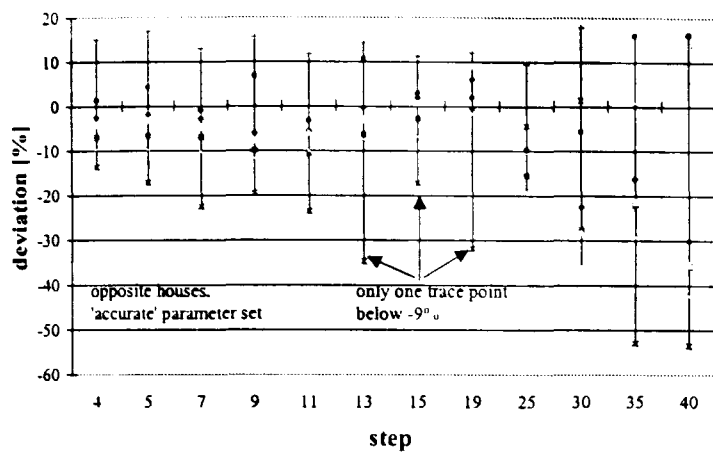
Table 6.7 Time demand of the direct and the sky patch approach for an annual calculation. The 'accurate' rtrace parameters were used and a step of 13

6.4.2 Accuracy dependent on the amount of patches

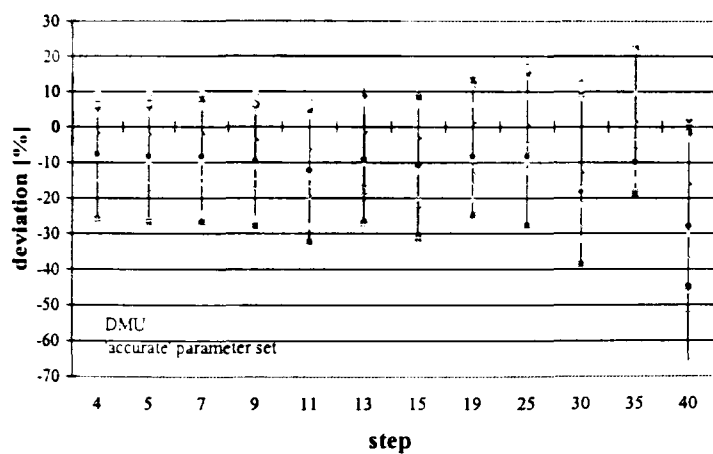
The results achieved with the patch approach were compared to the ones achieved with the direct method for cumulated values for April (see Chap. 6.3.5) and the scenes (A, C, D). The values that were computed with the direct method and the *accurate* parameter setting are used as reference (i.e. deviation = 0%). The deviations of the results using the patch approach with different steps are shown in Figures 6.21-6.23.

**Figure 6.21**

Deviation between the patch and the direct method for scene A (L-house), the spread refers to the seven sample points as given in Fig. 6.1

**Figure 6.22**

Deviation between the patch and the direct method for the scene C (opposing houses), the spread refers to the seven sample points as given in Fig. 6.2

**Figure 6.23**

Deviation between the patch and the direct method for scene E (DMU), the spread refers to 18 arbitrary chosen sample points

The diagrams generally show increasing deviations at increasing steps. However, at steps below about 15, the deviations remain at about constant values. Then, the deviation depends more on the scene and the location of the trace points than on the number of patches. It can be seen that the deviations at most trace points remain below 20% for steps smaller than 13. The large error bars at a step of 15 in Fig. 6.21 and at a step of 13, 15 and 19 in Fig. 6.22 are caused by one single trace point only.

A different ('higher') setting of the parameters was also tested but the influence on the accuracy was generally very small. However, the computation time increased, in some cases significantly.

6.4.3 Conclusions and recommendations on the number of patches

From the above examinations it is recommended to use the sky patch approach where a fast estimation of irradiance values is required and a lower accuracy is permitted. As a very general rule, it can be assumed that a step of 13 will lead to errors up to 20% and a step of 25 will produce errors around 30%. However, this assumption is only valid for typical urban structures and the calculation of cumulated irradiance data. In special cases the error may be very different.

When a solar system is to be installed some standard rules will usually be considered:

- it should **not** be placed towards the north
- it should **not** be installed in a dark corner of a building
- it should **not** be mounted at a location where it is heavily shaded.

Thus, the solar receiver will achieve a large share of the direct irradiation. Then, the RADIANCE predictions will also be more accurate because the main share of the irradiance is coming directly from the sun.

It is recommended to apply the *accurate* parameter setting as given in Chap. (6.3.6) also for the patch approach. A 'higher' setting will increase accuracy only slightly but can increase the computation time significantly.

7 EVALUATION AND EXAMINATIONS

The previous sections described methods of how to predict the yield of photovoltaic systems in an urban environment. The starting point is the (horizontal or normal) irradiance that is either provided by weather tapes or generated with a computer software, e.g., PVcad (Chap. 4.2.3). Then, the global irradiance on the PV modules is to be predicted either by IPROCESS or by PVcad. The advantage of IPROCESS is that it offers more flexibility to the user. For example, different sky models can be applied and the reflection of sun beams at surfaces with different reflection coefficients can be considered. The computed global irradiance on the PV modules is then fed to PVcad, and the PV system yield is calculated.

In the following Chap. 7.1, the different sky models are compared with each other and it is shown what happens if the ‘wrong’ sky model is applied. The two methods to calculate the irradiance on a tilted surface using the different Perez models (the ‘Tilted surface model’, Chap. 3.2.3.4 and the ‘All-weather sky model’ Chap. 3.3.4.2) are compared with each other. This model is also validated with measured values.

The different shading algorithms of IPROCESS and PVcad are compared with each other in Chap. 7.2.

General examinations of typical structures in an urban environment are presented in Chap. 7.3. These will assist system designers to decide where to place the receiver for solar energy systems. They should also help to estimate the influence of the building geometry and the facade (or surface) properties on the yield of a PV system.

7.1 Sky models

7.1.1 Comparing different sky models

Several models were developed to describe different sky luminance distributions ranging from dull overcast (Chap. 3.3.2) to a bright clear sky (Chap. 3.3.3). However, while calculating a time series of irradiance data, the sky conditions may vary in gradations between both extremes. Thus, further models were developed (Chap. 3.3.4-3.3.5) to describe an intermediate sky.

Figures 7.1-7.2 show what happens if a sky model is applied that does not match the actual conditions. For these figures, the irradiance on a vertical, south-facing wall was calculated applying the sky models: uniform sky (Equ. 3.32), overcast sky (Equ. 3.34), clear sky (Equ. 3.37), Matsuura intermediate sky (Equ. 3.47), or the Perez 'All-weather sky model' (Equ. 3.45). All of these models are implemented in IPROCESS.

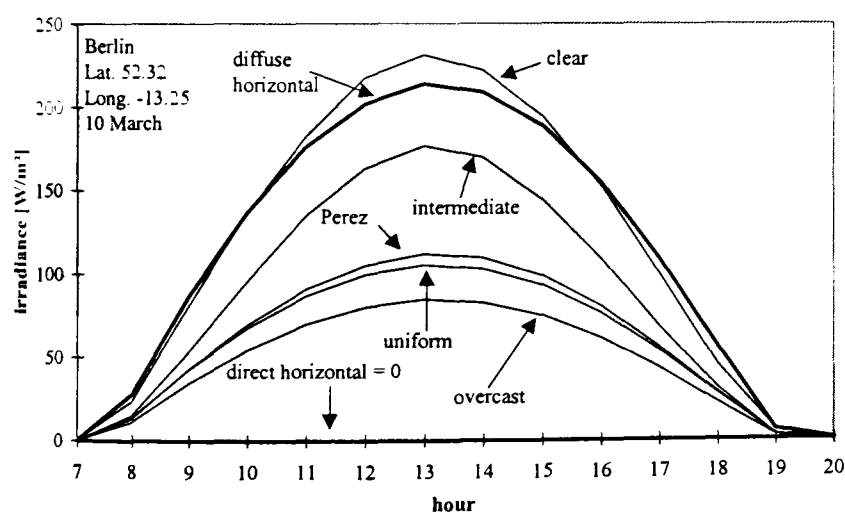


Figure 7.1
Irradiance on a vertical, south-facing surface on a dull, overcast day, calculated with different sky models

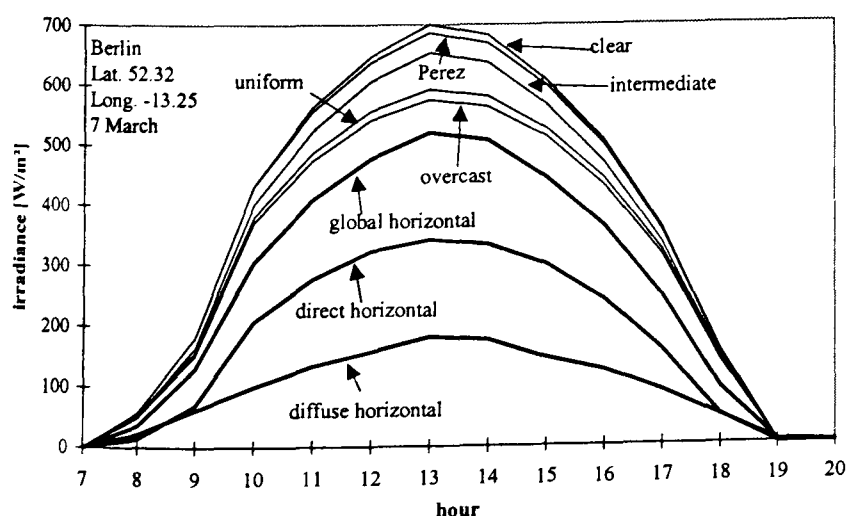


Figure 7.2
Irradiance on a vertical, south-facing surface on a clear day, calculated with different sky models

The real sky conditions of Fig. 7.1 were dull overcast, which is indicated by the low diffuse horizontal irradiance and the absence of any direct irradiance. Here, the overcast and uniform sky model predicts an irradiance on the wall of about one half of the horizontal irradiance. This is consistent with general considerations because the wall ‘sees’ only one half of the sky dome, and the sky brightness is relatively equally distributed over the hemisphere.

The clear sky model assigns a large part of the available luminance to a bright zone around the sun (which is not seen with a dull, overcast sky). Now, the southern sky is assumed to be very bright because the sun appears most frequently there. Thus, the clear sky model predicts too high on irradiance on the south-facing wall. As expected, the intermediate sky model predicts an irradiance between the overcast and the clear sky model.

The curves of Fig. 7.2 were computed for a relatively clear sky (the direct horizontal irradiation is about twice the diffuse horizontal irradiation) but at a low solar elevation (therefore the direct horizontal irradiance is relatively low). Now, the uniform and the overcast sky models predict too low on irradiance. They assign the available luminance symmetrically to the whole sky, also to the northern sky. However, this part is not ‘seen’ by the south-facing wall and not considered while calculating the irradiance. Since the brightness that is assigned to the northern sky is missing in the zone around the sun, the results on the wall are too low. Again, the intermediate sky model predicts irradiance values between the clear and the overcast sky models.

In both cases, the Perez model predicts values close to the results using the ‘right’ model. Thus, the Perez model that was also validated in comparisons with measured values [89] is recommended for time-varying simulations with fluctuating sky conditions.

7.1.2 Intermodel comparison

The Perez ‘All-weather sky model’ (Equ. 3.45) is implemented in IPROCESS. This model was compared with the Perez ‘Tilted surface model’ (Equ. 3.24) that is implemented e.g., in IRRAD [107] (Chap. 4.3.1) because the latter model was often validated [63] and became almost a standard used in many solar models (e.g. TRNSYS, INSEL, PVcad,

IRRAD). The comparison was made for a vertical, south-facing surface in Wuerzburg, Germany (lat. 49.9°, long. -9,54°).

Calculating the irradiance with IRRAD, the albedo was set to $\rho = 0.2$. For IPROCESS, a scene containing a ground plane with a reflectance also of $\rho = 0.2$ and the RADIANCE ‘upside-down sky’ was modelled. The latter was used because otherwise a black gap would appear between the edge of the (finite) ground plane and the (infinite) sky. The *rtrace* parameters were set to *accurate* (Tab. 6.5) and the direct method was used.

The results of the intermodel comparison are shown in Fig. 7.3. Here, the standard indicators to evaluate the performance of a mathematical model: Mean Bias Error (MBE) and Root Mean Square Error (RMSE) were used [129]. The MBE (Equ. 7.1) indicates a drift of the model that means whether it has a tendency to over- or underestimate the values. The RMSE (Equ. 7.2) registers the deviations of the single values and is therefore an indicator of the overall accuracy of the model. The variables Y and X refer to the predicted or measured values and the total number of samples is given by n .

$$MBE = \frac{1}{n} \sum_{i=1}^n (Y_i - X_i) \quad (7.1)$$

$$RMSE = \sqrt{\frac{1}{n} \sum_{i=1}^n (Y_i - X_i)^2} \quad (7.2)$$

The values that were predicted with the two Perez models are entered in Fig. 7.3. If the results were to match perfectly, all values would be situated on the diagonal. However, it can be seen that the two models show a very good correlation to each other, which is indicated by the small MBE and RMSE. For low irradiance values ($<500 \text{ W/m}^2$), the results of the both models vary little from each other. For values larger than 500 W/m^2 , the results of IPROCESS are slightly lower than those of IRRAD, but the deviations remain below 5%.

It should be noted that data smaller than 30 W/m^2 were removed from the records because there a small difference in the sun position has a large influence on the results. These

differences may be caused by rounding errors or by different algorithms calculating the sun's position and do not reflect differences in the sky models.

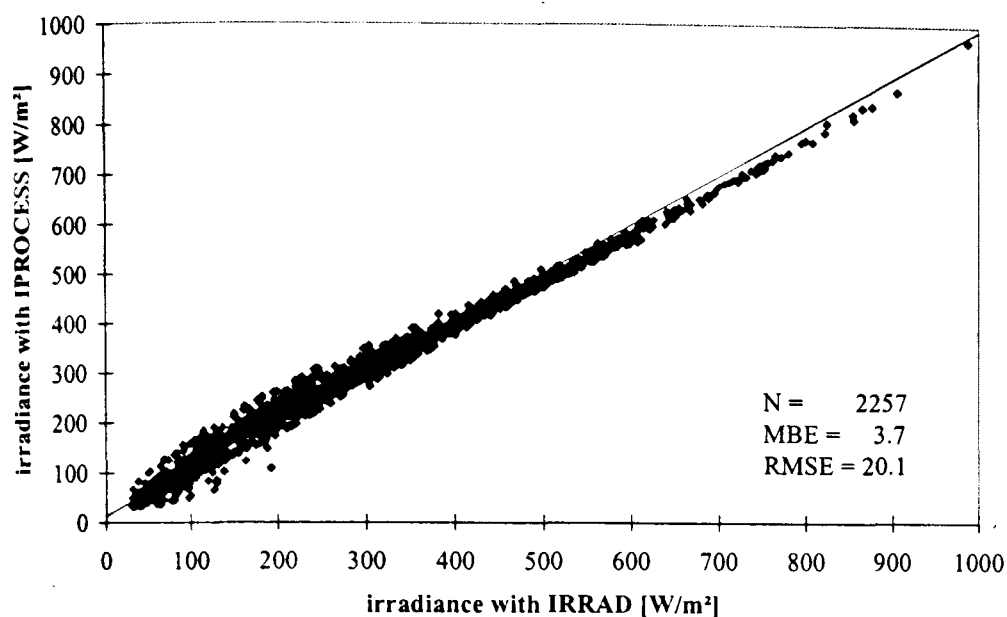


Figure 7.3
Comparison of the global irradiance on a vertical, south-facing surface, calculated with Perez' 'Tilted surface model' (IRRAD) and 'All-weather sky model' (IPROCESS)

The comparison shows that the 'All-weather' model performed comparably well to the well-validated 'Tilted surface' model if applied to calculate the irradiance on a tilted surface. The tilted surface models is used in most PV simulation programs (see Chap. 4.2).

7.1.3 Validation with measured values

Besides the intermodel comparison (Chap. 7.1.2), the irradiance data computed with IPROCESS were compared with measured values. These were recorded as hourly data at the station of Athalassa, Cyprus (lat. 35.09, long. -33.24). Here, the global horizontal and diffuse horizontal irradiance was measured together with the global irradiance on a vertical, south-facing surface [130].

As mentioned above, the RADIANCE scene was modelled with a ground plane (reflectance $\rho = 0.2$) and the 'upside-down sky'. The irradiance data on the south-facing wall were calculated using the *direct* method, the *accurate* parameter set, measured horizontal data of Athalassa as input, and the Perez sky model.

The result of the comparison is given in Fig. 7.4. It shows reasonable correlation between the measured and the calculated data. Again, values smaller than 30 W/m² and 10 further records that were obviously out of range (the measured global irradiance was inconsistent with that of the calculated sun position) were removed from the records.

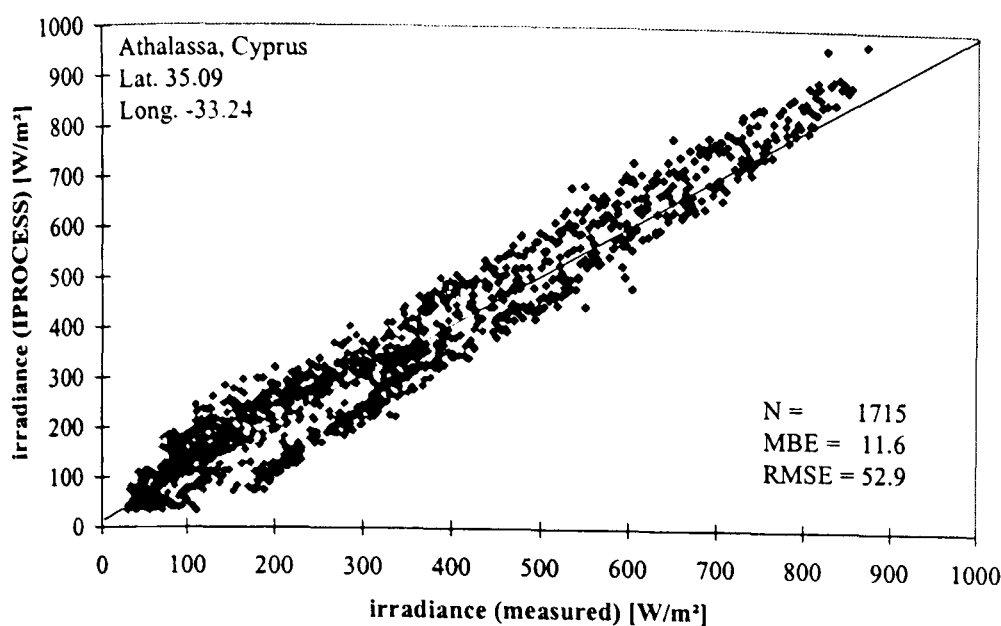


Figure 7.4
Comparison of measured data (station of Athalassa, Cyprus) with calculated (IPROCESS) values. The data refer to the global irradiance on a vertical, south-facing surface.

In an extensive comparison of data that were recorded at the Fraunhofer Institute for Solar Energy Systems in Freiburg, Germany, Reise [131] found similar results. For data measured at a vertical south-facing surface that were compared with values calculated with the 'All-weather' model of RADIANCE (but without ground plane), he found a MBE = 12.1 and a RMSE = 24.8. For other orientations (east, west or south with a tilt of 45°) or if additionally a ground plane with a reflectance of $\rho = 0.2$ was modelled, the accuracy even increased (Tab. 7.1).

Orientation of receiver plane	MBE	RMSE
south, 45° inclined, no ground plane	7.0	19.9
south, vertical, no ground plane	12.1	24.8
east, vertical, no ground plane	8.0	22.8
west, vertical, no ground plane	1.2	15.2
south, 45° inclined, with ground plane, ab = 1	2.2	18.1
south, 45° inclined, with ground plane, ab = 2	6.3	19.4
south, 45° inclined, with ground plane, ab = 3	6.4	19.5

Table 7.1 Comparison of irradiance values measured at the ISE, Freiburg, with simulated values (from Reise [131] with RADIANCE)

Besides the Perez sky model, Reise included the tilted surface models of Liu/Jordan (Chap. 2.2.3.1, Equ. 2.20), Temps/Coulson, Bugler/Hay/Kkambezedis, Klucher (Chap. 2.2.3.3, Equ. 2.22), Hay (Chap. 2.2.3.2, Equ. 2.21), Willmott, Skartveit/Olseth, Gueymard, Perez

(Chap. 2.2.3.4, Equ. 2.24) and Reindl in his comparison. Whereas the models Liu/Jordan, Klucher, Hay, Skartveit/Olseth, Perez 'Tilted Surface', and Reindl showed comparably small deviations for the MBE, no model performed similarly to the Perez sky model regarding the RMSE.

Further to the above mentioned examinations, Mardaljevic [125] validated RADIANCE using sky scanner measurements as source data to predict indoor illuminance values. The comparison of measured values with predicted values showed errors of MBE: -1.5% - 4.8% and RMSE: 9.8% - 16.1%. This demonstrated the reliability of the RADIANCE software (see discussion in 7.3.5).

7.2 Shading algorithms

The results from IPROCESS were compared with those from PVcad (Chap. 4.2.3) for a model scenario with shading. With IPROCESS, the effect of shading is calculated by RADIANCE using ray-tracing. PVcad was chosen because it offers a very convenient way of modelling PV systems in an urban environment.

To compare the algorithms, first the yields of the shaded PV generators were computed using exclusively PVcad. Then, the horizontal irradiance data generated by PVcad were used as input to calculate a time series of irradiance data (one per module) with IPROCESS. These data were fed back into PVcad to determine the yields of the PV generators.

7.2.1 Modelled scene and PV generators

An L-shaped house with the dimensions as given in Fig. 7.5 was modelled for the comparison. At its south-facing facade an array of totally 100 solar modules was mounted, arranged in 10 columns and 10 rows.

Then, PV generators that comprise ten-in-series connected modules (SIEMENS M110) linked to one inverter (SMA SWR 700) were modelled. For all cases the ten modules of one row or one column, respectively, belonged to one generator. Thus, in total twenty PV

generators were modelled. For the calculations with IPROCESS, the scene was modelled with a ground plane ($\rho = 0.2$), with the 'upside-down sky', and the surface of the walls were given a reflection coefficient of $\rho = 0.3$.

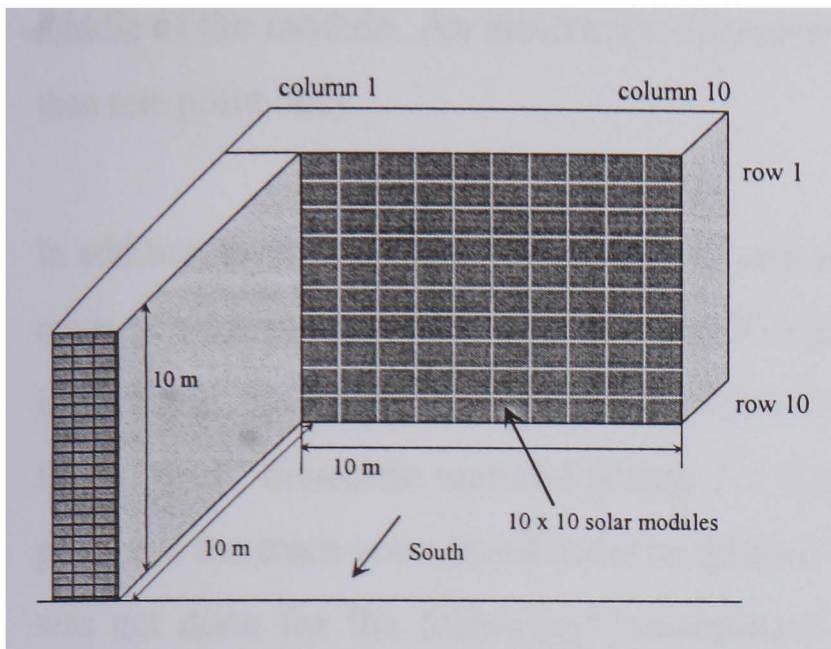


Figure 7.5
L-shaped house with an array of 10 x 10 solar modules at the south-facing facade

7.2.2 Shading algorithms of PVcad

The shading algorithms of PVcad differ greatly from the ray-tracing approach of IPROCESS. They will be briefly introduced following. PVcad calculates the yield of a shaded PV generator within the following set parameters:

1. The irradiance on each module is determined separately.
2. PVcad uses the Perez 'Tilted surface model' (Chap. 3.2.3.4) with the three parts: circumsolar (close to the sun), horizon band (a small band at the horizon), isotropic sky.
3. Reflections from any surface as well as the albedo are neglected.
4. An algorithm is used that creates a geometrical projection of the shading objects on the module plane(s). A grid of points is placed over each module and tested for shading. If one point of the grid is shaded, the direct irradiation and the circumsolar share of the diffuse irradiation is set to zero. Otherwise, the total irradiance is considered.
5. Two view factors (Equ. 3.63) are computed for each module, one for the horizon band and a second for the isotropic sky. The diffuse irradiation of the related two parts of the Perez model on the corresponding modules is reduced by these factors throughout the year.

Some of the above-mentioned items will most likely entail predictions from PVcad which are significantly lower than those from IPROCESS. Item (3) because the albedo and the reflection of sunbeams at surrounding surfaces are considered by IPROCESS and lead to a higher irradiation, and item (4) because IPROCESS usually uses only one trace point in the middle of the module. An arbitrarily chosen point within a grid is more frequently shaded than one point only.

In addition to what is mentioned above, losses due to the reflection of light from the glass cover of solar modules are considered in PVcad according to the equations of Fresnel. It is, in principle, possible for the values calculated by IPROCESS to consider this effect. To do this, a 'thick' dielectric material (Chap. 5.1.2) must be placed at the position of the sample point and the trace point itself must be located within the dielectric material. However, this was not done for the following examination because these losses remain below 6-12% [132] and the additional material would increase the computation time significantly.

7.2.3 Yield predictions using PVcad and IPROCESS

The yield predictions using PVcad and IPROCESS are shown in Figures 7.6-7.9. For these diagrams, the horizontal irradiance data were generated with PVcad for the location of Wuerzburg, Germany (lat. 49.8, long. -9.9). The yields for January are shown in Figures 7.6-7.7 and the yield of a complete year in Figures 7.8-7.9. The yield of an unshaded generator entered in the diagrams as rightmost column and upper row.

Despite of what is said in Chap. 7.2.2, the results show that nevertheless for the calculation of January (Figures 7.6-7.7), PVcad always predicts higher yields than IPROCESS. It can be seen that PVcad predicts almost a similar yield for all generators regardless of the placement of the modules. This does not tally with general considerations. The generator comprising the modules at the bottom of the building will yield a significantly lower energy than the generator comprising the modules at the top of the building. The same is valid for the annual predictions as shown in Figures 7.8-7.9. Thus, the shading algorithm of PVcad should be reviewed, and it is recommended to predict the yield of a PV generator using the ray-tracing algorithm of IPROCESS.

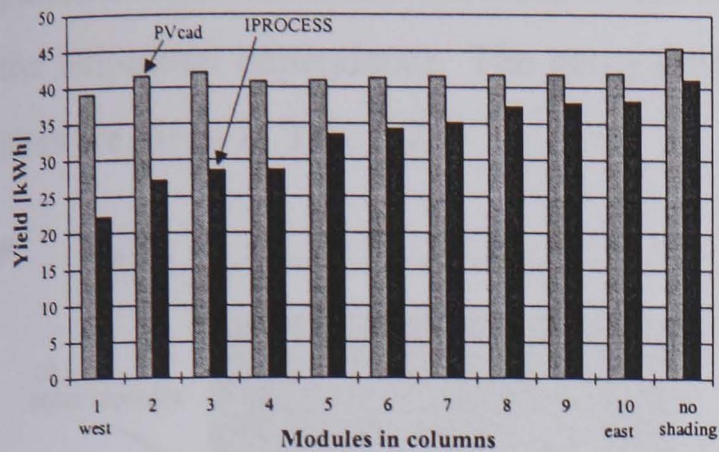


Figure 7.6 Yield of shaded PV generators in January. Each generator comprises ten solar modules (arranged in columns) on a building according to Fig. 7.5.

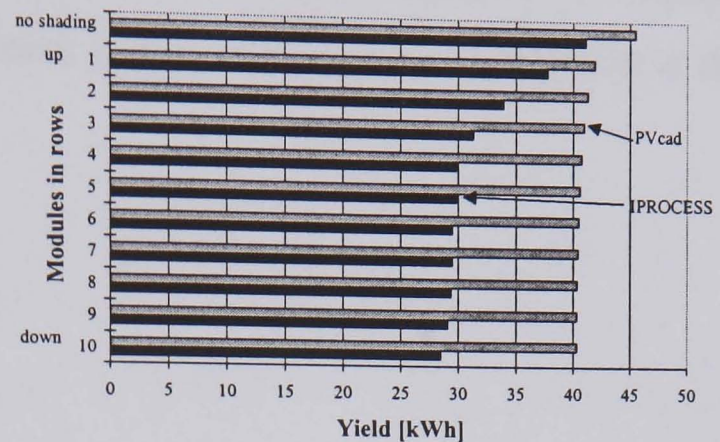


Figure 7.7 Similar to Fig. 7.6 but arranged in rows

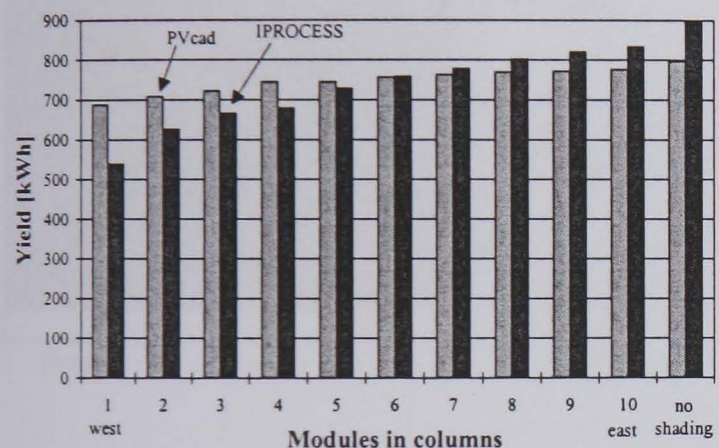


Figure 7.8 Similar to Fig. 7.6 but annual yield

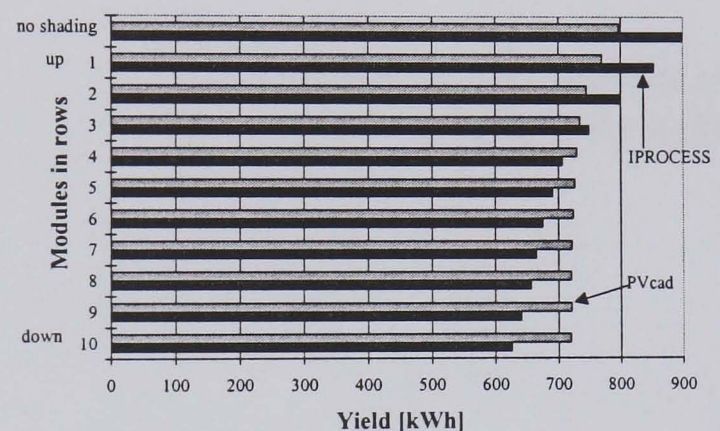


Figure 7.9 Similar to Fig. 7.7 but annual yield

7.3 Examinations of typical arrangements

This section will present general examinations of the inhomogeneous irradiance distribution on facades of buildings that are typical for urban environments. The aim is to give system designers an aid on where to place a PV array, how to wire the modules, and what the influence of the building geometry and of the surface properties will be. Two typical structures were examined: the L-shaped house as given in Fig. 7.5 and two opposing houses as given in Fig. 7.10. Again the RADIANCE scene was modelled with a ground plane ($\rho = 0.2$), the ‘upside-down sky’, and a reflection coefficient of $\rho = 0.3$ for the surfaces of the walls. The Perez sky model was used for all examinations.

The irradiance at the south-facing facades of both structures was computed using IPROCESS. Here, the trace points were placed in an 10 x 10 array so that they would match the PV modules as described Chap. 7.2.1. For the examinations, the structures were

placed in different locations, close to the equator or up to a latitude of about 50° to examine the latitudinal dependence. The geographical data and the global annual irradiation at the sites are given in Tab. 7.2.

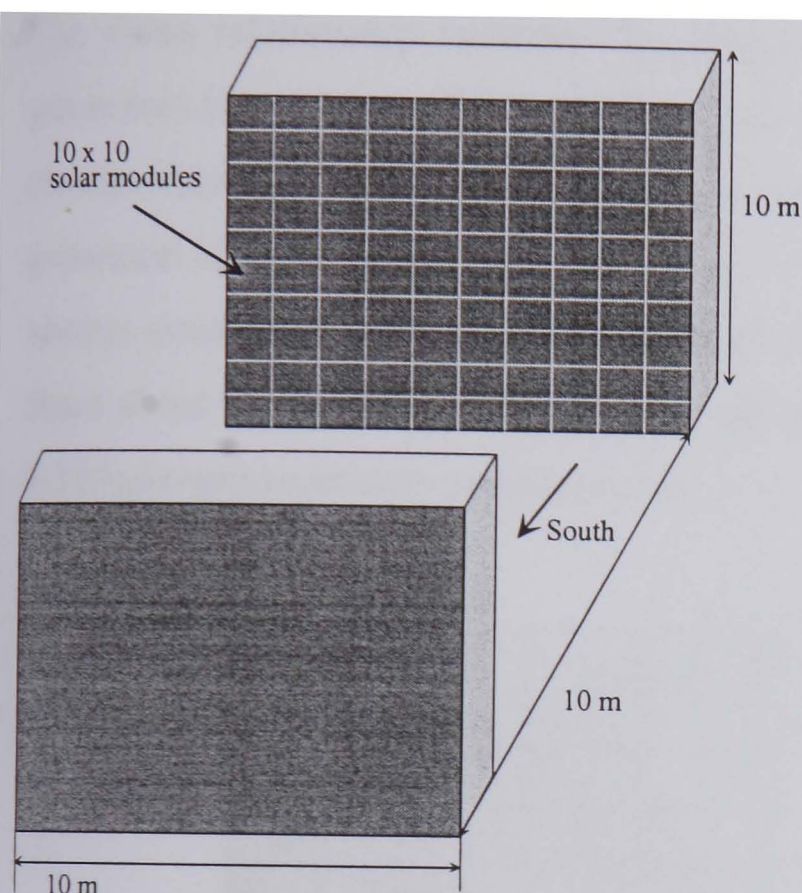


Figure 7.10
Opposing houses with an array of 10 x 10 solar modules at the south-facing facade

Location	Latitude (all north)	Longitude (+ west, - east)	Irradiation [kWh/m ² /a]
Kisangani, Zaire	0.5	-25.1	1,762.5
Odienne, Ivory Coast	9.5	7.6	1,956.5
Atar, Mauritania	20.5	13.7	2,092.7
Cairo, Egypt	30.5	-31.2	1,968.3
Rome, Italy	41.8	-12.6	1,542.7
Wuerzburg, Germany	49.8	-9.9	1,121.0

Table 7.2 Locations of examined sites and the annual global horizontal irradiation

7.3.1 Relationship between the irradiation distribution and the yield of a PV generator

The hourly irradiance on the 100 trace points of the L-shaped house was calculated for Wuezburg, Germany, and then all data of one trace point were cumulated (this was done using the converter of IPROCESS as described in Chap. 5.3.3). The results for cumulating

the data of January are shown in Fig. 7.11. Here, the same horizontal irradiance data and the same RADIANCE scene was used as for Figures 7.6-7.7. Thus, the irradiation can be compared with the PV yield.

The close relationship between the (long-term) irradiation and the yields of the PV generators (the values of Figures 7.6-7.7 that were calculated with IPROCESS) can be seen clearly. Generally, the modules with lowest irradiation determine the yield of the PV generator. If the rows are considered (Fig. 7.7), the modules with the lowest irradiation are always situated at the left side (Fig. 7.11). It can be seen that the modules of row 4-10 share about the same 'dark' area at the left side. Consequently, the PV generators of row 4-10 have approximately similar yields.

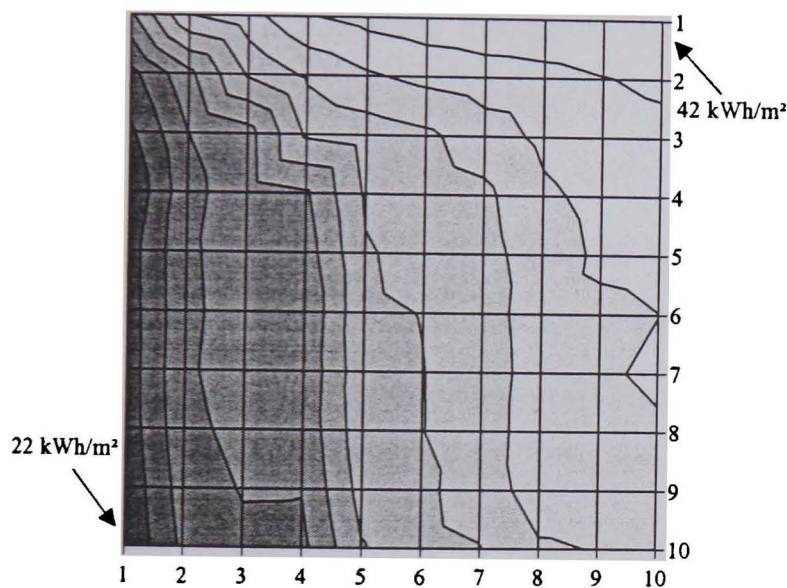


Figure 7.11
Irradiation in January at the trace points of the facade of the L-shaped house

Secondly, the generators of column 8-10 (Fig. 7.6) have approximately the same yields. In Fig. 7.11, it can be seen that the minimum irradiation of the modules of these columns is about equal. However, that the module with the lowest (long-term) irradiation determines the yield of the PV generator is only a general rule. Finally, the irradiance on the single modules at the single time steps determines the generator's yield.

Often, a system designer or an architect wants to know where the best area at a building to place a solar receiver is. To determine this, it is not always necessary to execute a complete PV energy simulation. From the above given results, it can be said that it is often sufficient to determine only the irradiation distribution and to conclude then the best 'solar' area of a building, i.e. which has the greatest incident irradiation.

7.3.2 Irradiation distribution at different locations

The distributions of the annual irradiation on the facade of an L-shaped house (Fig. 7.5) at the locations as given in Tab 7.2 are displayed in Figures 7.12-7.17. The images show the effect of the shading caused by the L-wing of the building dependent on the location.

As expected, the right upper corner always achieves the highest irradiation because it is hardly shaded. The irradiation at the left lower corner always amounts to about one half. Generally, the areas with equal irradiation extend diagonally, from the left upper corner to the right lower corner. This observation is true for all examined sites, regardless of the geographical latitude. An optimised wiring of a PV array would follow this structure. However, a yield prediction would be necessary to determine the extra energy of the PV generator, and then the system designer would have to decide if this compensates for the additional expenditure for the cabling.

The diagrams also show that the highest overall irradiation on a vertical facade can be expected in Atar, Cairo, and Rome, at a latitude of about $20^\circ \dots 40^\circ$. Although the sites south of Atar have a similar horizontal irradiation (Tab. 7.2), the illuminance of the vertical south-facing facade is low because of the low angle of incidence of the sunbeams. Further, in some months of the year, the sun appears in the north and no direct irradiance will strike the facade. European sites north of Rome generally have a low horizontal irradiation. Even the good angle of incidence of the sunbeams onto the facade does not increase the 'vertical' irradiation.

The irradiation distributions of the annual irradiation on the facade of the opposing houses (Fig. 7.10) are displayed in Figures 7.18-7.23. The images show the expected higher irradiation at the top of the facade in contrast to the area at the bottom. Whereas the difference between top and bottom is small in Kinsangani (about 18%), it reaches up to 35% in Wuerzburg. Here, the shading by the opposing house is more significant because of the low solar elevations. Again, the overall irradiation levels in Atar, Cairo, and Rome, are higher than in the other locations.

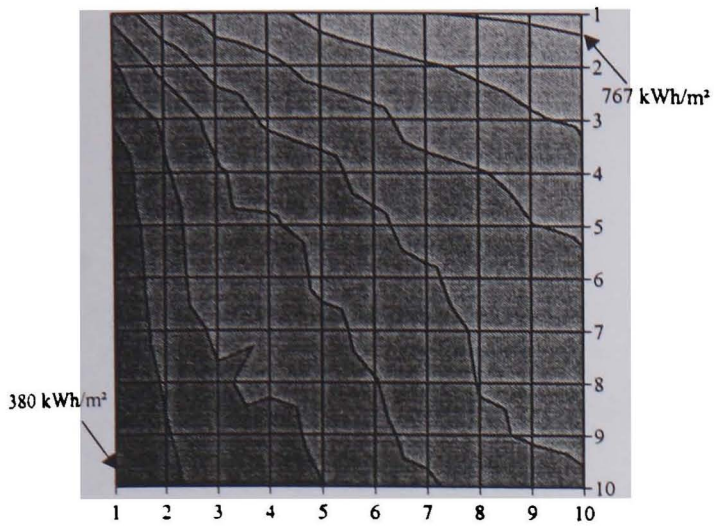


Figure 7.12
Distribution of the annual irradiation at the facade of the L-shaped house in Kisangani, Zaire (lat.: 0.5N)

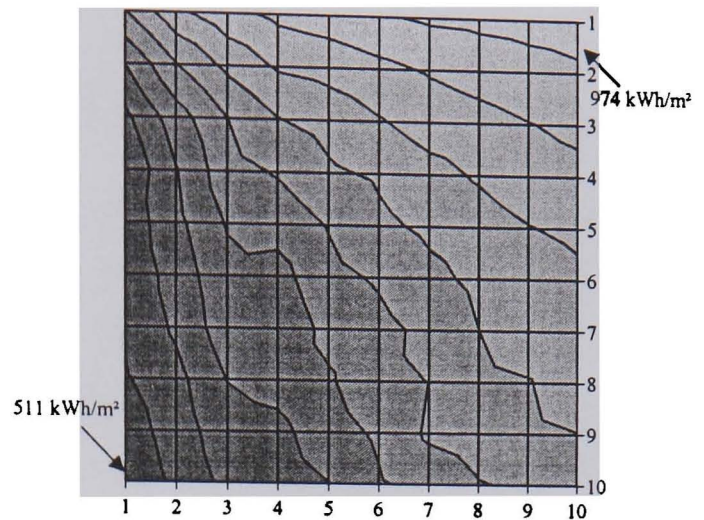


Figure 7.13
Similar to Fig. 7.12 but in Odiénne, Ivory Coast (lat.: 9.5N)

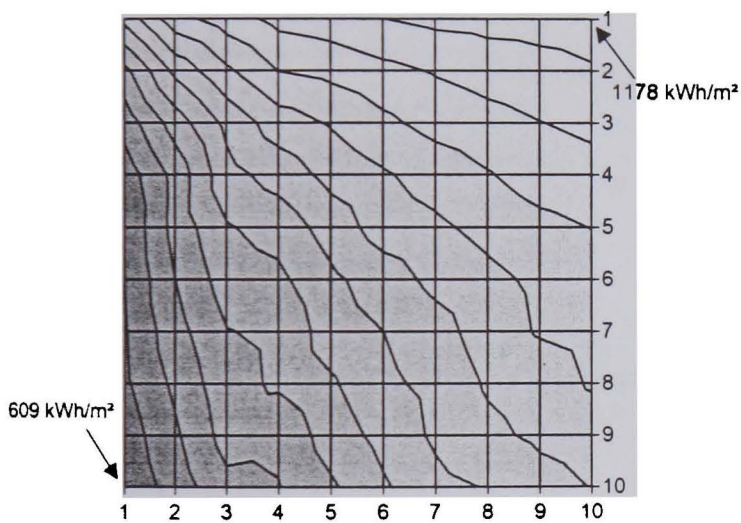


Figure 7.14
Similar to Fig. 7.12 but in Atar, Mauritania (lat.: 20.5N)

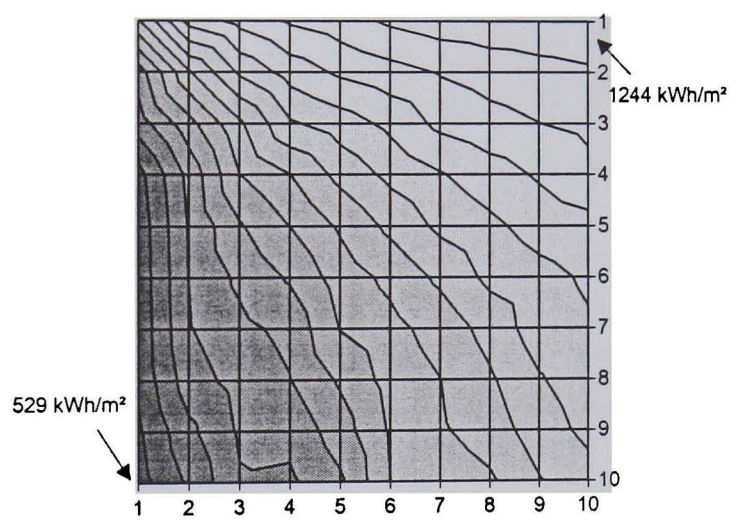


Figure 7.15
Similar to Fig. 7.12 but in Cairo, Egypt (lat.: 30.5N)

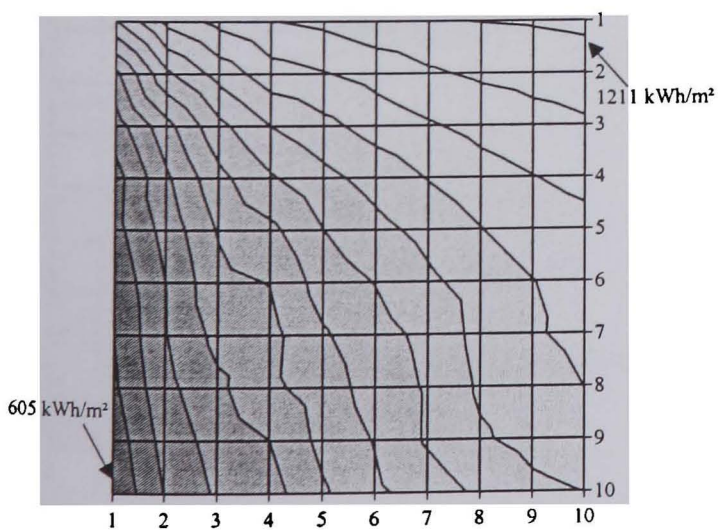


Figure 7.16
Similar to Fig. 7.12 but in Rome, Italy (lat.: 41.8N)

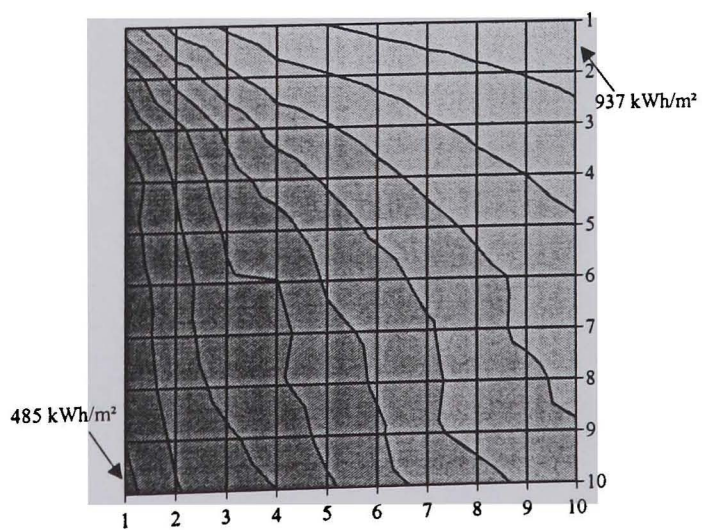


Figure 7.17
Similar to Fig. 7.12 but in Wuerzburg, Germany (lat.: 49.8N)

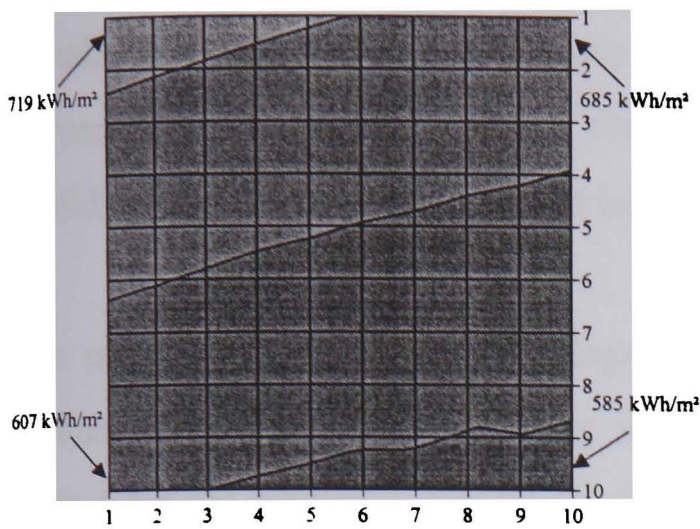


Figure 7.18
Distribution of the annual irradiation at the facade of the opposing houses in Kisangani, Zaire (lat.: 0.5N)

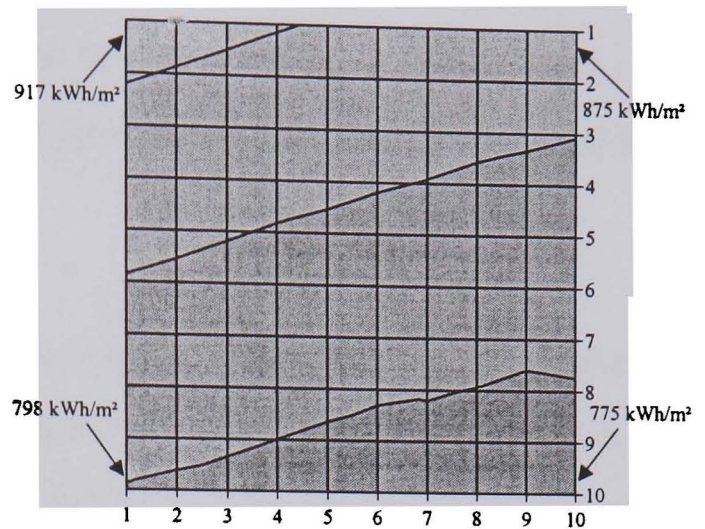


Figure 7.19
Similar to Fig. 7.18 but in Odienne, Ivory Coast (lat.: 9.5N)

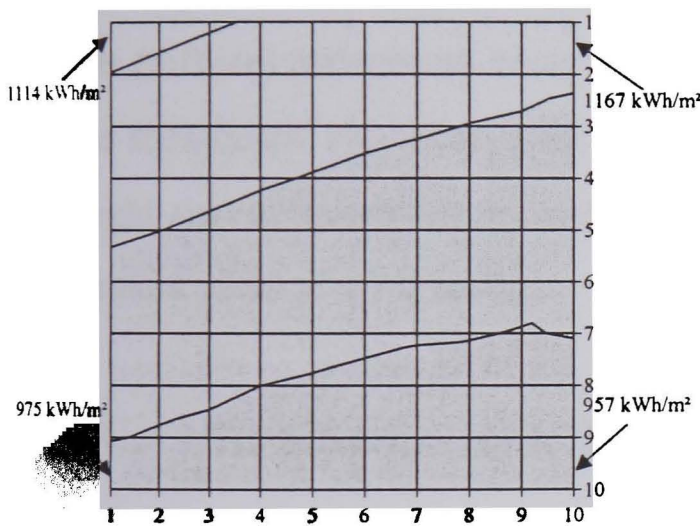


Figure 7.20
Similar to Fig. 7.18 but in Atar, Mauritania (lat.: 20.5N)

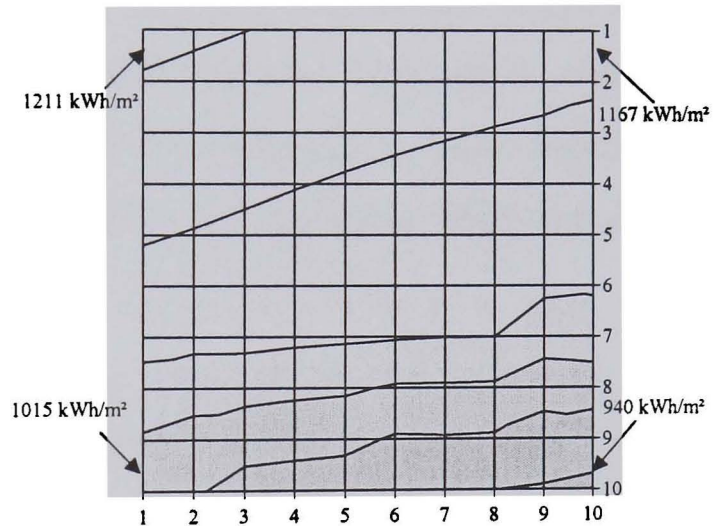


Figure 7.21
Similar to Fig. 7.18 but in Cairo, Egypt (lat.: 30.5N)

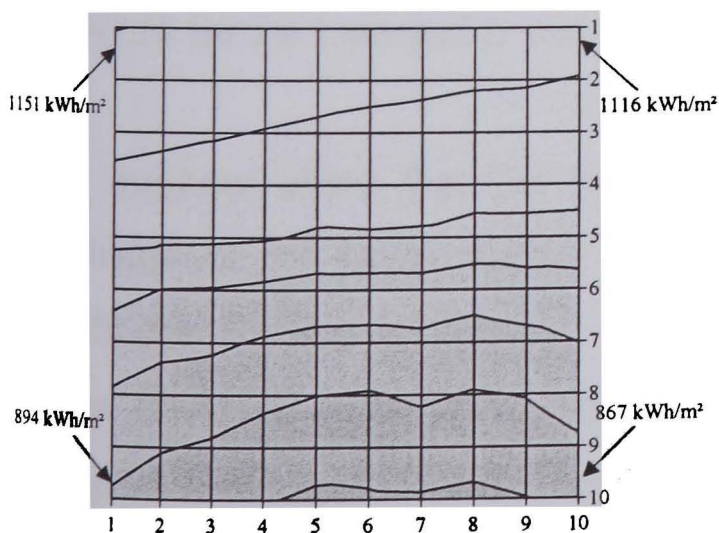


Figure 7.22
Similar to Fig. 7.18 but in Rome, Italy (lat.: 41.8N)

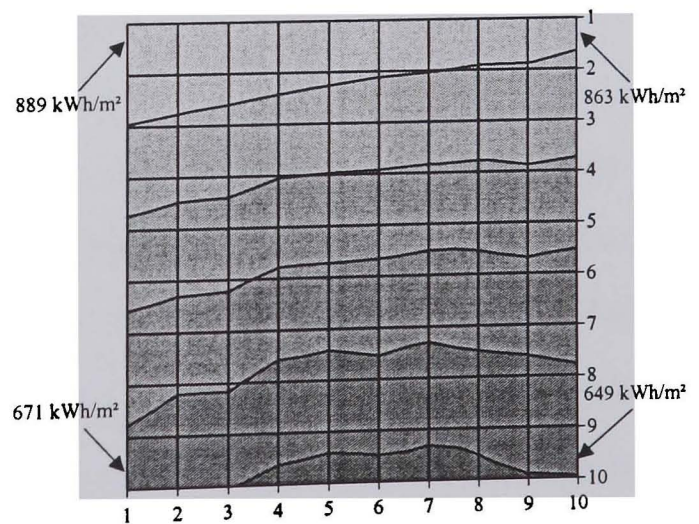


Figure 7.23
Similar to Fig. 7.18 but in Wuerzburg, Germany (lat.: 49.8N)

It can be seen that the effect of the opposing building on the azimuthal distribution of the irradiance is low. The characteristic ‘bumps’ that can be seen at the diagrams of Rome and Wuerzburg account for less than 5%. However, this depends on the distance between both buildings and is further examined in Chap. 7.3.4.

An unexpected result was the slope of the areas in Figures 7.18-7.21. This is obviously caused by the opposing building because, on repeating the calculations without it, the effect did not reappear. The higher irradiation at the left side of the building was caused by a higher horizontal irradiation in the afternoon. It seems that there is a small inaccuracy in the algorithm for generating the horizontal data, the direct and the diffuse data had a small time shift between them¹. It is an interesting result that this effect decreases when the reflectivity of the surfaces is increased (Figures 7.29 – 7.33). The explanation is that with a higher (diffuse) reflectivity more light is bouncing around and thus, the position of the sun is less significant. However, even in Figures 7.18 – 7.23 the difference between the left and the right side accounts for at most 5% and might be said to be negligible when calculating the annual yield of a PV system.

7.3.3 Irradiation distribution with different surface properties

The calculations as described in Chap. 7.3.2 were repeated for Wuerzburg to examine the influence of different reflection coefficients ρ . Coefficients from $\rho = 0.1 \dots 0.9$ were assigned to the surfaces of the houses. The resulting annual irradiation is shown in Figures 7.24-7.28 for the L-shaped house and in Figures 7.29-7.33 for the opposing houses.

The diagrams show that the principal distribution always remains similar. Also the irradiation at the rarely shaded corners is almost constant regardless of the reflection coefficient. By way of contrast, the irradiation at the lower left corner of the L-shaped house increases up to 25% with increasing ρ . Especially in shaded areas, the higher reflection coefficient leads to a higher irradiance and thus to a more symmetrical irradiation distribution. However, a reflection coefficient of $\rho > 0.4$ is unlikely for normal buildings.

¹ This error was reported to the author of PVcad.

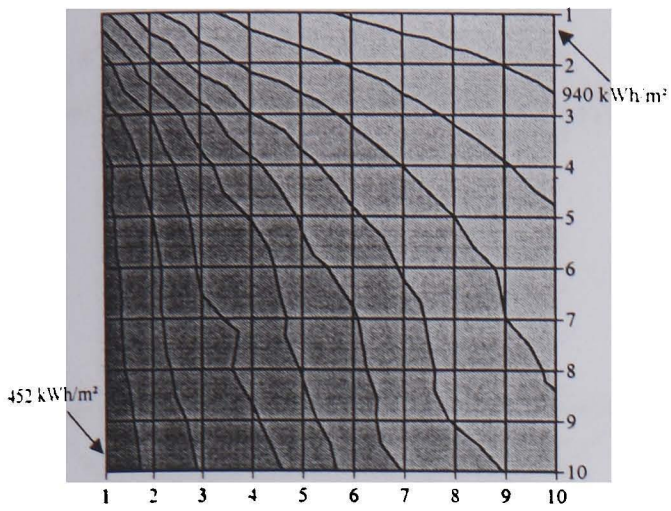


Figure 7.24
Distribution of the annual irradiation at the facade of the L-shaped house having an reflection coefficient of $\rho = 0.1$

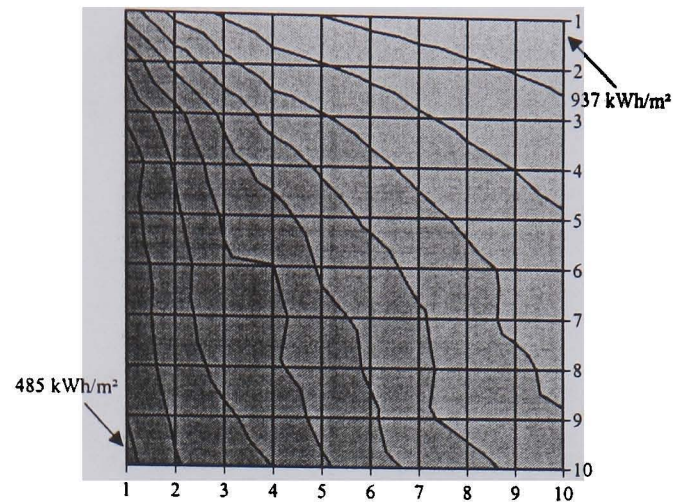


Figure 7.25
Similar to Fig. 7.24 but with a reflection coefficient of $\rho = 0.3$

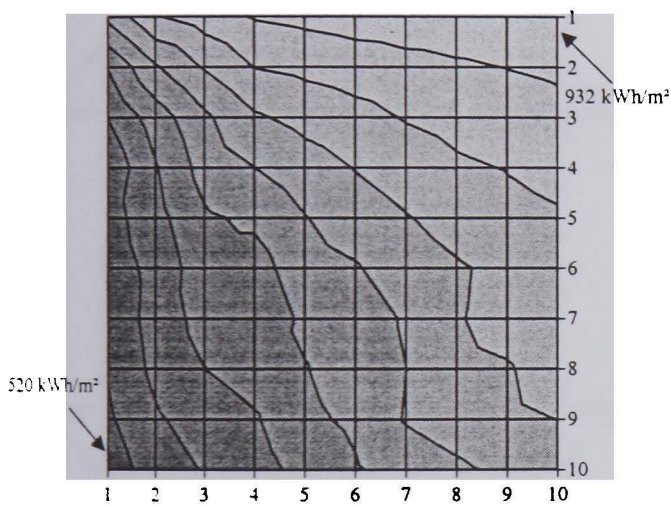


Figure 7.26
Similar to Fig. 7.24 but with a reflection coefficient of $\rho = 0.5$

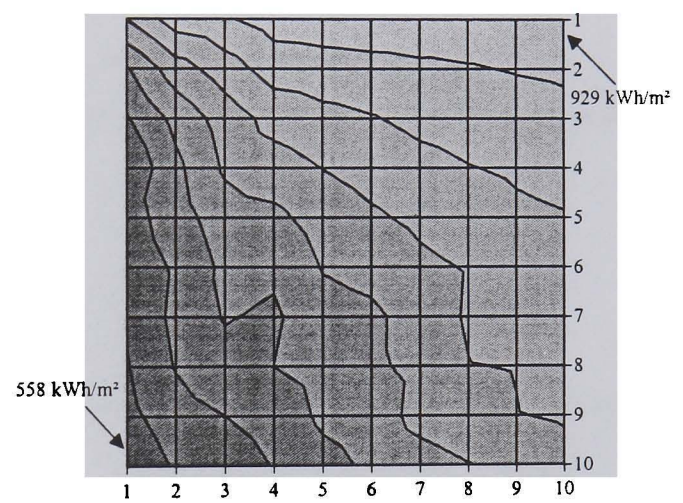


Figure 7.27
Similar to Fig. 7.24 but with a reflection coefficient of $\rho = 0.7$

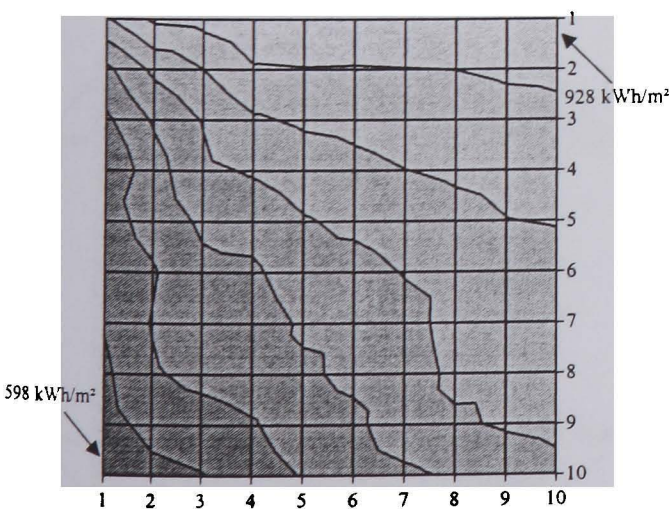


Figure 7.28
Similar to Fig. 7.24 but with a reflection coefficient of $\rho = 0.9$

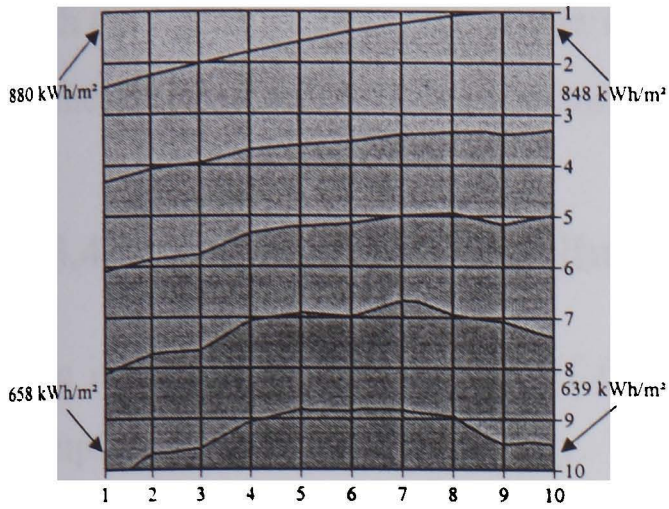


Figure 7.29
Distribution of the annual irradiation at the facade of the opposing houses having an reflection coefficient of $\rho = 0.1$

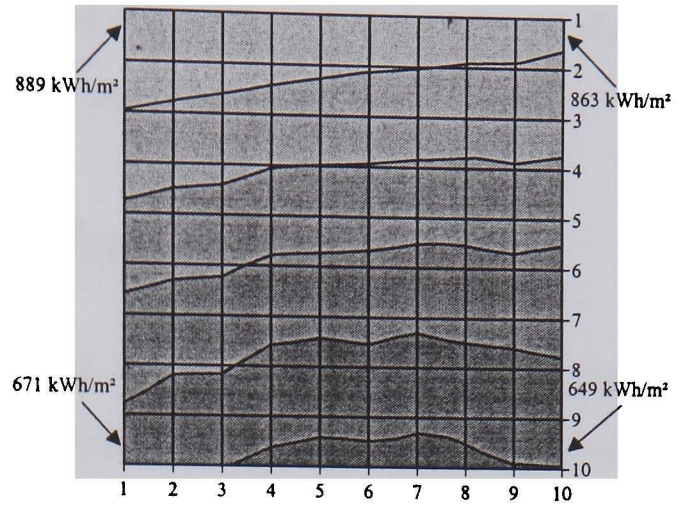


Figure 7.30
Similar to Fig. 7.29 but with a reflection coefficient of $\rho = 0.3$

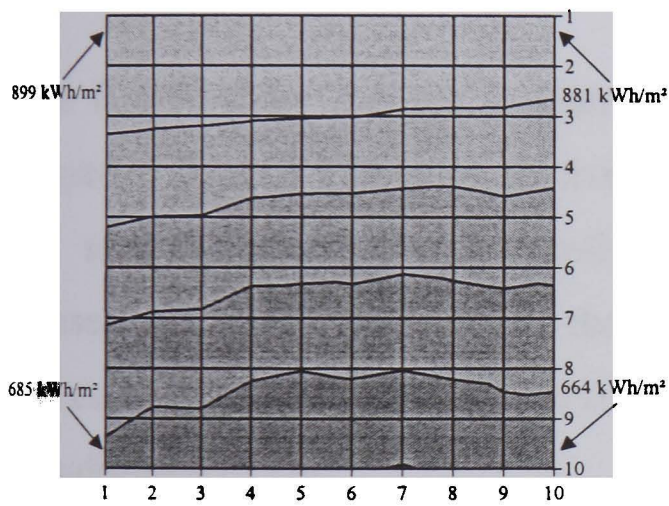


Figure 7.31
Similar to Fig. 7.29 but with a reflection coefficient of $\rho = 0.5$

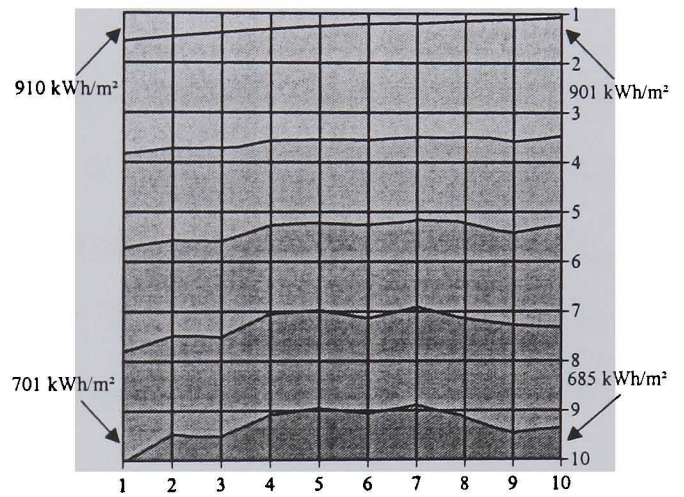


Figure 7.32
Similar to Fig. 7.29 but with a reflection coefficient of $\rho = 0.7$

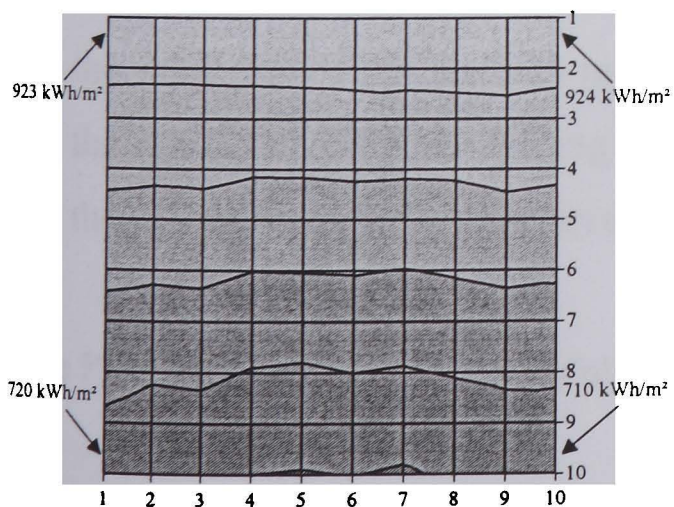


Figure 7.33
Similar to Fig. 7.29 but with a reflection coefficient of $\rho = 0.9$

The irradiation at the bottom of the facade of the opposite house increases by only 10% with the higher ρ . Here, the higher reflection coefficient did not lead to a significant change in the irradiation distribution because shading is not so decisive.

7.3.4 Irradiation distributions at different building distances

The influence of the distance of the opposing houses (Fig. 7.10) was examined for the sample of Wuerzburg, Germany. The same geographical data and irradiance values as mentioned before were applied, and the RADIANCE scene was modelled with ground plane ($\rho = 0.2$), with ‘upside-down sky’ and a reflection coefficient of $\rho = 0.3$ for the surfaces. Now, the irradiance distribution was calculated for a distance of 2 ... 10 m between both houses and is shown in Figures 7.34-7.38.

The figures show that the irradiation at the upper parts hardly varies. Here, the higher degree of shading decreases the irradiation only by up to 10%. At the bottom of the facade the situation changes significantly. The closer spacing leads to heavy shading, and consequently the dark ‘bump’ in the middle is growing. The irradiation in the middle of the lowest row (column 5) decreases from 634 kW/m²/a at a distance of 10 m to 114 kW/m²/a at a distance of 2m.

7.3.5 Further validation

A validation of the overall system would include the validation of three different models:

1. the validation of the used sky model (i.e. usually the Perez model)
2. the validation of the ray-tracing algorithms of RADIANCE
3. the validation of the PV model (i.e. Pvcad, PVEPO, or INSEL)

The Perez sky model is well validated with measured values as described in Chap. 7.1.3.

The RADIANCE system is also well validated for calculating the internal illuminance (e.g. [133]). In that work illuminance values that were measured inside a room were compared with values predicted by RADIANCE. The sky was modelled according to sky scanner measurements and thus, errors caused by a sky model could be excluded.

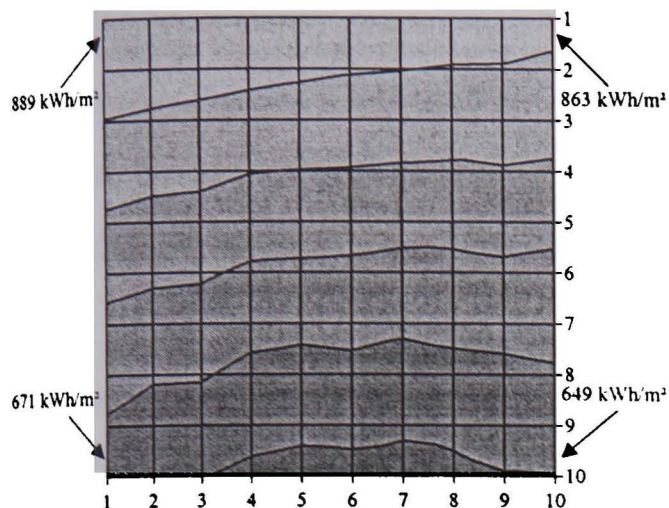


Figure 7.34
 Distribution of the annual irradiation at the facade of the opposing houses in Wuerzburg. The houses have a distance of 10 m from each other.

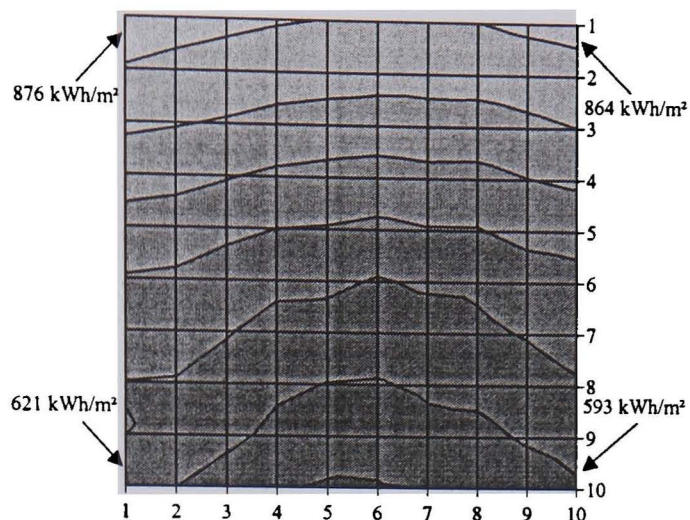


Figure 7.35
 Similar to Fig. 7.34 but with a distance of 8 m.

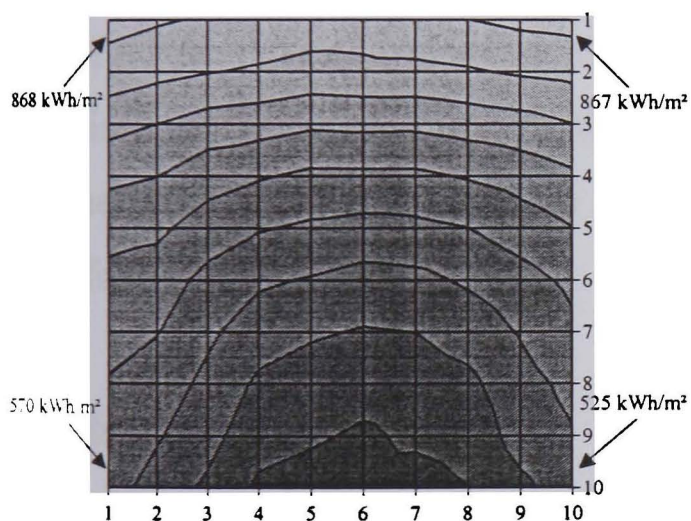


Figure 7.36
 Similar to Fig. 7.34 but with a distance of 6 m.

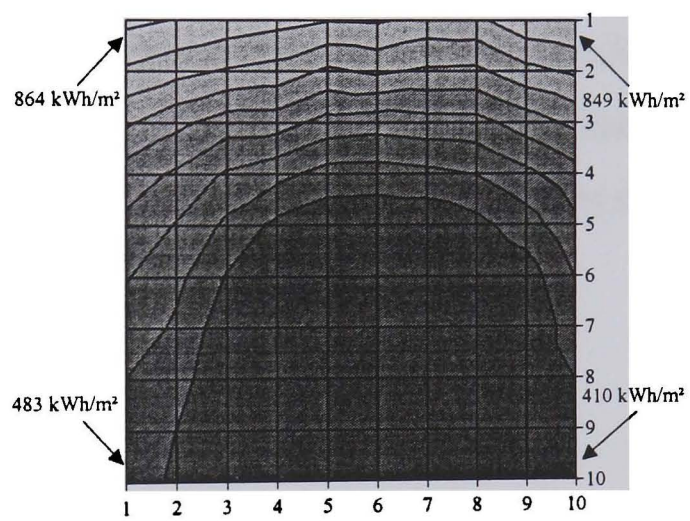


Figure 7.37
 Similar to Fig. 7.34 but with a distance of 4 m.

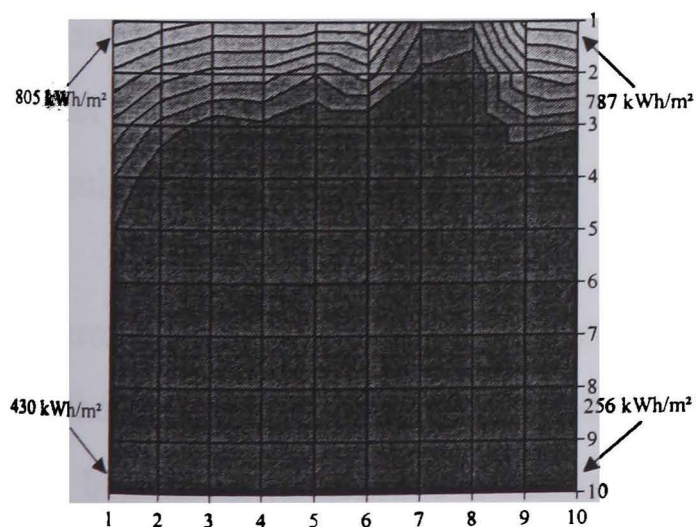


Figure 7.38
 Similar to Fig. 7.34 but with a distance of 2 m.

The results showed an MBE from -1.5% to 4.8% and an RMSE from 9.8% to 16.1% with RADIANCE parameters close to the defaults (except *ab*).

It can be assumed that the results will improve even further when looking at outdoor (irradiance) values. Here, the ambient calculation of RADIANCE (that calculates all the light in the scene that does not come directly from the sun) has a much less significant influence on the final result. The main contribution to the global irradiance at the trace points comes from the direct light which is easy to predict.

Thus, although one can feel reasonable of confident predicting correct values with IPROCESS, validation against measured irradiance values (using a correct description of the surrounding scene) would be useful further work.

To prove the overall system for predicting PV yield, validation of the PV models would be required. However, this is well beyond the scope of this work but is suggested as useful further work for others. Once the PV model is validated, a validation of the overall system can follow.

7.3.6 Conclusions

Invariably, any shading reduces the solar irradiation to a greater or lesser degree and should be avoided. However, this is not always possible since often aspects other than the energy yield must be considered. Solar facades of buildings are always multi-functional and must be subordinated to other constraints, e.g., to the building geometry, to optical reasons, or to other functions of the facade. Then, at least the best solution under the given circumstances should be found.

If architects or city planners are aware of the properties of solar systems and the influences of the buildings on PV systems, they can try to design buildings or city districts right from the beginning to achieve a maximum solar impact. The studies shown here will help to estimate the influence of the building geometry on solar systems. They will aid architects in optimising a building for solar energy and help system designers to find the best location for a solar receiver plane.



8 CONCLUSIONS

Predicting yields of solar energy systems in an urban environment is a complex task. The main problem is the non-linear behaviour of PV systems with respect to shading. As introduced in Chap. 2, a half-shaded PV array does **not** yield half of the total energy. The energy yield depends on the module wiring and on the system configuration. The starting point for yield predictions of a PV array is its inhomogeneous irradiance distribution caused by shading and reflections of sunbeams. Shading often occurs in an urban environment.

The work presented here has examined different algorithms and approaches to modelling PV systems in an urban environment. For this, different ‘Tilted surface models’ and ‘Sky luminance models’ were studied. One conclusion was that the Perez ‘All-weather sky model’ is suitable for the predictions of a time series of irradiance data.

The associated examination of PV models concluded that no model was ideal for predicting the yield of PV systems in an urban environment. Here, the models must be able to consider shading and reflections from surrounding structures since these can influence the yield of PV arrays significantly. The solution was to write an irradiance pre-processor program that would consider these factors and to connect this to a suitable PV model.

This pre-processor, IPROCESS, is based on the ray-tracing program RADIANCE. A way was found to enable a time-varying simulation with RADIANCE and to couple the output to the PV model Pvcad and to further solar models. Since the calculations with IPROCESS can take a long time (depending on the scene and the number of trace points) the daylight coefficient approach was modified and integrated in IPROCESS. Thus, a simulation run can be executed relatively quickly but often at the cost of accuracy.

The influence of the RADIANCE parameter settings on the analysis time and accuracy was examined. This led to the suggestion of three different parameter sets to enable a *fast*, *accurate*, or *detailed* simulation. A suitable number of daylight coefficients to generate a time series of irradiance data was also recommended.

Finally, the algorithms of IPROCESS were compared to those of other programs. Typical urban structures were examined to investigate the influence of the building's geometry, surface properties and location on the solar yield.

Normally, the irradiance distribution changes with each new structure. The computer code IPROCESS allows the investigation of the solar potential during the planning of a building or a city district when optimisations are still possible. Thus, it can contribute to designing better solar systems or buildings and to further disseminating solar applications.

8.1 Further work

Further work in this context would be to simplify the use of simulation programs so that even an inexperienced user can quickly achieve significant results. For this, the integration of IPROCESS with a PV model (e.g., PVcad) would be a good extension.

The validation of the shading and reflection algorithms using measured values has not been done. Others have evaluated RADIANCE for internal illumination predictions, as discussed in 7.3.5. Unfortunately irradiance data is usually collected at sites where hardly any shading occurs. A validation of IPROCESS and the associated PV model, with data from shaded PV generators, would increase the system's credibility. Furthermore, the losses at the glass cover of the PV modules (Chap. 7.2.2) requires further examinations.

One problem is still the time demand of the simulation. The ideal would be to achieve results within a second. Currently, however, this is not possible. It is expected that new computer generations will decrease the time demand significantly. Another option would be to employ the parallel computing strategies that are already available for RADIANCE.

A PEREZ AND BRUNGER MODELS

A.1 The Perez tilted surface model

In most simulation programs the Perez model is used to compute the diffuse irradiance on a tilted surface. In his publication 1987 [62], Perez simplified his earlier model from 1986 [61]. In fact two models are presented, one with a circumsolar region of 25° and one that reduces this region to a point (i.e. circumsolar region of 0°).

These models use empirically found coefficients F'_{nm} that depend on the Perez coordinates sky clearness parameter ϵl (originally only ϵ but here this symbol is already used in an other context) and sky brightness parameter Δ (Equ. 3.25 and 3.26).

The relative optical air mass m describes the inclined path of a sun beam through the atmosphere in relation to a perpendicular path when the sun is in the zenith [76].

$$m = \frac{p}{p_0} \frac{1}{\sin(\epsilon_s) + 0.50572 \cdot \left(\frac{180 \cdot \epsilon_s}{\pi} + 6.07995 \right)^{-1.6364}} \approx \frac{1}{\sin(\epsilon_s)} \quad (\text{A.1})$$

The approximation is valid for stations near sea level and solar elevations above 10° (ϵ_s in degree). The ratio of the atmospheric pressure at the station to the pressure at sea level is given by Equ. (A.2) and (A.3).

$$\frac{p}{p_0} = 1 - \frac{h}{10000} \text{ for } h < 4000 \quad (\text{A.2})$$

$$\frac{p}{p_0} = \exp \left[\frac{h}{10000} \left(-0.1174 - 0.0017 \frac{h}{10000} \right) \right] \text{ for } 4000 \leq h \leq 10000. \quad (\text{A.3})$$

The factors F'_{nm} of the Perez model depend on a set of empirically found coefficients as given in the following chapters.

$$F'_1 = F'_{11(\varepsilon l)} + F'_{12(\varepsilon l)} \cdot \Delta + F'_{13(\varepsilon l)} \cdot \theta_s \quad (\text{A.4})$$

$$F'_2 = F'_{21(\varepsilon l)} + F'_{22(\varepsilon l)} \cdot \Delta + F'_{23(\varepsilon l)} \cdot \theta_s \quad (\text{A.5})$$

A.1.1 Circumsolar region 25°

The more complex model has a half angle of the circumsolar region of 25°. The diffuse irradiation on a tilted surface is calculated according to Equ. (A.6).

$$I_{d,t} = I_{d,h} \left[\left(1 - F'_1 \right) \frac{1 + \cos(\beta)}{2} + F'_1 \frac{a}{c} + F'_2 \cdot \sin(\beta) \right] \quad (\text{A.6})$$

εl	F'_{11}	F'_{12}	F'_{13}	F'_{21}	F'_{22}	F'_{23}
1.000 - 1.056	-0.011	0.748	-0.080	-0.048	0.073	-0.024
1.056 - 1.253	-0.038	1.115	-0.109	-0.023	0.106	-0.037
1.253 - 1.586	0.166	0.909	-0.179	0.062	-0.021	-0.050
1.586 - 2.134	0.419	0.646	-0.262	0.140	-0.167	-0.042
2.134 - 3.230	0.710	0.025	-0.290	0.243	-0.511	-0.004
3.230 - 5.980	0.857	-0.370	-0.279	0.267	-0.792	0.076
5.980 - 10.080	0.734	-0.073	-0.228	0.231	-1.180	0.199
> 10.080	0.421	0.0661	0.097	0.119	-2.125	0.446

Table A.1 Original Perez coefficients for 25° model

The location of this region is specified by the ratio a/c

$$\frac{a}{c} = \frac{\max[0, \cos(\gamma_s)]}{\max[\cos(85), \cos(\theta_s)]} \quad (\text{A.7})$$

In the original, publication the coefficient of Tab. A.1 had been given, but in a later evaluation [64] with measurements of several stations, the values had been reviewed and the data of Tab. A.2 had been found. This later data set is used, for example, in the building simulation program TRNSYS [52].

ϵl	F'11	F'12	F'13	F'21	F'22	F'23
1.000 - 1.065	-0.196	1.084	-0.006	-0.114	0.180	-0.019
1.065 - 1.230	0.236	0.519	-0.180	-0.011	0.020	-0.038
1.230 - 1.500	0.454	0.321	-0.255	0.072	-0.098	-0.046
1.500 - 1.950	0.866	-0.381	-0.375	0.203	-0.043	-0.049
1.950 - 2.800	1.026	-0.711	-0.426	0.273	-0.602	-0.061
2.800 - 4.500	0.978	-0.986	-0.350	0.280	-0.915	-0.024
4.500 - 6.200	0.748	-0.913	-0.236	0.173	-1.045	0.065
> 6.2000	0.318	-0.757	0.103	0.062	-0.698	0.236

Table A.2 Second set of Perez coefficients

After continuing the research [93] the coefficients are modified again to obtain higher accuracy and less site dependence, but Perez pointed out that they now reached an asymptotic level of optimisation.

A.1.2 Circumsolar region 0°

The simpler model that reduces the circumsolar region to a point was also introduced by Perez in 1987 [62], but with different coefficients.

$$I_{d,t} = I_{d,h} \left[\left(1 - F_1'\right) \frac{1 + \cos(\beta)}{2} + F_1' \frac{\cos(\theta_t)}{\cos(\theta_s)} + F_2' \cdot \sin(\beta) \right] \quad (\text{A.8})$$

ϵl	F'_{11}	F'_{12}	F'_{13}	F'_{21}	F'_{22}	F'_{23}
1.000 - 1.056	0.041	0.621	-0.105	-0.040	0.074	-0.031
1.056 - 1.253	0.054	0.966	-0.166	-0.016	0.114	-0.045
1.253 - 1.586	0.227	0.866	-0.250	0.069	-0.002	-0.062
1.586 - 2.134	0.486	0.670	-0.373	0.148	-0.137	-0.056
2.134 - 3.230	0.819	0.406	-0.465	0.268	-0.497	-0.029
3.230 - 5.980	1.020	-0.260	-0.514	0.306	-0.804	0.046
5.980 - 10.080	1.009	-0.708	-0.433	0.287	-1.286	0.166
> 10.080	0.936	-1.121	-0.352	0.226	-2.449	0.383

Table A.3 Perez coefficients for 0° model

A.2 The anisotropic sky radiance model of Brunger

Brunger's sky model [82] is calibrated to four empirically found coefficients. They are given in a matrix (Tab. A.4) dependent on the diffuse fraction κ (Equ. 3.43) and the atmospheric clearness index κ_t (Equ. 3.44).

$\kappa \backslash \kappa_t$	0.05	0.15	0.25	0.35	0.45	0.55	0.65	0.75	0.85
0.95	0.1864 0.1979 0.0000 1.0000	0.2002 0.1772 0.0000 1.0000	0.1380 0.0930 0.2890 0.9667	0.1508 0.5472 0.6659 1.6755	0.1718 0.0566 0.8734 2.4129	0.2060 -0.0294 2.9511 3.7221			
0.85	0.1431 0.142 2.636 5.525		0.3477 -0.2153 5.3170 4.4211	0.2664 -0.1559 1.7758 2.8590	0.2139 0.0307 1.6099 3.7260	0.1520 0.1497 1.8315 4.6125	0.1151 0.1805 2.2284 4.1553		
0.75			0.3687 -0.2927 2.6268 2.8413	0.2684 -0.1615 4.5224 4.0842	0.2019 -0.1275 1.4096 2.2453	0.1870 -0.0632 1.2819 2.5932	0.1842 0.0253 1.3080 3.1127	0.1566 0.3003 1.8486 14.7440	
0.65			0.3851 -0.2726 4.1962 5.2590	0.2843 -0.1645 5.2960 4.3678	0.2713 -0.1837 2.8220 3.4860	0.1597 -0.1715 1.2964 1.9183	0.2088 -0.0520 1.3225 2.8364	0.1273 -0.0500 1.5961 2.0993	
0.55			0.6079 -0.4838 11.078 4.5880	0.2892 -0.1953 2.1346 3.7268	0.2816 -0.1945 3.8606 3.7447	0.2465 -0.1245 2.9163 4.0760	0.2070 -0.0927 1.1098 2.5586	0.2477 -0.0711 1.5836 3.4500	
0.45				0.2337 -0.1015 11.7920 5.3698	0.2822 -0.1842 6.0300 4.5241	0.2916 -0.2065 2.7327 3.7624	0.2583 -0.1654 1.9525 3.3796	0.2457 -0.1398 1.5120 2.9640	0.2315 -0.2028 1.5803 2.3229
0.35					0.3162 -0.2039 6.2226 5.8975	0.3006 -0.2172 4.5443 4.2660	0.2871 -0.2184 2.6467 3.5940	0.2491 -0.2224 1.5992 2.6404	0.2510 -0.0907 0.9733 2.6775
0.25		a ₀ a ₁ a ₂ a ₃				0.3417 -0.2574 4.1918 4.3268	0.3153 -0.2338 3.8860 4.3920	0.3071 -0.2576 2.3127 3.5189	0.2971 -0.3126 1.3594 2.3970
0.15							0.3360 -0.2600 4.2481 4.3727	0.3243 -0.3003 1.9157 3.2680	0.3061 -0.4531 1.6120 2.3190

Table A.4 Coefficients for the sky model of Brunger

A.3 The Perez 'All weather model'

The coefficients of the Perez 'All-weather model' depend, similarly to the tilted surface model, on sky brightness parameter Δ and sky clearness parameter ϵl .

ϵl	a ₁ a ₂ a ₃ a ₄	b ₁ b ₂ b ₃ b ₄	c ₁ c ₂ c ₃ c ₄	d ₁ d ₂ d ₃ d ₄	e ₁ e ₂ e ₃ e ₄
1.000 - 1.065	1.3525 -0.2576 -0.2690 -1.4366	-0.7670 0.0007 1.2734 -0.1233	2.8000 0.6004 1.2375 1.0000	1.8734 0.6297 0.9738 0.2890	0.0356 -0.1246 -0.5718 0.9938
1.065 - 1.230	-1.2219 -0.7730 1.1418 1.1016	-0.2054 0.0367 -3.9128 0.9156	6.9750 0.1774 6.4477 -0.1293	-1.5798 -0.5081 -1.7812 0.1080	0.2624 0.0672 -0.2190 -0.4285
1.230 - 1.500	-1.1000 -0.2515 0.8952 0.0156	0.2782 -0.1812 -4.5000 1.1766	24.7219 -13.0812 -37.7000 34.8438	-5.0000 1.5218 3.9229 -2.6204	-0.0156 0.1597 0.4199 -0.5562
1.500 - 1.950	-0.5484 -0.6654 -0.2672 0.7117	0.7234 -0.6219 -5.6812 2.6297	33.3389 -18.3000 -62.2500 52.0781	-3.5000 0.0016 1.1477 0.1062	0.4659 -0.3296 -0.0876 -0.0329
1.950 - 2.800	-0.6000 -0.3566 -2.5000 2.3250	0.2937 0.0496 -5.6812 1.8415	21.0000 -4.7656 -21.5906 7.2492	-3.5000 -0.1554 1.4062 0.3988	0.0032 0.0766 -0.0656 -0.1294
2.800 - 4.500	-1.0156 -0.3670 1.0078 1.4051	0.2875 -0.5328 -0.3850 3.3750	14.0000 -0.9999 -7.1406 7.5469	-3.4000 -0.1078 -1.0750 1.5702	-0.0672 0.4016 0.3017 -0.4844
4.500 - 6.200	-1.0000 0.0211 0.5025 -0.5119	-0.3000 0.1922 0.7023 -1.6317	19.000 -5.0000 1.2438 -1.9094	-4.0000 0.0250 0.3844 0.2656	1.0468 -0.3788 -2.4517 1.4656
> 6.200	-1.0500 0.0289 0.4260 0.3590	-0.3250 0.1156 0.7781 0.0025	31.0625 -14.5000 -46.1148 55.3750	-7.2312 0.4050 13.3500 0.6234	1.5000 -0.6426 1.8564 0.5636

Table A.5 Coefficients for the Perez 'All-weather sky model'

The empirically found coefficients are given in Tab. A.5 with $x = a, b, c, d, e$ according to Equ. (A.9 – A.11).

$$x = x_{1(\varepsilon)} + x_{2(\varepsilon)} \theta_s + \Delta(x_{3(\varepsilon)} + x_{4(\varepsilon)} \theta_s). \quad (\text{A.9})$$

For $1 \leq \varepsilon l \leq 1.065$ Equ. (A.10) and (A.11) must be used.

$$1 \leq \varepsilon l \leq 1.065 \quad c = \exp\left(\left(\Delta(c_1 + c_2 \theta_s)\right)^{c_3}\right) - c_4 \quad (\text{A.10})$$

$$1 \leq \varepsilon l \leq 1.065 \quad d = -\exp\left(\Delta(d_1 + d_2 \theta_s)\right) + d_3 + \Delta d_4 \quad (\text{A.11})$$

B LIST OF PV MODELS

The following table presents a survey of PV models taken from ETSU [96], Kaiser [97] and from the author's personal contacts.

Tool	Company / Institute	Address	Fax / Tel	Contact
ASHLING	National Microelectronics Research Centre	Lee Maltings Prospect Row Cork (Ireland)	00353 -21 270 271	Mr. D. Mulcahy
INSEL	Universität Oldenburg Fachbereich Physik	P. O. Box 2503 D- 26111 Oldenburg	0049 - 441 798-3326	Dr. Jürgen Schumacher
ITE-BOSS	Universität Stuttgart Institut für Theorie der Elektrotechnik	Pfaffenwald- ring 47 D- 70550 Stuttgart	0049 - 711 121-0	Mr. Zahir
PHOTO	Helsinki University of Technology, Dept Technical Physics	02150 Espoo, Finland	00358 - 451 3195	Mr. K. Peippo
POWA- COST	Dr. A. A. Eberhard	Private Bag Rondebosch 7700 South Africa		Mr. M. Davis
PV	Oberösterreichische Kraftwerke AG	Böhmerwaldstr. 3 A- 4021 Linz	0043 - 732 6593 3547	Mr. Gabriel
PVcad (ISET)	ISET Institut für Solare Energie- versorgungstechnik	Königstor 59 D- 34119 Kassel	0049 - 561 7294 100	Mr. M. Viotto
PV CAD (PV IR)	PV Resources International	1440 W Mesoto Ave. Mesa, Arizona, 85202	001 - 602 6108254	Mr. W. Kaszeta
PV Calc	Oberösterreichische Kraftwerke AG	P. O. Box 298 A- 4021 Linz	0043 - 732 6593 3547	Mr. H. Wilk
PV DIM	Jensolar GmbH	F.-Engels Str. 11a D- 07749 Jena		Mr. M. Gladitz

Tool	Company / Institute	Address	Fax / Tel	Contact
PVEPO	Lehrstuhl für Technische Thermodynamik RWTH Aachen	Schinkelstr. 8 D-52056 Aachen	0049 - 241 805 399	Mrs. Monika Grötzner
PV F-Chart	F-Chart Software	4406 Fox Bluff Rd Middleton, WI 53562	001 - 606 836 8536	Mr. S. A. Klein
PV FORM	Sandia National Laboratory	Albuquerque New Mexico, NM 87185	001 - 505 844 4383	
PV ISRAEL	Ben-Gurion University of the Negev Blaustein Institute for Desert Research	Sede Boqer Campus Israel		
PV NetSim	Mr. Thomas Schilla	Marienstr. 18 D- 73262 Reichenbach	0049 - 7153 590 994	Mr. T. Schilla
PV Node	ZSW Baden-Württemberg	Heßbrühlstr. 21c D- 70565 Stuttgart	0049 - 711 7870 236	Mr. Stellbogen
PV SOL	Dr.-Ing. G. Valentin	Köpenickerstr. 9 D- 10997 Berlin	0049 - 30 611 917	Mr. Valentin
PVS for Windows	Econzept Energieplanung GmbH	Wiesentalstr 29 D- 79115 Freiburg	0049 -761 40 166 27	Mr. Schnellbach
PVSYST	GAP University of Geneva	158 rue de Florissant CH- 1231 Conches	0041 - 22 347 86 49	Mr. A. Mernoud
PV-TAS	UECONSULT GmbH	Augustinusstr. 11c D- 50226 Frechen	0049 - 0223 465095	
SAM	ENGCOTEC GmbH	P. O. Box 10 12 62 D- 70011 Stuttgart	0049 - 711 222 96 777	Mr. T. Schilla Mr. Schweizer
SHADE	ZSW Baden-Württemberg	Heßbrühlstr. 21c D- 70565 Stuttgart	0049 - 711 7870 236	Mr. Stellbogen
SOMES	Utrecht University Department of Science, Technology & Society	Padualaan 14 NL- 3584 CH Utrecht	0031 - 30 253 7601	Mr. van Dijk
TRNSYS	Transolar Energietechnik GmbH	Nobelstr. 15 D- 70569 Stuttgart		
WAT-SUN PV	WATSUN Simulation Lab.	University of Waterloo, Canada Ontario N2L 3GL	001 - 519 888 6197	Mr. D. Thevenard

Table B.1 Survey of known PV simulation programs including contact addresses.

C RADIANCE: INPUT AND DEFAULTS

C.1 A simple RADIANCE scene description

A simple scene which consists of just one round light (centre $[x, y, z] = [10, 10, 10]$, radius = 1, emissivity $[r, g, b] = [50, 50, 50]$) and a blue floating ball light (centre $[x, y, z] = [0, 0, 3]$, radius = 1, emissivity $[r, g, b] = [0.1, 0.1, 0.5]$) might be entered as following.

```
# material of a lantern, void means no modifier
void light lamp
0
0
3 50 50 50
# No. red_emission green_emission blue_emission

# surface of the lantern, the lantern it self
lamp sphere lantern
0
0
4 10 10 10 1
# No. x_centre y_centre z_centre radius

# material of the ball
void plastic blue
0
0
5 0.1 0.1 0.5 0 0
# No. red_reflectivity green_reflectivity blue_reflectivity specularity roughness

# surface of the ball
blue light ball
0
0
3 0 0 3 1
# No. x_centre y_centre z_centre radius
```

C.2 RADIANCE *rtrace* defaults

Parameter	<i>rtrace</i> ADELINE 2.0
# irradiance calculation off	-i-
# x resolution	-x 0
# y resolution	-y 0
# back face visibility on	-bv+
# direct threshold	-dt 0.050000
# direct certainty	-dc 0.500000
# direct jitter	-dj 0.000000
# direct sampling	-ds 0.200000
# direct relays	-dr 2
# direct pretest density	-dp 512
# direct visibility on	-dv+
# specular jitter	-sj 1.000000
# specular threshold	-st 0.150000
# ambient value	-av 0.0000 0.0000 0.0000
# ambient value weight	-aw 0
# ambient bounces	-ab 0
# ambient accuracy	-aa 0.200000
# ambient resolution	-ar 128
# ambient divisions	-ad 512
# ambient super-samples	-as 0
# extinction coefficient	-me 0.00e+000 0.00e+000 0.00e+000
# scattering albedo	-ma 0.0000 0.0000 0.0000
# scattering eccentricity	-mg 0.000000
# mist sampling distance	-ms 0.000000
# limit reflection	-lr 6
# limit weight	-lw 0.004000
# format input/output = ascii/ascii	-faa
# output value	-ov
# warning messages on	-w+

D COUPLING IPROCESS TO TRNSYS

IPROCESS can be used as an irradiance pre-processor to the thermal building model TRNSYS. Often, the thermal behaviour of a building will be predicted but the solar irradiance on walls, windows or thermal collectors is uncertain because of the influence of shading and reflections. These may be caused by the building itself, for example by atria or courtyards, or by neighbour buildings. TRNSYS has a built-in type (TYPE 34) that can consider shading from overhangs and wingwalls but often, buildings have a much more complex geometry.

To use the output data from IPROCESS for TRNSYS, the output format option '*no header*' or '*global irradiance + temp*' should be chosen. Common to both formats is that the records start directly in the first line of the generated file and no header is printed. The numbers of digits and the position of the first digit of each data (this information is required by the data reader) are given in Tab. E.2.

The TRNSYS Type 9 - Data Reader [52] is used to read data from external files. Often weather data are read from a file containing a Typical Meteorological Year (TMY). A special mode of the data reader, Mode 1: TMY READER MODE, matches to this format. Other data can be read by using the mode 2, Mode 2: STANDARD DATA READER, which offers two options:

- unformatted reading (reads data after data, separated by a space or comma)
- formatted reading (uses the FORTRAN code to specify the position and length of the data)

D.1 Unformatted reading

An example how the Data Reader is used for unformatted reading is given below. The text in italic is only an explanation and must not appear in the TRNSYS DEK-file.

```
UNIT 2 TYPE 9 DATA READER (FREE)
PARAMETERS 14
2          mode 2
3          number of values to be read in total
1          time interval in hours
-3 2 5     read the 3rd value, do not interpolate (-), multiply with 2 and add 5
-4 11 0    read the 4th value, do not interpolate (-) and multiply with 11
6 0.5 7    read the 6th value, interpolate it with the last value, multiply with 0.5
and add 7
13         logical unit number of the input file
-1         unformatted reading
```

Unfortunately there seems to be a small bug in the TRNSYS code. As soon as the 11th value is to be read, the Data Reader interpolates the values regardless of how the parameters are set. Further, it is not possible to read more than a total of 18 values. Thus, it is preferable to use the formatted Data Reader.

D.2 Formatted reading

An example for the formatted Data Reader is given below. Again the text in italic must not appear in the DEK-file.

```
UNIT 2 TYPE 9 DATA READER (FORMATTED)
PARAMETERS 17
2          mode 2
4          number of values to be read in total
1          time interval in hours
-1 1 0     read the 1st value and do not interpolate (-)
-2 11 0    read the 2nd value, do not interpolate (-), multiply with 11
-3 0.5 7   read the 3rd value, do not interpolate (-), multiply with 0.5 and add 7
4 1 0     read the 4th value and interpolate it with the last value
13         logical unit number of the input file
```

```
1          formatted reading
(F4.0, 21X, F6.0, F8.2, 8X, F8.0)
```

The last '1' determines the formatted reading. Then, TRNSYS expects a line embedded in parenthesis that gives the FORTRAN format of the data to be read. All records must have the same format. Although more symbols can be used, the two letters X and F are sufficient to describe the format of the records.

- X to skip the specified number of digits, e.g. 21X means to skip 21 digits
- F to read a float number, e.g. F6.1 means to read a total of 6 digits, consisting of 4 numbers, one comma and one digit after the comma

Output files generated by IPROCESS using the option *no header* can be read with the format specification as given in the example above. This would read the values: day, temp, beam_h and glo001 from the file.

To read the data from a file generated with the option *global irradiance + temp* (Tab. E.3) the following lines can be used. This, would read the temperature and the irradiance values glo001 ... glo005.

```
UNIT 2 TYPE 9 DATA READER (FORMATTED)
PARAMETERS 23
2 6 1 -1 1 0 -2 1 0 -3 1 0 -4 1 0 -5 1 0 -6 1 0 13 1
(F6.0, F8.0, F8.0, F8.0, F8.0, F8.0)
```

Two limitations of TRNSYS must be observed:

- i) one data reader (Type 9) can read only 18 different values for one time step and
- ii) in total, up to five data readers can be specified in one DEK-file.

Thus, a maximum of 90 different irradiance values that are scattered over a receiver plane can be used for a simulation.

E IPROCESS MANUAL

E.1 Preliminary remarks

Before working with IPROCESS please make sure that the program is properly installed on your machine. IPROCESS requires also an installation of RADIANCE (for PC) that is delivered in the ADELIN package. While installing, several files are copied to the selected directory. It is recommended shift the new programs, *dcalc.exe*, *pcalc.exe*, *pcoef.exe*, *gensky1.exe*, and *gendayli1.exe*, to the binary directory of ADELIN (e.g. C:\ADELINE\BIN). The file *perezlum.cal* must be copied to the raylib directory of ADELIN (e.g. C:\ADELINE\RAYLIB).

E.2 Introduction

IPROCESS is a program to calculate the irradiance at arbitrarily chosen (trace) points in a modelled scene. Usually, the trace points are placed on a receiver plane of a solar system and the results are used for energy yield predictions. Structures that surround the solar system can be modelled and their influence regarding shading or reflections is considered in the irradiance calculations.

The scene must be described in a plain ASCII file that can be written with a simple text editor. Another option is to model the scene with a 3D-CAD program (e.g. AutoCAD) and converted it to the ASCII file. The latter method is recommended for complex scenes.

The co-ordinates of the trace points must entered into a second ASCII file. It can be produced with the aid of a built-in visualisation tool that helps to find the required data.

The screenshot shows the 'Irradiance processor' window with the following fields and values:

Location			
Site name	Latitude south=minus	Longitude east=minus	Time meridian east=minus
D-Stuttgart	48.47	-9.12	-15.0

Irradiance			
File type	Time mode	Factor to Wh/m ² or select units	Start time day month
try: DIRh DIFh T	solar time	1	1 1

Irradiance file: sample.try

Scene and output			
Scene file path	Scene file 1	Scene file 2	Scene file 3
C:\IPROCESS\	sample.rad		

Coordinates file: sample.inp

Coefficients file: step.cof

Output file: C:\IPROCESS\stuttgart.out

Format of output file: standard (with header)

Time period		Algorithm	Sky model
start	stop		
1 1	31 12	<input checked="" type="radio"/> direct	PEREZ
		<input type="radio"/> patch sky	RTRACE options: -l -aa 0.4 -ab 2 -ad 64

Figure E.1
Input
mask of
IPROCESS

Three formats of the necessary climate data file (horizontal irradiance and temperature) are accepted. Two different calculation algorithms can be selected: the direct method should be used if a short time period is regarded and a higher accuracy is required. The patch method is somewhat less accurate but much faster at long time periods, i.e. the calculation of a complete year.

In the following chapter the different options and opportunities are described. The headers refer to the main frames of the IPROCESS surface (Fig. E.1).

E.3 Features

E.3.1 Location

The user can enter the geographical location of the scene either directly in the foreseen fields or select a site from the database by clicking on the *Location* button. Adding and removing of records is supported. The information of the standard meridian of the site is only required if the weather data are recorded at local time. Otherwise they are neglected.

E.3.2 Irradiance

In the field *Irradiance file* the user has to enter the path to the file containing the weather data. By clicking on the *Data* button, a file can be selected from a list. The data must be supplied in one of the three formats given in Tab. E.1.

Format	1 st column	2 nd column	3 rd column	4 th column	5 th column
TMY	arbitrarily	arbitrarily	direct normal	global horizontal	temperature
TRY	direct horizontal	diffuse horizontal	temperature	-	-

Format	1 st - 5 th column	6 th column	7 th column	8 th column
SCT	five columns with arbitrarily values	temperature	global horizontal	global diffuse

Table E.1: Accepted formats of irradiance data files

In files of the TMY or TRY format, the records must start in the first line. The SCT format assumes a header of seven lines. This format is fitted to data files generated with PV model PVcad.

The entries of the further boxes of this frame must be done as follows:

- *File type*

The selected type must fit to data file containing the weather data.

- *Time mode*

Here, it must be entered if the data were recorded at *solar time* or *local time*. Solar time means the sun reaches its highest elevation at 12:00 noon. If the data were recorded at local time, the sun position is calculated considering the deviation of the site to the *standard meridian* and the equation of time. The TRY and TMY data refer to solar time and the SCT data to local time.

- *Factor to Wh/m² or select units*

IPROCESS calculates irradiance in Wh/m². If the data are supplied in a different format their units can be selected in this box or the factor to convert the data to Wh/m² must be entered.

- *Start time*

The day when the first record starts must be entered in this box.

E.3.3 Scene and output

E.3.3.1 Scene description

The scene with the receiver plane and surrounding structures must be described in an ASCII file according to the rules of a RADIANCE scene description. The geometrical information and surface properties can be supplied in up to three different files (for example one with surface properties and one with geometrical data) that will be merged during the simulation. Care must be taken that the modifier of a surface is mentioned before the surface is referred to (i.e. the file with the surface modifier must appear left from the file with the surface itself).

By clicking on the *Scene* button, the files can be selected from a list. At minimum one file must be selected to perform an irradiance calculation (however, this file may be empty). The scene files can be opened with a text editor for manually editing or browsing within IPROCESS.

By clicking on the *Create files* button a form is opened that allows to generate the ASCII file from a DXF file. This is usually created with 3D AutoCAD and the rules given in the RADIANCE DXFCONV manual must be followed to ensure a proper conversion.

If a DXF file is selected and the *Create file* button clicked, two files will be generated. One containing the materials and the other containing the geometrical data. Since the AutoCAD material properties do not match to RADIANCE they cannot be generated automatically but they are set to predefined defaults. The user has to enter the correct material properties manually.

E.3.3.2 Ray files

The ray file contains the co-ordinates of the points of interest (trace points). These are often the centres of PV modules, thermal collectors or windows. It depends on the requirements of the user if one point should symbolise the complete PV array or if a set of data should be generated, e.g. one value for each PV module.

Additionally to the coordinates, the direction must be entered. This is usually the normal vector of the surface (e.g. 0/0/1 for a horizontal surface). Thus, for each point 6 data are required, three for the coordinates and three for the direction. Always the x-vector points to the east, the y-vector towards north, and the z-vector to the zenith.

If the data are already entered to a file it can be selected from a list by clicking on the *Ray* button. The data can be also extracted from a visualised scene by clicking on the *Create file* button. This will load a form where first the name of the ray file is to be entered into the *Visualise scene* box. The two buttons below (*With VIEW* - *with OBJVIEW*), will display the scene on the screen. Depending on the scene size, its complexity, the view point, and the view direction, either method will work better. However, very large scenes cannot be visualise. If the button *Including trace points* is selected already entered trace points are displayed within the scene in form of arrows.

Once the scene is visualised, the *t*-command can be used to extract the coordinates of an arbitrarily point that is selected with the mouse. These coordinates must be entered into the *Create ray file* form at *Enter coordinates - Sample point*. The same data will immediately appear under *Data written to file - Sample point*. If the surface normal is known the vector can be entered under *Direction*, otherwise two further points on the plain must be entered (anticlockwise) under *Second* and *Third point*. Then, the normal vector is determined automatically and will appear under *Direction*. If the data are correct, they can be added to the ray file by clicking on the *Add data to ray file* button. The user should take care that the sample point is not falsely hidden behind the surface. This may happen due to rounding errors. It is always recommended to place the points slightly in front of the plane.

Once the scene is visualised, *rview* commands allow moving around to select a certain view and to find the right plain. Further commands are listed in the RADIANCE *rview* manual.

E.3.3.3 Coefficient file

This box is only active if the *Patch sky* method is selected. Then the entered file has to contain pre-calculated coefficients that will be used for the irradiance computation. If such a file does not exist it must be created first by clicking on the *Coefficient - Create file* button.

In the appearing form, the *file name* and the *step* are to be entered. The latter defines the angle between two patches and thus, the total number of patches. A small step will lead to a large number of patches, a higher accuracy and a long computation time. As a very general rule that however needs to be validated for each specific scene and sample point, a step of 13 will increase the inaccuracy by max. 20% and a step of 25 by about 30% in contrast to the direct method. The file will be generated when the *Create* button is pushed in the *Coefficient file* form.

E.3.3.4 Output file

In the *Output file* box the path and name of the resulting file is to be entered. It can be generated in the following formats:

Standard (with header)

This selection will generate the most extensive file. It comprises a header that specifies the used data files, the sky model, the simulation parameters, the time mode and a label for each column. At each record the day, hour, solar zenith angle, solar azimuth angel, temperature, beam horizontal irradiance, diffuse horizontal irradiance, and the calculated global irradiance at the trace points are printed.

	day	hour	sol_ze	sol_azi	temp	beam_h	diff_h	glo001	glo002
Sample	182	6	84.97	-123.43	5	0.00	5	5	5

Table E.2: Output format using the option 'Standard (with header)'

No Header

The file generated with this option contains the same record as given above but without a header. The first record starts directly in the first line.

Global irradiance + temp

Using this choice will generate a file without a header. Each record contains the temperature in the first column and the global irradiance at the trace points in the following columns.

	temp	glo001	glo002	glo003	glo004	glo005
Sample	14	5	6	5	7	8

Table E.3: Output format using the option 'Global irradiance + temp'

Output for PVEPO

This option will produce a file with a format fitted to the PV model PVEPO. It contains no header and at each record the data are given in the following order: number of the trace point, day of the year (1 ... 365), hour, global irradiance, temperature. Since each trace point requires one line per hour the file may become very long if many points are to be traced.

No.	day	hour	glo_no	temp
1	1	6	5	5
2	1	6	6	5
3	1	6	5	5
.
1	1	7	18	6
2	1	7	18	6
.

Table E.4: Output format using the option 'Output for PVEPO'

Output for PVcad

The file generated with this option is fitted to the PV model PVcad. It contains a header with the label of the columns and then: day, month, year, hour, minute, temperature, global irradiance. However, some data are not used within PVcad, thus the minute is always set to 0. Further, PVcad requires the input of any year, thus the year is always set to 1990. This must be entered in PVcad to run a simulation. It should be noticed that PVcad counts the hours from 0 to 23. Thus, in contrast to other irradiance data the values at the full hour refer to the succeeding hour. For example the data of 10:00 refer to the interval from 10:00 to 11:00.

<i>Day</i>	<i>Month</i>	<i>Year</i>	<i>Hour</i>	<i>Minute</i>	<i>T_amb</i>	<i>MOD_1</i>	<i>MOD_2</i>
Tag	Monat	Jahr	Stunde	Minute	T_umg	MOD_1	MOD_2
1	1	1990	6	0	5	5	5
1	1	1990	7	0	6	18	18
1	1	1990	8	0	6	102	102

Table E.5: Output format using the option 'Output for PVcad'

E.3.4 Time period

In these boxes the simulation *start* and *stop time* are to be entered.

E.3.5 Algorithm

IPROCESS offers the options to choose between the *direct* method or the *patch* approach. If the latter method is used the sky is divided into several patches. The contribution of each patch to the irradiance at a specific trace point is determined with ray-tracing and at a normalised sky brightness. This contribution, a so-called form factor, of each patch and each sample point is stored in a file. In the succeeding simulation, the real sky luminance distribution is generated and the irradiance is calculated using the form factors.

By this way the computation can run much faster because the time consuming ray-tracing is executed only one time but the results are less accurate.

E.3.6 Sky model

A sky model can be selected from an extensive list. However, for a long-term simulation always the *Perez* sky model is recommended. Using the sky patch approach the *Brunger* model will also perform well. The other models are for experimental purpose or for single days with a constant sky characteristic.

E.3.7 RTRACE options

This option specifies the accuracy and the time demand of the calculations. Three predefined parameter sets can be used: *fast - accurate - detailed*. It is also possible to enter user defined parameters but be sure to enter the *-I* parameter if the irradiance is to be calculated.

E.3.8 Start

After all boxes are filled and each options are entered the simulation can start by clicking on the *Start* button. The entered data are checked and if inconsistent error messages are produced.

The simulation will run in a DOS window. Among other information, the current day and hour are displayed to follow the progress. The computation may take a long time, dependent on the parameters, the number of trace points, the scene size and complexity.

E.3.9 Convert

The menu item *Convert* allows to convert output files from the formats *standard, no header, PVcad* or *PVEPO* to the formats *PVcad, PVEPO* or to a file with *Summarised data*.

If the latter is chosen a file will be created where all the irradiance values for one trace point are totalled for the given time interval. This might be helpful if several trace points at one facade were used. From the resulting file it is possible to see at which corner the highest irradiation (in total) is expected to occur.

E.4 Typical working routine

In the following, a typical working routine to generate a file with separate irradiance data for different sample points is introduced. The direct method and a sky model according to Perez will be used and the *rtrace* options are set to fast. It is assumed that a data file with hourly irradiance values in the right format is either available or could be generated with PVcad.

Several sample files (sample.*) can be used to start a first simulation

E.4.1 Preparation of input files

First, the necessary input files must be provided. The scene file is either created with a text editor or it is converted from a DXF (AutoCAD) file. Then, the file with the trace points is to be created. Again, this can be done with a text editor or with aid of IPROCESS (Chap. E.E.3.3.2).

E.4.2 Entering the settings in IPROCESS

Now, the IPROCESS main form can be filled. The location can be entered directly or chosen from the database. The path and name of the irradiance file is to entered is the *Irradiance file* box and the properties of the file in the related fields according to Chap. E.E.3. The path and name of the (already existing) input files must be entered into the *Scene file* and *Ray file* boxes. An arbitrarily name and format can be chosen for the resulting *Output file*.

Now the desired time period is to be entered and the *direct* option should be selected. Finally, the *Perez sky model* should be chosen and the *RTRACE options* should be set to *fast*.

E.4.3 Running the simulation

After all entries are done the simulation can be started by clicking on the *Start* button. It must be mentioned that in some few cases the Perez sky model will result in untrustworthy

values. These are caused by a mismatch of the actual calculated sun position and the read irradiance value (read from the data file). In such cases the string "xxxxxxx" is printed instead of the value. In case of doubts, the output file should be checked on the occurrence of this string.

COMPUTATION OF ILLUMINANCE AND IRRADIANCE IN URBAN STRUCTURES

C. Schweizer

Engcotec GmbH, PO Box 10 12 62, D - 70011 Stuttgart, Germany,
Tel + 49 - 711 - 222 96 772, Fax + 49 - 711 - 222 96 777

U. Eicker

Fachhochschule Stuttgart - Hochschule für Technik, Egle-Institut
Schelling-Str. 24, D - 70174 Stuttgart, Germany,

Tel + 49 - 711 - 121 2831, Fax +49 - 711 - 121 2666

K. Lomas

Institute of Energy and Sustainable Development, De Montfort University,
Leicester LE1 9BH, UK; Tel + 44 - 116 - 257 7445, Fax + 44 - 116 - 257 7449

ABSTRACT: Shading is a major reason for decreased performance of PV systems and should be avoided wherever possible [[1]]. However, in some cases shading is unavoidable. In urban environments, neighbour buildings are often an obstacle to sunlight, specially for a vertically mounted, facade-integrated solar receiver. Shading must be considered in the system yield predictions. A new software program IPROCESS allows detailed shading calculation for virtually any environment. The calculation method ray-tracing considers not only losses due to shading but also gains due to reflections of the sunbeams by the surrounding buildings. The software IPROCESS follows a general approach that makes it useful not only for PV system simulation but also for other solar systems, such as thermal receiver, Transparent Insulation Material or daylighting.

KEYWORDS: Ray-Tracing - 1: Facade - 2: Building Integration - 3

1. INTRODUCTION

An increasing number of facade integrated PV systems or thermal air collectors are installed on non-domestic buildings. These are often situated in an urban environment where neighbour buildings have a strong influence on the spatial irradiance distribution. If the yield of a solar system in such an environment is to be predicted, the surroundings must be taken into consideration.

The aim of the work is to develop a computer program IPROCESS that predicts the time-varying solar light and energy distribution in complex urban structures. The program can be used as a shading pre-processor to calculate irradiance on arbitrarily orientated solar receivers considering shading and reflections.

The results of the new program can be used as input to a conventional solar system simulation. Primarily the work is targeted at PV systems, due to their high sensitivity to shading, but other solar system simulations will also benefit from IPROCESS.

2. METHOD

In principle, the ray-tracing approach is able to calculate solar shading. The sample point at which irradiance is to be predicted must be specified (Fig. 1). From there a bundle of rays is sent out and traced.

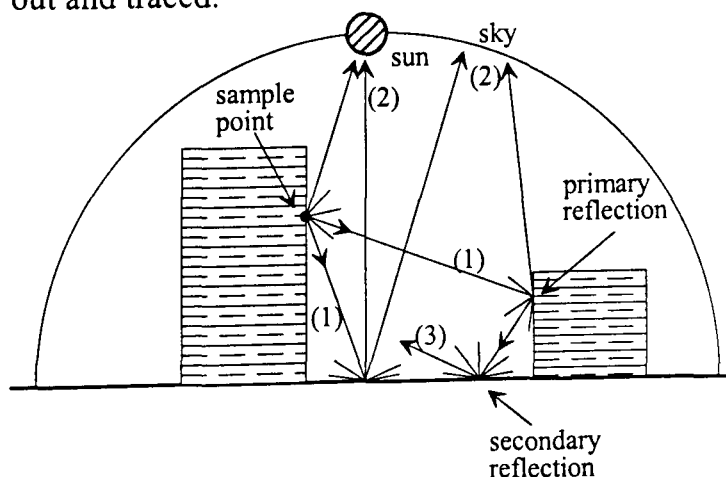


Figure 1: Backwards ray-tracing

Rays are traced until they hit a surface (1), a light source (2) or until they are attenuated by repeated reflections (3). With this approach,

virtually any architectural space can be modelled and simulated. No limitations are placed on the complexity of the scene or the accuracy that can be expected.

Different angular and specular reflection characteristics of surfaces are described by a Bidirectional Reflectance Distribution Function. Thus, different surface characteristics (for example concrete or glass facades) and even different colours of surrounding buildings can be considered (Figure 2). This could be important for coloured PV modules.

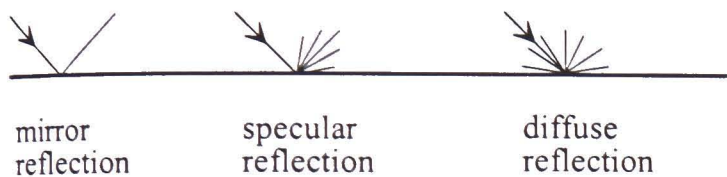


Figure 2: Different surface characteristics

3. IMPLEMENTATION

To implement the ray-tracing approach in a program the core of the validated program RADIANCE [[2]] was used. Originally it was written to generate photo-realistic images of architectural spaces where the sample point represents the place of the camera.

The limitation of RADIANCE is its static calculation of a given scene with a determined sky luminance distribution, e.g. CIE standard overcast sky. For use as a shading processor it is necessary to execute a dynamic simulation. This was done here by repeated calculations at corresponding sky luminance distributions. The sky models from PEREZ (All weather sky model) [[3]] and BRUNGER were found to be suitable [[4]].

4. EXPERIMENT

4.1 L-Shape

As an exemplary study, the arrangement of buildings shown in Fig. 3 was examined.

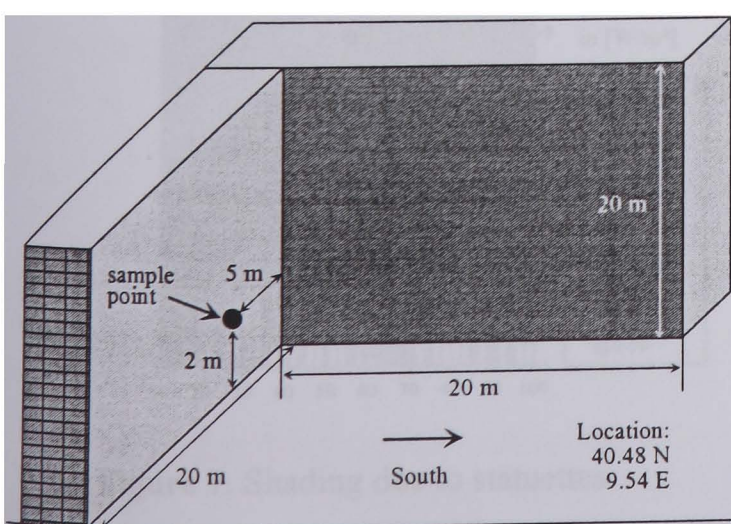


Figure 3: Two buildings in L-shape

The irradiance on the sample point was examined with different configurations for June 18 and the German Test Reference Year 5 (Wuerzburg).

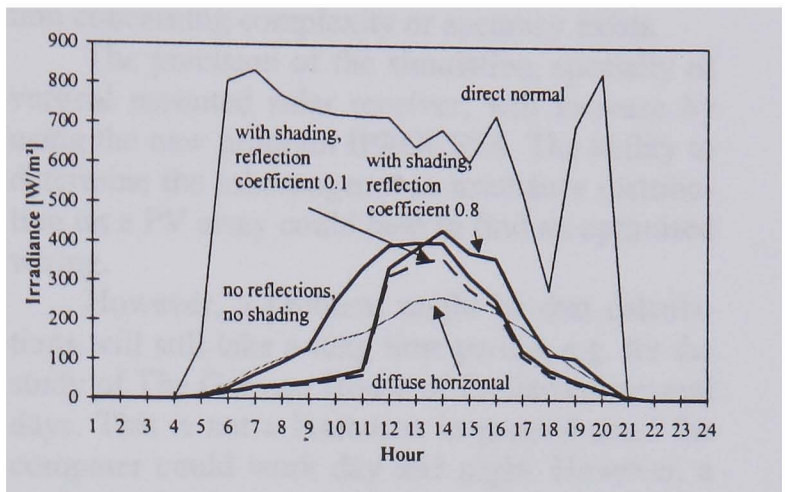


Figure 4: Irradiance at June 18

In a first simulation the rear building was not included. The curve 'no reflections, no shading' follows the typical course for a vertical, south-facing surface (Fig. 4). The curves where the facade of the rear building is modelled display the shading until 11:00. With a reflection coefficient of $\rho = 0.8$, the irradiance at the sample point is significantly increased in the afternoon compared to the curve for $\rho = 0.1$.

When a solar system is placed on a facade, its yield is of interest. This requires information about the irradiation over a time period, for example a complete year.

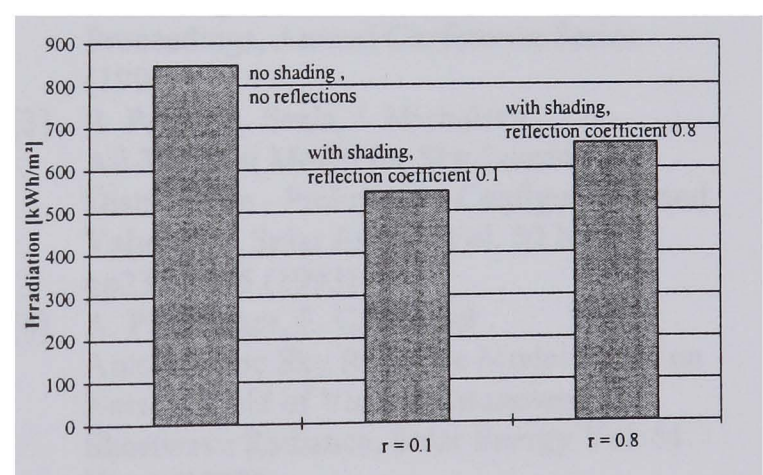


Figure 5: Annual irradiation

The results of an annual calculation for the above given arrangement are displayed in Fig. 5. If the rear building has a facade with a reflection coefficient of $\rho = 0.1$ (dull concrete) it causes a decreased irradiation at the sample point of 35.5%. A facade with a reflection coefficient of $\rho = 0.8$ (highly reflective glazing) reduces the annual irradiation by only 22.2%.

4.1 Historical Building

To calculate the inhomogeneous irradiance distribution on a surface, several sample points could be placed close together. If a PV generator is to be installed on a surface, the simulation could help to find an optimised electrical wiring or system design.

A PV system will be installed on a historical building (Fig. 6). For architectural reasons, the PV array cannot be installed without shading. Towers at the edge of the building and statuettes will decrease the performance.



Figure 6: Historical building

The losses due to different system layouts were examined. Two alternatives were discussed: a system with module inverter and a system with string inverter, five modules per string.

The study predicted yields of:

- 93% with module inverter
- 89% with string inverter

compared to an unshaded installation.

The momentary irradiance at the PV array, which consists of 10 x 10 modules, at the 12. January at 10:00 is displayed in Fig. 7. Due to the low solar elevation of $\varepsilon = 25.6^\circ$ the front modules are shaded by the statuettes. For this irradiance distribution a string wiring parallel to the front would perform better than a perpendicular wiring.

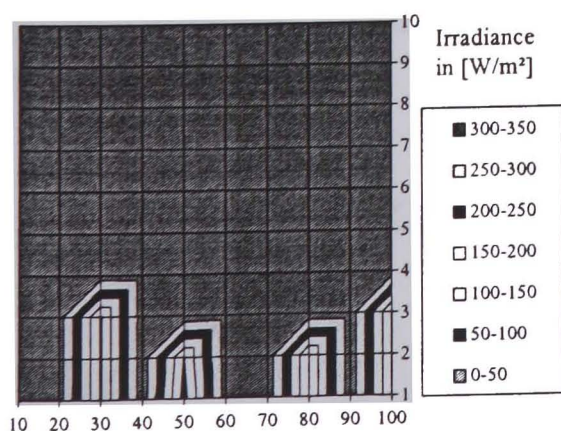


Figure 7: Shading due to statuettes

5 CONCLUSION

The new tool is well suited to calculating the irradiance distribution in an urban environment considering shading and reflections. Virtually any architectural space can be modelled and no limitation concerning complexity or accuracy exists.

The precision of the simulation, specially of vertical mounted solar receiver, will increase by using the new program IPROCESS. The ability to determine the inhomogeneous irradiance distribution on a PV array could help to find an optimised wiring.

However, a problem might be that calculations will still take a long time period, e.g. for the study of The German House of Parliament several days. This is not a limitation in general since the computer could work day and night. However, a method of reducing the computation time is the sky patch approach [[5]]. The sky is divided into several patches and coefficients for each patch are computed. They can be reused in a later annual calculation. However, faster calculation decreases the accuracy. Further work will concentrate on this aspect.

REFERENCES

- [1] C. Schweizer, D. Stellbogen, W. H. Bloss, Protective Diodes in PV Systems, Institute of Physical Electronic, University of Stuttgart, Germany (1992)
- [2] G. J. Ward
The RADIANCE Lighting Simulation and Rendering System, Computer Graphics Proceedings, Annual Conference Series (1994)
- [3] R. Perez, R. Seals, J. Michalsky
All-Weather Model for Sky Luminance Distribution - Preliminary Configuration and Validation, Solar Energy Vol. 50 No. 3 pp235 - 245 (1993)
- [4] A. P. Brunger, F. C. Hooper
Anisotropic Sky Radiance Model Based on Narrow Field of View Measurement of Shortwave Radiance, Solar Energy Vol. 51 No. 1 (1993)
- [5] P. Cropper, K. J. Lomas, A. Lyons, J. Mardaljevic
A Dynamic Lighting System: Background and Prototype, Proc. Lux Europa 97, Amsterdam, pp 480 - 492 (1997)

DYNAMIC CALCULATION OF DAYLIGHTING IN URBAN STRUCTURES

C. Schweizer¹, U. Eicker², K. Lomas¹

¹ Institute of Energy and Sustainable Development, De Montfort University, Leicester LE1 9BH, UK; Tel +44-116-257 7445, Fax +44-116-257 7449

² Fachhochschule Stuttgart - Hochschule für Technik, Egle-Institut Schelling-Str. 24, D - 70174 Stuttgart, Germany, Tel +49-711-121 2831, Fax +49-711-121 2666

ABSTRACT

Modern applications for energy saving in buildings need to include daylighting. Natural illumination will not only reduce the demand of electrical energy for fixtures but will also reduce the energy demand of air conditioning during a hot period. Conventional approaches consider the natural illumination of architectural spaces by using a statically sky lumination distribution, e.g. the standard overcast sky according to the German DIN (DIN, 1983).

This approach is not sufficient if energy saving should be calculated since it does not take the fluctuating sky lumination at the site of the building into account. This defect can be overcome by extend an existing illumination simulation program that computes only statically by a dynamic routine.

KEYWORDS

Daylighting, dynamic calculation, illuminance, illumination, irradiance, shading, ray-tracing

DYNAMIC CALCULATION OF DAYLIGHTING

Daylighting

A software that could calculate energy savings by daylighting is an extension to the building simulation program TRNSYS, the module TRNSYS -LIGHT (Dietrich, 1994). This program allows static and dynamic simulation of rectangular rooms. Results might be the illumination in Lux at the floor. This is shown in Fig. 1, where the illumination of a

simulated room is displayed. This room has partly shaded front window and a French window at the left side, from where most of the illumination is coming in.

It is foreseen to couple the output of TRNSYS-LIGHT to a dynamic TRNSYS simulation and to calculate annual energy savings that will be gained by optional switched artificial illumination. The main limitations of the program are that only rectangular rooms are permitted and that neither the surrounding of the simulated room nor atria situations can be considered.

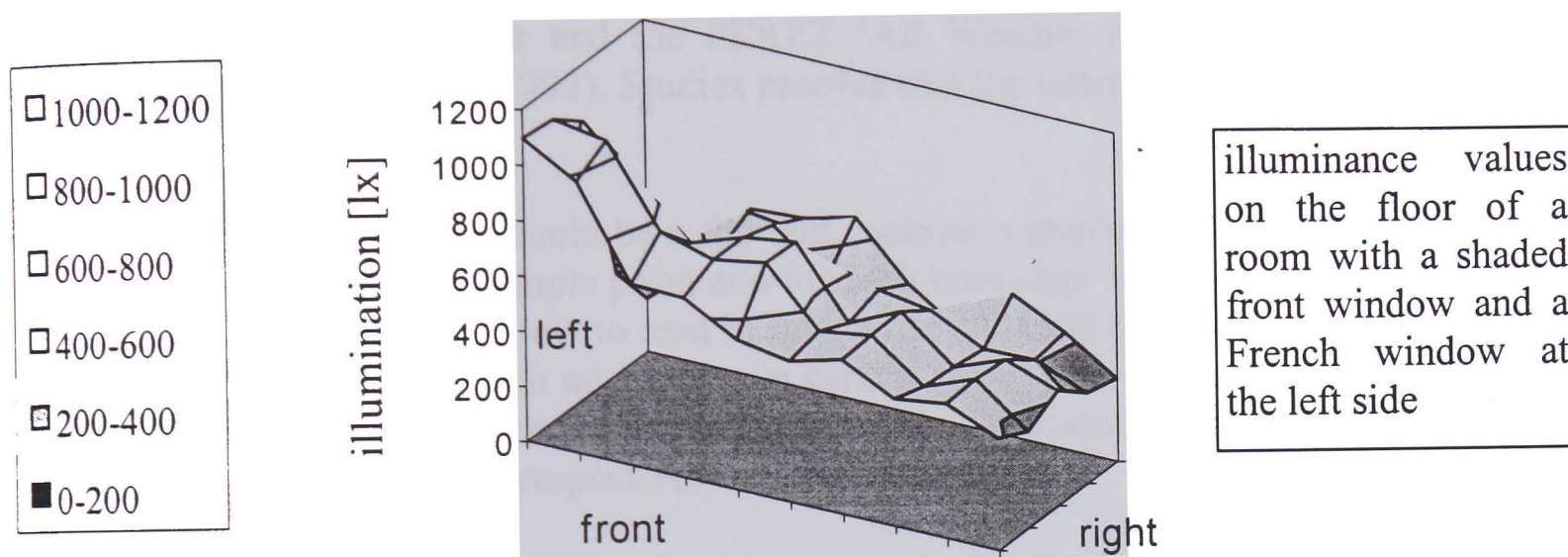


Fig. 1 Static daylighting simulation with TRNSYS-LIGHT

These limitations can be overcome by the ray-tracing program RADIANCE (Ward, 1994). It is originally designed to produce photo-realistic images of architectural spaces. Such an image, of the room simulated in Fig. 1, is shown in Fig. 2. The view point is at the right-hand side and the direction towards the left-hand side. The increased brightness at the left corner can be seen clearly.

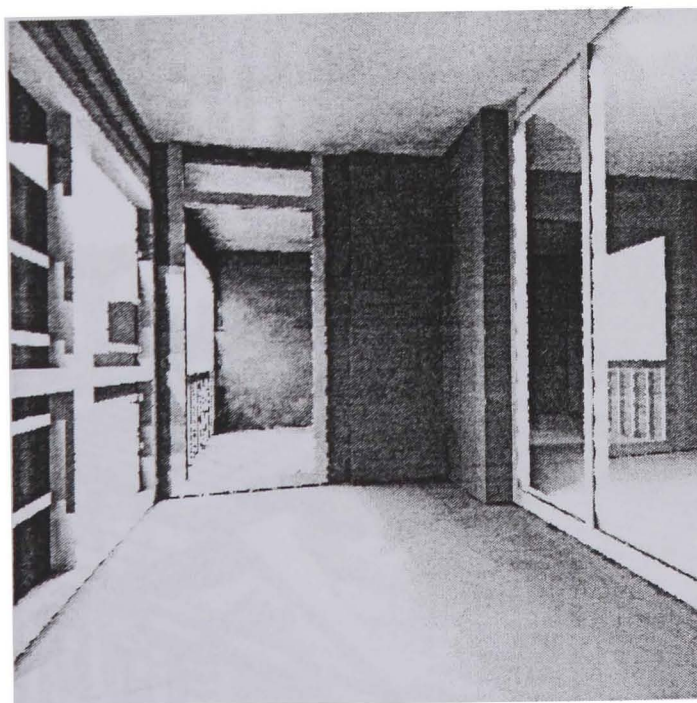


Fig. 2 Image of the room generated with RADIANCE, view from the right-hand side

RADIANCE allows to simulate virtually any architectural space, thus, also further buildings in the neighbourhood can be included. So far, RADIANCE is limited to static simulations. Besides the generation of photo-realistic images also the illuminance at specified points can be calculated.

A new extension now allows a dynamic calculation, e.g. for a complete year. This is done by repeated RADIANCE calls. For each time step the climatic data are read in (direct and diffuse irradiance from a separate file), the sun position is calculated according to the time and the location and then the corresponding sky luminance distribution is computed. Different sky models can be chosen (uniform, CIE standard overcast, standard intermediate, standard clear and the PEREZ 'All Weather Model for Sky Luminance Distribution' (Perez *et al.*, 1993). Studies proved that the latter is well suited for changing skies.

The output of the program could be a file that contains a matrix with computed brightness values for each specified sample point and for each time step. Existing building simulation programs (e.g. TRNSYS) allow to read in such a file and built up a virtual control strategy. This is for example to switch on fixtures in certain areas if the corresponding illumination decreases 500 Lux. The required energy can be calculated and also additional heat production or cooling load, respectively.

Irradiance

In principle, irradiance is the integrated illuminance over the solid angle. Thus, the new RADIANCE extension cannot only be used to evaluate illuminance values inside a room but also to calculate outside illuminance and irradiance values. The latter is specially important for solar energy systems in urban environments. These often consists of vertically mounted receivers, e.g. photovoltaic (PV) facades, air collectors or Transparent Insulation, which may be subject to complex shading and reflections of nearby standing buildings. So far, hardly any solar simulation program can deal well with shading and no one is known to the author that could also consider increased irradiation due reflections at surrounding buildings. This leakage can be also overcome with the new RADIANCE extension. Irradiance can be predicted on arbitrarily orientated surfaces in virtually any environment.

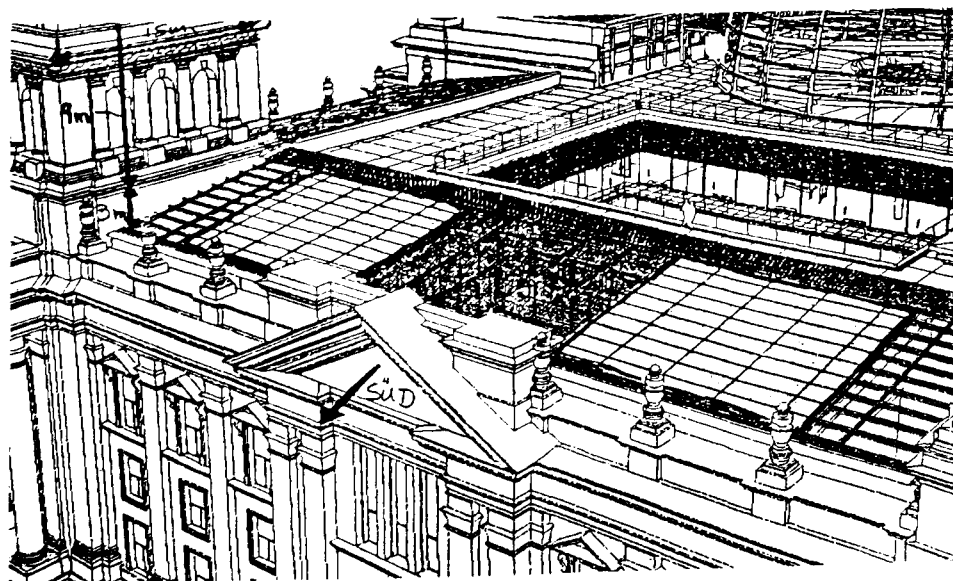


Fig. 3 Historical building Berlin, Germany

Specially for PV generators, which are very sensitive to shading, this is very important. The flexibility of RADIANCE to predict irradiance on different points of a planned PV-array can help to find an optimized wiring of the PV generator to minimize shading losses that might occur due to some building incorporated parts.

Fig. 3 shows a historical building in Berlin where a PV generator should be mounted. The two bright areas indicate the PV arrays. Due to the building itself, the modules in the front will be shaded at certain hours by different towers. The irradiance on the modules (each array with 5 x 10 modules) was predicted with the new program. Values at the leftmost row of modules are displayed in Fig. 4.

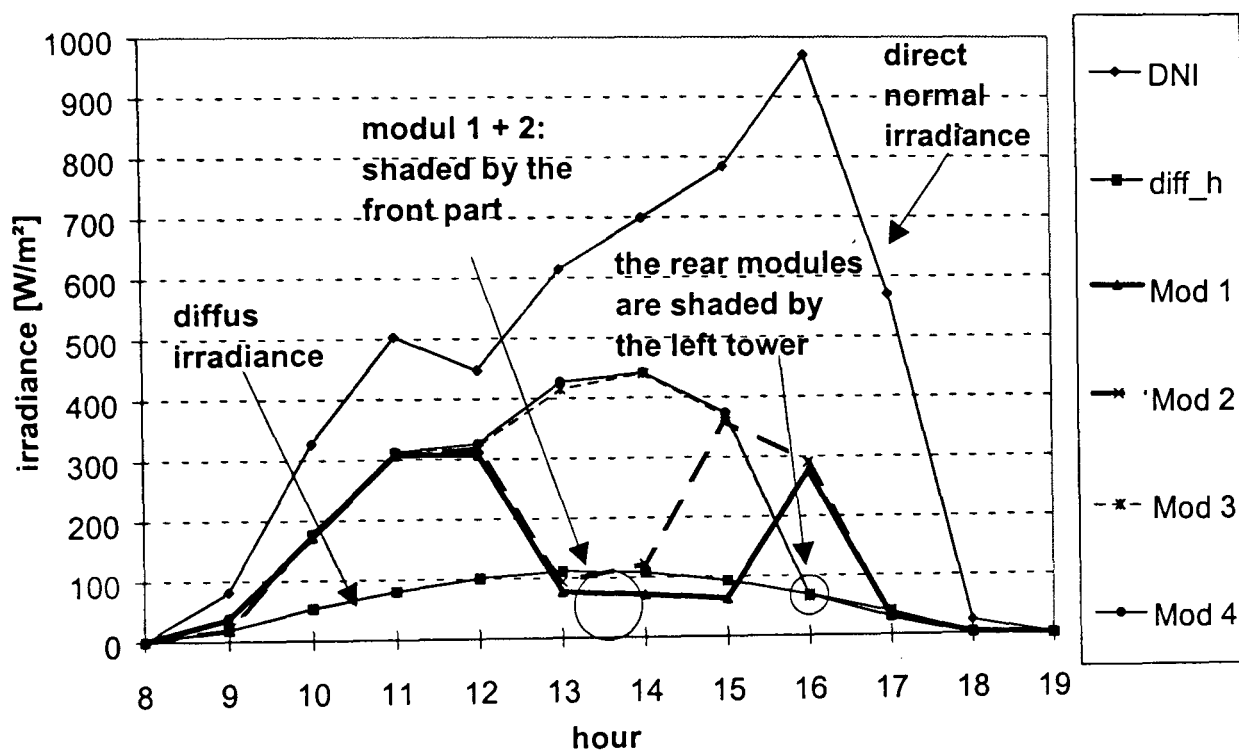


Fig. 4 Irradiance on the leftmost row of PV modules

Figure. 4 shows the different irradiance at different hours. Originally ten modules are in one row but the seven rear modules obtain the same irradiance and their curves are identically to the one of module 4.

CONCLUSION

The new tool is well suited to execute a dynamic daylight simulation. The output can be coupled to a conventional thermal building simulation. Additionally, the irradiance on arbitrarily planes in an urban structure can be predicted. This could be done for virtually any architectural space (including further buildings) and even reflections can be taken into consideration. The ability to predict irradiance on each module of a PV array allows to optimize the wiring of a PV generator.

Further work in this regard will be to demonstrate to coupling of the output of the tool to a PV simulation program.

REFERENCES

- Dietrich, U. (1994). **Tageslichtmodell TYP 70 für TRNSYS**, TRNSYS-News, Transsolar Energietechnik GmbH Stuttgart, Germany
- DIN 5034 (1983). **Tageslicht in Innenräumen**, Deutsche Industrienorm, Beuth Verlag, Berlin, Germany
- Perez, R., R. Seals and J. Michalsky (1993). **All-Weather Model for Sky Luminance Distribution** - Preliminary Configuration and Validation, **Solar Energy Vol. 50** No. 3 pp235 - 245
- Ward, G. J. (1994). **The RADIANCE Lighting Simulation and Rendering System**, Computer Graphics Proceedings, Annual Conference Series

SOLAR IRRADIATION IN AN URBAN STRUCTURE

CHRISTIAN SCHWEIZER⁽¹⁾, URSULA EICKER⁽²⁾, KEVIN LOMAS⁽³⁾

(1) ENGCOTEC GmbH

PO Box 10 12 62

D-70011 Stuttgart, Germany

Tel +49 / 711 / 222 967-72, Fax +49 / 711 / 222 967-77

(2) Fachhochschule Stuttgart - Hochschule für Technik

Schelling-Str. 24

Stuttgart, Germany

Tel +49 / 711 / 121-2831, Fax +49 / 711 / 121-2666

(3) De Montfort University, Leicester

Institute of Energy and Sustainable Development

Leicester LE1 9BH, United Kingdom

Tel +44 / 116 / 257-7445, Fax +44 / 116 / 257-7449

ABSTRACT - Several mathematical models and computer programs exist to determine the solar irradiance on an arbitrarily orientated solar receiver [1-4]. Unfortunately, these models are not longer valid for systems, operating in an urban environment. Here, site dependant circumstances like buildings in the neighbourhood have a strong influence on the received irradiance: they shade a part of the sky and block or reflect the sun light. To determine the correct irradiance is difficult, especially for a vertically mounted (for example facade integrated) solar receiver. They obtain a considerable part of their insolation through reflections and are often subject of shading.

This paper introduces a new software tool that allows computation of irradiance considering shading and reflections. The program uses a ray-tracing technique [5] (the core of the lighting simulation program RADIANCE [6]) to predict the irradiance in virtually any environment. In a study, typical architectural arrangements, which are often found in urban structures and their effects on the yield of solar systems were examined.

1. INTRODUCTION

It is still a problem to determine the solar irradiance on receivers in an urban environment. Site dependant influences due to buildings in the neighbourhood are usually neglected by mathematical models, and yet, no easy-to-use software tool exists to calculate irradiance considering complex shading and reflections.

A new computer program, IPROCESS, using a ray-tracing technique, was developed to overcome these limitations. It permits precise irradiance calculation in almost any environment. Not only geometrical characteristics of architectural spaces but also different surface properties are included in the simulation [7]. IPROCESS is a very helpful irradiance pre-processor to a standard solar thermal or PV model.

2. STUDY OF AN L-SHAPED HOUSE

As an example, the irradiance at a sample point on an L-shaped building was studied. Its location and the geometrical dimensions of the house are given in Figure 1. A ground reflectivity of $\rho = 0.2$ was assumed for all calculation.

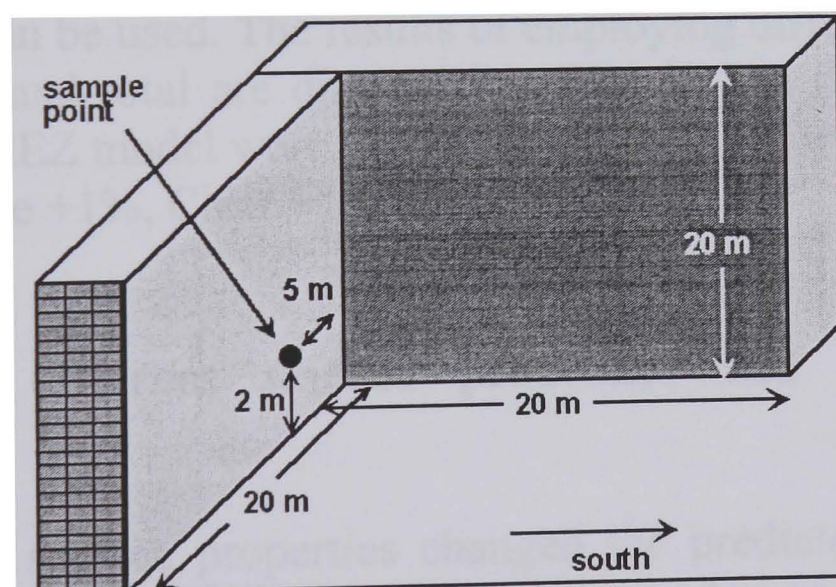


Fig. 1 L-shaped building, latitude: 48.48 N, longitude: 9.54 E

2.1 Effects of using different sky models

The effect of using different standard sky luminance models was examined, by assuming, regardless of the real sky conditions, that the description of the sky was uniform [8], overcast [9], clear [10], intermediate [11] or according to Perez [12].

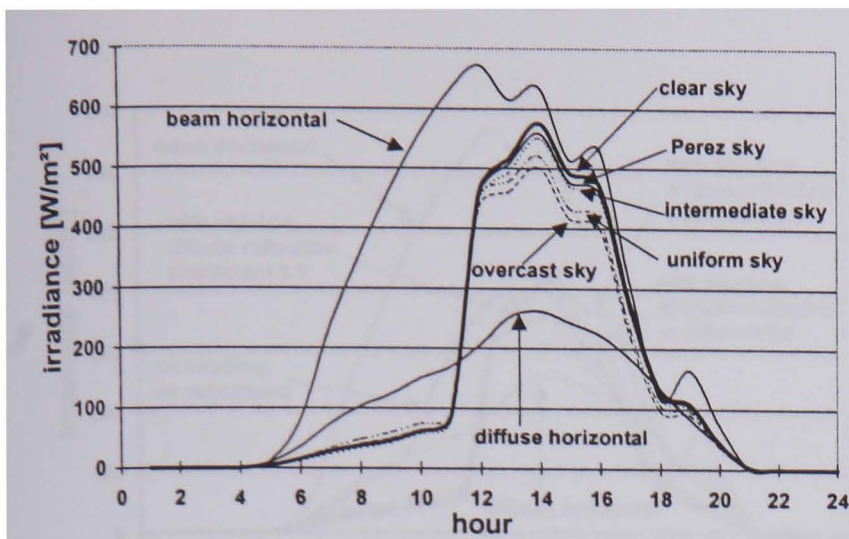


Fig. 2 Irradiance at the sample point, June 18, calculated with different sky models for a sunny day

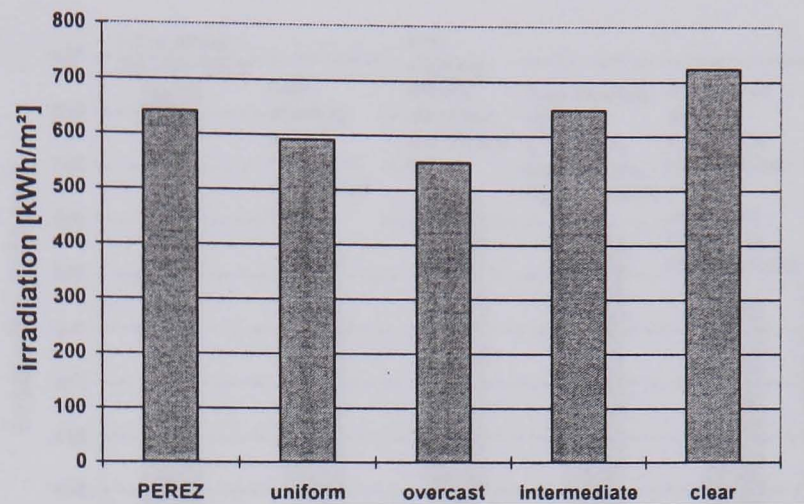


Fig. 3 Irradiation as annual sum calculated with different sky models

On a bright sunny day the overcast sky model predicted lower values than the clear sky model at hours, when the sun was 'visible' from the sample point (e.g. Fig. 2). The reason for this effect is that the overcast sky model neglects the bright zone of the sky around the sun. Thus, a certain share of the diffuse irradiance is not included.

In an annual simulation, the fluctuating sky properties must be taken into consideration. The 'Intermediate sky model' [11] or the PEREZ 'All-Weather Sky Model' [12] can be used. The results of employing different sky models for calculating the annual total are displayed in Fig. 3. The differences from the well-validated PEREZ model were, for the situation: Uniform -7.9%, Overcast -14.1%, Intermediate +1%, Clear +12.7%:

2.2 Effects of different surface properties and different shading algorithms

The way different surface properties changed the predicted irradiance at the sample point was examined. The irradiance increased at certain hours by about 10 - 15% (e.g. Fig. 4) if the reflection coefficient of the walls was set to $\rho = 0.8$ instead of

$\rho = 0.1$. Over a complete year the different reflection coefficients caused a difference of 17% (2nd and 3rd column in Fig. 5). Here, a fully diffusing reflection characteristic was assumed. When a purely specular reflection characteristic was assigned to the walls, the irradiance decreased because the sun's position does not always match the reflection angle (Fig. 4).

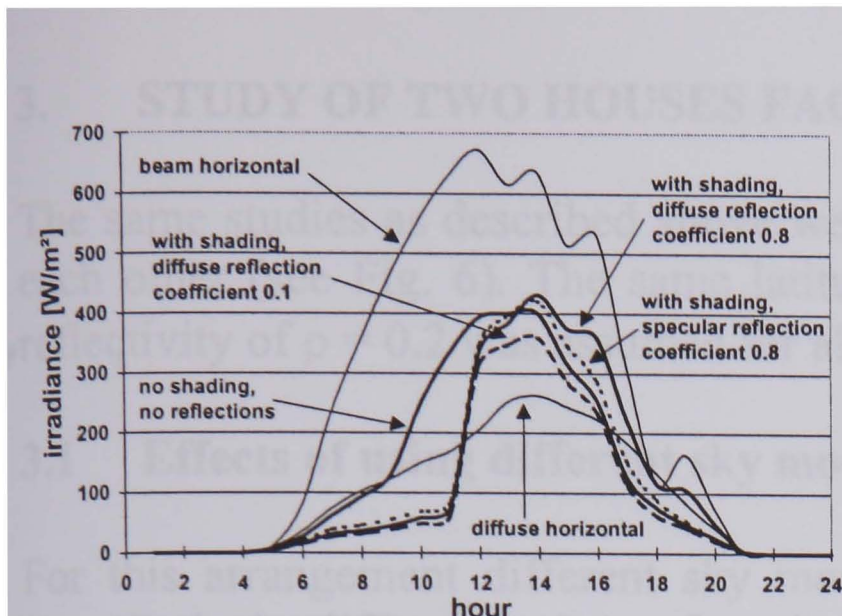


Fig. 4 Irradiance at the sample point, June 18, calculated with different surface properties

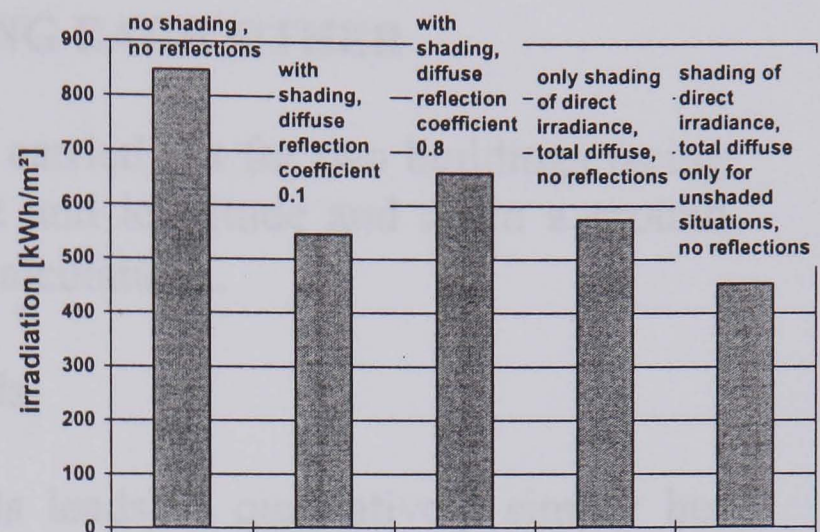


Fig. 5 Total annual irradiation, calculated with different surface properties and different algorithms

Some recently developed simulation programs are able to include shading but not reflections in the predictions. Two shading algorithms, often used by programs, which do not take the diffuse shading into consideration were studied:

- i) By a geometrical model it is determined if the sun beams can reach the sample point. If so, the global irradiance at the sample point is calculated by adding the beam and the total diffuse irradiance. If not, the total diffuse irradiance is used (the expression total diffuse irradiance shall clarify that masking of the sky vault, which reduces the diffuse irradiance, is not considered).
- ii) By a geometrical model it is determined if the sun's rays can reach the sample point. If so, the irradiance at the sample point is calculated by adding the beam and the total diffuse irradiance. If not, neither the beam nor the diffuse irradiance is used.

A limitation of these algorithms is that they do not account for the 'diffuse shading'. A neighbour building that blocks the view to a part of the sky reduces the diffuse irradiation on the sample point, which is not considered by these algorithms. Results are given in Fig. 5 (4th and 5th column). Since the second method adds the total diffuse irradiance only for unshaded situations, it predicts a lower annual sum (here 20%).

3. STUDY OF TWO HOUSES FACING EACH OTHER

The same studies as described above were carried out for two buildings facing each other (see Fig. 6). The same latitude and longitude and again a ground reflectivity of $\rho = 0.2$ was assumed for all calculations.

3.1 Effects of using different sky models

For this arrangement different sky models leads to qualitatively similar but quantitatively different values of total annual incident irradiance (Fig. 7). The differences from the Perez model are: Uniform -5.2%, Overcast -9.6%, Intermediate +1%, Clear +8.0%.

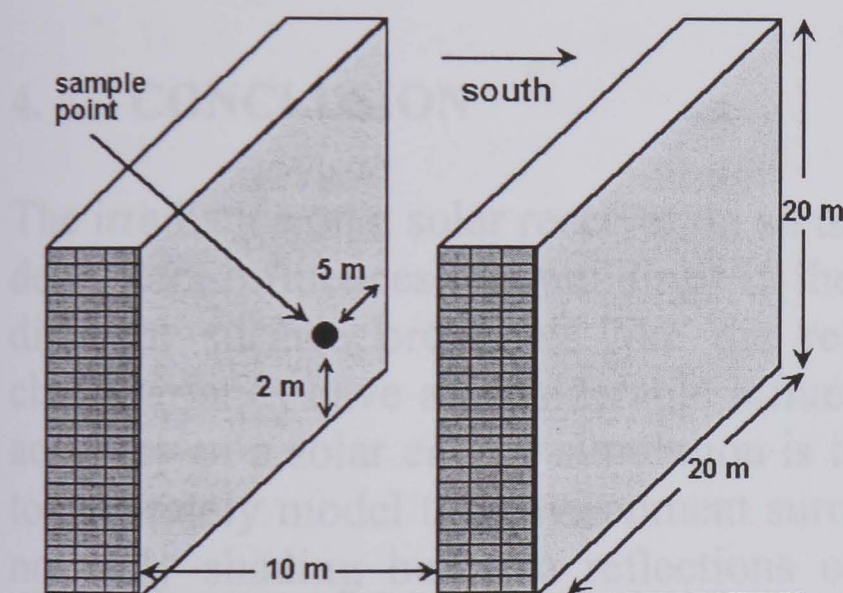


Fig. 6 Two buildings facing each other, latitude: 48.48 N, longitude: 9.54 E

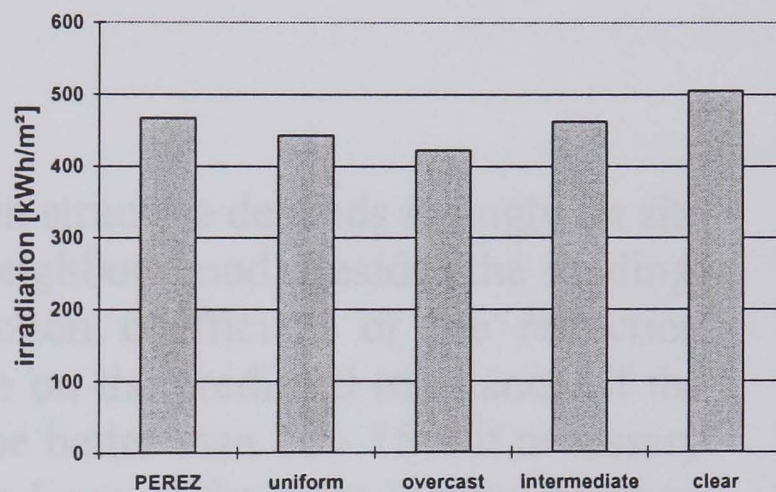


Fig. 7 Total annual irradiation calculated with different sky models

3.2 Effects of different surface properties and different shading algorithms

On the days studied, the different reflection coefficients still cause a difference of about 10 - 15% but the curves for a diffuse and a specular reflection characteristic hardly vary from each other (Fig. 8).

The total annual irradiation calculation with $\rho = 0.8$ is 14.2% higher than with $\rho = 0.1$ and the results for the two shading algorithms differed by 19% (Fig. 9).

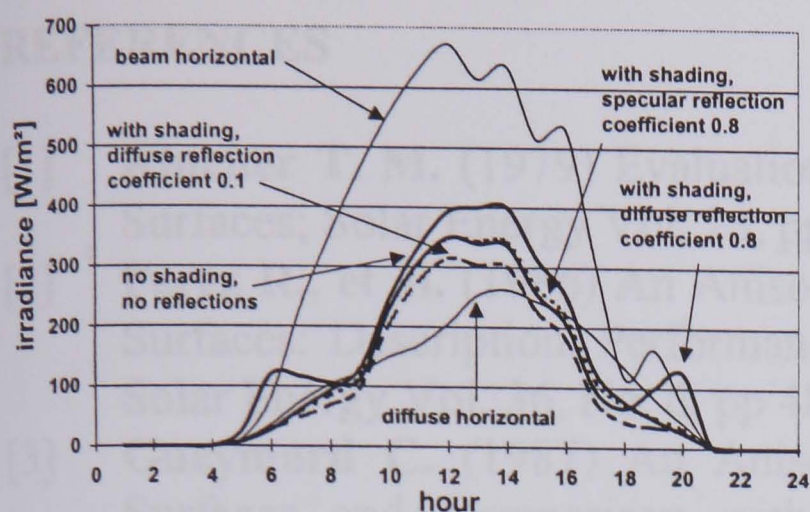


Fig. 8 Irradiance at the sample point, calculated with different surface properties

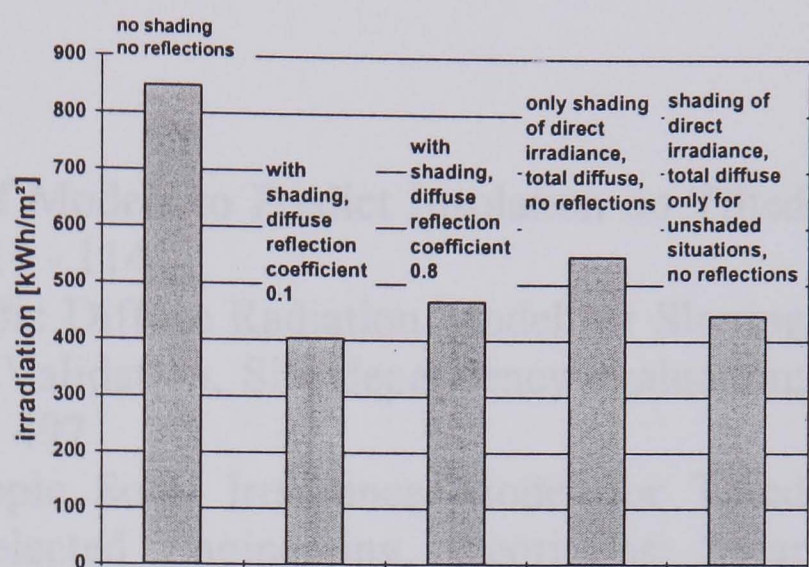


Fig. 9 Irradiation as annual sum calculated with different surface properties and different algorithms

4. CONCLUSION

The irradiance on a solar receiver on an urban structure depends strongly on site dependant influences, i.e. buildings in the neighbourhood. Besides the shading, different surface properties like the reflection coefficient or the reflection characteristics have a considerable influence on the predicted irradiance. If the accuracy of a solar energy simulation is to be better than 10 - 15% it necessary to accurately model the environment surroundings of the solar system. Further, not only shading but also reflections of direct and diffuse irradiation from neighbour buildings must be included in the simulation.

The new software tool, IPROCESS, can fulfil these tasks. The program uses a ray-tracing method and can be used as irradiance pre-processor to standard solar thermal or PV models.

REFERENCES

- [1] **Klucher T. M.** (1979) Evaluation of Models to Predict Insolation on Tilted Surfaces; Solar Energy Vol. 23, pp 111 - 114
- [2] **Perez R., et al.** (1986) An Anisotropic Diffuse Radiation Model for Sloping Surfaces: Description, Performance, Validation, Site dependency evaluation; Solar Energy Vol. 36, No. 6, pp 481 - 497
- [3] **Gueymard C.** (1987) An Anisotropic Solar Irradiance Model for Tilted Surfaces and Comparison with Selected Engineering Algorithms; Solar Energy Vol. 38, No. 5, pp 367 - 386
- [4] **Brunger, A. P.; Hooper, F. C.** (1993) Anisotropic Sky Radiance Model Based on Narrow Field of View Measurement of Shortwave Radiance; Solar Energy Vol. 51, No. 1, pp 53 - 64
- [5] **Watt A.** (1990) Fundamentals of Three-Dimensional Computer Graphics; Addison-Wesley Publishing Company, Inc.
- [6] **Ward G. J.** (1994) The RADIANCE Lighting Simulation and Rendering System; Computer Graphics Proceedings, Annual Conference Series
- [7] **Schweizer C., Eicker U. Lomas K.** (1998) Computation of Illuminance and Irradiance in Urban Structures, Proceedings of the 2nd World Conference and Exhibition on Photovoltaic Solar Energy Conversion, Vienna, Austria
- [8] **Duffie J. A., Beckmann W. A.** (1974) Solar energy thermal processes; Solar Energy Laboratory University of Wisconsin - Madison, John Wiley & Sons New York, USA
- [9] **DIN 5034** (1983) Tageslicht in Innenräumen; Deutsche Industrienorm, Beuth Verlag, Berlin und Köln
Daylight in Rooms; German Industrial Norm, Beuth-publication, Berlin and Cologne
- [10] **CIE Technical Committee 4.2** (1973) Standardization of Luminance on Clear Skies; CIE Publications No. 22 Commission International de l'Eclairage, Paris
- [11] **Matsuura K.** (1987) Luminance Distributions of Various Reference Skies; CIE Technical Report of TC 3-09
- [12] **Perez R., Seals R., Michalsky J.** (1993) All-Weather Model for Sky Luminance Distribution - Preliminary Configuration and Validation; Solar Energy Vol. 50, No. 3, pp 235-245

LIST OF PUBLICATIONS AND RELATED WORK

- **Schweizer C., Stellbogen D.:** IRRAD: Ein Programm zur Berechnung der solaren Einstrahlung auf feste und nachgeführte Flächen, unveröffentlichte Programmbeschreibung, Zentrum für Sonnenenergie- und Wasserstoff-Forschung ZSW, Stuttgart (1990)
IRRAD: A Program to Calculate Solar Irradiation on Fixed and Tracked Surfaces, unpublished manual, Center for Solar Energy- and Hydrogen-Research, ZSW, Stuttgart, Germany (1990)
- **Schweizer C., Stellbogen D., Bloss W. H.:** Schutzdioden in PV-Generatoren, Semesterarbeit, Institut für Physikalische Elektronik, Universität Stuttgart (1992)
Protective Diodes in PV Generators, Scientific work at the Institute for Physical Electronic, University of Stuttgart, Germany (1992)
- **Schweizer C.:** Dynamic simulation of Solar energy Systems in Urban environments, Interim Reports I-IX, Institute of Energy and Sustainable Development, De Montfort University Leicester (1995-1999)
- **Eicker U., Schweizer C.:** Daylighting of a social building in Ferney/Voltaire, Report for the European Commission, APAS RENA-CT94-0007 (1996)
- **Samak I., Loza R., Schelb R., Schweizer C., Munzert M.:** Factory of the Future, The World's Largest Photovoltaic System to be Incorporated into one Building; Proceedings of the 14th European Photovoltaic Solar Energy Conference, pp 1864-1867, Barcelona, Spain (1997)

-
- **Schweizer C., Eicker U. Lomas K.:** Dynamische Tageslichtberechnung in städtischer Umgebung, Fachhochschule Stuttgart, Hochschule für Technik, Forschungsbericht 1997 Band 40, pp 59-72 (1997)
Dynamic Calculation of Daylighting in an Urban Environment, Polytechnique Stuttgart, Research Report 1997, Vol. 40 pp 59-72 (1997)
Additionally published in the Proceedings of the 'Meeting of Building Physicist', Polytechnique Stuttgart, Vol. 38, pp 61-78, Germany (1997)
 - **Schweizer C., Eicker U. Lomas K.:** Prognose der solaren Einstrahlung auf PV-Module unter Berücksichtigung komplexer Verschattung und Reflexionen; Tagungsband des 13. Symposium Photovoltaische Solarenergie, Staffelstein, pp. 112-116 (1998)
Prognosis of the Solar Irradiation on PV modules considering complex shading and reflections, Proceedings of the 13th Symposium PV Solar Energy, Staffelstein, Germany, pp 112-116 (1998)
 - **Schweizer C., Eicker U. Lomas K.:** Computation of Illuminance and Irradiance in Urban Structures, Proceedings of the 2nd World Conference and Exhibition on Photovoltaic Solar Energy Conversion, Vienna, Austria (1998)
 - **Schweizer C., Eicker U. Lomas K.:** Dynamic Calculation of Daylighting in Urban Structures, Renewable Energy Vol. 15, pp. 360 - 363 (1998)
 - **Schweizer C., Eicker U. Lomas K.:** Solar Irradiation in an Urban Structure, Proceedings of the second ISES-Europe Solar Congress, EuroSun 1998, Portoroc, Slovenia (1998)

REFERENCES

- 1 **Ladener H.:** Solaranlagen; Planung, Bau & Selbstbau von Solarsystemen zur Warmwasserbereitung und Raumheizung, ökobuch Verlag Staufen (1993)
Solar systems; Design, erection & self-installation of solar systems for domestic hot water and space heating, ökobuch publishing, Staufen, Germany (1993)
- 2 **Schindler J., Zittel W.:** Wirtschaftliche Umbrüche durch nahende Erschöpfbarkeit fossiler Ressourcen, Solarzeitalter, Heft 2, Seiten 12-18 (1999)
Upheaval in economics due to exhausted fossil resources in the near future, Solarzeitalter, Vol 2, pp. 12-18 (1999)
- 3 **Quaschnig V.:** Simulation der Abschattungsverluste bei solarelektrischen Systemen, Dissertation an dem Fachbereich Elektrotechnik der Technischen Universität Berlin (1996)
Simulation of shading losses in solar electric systems, dissertation at the Dept. of Electrical Engineering, Technical University of Berlin Germany, (1996)
- 4 **Scheer H.:** Konsens über "Atomausstieg" - ein Bumerang für den Einstieg in die ökologische Energiewende, Solarzeitalter, Heft 2, Seiten 1-3 (1999)
Consensus about the opting out of nuclear energy - a boomerang for the entry in the ecological energy reform, Solarzeitalter, Vol. 2, pp. 1-3 (1999)
- 5 **Schöfer E.:** David und die Saurier, Solarzeitalter, Heft 2, Seiten 10-11 (1999)
David and the saurian, Solarzeitalter, Vol. 2, pp. 10-11 (1999)

-
- 6 **Tributsch H.:** Das Aufgabenfeld für Solarenergieforschung und -technologie, Solarzeitalter, Heft 2, Seiten 6-9 (1999)
The scope of duties of solar energy research and technology, Solarzeitalter, Vol. 2, pp. 6-9 (1999)
 - 7 **Mener G.:** War die Energiewende zu Beginn des 20. Jahrhunderts möglich? Sonnenenergie Heft 5, Seiten 40-43 (1998)
Had the change of electrical power supply been possible at the beginning of the 20th century? Sonnenenergie Vol. 3, pp. 40-43 (1998)
 - 8 **Püttmann H. et al.:** Bau-Handbuch, Technischer Ausbau, RWE, Essen (1987/88)
Building handbook, technical completion, RWE, Essen, Germany (1987/88)
 - 9 **Kiss M. G.:** Energiekonzepte in der Bauplanung: Thesen, Arbeitsmethoden, Beispiele, Bauverlag Wiesbaden, Schriftenreihe Bau, Energie, Wirtschaftlichkeit (1983)
Energetically conception in planing of buildings: theses, working methods, samples, Bauverlag Wiesbaden, Germany, series: construction, energy, profitability (1983)
 - 10 **Glück B.:** Komplexe Simulation, Voraussetzung zur Energieoptimierung, HLH Band 46 Nr. 3 (1995)
Complex simulation, prerequisites to an energetically optimization, HLH volume 46 No. 3 (1995)
 - 11 **Crisp V., Littlefair P., Cooper I., McKennan G.:** Daylighting as a passive solar energy option: An assessment of its potential on non-domestic design, BRE Report BR 129, Building Research Establishment, Garston, Watford UK (1988)
 - 12 **Szerman M.:** Auswirkung der Tageslichtnutzung auf das energetische Verhalten von Bürogebäuden, Dissertation am Institut für Baukonstruktion, Universität Stuttgart (1994)
Effects of daylighting on the energetically behaviour of non-domestic buildings, dissertation at the Department of Building Construction, University of Stuttgart, Germany (1994)

-
- 13 **Goretzki P.:** Passive Sonnenenergienutzung in der Bauleitplanung, Dissertation an der Universität Stuttgart (1994)*Passive utilisation of solar energy in architectural planing, dissertation at the University of Stuttgart, Germany (1994)*
 - 14 **Stohler F.:** Heizen mit alternativen Energien, AT-Verlag, Aarau, Schweiz (1981)*Heating with alternative energies, AT-publication, Aarau, Switzerland (1981)*
 - 15 **Feist W.:** The passive houses at Darmstadt / Germany, Institute Housing and Environment, Annastr. 15, D-64285 Darmstadt, Germany (1995)
 - 16 **Goetzberger A.:** The energetically self-sufficient solar house, Freiburg, Fraunhofer-Institute for Solar Energy Systems, Freiburg, Germany, workshop on Renewable Energy, Islamabad, Pakistan (1994)
 - 17 **Siemens Solar:** Product information, Siemens Solar GmbH, Frankfurter Ring 152, D-80915 München, Germany (1998)
 - 18 **Räuber A.:** Weltweite PV-Aktivitäten - eine kritische Bewertung, Tagungsband 13. Symposium Photovoltaische Solarenergie, Seiten 26-33, Staffelstein (1998)*World-wide PV activities - a critical valuation, Proceedings of the 13th Symposium PV Solar Energy, pp. 26-33, Staffelstein, Germany (1998)*
 - 19 **Schmid J.:** Photovoltaik als global Energiequelle, Solarzeitalter, Heft 2, Seiten 19-23 (1999)*Photovoltaic as global source of energy, Solarzeitalter, Vol. 2, pp. 19-23 (1999)*
 - 20 **Ladener H.:** Solare Stromversorgung: Grundlagen, Planung, Anwendung, ökobuch Verlag Staufen (1996)*Solar power supply: basics, planning, applications, ökobuch publishing, Staufen, Germany (1996)*
 - 21 **Hering E. et al.:** Elektronik für Ingenieure, VDI Verlag, Düsseldorf (1994)*Electrical engineering for engineers, VDI publishing, Düsseldorf, Germany (1994)*

-
- 22 **Köthe, H. K.:** Stromversorgung mit Solarzellen: Methoden und Anlagen für die Energieaufbereitung, Franzis-Verlag, München (1988)
Power supply by solar cells: methods and systems for the energy process, Franzis publishing, Munich, Germany (1988)
- 23 **Jäger F., Räuber A.:** Photovoltaik: Strom aus der Sonne, Müller Verlag, Karlsruhe (1990)
Photovoltaic: Power from the sun, Müller publishing, Karlsruhe, Germany (1990)
- 24 **Siemens Solar:** Technical Data, Solar module SM 55, Siemens Solar GmbH, Frankfurter Ring 152, D-80915 München, Germany (1998)
- 25 **Daimler-Benz:** Umweltbericht 1998, Daimler-Benz AG, Kommunikation, D-70546 Stuttgart (1998)
Environment report 1998, Daimler-Benz AG, Communication, 70546 Stuttgart, Germany (1998)
- 26 **Heinzel A., Ledjeff K.:** Wasserstofftechnik im Energieautarken Solarhaus, Freiburg, Fraunhofer-Institut für Solare Energiesysteme, Freiburg, Achema, Frankfurt (1994)
Hydrogen technique in the energetically self-sufficient solar house, Freiburg, Fraunhofer-Institute for Solar Energy Systems, Freiburg, Achema, Frankfurt Germany (1994)
- 27 **Keller G.:** Darstellung unterschiedlicher MPP-Regelungsverfahren, Tagungsband 10. Symposium Photovoltaische Solarenergie, Seiten 537-541, Staffelstein (1995)
Description of different MPP control procedures, Proceedings of the 10th Symposium PV Solar Energy, pp. 537-541, Staffelstein, Germany (1995)
- 28 **Adelmann P.:** MPP-Tracking, Digitale Regelungen für MPP-Tracker, Sonnenenergie Heft 3 (1988)
MPP tracking, Digital Control for MPP Tracker, Sonnenenergie Vol. 3 (1988)
- 29 **Gfrörer W.:** Wechselrichter für Solaranlagen, Franzis-Verlag, Poing (1998)
Inverter for solar systems, Franzis publishing, Poing, Germany (1998)

-
- 30 **Edelmoser K. H., Himmelstoss F. A.:** High efficiency DC-AC inverters for solar application, Proceedings of the Fourteenth European Photovoltaic Solar Energy Conference, Barcelona, Spain (1997)
- 31 **Schmidt H., Sauer D. U.:** Wechselrichter-Wirkungsgrade, Praxisgerechte Modellierung und Abschätzung, Sonnenenergie, Heft 4 / August (1996)
Efficiencies of inverters, Modelling and estimations for the practice, Sonnenenergie, Vol. 4, August (1996)
- 32 **SMA Regelsysteme:** Product information, Inverter: Sunny Boy, SMA Regelsysteme GmbH, Hannoversche Str. 1-5, 34266 Niestetal, Germany (1999)
- 33 **Würth Elektronik:** Product information, Inverter: WE 500 NWR, Würth Elektronik GmbH & Co.KG, Zeilbaumweg 15, 74613 Öhringen, Germany (1998)
- 34 **Dorf Müller:** Product information, Inverter: DMI, Dorf Müller Solaranlagen GmbH, Gottlieb-Daimler-Str. 15, 71394 Kernen, Germany (1998)
- 35 **Schweizer C., Eicker U. Lomas K.:** Computation of illuminance and irradiance in urban structures, Proceedings of the 2nd World Conference and Exhibition on Photovoltaic Solar Energy Conversion, Vienna, Austria (1998)
- 36 **Kukulka J. R.:** Solar cell with integrated bypass diode and method, Renewable Energy, Vol. 12 Issue 3, (1997)
- 37 **Green M. A., Hasyim E. S., Wenham S. R.:** Thermal performance of integral bypass diode solar cell modules, Solar Cells Vol. 19 pp. 109-122 (1986)
- 38 **Laukamp H., Kresse A., Leithold W.:** PV-Module ohne Bypass-Dioden, Tagungsband 13. Symposium Photovoltaische Solarenergie, Staffelstein (1998)
PV modules without bypass diodes, Proceedings of the 13th Symposium PV Solar Energy, Staffelstein, Germany (1998)

-
- 39 **Laukamp H.:** Eine "Structural-Glazing" Photovoltaik Fassade: Das "Solarzentrum Freiburg", Tagungsband 10. Symposium Photovoltaische Solarenergie, Staffelstein (1995)
A "structural-glazing" photovoltaic facade: the solar centre Freiburg, Proceedings of the 10th Symposium PV Solar Energy, Staffelstein, Germany (1995)
- 40 **Schneider A.:** Das solare Regierungsviertel, Photon, Vol. 1, Seiten 45-52 (1999)
The solar government quarter, Photon, Vol. 1, pp. 45-52 (1999)
- 41 **Tietze U., Schenk Ch.:** Halbleiter-Schaltungstechnik, Springer-Verlag Berlin (1993)
Semiconductor circuit design, Springer publishing Berlin, Germany (1993)
- 42 **Schweizer C.:** Schutzdioden in PV-Generatoren, Semesterarbeit am Institut für Physikalische Elektronik, Universität Stuttgart, (1992)
Protective diodes in photovoltaic systems, Study report at the Department of Physical Electronic, University of Stuttgart, Germany (1992)
- 43 **Samak I., Loza R., Schelb R., Schweizer C., Munzert M.:** The world's largest photovoltaic system to be incorporated into one building, Proceedings of the Fourteenth European Photovoltaic Solar Energy Conference, Barcelona, Spain (1997)
- 44 **Schweizer C., Eicker U. Lomas K.:** Dynamic calculation of daylighting in urban structures, Renewable Energy 15, pp. 360-363 (1998)
- 45 **Fröhlich C., Brusa R. W.:** Solar radiation and its variation in time, Solar Physics 74, pp. 209-215 (1981)
- 46 **Fisch M. N.:** Solartechnik I, Universität Stuttgart, Institut für Thermodynamik und Wärmetechnik, Pfaffenwaldring 6, D - 70569 Stuttgart (1991)
Solar technology I, University of Stuttgart, Department of Thermodynamics and Heat Engineering, Pfaffenwaldring 6, D - 70569 Stuttgart, Germany (1991)

-
- 47 **Duffie J. A., Beckmann W. A.:** Solar energy thermal processes, Solar Energy Laboratory University of Wisconsin - Madison, John Wiley & Sons New York, USA (1974)
- 48 **Plate E.:** Engineering meteorology, Fundamentals of meteorology and their application to problems in environmental and civil engineering, Elsevier scientific publishing company, Amsterdam (1982)
- 49 **Iqbal M.:** An introduction to solar radiation, Department of Mechanical Engineering, The University of British Columbia, Vancouver, Academic Press Toronto (1983)
- 50 **The Times:** Atlas of the world, Times Books Ltd., 16 Golden Square, London W1R 4BN and John Bartholomew & Son Ltd., Edinburgh, Great Britain (1986)
- 51 **Spencer J. W.:** Fourier series representation of the position of the sun, Search 2 (5), Science technology and society, pp. 172, Sydney (1971)
- 52 **Klein S. A., et al.:** TRNSYS 14.1, A transient system simulation program, Reference manual, Solar Energy Laboratory University of Wisconsin, Madison USA (1994)
- 53 **Quaschnig V., Hanitsch R.:** Der Einfluß von Abschattungen auf Photovoltaikanlagen in der Landwirtschaft, Institut für Elektrische Maschinen, Technische Universität Berlin, 19. Konferenz CIGR Sektion IV, Stuttgart (1995)
Influence of shading on agriculturally photovoltaic systems, Department of Electrical Machines, Berlin University of Technology, 19. Conference CIGR Section IV, Stuttgart, Germany (1995)
- 54 **Liebelt C.:** Leuchtdichte- und Strahldichteverteilung des Himmels, Dissertaion an der Fakultät für Elektrotechnik, Universität Karlsruhe (1987)
Light and radiance distribution in the sky, dissertation at the Department of Electrical Engineering, University of Karlsruhe, Germany (1978)

-
- 55 **Gueymard C.:** An anisotropic solar irradiance model for tilted surfaces and comparison with selected engineering algorithms, *Solar Energy* Vol. 38, No. 5, pp. 367 - 386 USA (1987)
- 56 **Kipp & Zonen:** Meteorological radiation sensors, Kipp & Zonen Delft BV, Mercuriusweg 1, NL 2600 AM Delft, The Netherlands (1997)
- 57 **Auer F., Windel C.:** Pyranometer oder Solarzelle, Fakten und Empfehlungen auf der Basis zweijähriger Vergleichsmessungen der solaren Strahlung, *Sonnenenergie* Heft 2, Seiten 28-29, April (1993)
Pyranometer or solar cell, facts and recommendations on a basis of a two-year comparative measurement, Sonnenenergie Vol. 2, pp. 28-29, April (1993)
- 58 **Liu B. Y. H., Jordan R. C.:** The long-term average performance of flat-plate solar energy collectors, *Solar Energy* Vol. 7, pp. 53 (1963)
- 59 **Hay J. E., Davis J. A.:** Calculation of the solar radiation incident on an inclined surface, Proc. 1st Canadian Solar Radiation Data Workshop J. E. Hay and T. K. Won, Toronto, pp. 59 - 72 (1980)
- 60 **Klucher T. M.:** Evaluation of models to predict insolation on tilted surfaces, *Solar Energy* Vol. 23, pp. 111 - 114 (1979)
- 61 **Perez R., et al.:** An anisotropic diffuse radiation model for sloping surfaces: Description, performance, validation, site dependency evaluation, *Solar Energy* Vol. 36, No. 6, pp. 481 - 497 (1986)
- 62 **Perez R., Seals R.:** A new simplified version of the Perez diffuse irradiance model for tilted surfaces, *Solar Energy* Vol. 39, No. 3, pp. 221 - 231 (1987)
- 63 **Reindl D. T., Beckmann W. A., Duffie J. A.:** Evaluation of hourly tilted surface radiation models, *Solar Energy* Vol. 45, No. 1, pp. 9 - 17 (1990)
- 64 **Perez R., Stewart R., Seals R., Guertin T.:** The development and verification of the Perez diffuse radiation model, Sandia Report SAND 88-7030, Sandia National Laboratories, Albuquerque, New Mexico USA (1988)

-
- 65 **Robledo L., Soler A.:** Point-source Perez illuminance model: Dependence of coefficients on surface orientation at Madrid, *International journal of lighting research and technology*, Vol. 28, No. 3, pp. 141-148 (1996)
- 66 **Burek S. A., Norton B., Probert S. D.:** Analytical and experimental methods for shadowband correction factors for solarimeters on inclined planes under isotropically diffuse and overcast skies, *Solar Energy* Vol. 40, No. 2, pp. 151 - 160 (1988)
- 67 **Le Baron B. A., Michalsky J. J., Perez R.:** A simple procedure for correcting shadowband data for all sky conditions, *Solar Energy* Vol. 44, No. 5, pp. 249 - 256 (1990)
- 68 **Ineichen P., Perez R., Seals R.:** The importance of correct albedo determination for adequately modelling energy received by tilted surfaces, *Solar Energy* Vol. 39, pp. 301 - 305 (1987)
- 69 **Nkemdirim L. C.:** A note on the albedo of surfaces, *Applied Meteorology* Vol. 11 pp. 867 - 875 (1972)
- 70 **Nkemdirim L. C.:** A note on the journal, latitudinal and seasonal variation of the surface reflection coefficient, *Applied Meteorology* Vol. 14 pp. 1603 - 1608 (1975)
- 71 **Ineichen P., Guisan O., Perez R.:** Ground-Reflected radiation and albedo, *Solar Energy* Vol. 44, No. 4, pp. 207 - 214 (1990)
- 72 **Quaschnig V., Hanitsch R.:** Shade calculations in photovoltaic systems, Department of Electrical Machines, Berlin University of Technology, ISES Conference Harare (1995)
- 73 **Schulze R.:** *Strahlenklima der Erde*, Wissenschaftliche Forschungsberichte, Steinkopf-Verlag Darmstadt (1970)
Radiation climate of the earth, Scientific research reports, published by Steinkopf, Darmstadt, Germany (1970)

-
- 74 **DIN 5034:** Tageslicht in Innenräumen, Deutsche Industrienorm, Beuth Verlag, Berlin und Köln (1983)
Daylight in rooms, German industrial norm, published by Beuth, Berlin and Cologne, Germany (1983)
- 75 **Müller S., Kresse W., Gatenby N., Schöffel F.:** A radiosity approach for the simulation of daylight, Fraunhofer-Institute for Computer Graphics, Wilhelminenstr. 7, 64283 Darmstadt, Germany, Eurographics (1996)
- 76 **Tregenza P., Sharples S.:** Daylighting algorithms, ETSU S 1350, School of Architectural Studies, University of Sheffield (1993)
- 77 **Littlefair P. J.:** A Comparison of sky luminance models with measured data from Garston, UK, Solar Energy Vol. 53, No 4, pp. 315 - 322 (1994)
- 78 **Czeplak G.:** Investigation of impact of cloud amount and height on luminous efficacy, IEA-SHCP, Task 17, Subtask E. (1996)
- 79 **Littlefair P. J.:** The luminous efficacy of daylight: A review, International journal of lighting research and technology, Vol. 17, pp. 162-182 (1985)
- 80 **Muneer T., Angus R. C.:** Luminous efficacy: Evaluation of models for the United Kingdom, International journal of lighting research and technology, Vol. 27, No. 2, pp. 71-77 (1995)
- 81 **Michalsky J., Perez R., Seals R.:** Evaluations of algorithms for sky luminance distribution, Prospects for performance improvements, World Solar Congress, Vol. 1 Part II, Denver, pp. 1049 - 1054 (1991)
- 82 **Brunger, A. P., Hooper, F. C.:** Anisotropic sky radiance model based on narrow field of view measurement of shortwave radiance, Solar Energy, Vol. 51, No. 1 (1993)
- 83 **Coulson K. L.:** Polarization and intensity of light in the atmosphere, A. DEEPAK Publishing, Hampton, Virginia USA (1988)

-
- 84 **Perez R., Seals R., Michalsky J.:** All-weather model for sky luminance distribution - preliminary configuration and validation, *Solar Energy* Vol. 50, No. 3, pp. 235-245 (1993)
- 85 **Enarum D., Littlefair, P.:** Luminance models for overcast skies: Assessment using measured data, *International journal of lighting research and technology*, Vol. 27, No. 1 (1995)
- 86 **Kittler R., Valko P.:** Radiance distribution on densely overcast skies: Comparison with CIE luminance standard, *Solar Energy* Vol. 51 No 5, pp. 349 - 355 (1993)
- 87 **CIE Technical Committee 4.2:** Standardization of luminance on clear skies, CIE Publications No. 22 Commission International de l'Eclairage, Paris (1973)
- 88 **Brunger A. P., Hooper F. C.:** Measured shortwave sky radiance in an urban atmosphere, *Solar Energy* Vol. 47, No 2, pp. 137 - 142 (1991)
- 89 **Ineichen P., Molineaux B., Perez R.:** Sky luminance data validation: Comparison of seven models with four data banks, *Solar Energy* Vol. 52, No 4, pp. 337 - 346 (1994)
- 90 **Perez R., et al.:** Geostatistical properties and modelling of random cloud pattern for real skies, *Solar Energy* Vol. 51, No. 1, pp. 7 - 18 (1993)
- 91 **Matsuura K.:** Luminance distributions of various reference skies, CIE Technical Report of TC 3-09 (1987)
- 92 **Harrison A. W.:** Directional sky luminance versus cloud cover and solar position, *Solar Energy* Vol. 46 No 1, pp. 13 - 19 (1991)
- 93 **Perez R., Ineichen P., Seals R., Michalsky J., Stewart R.:** Modelling daylight availability and irradiance components from direct and global irradiance, *Solar Energy* Vol. 44, No. 5, pp. 271 - 289 (1990)

-
- 94 **Mermoud A.:** PVSYST, Version 2.0, User's Manual, Group of Applied Physics (GAP) and University Centre for the Study of Energy Problems (CUEPE), University of Geneva, Switzerland (1996)
- 95 **Stellbogen D., Geyer D.:** F&E-Vorhaben "Rechnerprogramm zur Auslegung von Photovoltaik-Fassaden", Abschlußbericht: Arbeitsteil "Einstrahlungs- und Schattenberechnung", Zentrum für Sonnenergie- und Wasserstoff-Forschung (Nov. 1998)
R&D Project "Computer model for Photovoltaic Facades", Final Report of the part: "Irradiance and Shading Calculations", Centre for Solar Energy and Hydrogen Research (Nov. 1998)
- 96 **ETSU Report,** Photovoltaics in Buildings, A survey of design tools, Palace Wharf, Rainville Road, London W6 9HN, UK (Nov. 1997)
- 97 **Kaiser R., Reise C.:** PV system simulation programs, International Energy Agency IEA, Task 16 Photovoltaics in Buildings, Fraunhofer Institute for Solar Energy Systems ISE, Oltmannsstr. 5, 79100 Freiburg, Germany (May 1996)
- 98 **Schilla T., Hill R., Bucher:** PVNetSim: a versatile PV simulation software based on the Design Centre program Schematics, PSpice and Probe, Proceedings of the Fourteenth European Photovoltaic Solar Energy Conference, Barcelona, Spain (1997)
- 99 **MicroSim PSpice A/D:** Circuit Analysis Reference Manual, Version 7.1, MicroSim Corporation, 20 Fairbanks, Irvine, California 92618 (October 1996)
- 100 **MicroSim Schematics:** User's Guide, Version 7.1, MicroSim Corporation, 20 Fairbanks, Irvine, California 92618 (October 1996)
- 101 **FhG-ISE:** 1000-Dächer Meß- und Auswertprogramm, Jahresjournal 1997, Fraunhofer Institut für Solar Energiesysteme, Oltmannsstr. 5, 79100 Freiburg (1997)
1000 roof measurement and evaluation program, Annual Journal 1997, Fraunhofer Institute for Solar Systems, Oltmannsstr. 5, 79100 Freiburg, Germany (1997)

-
- 102 **Blümel E. et al.:** Entwicklung von Testreferenzjahren (TRY) für Klimaregionen der Bundesrepublik Deutschland, BMFT Forschungsbericht T 86-051, Juli (1986)
Development of test reference years (TRY) for climate regions in Germany, BMFT research report T 86-051, July (1986)
- 103 **Viotto M., Punkrop D., Stellbogen D.:** Auslegung von Solarfassaden mit PVcad, Ein Werkzeug für den Planer, Tagungsband 13. Symposium Photovoltaische Solarenergie, Staffelstein, Deutschland (1998)
Dimensioning of solar facades with PVcad, a tool for the planner, Proceedings of the 13th Symposium PV Solar Energy, Staffelstein, Germany (1998)
- 104 **INSEL:** Interactive Simulation of Renewable Electrical Energy Supply Systems, University of Oldenburg, Faculty of Physics, Department of Energy and Semiconductor Research, Carl-von-Ossietzky Str. 9-11, D-26129 Oldenburg, Germany (1998)
- 105 **PVcad V 1.10:** Ein Auslegungswerkzeug für Solarfassaden, Institut für Solare Energieversorgungstechnik ISET e.V., Königstor 59, 34119 Kassel (1999)
A tool to design solar facades, Institute for solar energy supply, Königstor 59, D-34119 Kassel, Germany (1999)
- 106 **Grötzner M., Roosen P.:** PVEPO - Optimierungswerkzeug für die Verschaltung von Photovoltaik-Fassaden, Tagungsband 13. Symposium Photovoltaische Solarenergie, Staffelstein, Deutschland (1998)
PVEPO - A tool to optimise the wiring of PV facades, Proceedings 13th Symposium PV Solar Energy, Staffelstein, Germany (1998)
- 107 **Schweizer C., Stellbogen D.:** IRRAD, ein Programm zur Berechnung der solaren Einstrahlung auf geneigte Flächen (nicht veröffentlicht), Zentrum für Sonnenenergie- und Wasserstoff-Forschung, Stuttgart (1990)
IRRAD, a program to calculate solar irradiation on tilted surfaces (not published), Centre for Solar Energy- and Hydrogen-Research, Stuttgart, Germany (1990)

-
- 108 **Niewianda A., Heidt F. D.:** Sombrero, A PC-tool to calculate shadows on arbitrarily oriented surfaces, Department of Physics, University of Siegen, Germany (1995)
- 109 **Quaschnig V., Hanitsch R.:** Sundi manual, Department of Electrical Machines, Berlin University of Technology, 19th Conference CIGR Section IV, Stuttgart, Germany (1995)
- 110 **Stellbogen D.:** Shade / PV-Node, Centre for Solar Energy and Hydrogen Research, Stuttgart, Germany (1995)
- 111 **Watt A.:** Fundamentals of three-dimensional computer graphics, Addison-Wesley Publishing Company, Inc. (1990)
- 112 **Ward G. J.:** The RADIANCE lighting simulation and rendering system, Computer Graphics Proceedings, Annual Conference Series (1994)
- 113 **Ward Larson G., Shakespere R.:** Rendering with Radiance, The Art and Science of Lighting Visualization, Morgan Kaufmann Publishers, San Francisco, California, USA (1998)
- 114 **Autodesk:** AutoCAD Release 14, Autodesk BV, Rue du Puits-Godet 6, 2000 Neuchatel, Switzerland
- 115 **Eicker U.:** Urban planning studies with new PV/thermal building components, Architectural integration of new components in three major European housing projects, First interim progress report, APAS Contract No. RENA-CT94-007, Hochschule für Technik, Schellingstr. 24, D-70174 Stuttgart, Germany (1995)
- 116 **Schweizer C., Eicker U., Lomas K.:** Solar Irradiation in an Urban Structure, Proceedings of the second ISES-Europe Solar Congress, EuroSun 1998, Portoroc, Slovenia (1998)
- 117 **Schweizer C:** IPROCESS, Manual, Am Sonnenweg 58, 70619 Stuttgart, Germany (1999)

-
- 118 **Erhorn et al.:** ADELIN 2.0 Advanced Daylighting and Electric Lighting Integrated New Environment, International Energy Agency (IEA) Solar Heating and Cooling Task 12, Fraunhofer-Institut für Bauphysik, Nobelstr. 12, D-70569 Stuttgart, Germany (1996)
- 119 **Ward G. J., et al.:** ADELIN 2.0, RADIANCE reference manual, International Energy Agency: Solar Heating and Cooling Task 12, Lawrence Berkeley Laboratories, Berkeley, CA (1996)
- 120 **Ward G. J., et al.:** ADELIN 2.0, RADIANCE user's manual, International Energy Agency: Solar Heating and Cooling Task 12, Lawrence Berkeley Laboratories, Berkeley, CA (1996)
- 121 **Delaunay J.:** GENDAYLIT, to generate a RADIANCE description of the daylight sources using the PEREZ models for diffuse and direct components, Fraunhofer-Institute for Solar Energy Systems, Freiburg, Germany (1994)
- 122 **Kovach A.:** Effect of Partial Shading on the Energy Performance of Photovoltaic Arrays Integrated onto Buildings, Dissertation, Fortschr.-Bericht VDI Reihe 6 Nr. 329, Düsseldorf, Germany (1995)
- 123 **Tregenza P., Waters I. M.:** Daylight coefficients, *Lighting Research and Technology*, Vol. 15 (2), pp. 65-71 (1983)
- 124 **Cropper P.:** Deriving daylight coefficients from a discretised sky dome, Interim Report: 4, Institute of Energy and Sustainable Development, De Montfort University Leicester, UK (1996)
- 125 **Mardaljevic J.:** Notes on (1) Daylighting Applications, (2) Advanced Daylighting Calculations and (3) Validation Studies in Rendering with RADIANCE: A Practical Tool for Global Illumination ACM SIGGRAPH (1998)
- 126 **Cesarano A., Bellia L., Minichiello F., Sibilio S.:** Sky luminance models: Sensitivity to sky-dome subdivision, *Lighting Research and Technology*, Vol. 28 (3), pp. 131-140 (1996)

-
- 127 **Tregenza P. R.:** Subdivision of the sky hemisphere for luminance measurements, *Lighting Research and Technology*, Vol. 19, pp. 13-14 (1987)
- 128 **Microsoft:** VISUAL BASIC, Programming System for Windows, Professional Edition, Microsoft Corporation
- 129 **Bronstein I. N., Semendjajew K. A.:** Taschenbuch der Mathematik, Verlag Harri Deutsch, Thun und Frankfurt (1987)
Paperback of Mathematics, published by Harri Deutsch, Thun, Switzerland, and Frankfurt, Germany (1987)
- 130 **Hadjoannou:** A set of irradiance data personally received from Mr. Hadjoannou, Ministry of Agriculture, Natural Resources & Environment, Meteorological Service CY-1418 Nicosia, Cyprus (1996)
- 131 **Reise C., Hofer F.:** Modelle für Licht und Zwielight, Dokumentation der Einstrahlungsumrechnung in diversen Simulationssystemen und -Programmen, Fraunhofer Institut für Solare Energiesysteme (1997)
Models for Light and Twilight, Documentation of converting irradiance in different simulation systems, Fraunhofer Institute for Solar Energy Systems (1997)
- 132 **Lanzerstorfer S.:** Simulation der Reflexionsverluste eines kristallinen Solarmoduls und deren Auswirkungen auf den Stromertrag, Tagungsband 10. Symposium Photovoltaische Solarenergie, Staffelstein (1995)
Simulation of the reflection losses of a crystalline solar module and the influence on the energy yield, Proceedings of the 10th Symposium PV Solar Energy, Staffelstein, Germany (1995)
- 133 **Mardaljevic J.:** Daylight Simulation: Validation, Sky Models and Daylight Coefficients, Thesis draft, Institute of Energy and Sustainable Development, De Montfort University Leicester, UK (1999)

Curriculum Vitae

Name Christian Schweizer
Citizenship Germany
Birthplace Hamburg, Germany
Date of Birth 13 September 1966

Education

Primary School Böblingen, Germany	1972 - 1975
German school Brussels, Belgium	1975 - 1978
Secondary School education Böblingen, Germany Degree: Abitur	1978 - 1986 June 1986
University of Stuttgart, Germany Department of Electrical Engineering Degree: Diplom-Ingenieur	1987 - 1993 June 1993
De Montfort University Leicester, UK Institute of Energy and Sustainable Development Degree: Doctor of Philosophy	1995 - 1999 January 2000

Work Experience

Trainee at Mercedes-Benz Stuttgart, Germany	1988
Assistant at Centre for Solar Energy- and Hydrogen Research, ZSW, Stuttgart, Germany	1990
Trainee at IBM, Research Institute Böblingen, Germany	1991
ENGCOTEC GmbH, Stuttgart, Germany Current position: Project Manager	since 1993